UNIVERSIDADE FEDERAL DE SANTA CATARINA
CAMPUS REITOR JOÃO DAVID FERREIRA LIMA
CENTRO DE CIÊNCIAS DA SAÚDE
PROGRAMA DE PÓS-GRADUAÇÃO EM NANOTECNOLOGIA FARMACÊUTICA

Carine Zuglianello

Desenvolvimento e avaliação das propriedades biofarmacêuticas e farmacológicas de nanopartículas de polieletrólitos constituídas de pranlintida e sulfato de dextrana com vistas a potencial aplicação para administração nasal no tratamento do Alzheimer

Florianópolis
2021

Carine Zuglianello

Desenvolvimento e avaliação das propriedades biofarmacêuticas e farmacológicas de nanopartículas de polieletrólitos constituídas de pranlintida e sulfato de dextrana com vistas a potencial aplicação para administração nasal no tratamento do Alzheimer

Tese submetida ao Programa de Pós-graduação em Nanotecnologia Farmacêutica da Universidade Federal de Santa Catarina para a obtenção do título de Doutora em Nanotecnologia Farmacêutica.
Orientadora: Profa. Dra. Elenara Maria Teixeira Lemos-Senna.

Florianópolis
2021

Ficha de identificação da obra elaborada pelo autor,
através do Programa de Geração Automática da Biblioteca Universitária da UFSC.

Zuglianello, Carine
Desenvolvimento e avaliação das propriedades biofarmacêuticas e farmacológicas de nanopartículas de polieletrólitos constituídas de pranlintida e sulfato de dextrana com vistas a potencial aplicação para administração nasal no tratamento do Alzheimer / Carine Zuglianello ; orientadora, Elenara Lemos-Senna, 2021.
210 p.

Tese (doutorado) - Universidade Federal de Santa Catarina, Centro de Ciências da Saúde, Programa de Pós Graduação em Nanotecnologia Farmacêutica, Florianópolis, 2021.

Inclui referências.

1. Nanotecnologia Farmacêutica. 2. Pranlintida. 3. Nanocarreador. 4. Doença de Alzheimer. 5. Administração nasal. I. Lemos-Senna, Elenara. II. Universidade Federal de Santa Catarina. Programa de Pós-Graduação em Nanotecnologia Farmacêutica. III. Título.

Carine Zuglianello

Desenvolvimento e avaliação das propriedades biofarmacêuticas e farmacológicas de nanopartículas de polieletrólitos constituídas de pranlintida e sulfato de dextrana com vistas a potencial aplicação para administração nasal no tratamento do Alzheimer

O presente trabalho em nível de doutorado foi avaliado e aprovado por banca examinadora composta pelos seguintes membros:

Profa. Dra. Cristiana Lima Dora
Universidade Federal do Rio Grande (FURG)

Prof. Dr. Eduardo Luiz Gasnhar Moreira
Universidade Federal de Santa Catarina (UFSC)

Profa. Dra. Maria Palmira Daflon Gremião
Universidade Estadual Paulista Júlio de Mesquita Filho (UNESP/Araraquara)

Certificamos que esta é a **versão original e final** do trabalho de conclusão que foi julgado adequado para obtenção do título de doutor em Nanotecnologia Farmacêutica.

Documento assinado digitalmente
Elenara Maria Teixeira Lemos Senna
Data: 22/03/2021 12:41:14-0300
CPF: 607.080.000-10
Verifique as assinaturas em https://v.ufsc.br

Profa. Dra. Elenara Maria Teixeira Lemos-Senna
Coordenadora Local do PPGNanoFarma (UFSC)

Documento assinado digitalmente
Elenara Maria Teixeira Lemos Senna
Data: 22/03/2021 12:41:47-0300
CPF: 607.080.000-10
Verifique as assinaturas em https://v.ufsc.br

Profa. Dra. Elenara Maria Teixeira Lemos-Senna
Orientadora

Florianópolis, 2021.

Este trabalho é dedicado aos meus ascendentes, especialmente aos meus bisavôs Elvira (*in memoriam*) & Rudi (*in memoriam*) e Gema (*in memoriam*) & Vergílio (*in memoriam*), aos meus avôs Protásio (*in memoriam*) e Ramis (*in memoriam*) e às minhas avós Naldi e Mercedes.

What is the ultimate truth about ourselves? Various answers suggest themselves. We are a bit of stellar matter gone wrong. We are physical machinery—puppets that strut and talk and laugh and die as the hand of time pulls the strings beneath. But there is one elementary inescapable answer. We are that which asks the question.

(EDDINGTON, 1935).

AGRADECIMENTOS

Agradeço, em especial, a minha orientadora, Profa. Dra. Elenara Lemos-Senna, que me apoiou e por vezes me conduziu durante o percurso de doutoramento. Agradeço aos colegas que participaram da realização e interpretação de experimentos, emprestando sua experiência e dedicação: Vanessa (CEBIME/UFSC), Andrés (PPGQ/UFSC), Nícolas (Farmácia/UFSC), Jonathan (PPGFarmaco/UFSC) Bruna (PPGNeuro/UFSC) e Angela (PGFar/UFSC), assim como aos professores, que me receberam em seus laboratórios: Profa. Dra. Nereide (PPGNanoFarma/UFPE) e Prof. Dr. Humberto (Ciências Farmacêuticas/UPPB), Prof. Dr. Alfeu (PPGFarmaco/UFSC) e Prof. Dr. Rui (PPGNeuro/UFSC), ou compuseram as bancas de qualificação e/ou defesa: Profa. Dra. Palmira (UNESP), Prof. Dr. Hernán (CEBIME, UFSC), Profa. Dra. Cristiana (FURG) e Prof. Dr. Eduardo (PPGNeuro/UFSC). Agradeço às agências de fomento, CAPES e CNPq e FAPESP. Agradeço à minha família, por todo o suporte que recebi, principalmente ao meu irmão, Daniel e ao meu esposo, Jocemar. Agradeço a todos familiares e amigos que torceram por mim, de longe, e as amizades que construí no dia a dia, no Laboratório de Farmacotécnica da UFSC. Vocês tornaram a concretização do meu sonho possível, e suas contribuições foram para além do enriquecimento dessa pesquisa, impactando também meu desenvolvimento pessoal.

RESUMO

A pranlintida (Pram) é um peptídeo análogo da amilina humana, aprovada pelo FDA para tratamento do diabetes mellitus (DM) dos tipos 1 e 2, em combinação com a insulina, e para tratamento da obesidade. Além disso, tem demonstrado efeitos promissores em diversos modelos de doença de Alzheimer (DA), no que parece agir como um antagonista funcional do receptor de amilina, revertendo danos causados por oligômeros tóxicos do peptídeo beta-amiloide (Aβ). Em contraponto aos interessantes efeitos terapêuticos, suas propriedades farmacocinéticas compreendem curto tempo de meia-vida e rápida eliminação, após infusão intravenosa. A via de administração subcutânea, em esquema de múltiplas doses diárias também é um inconveniente para os pacientes. Com o intuito de contornar estes inconvenientes, este trabalho teve como objetivo desenvolver nanocarreadores para administração nasal da Pram e avaliar a sua potencial utlização no tratamento da DA. Inicialmente a complexação da Pram, catiônica em pH 4, com sulfato de dextrana (DexS), um polissacarídeo aniônico, foi utilizada para obtenção de nanopartículas de polieletrólitos (DexS/Pram NPs) com concentração de fármaco semelhante a presente no produto comercial, destinado a administração subcutânea (Symlin®). A adição de uma solução de Pram a uma solução de DexS, em uma estreita faixa de concentrações e razão molar, permitiu a obtenção de nanopartículas de polieletrólitos de tamanho nanométrico e com baixa dispersão de tamanho. A formação dos complexos ocorreu por interações eletrostáticas e ligações de hidrogênio espontâneas, além de interações hidrofóbicas, que levaram a modificações estruturais no peptídeo, permitindo sua estabilização na forma bioativa de α-hélice. Porém os complexos não foram estáveis em fluido nasal simulado (FNS), ocorrendo completa dissociação do fármaco. Algumas estratégias foram testadas para estabilização coloidal dos complexos, tendo a associação a superfície de gotículas de uma nanoemulsão demonstrado ser mais promissora, por não causar deslocamento da pranlintida dos complexos e não acrescentar componentes tóxicos à composição das nanopartículas. A permeação *in vitro* através da mucosa nasal suína foi avaliada utilizando células de difusão de Franz e FNS como meio aceptor. A permeação da Pram a partir das nanoemulsões revestidas pelos complexos ($NE_{DexS/Pram}$) ocorreu de forma sustentada ao longo do tempo, e foi menor nas primeiras horas, enquanto a retenção na mucosa não foi afetada em relação ao peptídeo, administrado na forma de solução. Nos estudos de mucodifusão, a associação ao nanocarreador aumentou a difusão da Pram através de um gel fluido de mucina, o que foi atribuído às propriedades mucolíticas da DexS. Finalmente, os efeitos dos tratamentos com Pram livre ou associada ao nanocarreador ($NE_{DexS/Pram}$), por via nasal, e da Pram livre por via intraperitoneal, na dose de 100 µg/kg/dia foram avaliados em estudos *in vivo*, utilizando modelo animal de DA induzido pela administração intracerebroventricular de oligômeros de $A\beta_{1-42}$. Nos testes comportamentais específicos para memória e cognição, o tratamento com $NE_{DexS/Pram}$ melhorou o desempenho dos animais, enquanto o tratamento com a solução de Pram, administrada por via nasal ou intraperitoneal, não modificou o desempenho dos animais em relação ao controle. Esses resultados estão de acordo com as propriedades esperadas para as nanoemulsões, que foram formuladas para manter a estabilidade da Pram nos fluidos biológicos e mucosa nasal, aumentar a área superficial de contato com a mucosa e promover sua difusão através da camada de muco. Estudos de biodistribuição e toxicidade crônica precisam ser realizados para afirmar os possíveis benefícios do fármaco nas formas livre e nanocarreado no tratamento da DA.

Palavras-chave: Pranlintida. Nanocarreador. Doença de Alzheimer. Administração nasal.

ABSTRACT

Pramlintide (Pram) is a human amylin analog peptide, approved by the FDA for the treatment of diabetes mellitus (DM) types 1 and 2 in association with insulin, and obesity. Besides, Pram has demonstrated promising beneficial effects in several Alzheimer's disease (AD) models, in what appears to act as a functional amylin receptor antagonist, reversing damage caused by toxic oligomers of the beta-amyloid (Aβ) peptide oligomers. Despite its interesting therapeutic effects, Pram has a short half-life time and a fast elimination after intravenous injection. The subcutaneous administration, in a multiple-doses scheme, is also inconvenient for patients. To circumvent these drawbacks, this work aimed to develop Pram-loaded nanocarriers for nasal administration and to evaluate its potential application in the treatment of the DA. Firstly, the complexation of Pram, which is positively charged in pH 4.0, with dextran sulfate (DexS), an anionic polysaccharide, was used to obtain polyelectrolyte nanoparticles (DexS/Pram NPs), with a drug content similar to the subcutaneous formulation, marketed as Symlin®. The addition of a Pram solution to a DexS solution, in a narrow concentration and molar ratio range, allowed the formation of polyelectrolyte particles (DexS/Pram NPs) displaying nanometric size and narrow particle size distribution. The formation of the complexes occurred through electrostatic interactions and hydrogen bonds, in addition to hydrophobic interactions, which led to structural changes in the peptide, allowing its stabilization in the bioactive form of α-helix. Despite that, the complexes were not stable in simulated nasal electrolyte solution (SNES), occurring the complete dissociation of the drug. Some strategies were tested for colloidal stabilization of the complexes, and the association onto the droplet surface of a nanoemulsion (PEC-$NE_{DexS/Pram}$) demonstrated to be promising, as it did not cause the displacement of the Pram after incubation of the complexes in SNES and did not add toxic components to the formulations. *In vitro* permeation of the Pram across porcine nasal mucosa was evaluated using Franz diffusion cells and SNES as acceptor medium. Pram permeation from the PEC-$NE_{DexS/Pram}$ occurred in a sustained manner over time, and was lower in the first hours, while the amount of Pram retained in the mucosa did not differ after the application of the free peptide or the PEC-$NE_{DexS/Pram}$. In muco-diffusion studies, Pram association to the nanocarrier increased its diffusion across the mucin gel, which was attributed to the mucolytic properties of DexS. Finally, *in vivo* studies were carried out using the experimental model of AD induced by intracerebroventricular injection of $A\beta_{1-42}$ oligomers. The effects of intranasal treatment with Pram, free and associated with nanocarrier, at the dose of 100 µg/kg/day were evaluated. In the behavioral tests of memory and cognition, the treatment with the $NE_{DexS/Pram}$ improved the animal performance, while the treatment with the Pram solution by nasal or intraperitoneal routes did not alter the animal performance, regarding the control group. These results are in accordance with the expected nanoemulsion properties, which were developed to maintain Pram stability in biological fluids and nasal mucosa, enhance the surface contact area with the mucosa and promote the diffusion across the mucus layer. However, biodistribution and chronic toxicity studies must be performed to prove the beneficial properties of Pram, free and associated with the nanocarrier, in the AD treatment after nasal administration.

Keywords: Pramlintide. Nanocarrier. Alzheimer´s Disease. Nasal administration.

LISTA DE FIGURAS

CAPÍTULO I, Manuscrito 1 – Dextran Sulfate/Pramlintide Polyelectrolyte Nanoparticles as a promising Delivery System: Optimization, evaluation of Supramolecular Interactions and effect on Conformational Stability of the Peptide Drug

CAPÍTULO III, Manuscrito 3 – Intranasal administration of dextran sulfate/pramlintide polyelectrolyte complex-coated nanoemulsions restores cognitive impairment induced by β-Amyloid peptide oligomers in an animal model of Alzheimer´s disease

APÊNDICE A – ESTRATÉGIAS PARA ESTABILIZAÇÃO DE NANOPARTÍCULAS DE POLIELETRÓLITOS EM MEIOS COM FORÇA IÔNICA COMPATÍVEL A DOS MEIOS BIOLÓGICOS

APÊNDICE B – VALIDAÇÃO PARCIAL DE MÉTODO UTILIZADO PARA QUANTIFICAÇÃO DE PRANLINTIDA EM AMOSTRAS DE EXPERIMENTOS DE MUCODISUSÃO E PERMEAÇÃO EM MUCOSA NASAL SUÍNA

LISTA DE QUADROS

LISTA DE TABELAS

CAPÍTULO I, Manuscrito 1 – Dextran Sulfate/Pramlintide Polyelectrolyte Nanoparticles as a promising Delivery System: Optimization, evaluation of Supramolecular Interactions and effect on Conformational Stability of the Peptide Drug

CAPÍTULO II, Manuscrito 2 – Polysaccharide/peptide complexes stabilized around nanoemulsion droplets: an application for nasal administration of pramlintide

CAPÍTULO III, Intranasal administration of dextran sulfate/pramlintide polyelectrolyte complex-coated nanoemulsions restores cognitive impairment induced by β-Amyloid peptide oligomers in an animal model of Alzheimer´s disease

APÊNDICE A – ESTRATÉGIAS PARA ESTABILIZAÇÃO DE NANOPARTÍCULAS DE POLIELETRÓLITOS EM MEIOS COM FORÇA IÔNICA COMPATÍVEL A DOS MEIOS BIOLÓGICOS

LISTA DE ABREVIATURAS E SIGLAS

129/SvEv
An inbred mouse strain popular for use in genetic knockout studies., 46

3xTgAD
Triple-transgenic Alzheimer's disease, 42, 44, 45

5xFAD
Express human APP and PSEN1 transgenes with a total of five AD-linked mutations, 42, 44, 45, 46, 48

AC253
An amylin receptor antagonist, 45, 46

ADAM-10
ADAM metallopeptidase domain 10, 45
AE
Association efficiency, 84

Amy
Amilina, 44, 45
Amylin, 44

Amy_R
Receptores de amilina, 38

AP
Área postrema, 37

APP,
Amyloid precursor protein, 31, 42, 44, 45, 47, 48

APP/PS1
Double transgenic mouse overexpresses mutated forms of the genes for human amyloid precursor protein (APPsw) and presenilin 1 (m146L), 43, 44, 45, 47

ATP5b
Gene que codifica a enzima mitocondrial subunidade β de ATP-sintase F1, 46

Aβ
Proteína β-amiloide, 33, 34, 31, 32, 33, 35, 42, 43, 44, 45, 46, 47, 48, 131, 136

B4GALNT1
Enzima β-1,4 galactosaminil transferase-1, 48

BACE-1
Beta-secretase, 45, 47, 131

BHE
Barreira hematoencefálica, 44, 46

c.a.
Cerca de aproximadamente, 41

CalcR
Receptor de calcitonina, 37

CD
Circular dichroism, 41, 89, 91

CD68
Cluster of differentiation 68, 44

CDK5
Cyclin Dependent Kinase 5, 44, 45, 46

CEUA
Comissão de Ética no Uso de Animais, 215

COX-2
Ciclo-oxigenase-2, 44

DA
Doença de Alzheimer, 21, 22, 31, 32, 33, 34, 35, 41, 42, 43, 44, 45, 46, 47, 48, 56, 131

DCF
Diclorofluoresceína, 47

DexS
Dextran sulfate, 35, 36, 41, 73, 75, 77, 78, 79, 80, 81, 82, 83, 84, 85, 86, 87, 88, 89, 90, 91, 92, 98, 99

DexS/Pram NPs
Dextran sulfate/pramlintide nanoparticles, 79

DLS
Dynamic light scattering, 79

DM
Diabetes mellitus, 33, 34, 35, 36, 38, 41, 42, 49

DM1
Diabetes mellitus tipo 1, 33, 34, 35, 42

DM2
Diabetes mellitus tipo 2, 33, 34, 35, 42

DMSO
Dimethyl sulfoxide, 80

ERK
Extracellular signal-regulated kinase, 45

FCE
Fluido cerebrospinal, 44, 51

FDA
Food and Drug Administration, 21, 38

FNS
Fluído nasal simulado, 103, 207, 208, 210

FTIR
Fourier-transform infrared spectroscopy, 81, 88

GABA
Ácido gama-aminobutírico, 37

GAG
glicosaminoglicano, 69, 90

GFAP
glial fibrillary acid protein, 32

GM1
Monosialotetrahexosylganglioside-1, 48

GM2
Monosialotetrahexosylganglioside-2, 48

GPCRs
Receptores acoplados a proteínas G, 37

GP-x
Glutationa peroxidase, 45, 47

His
Histidina, 39

HO-1
Heme oxygenase- 1, 44, 45, 47

HPSEC
High-performance size exclusion chromatography, 78, 83

i.c.v.
Intracerebroventricular, 131

i.p.
Intraperitoneal, 44

i.v.
intravenosa, 41

Iba-1
Ionized calcium- binding adaptor molecule-1, 44

IL
Interleucina, 38, 44

ITC
Isothermal calorimetry titration, 81

LC-UV
Liquid chromatography with ultraviolet detection, 82

LRP1
Proteína-1 relacionada ao receptor de lipoproteína de baixa densidade, 46

MHC
major histocompatibility complex, 32

M_n
number average molecular weight, 83

MnSOD
Manganês super-óxido dismutase, 45, 47

M_w
Molecular weight, 83

MWM
Morris water maze, 44

NFT
Neurofibrilary tangles, 31

NLRP3
NOD-, LRR- and pyrin domain-containing protein 3, 38

NPBL
Núcleo parabraquial lateral, 37, 38

NPs
Nanoparticles, 35, 36, 41, 75, 79, 80, 81, 82, 84, 85, 88, 89, 91, 92, 98, 99

OMS
Organização Mundial de Saúde, 34

OR
Object recognition, 44

PAG
Precursor recombinante da pranlintida, com um resíduo glicina adicionado a carbonila terminal, 39

PBS
Phosphate buffer saline, 47

PdI
Polydispersity index, 36, 82, 83, 84, 91, 92

PEs
Polieletrólitos, 52, 53

pH
Potencial hidrogeniônico, 35, 36, 38, 41, 52, 53, 56, 76, 77, 78, 79, 80, 82, 83, 89, 90, 91, 93, 99

PHF-1
PHD Finger Protein 1, 48

p-IR
Phosphorylated insulin receptor, 47

PLGA
Poli(ácido lático-co-ácido glicólico), 56
POMC
Pró-opiomelanocortina, 38

p-PI3K
fosfatidilinositol 3-quinase fosforilada, 47

Pram
Pranlintida, Pramlintide, 35, 36, 41, 44, 45, 73, 75, 76, 77, 78, 79, 80, 81, 82, 83, 84, 85, 86, 87, 88, 89, 90, 91, 92, 98, 99

Pro, P
Prolina, 38

PS
Presenelina, 43

PSD95
Postsynaptic density protein 95, 44, 48

p-tau
phosphorylated tau protein, 44, 47, 48

RAGE
receptor for advanced glication end-products, 32

RAMPs
Proteínas modificadoras da atividade de receptores, 37, 46

SAMP-8
Senescence-accelerated prone mouse, 44

Ser
Serina, 38

SH-SY5Y
Neuroblastoma cell line, 47

siRNA
Small interfering RNA, 46

SNAP-25
Synaptosomal-Associated Protein, 25kDa, 136

SPPS
Solid phase peptide synthesis, 39

TBARs
Thiobarbituric acid reactive substances, 47

TEM
Transmission electron microscopy, 35, 80, 85, 86

TFA
Trifluoroacetic acid, 36, 99

Tg2576
AD mouse model carries a mutant APP (APP695SWE) found in human familial AD and produces excess Aβ., 42, 44, 46

TgCRND8
Amyloid Precursor Protein Transgenic Mice Exhibit an Altered γ-Secretase Processing and an Aggressive, Additive Amyloid Pathology, 44

TGI
Trato gastrointestinal, 51

TgSwDI
Camundongo transgênico, modelo para angiopatia amiloide cerebral e DA, 43, 48, 131

TNF
Fator de necrose tumoral, 38

TPRV4
Transient receptor potential cation channel subfamily V member 4 is an ion channel protein, 38

LISTA DE SÍMBOLOS

[Q]
Molar concentration of suppressor agent, 81

ΔG
Standard Gibb's free energy, 81

D_h^{NP}
Diffusion coefficient of the nanoparticle, 79

F
fluorescence intensity in the presence of several concentrations of the quenching, 81

F_0
fluorescence intensity in the absence of the quenching, 81

k
Boltzmann constant, 79

Kq
Suppression rate constant, 81

K_{SV}
Stern–Volmer constant, 81

Ka
Constant of association, 81

R
Gas constant, 81

T
Absolute temperature, 79, 81

Γ
Relation frequency, 84

ΔH
Enthalpy change, 87

η
Viscosity, 79

λ
Wavelength, 78, 79

Γ
Relation frequency, 84

τ
Relaxation time, 81, 84

τ_0
Fluorophore half-life in the absence of suppressor, 81

SUMÁRIO

1 INTRODUÇÃO

Nas últimas décadas os avanços na biotecnologia impulsionaram a chegada ao mercado de muitas proteínas e peptídeos terapêuticos (PATEL; GAUDANA; MITRA, 2014). A administração de proteínas e peptídeos na conformação ativa representa um grande desafio para a indústria farmacêutica, apesar de serem moléculas muito potentes e com mecanismos de ação específicos. Propriedades físico-químicas e biológicas, como alto peso molecular, baixa permeabilidade no trato gastrointestinal, baixa estabilidade frente ao pH ácido do estômago e à ação de enzimas proteolíticas, entravam sua administração oral. Por outro lado, as vias parenterais injetáveis, comumente usadas na administração destes fármacos, são vias invasivas que podem levar à redução da adesão do paciente ao tratamento e aumentar os custos da terapia, especialmente quando o tratamento de doenças crônicas é requerido (ANDRADE *et al.*, 2011).

A pranlintida é um análogo da amilina humana, aprovado pelo FDA, para tratamento de pacientes com diabetes mellitus dos tipos 1 e 2, em combinação com a insulina (HAY *et al.*, 2015; YUAN *et al.*, 2017) e no tratamento da obesidade, com efeitos importantes principalmente em combinação com a metreleptina (RAVUSSIN *et al.*, 2009). Além da sua utilização no tratamento da diabetes, o uso da pranlintida tem sido alvo de estudos em diversos modelos da Doença de Alzheimer (DA) (ADLER *et al.*, 2014; MOHAMED *et al.*, 2017; WANG, ERMING *et al.*, 2017; ZHU, HAIHAO *et al.*, 2017; GAN *et al.*, 2019; PATRICK *et al.*, 2019; MOUSA *et al.*, 2020). Os resultados sugerem que este peptídeo age como um antagonista funcional do receptor da amilina, revertendo os efeitos deletérios da beta-amiloide, além de conduzir à melhora da memória e cognição tendo, portanto, um grande potencial de utilização no tratamento da DA (ADLER *et al.*, 2014; KIMURA *et al.*, 2017; ZHU, HAIHAO *et al.*, 2017). A DA e o diabetes são duas das epidemias mais prevalentes atualmente e afetam a qualidade e a expectativa de vida da população (SEN; CHAKRABORTY; DE, 2016; ARNOLD *et al.*, 2018).

Apesar dos interessantes resultados clínicos no tratamento do diabetes e obesidade e pré-clínicos, no tratamento do Alzheimer, as propriedades farmacocinéticas da pranlintida não são ideais: ela possui um curto tempo de meia-vida (cerca de aproximadamente 48 minutos) e uma rápida eliminação (2 h – 3 h após o término da infusão i.v.). Além disso, sua administração injetável (duas a três vezes ao dia) e o surgimento de náuseas representam inconvenientes para os pacientes (RUBIN; PEYROT, 2007). Mesmo com as diferenças estruturais em relação à amilina humana, que tornam a pranlintida mais solúvel, alguns trabalhos demonstraram que ela pode formar agregados amiloides em determinadas condições (DA SILVA *et al.*, 2016;

ŁOBODA; ROWIŃSKA-ŻYREK, 2017). Estratégias como peguilação (GUERREIRO *et al.*, 2013), glicosilação (TOMABECHI *et al.*, 2013; YULE *et al.*, 2016) ou modificações na estrutura da amilina (ou da pranlintida) (FRIGORI, 2017) para obtenção de um análogo com características melhoradas têm sido sugeridas.

O uso de sistemas nanotecnológicos constitui uma importante estratégia para aumentar a absorção de peptídeos terapêuticos por vias não-parenterais, contornando as limitações e aumentando a eficácia desses fármacos. As nanopartículas mais estudadas para a veiculação de fármacos (incluindo peptídeos) são as de composições polimérica e lipídica (JALLOUK *et al.*, 2015). Devido ao método de produção mais brando, os nanocomplexos, também chamados nanoplexos – complexos formados por interações eletrostáticas entre uma molécula carregada e um polieletrólito – tem se destacado para a veiculação de peptídeos terapêuticos (BERRILL *et al.*, 2011; WU, FU-GEN GEN *et al.*, 2016). Conforme relatado, a formação de complexos entre polieletrólitos pode modular a atividade e a estabilidade de peptídeos funcionais (GAO *et al.*, 2010; SHIMADA *et al.*, 2015).

Entre as vias de administração não-invasivas, a via nasal tem obtido maior sucesso para liberação sistêmica de peptídeos como, por exemplo, buserelina, oxitocina e calcitonina, disponíveis comercialmente na forma de sprays (CHONKAR; NAYAK; UDUPA, 2015). A permeabilidade relativamente elevada, a resposta imunogênica da mucosa, a abundante vascularização, que favorece um rápido início de ação, aliadas à aceitação pelos pacientes, tem impulsionado o interesse na utilização da via nasal para administração de fármacos com efeitos sistêmicos e de vacinas, como alternativa as vias oral e parenteral (KUMAR, AMRISH; PANDEY; JAIN, 2016). Além disso, a via nasal se destaca por possibilitar a veiculação direta de fármacos para o sistema nervoso central, pela presença de terminações nervosas olfatórias e trigeminais na cavidade nasal (CHONKAR; NAYAK; UDUPA, 2015). Por outro lado, a presença do mecanismo de depuração mucociliar limita o tempo de permanência da forma farmacêutica na mucosa, fazendo com que sejam necessárias estratégias para o aumento da retenção e absorção do fármaco através dela. Em especial, o uso de sistemas mucopenetrantes e/ou mucoadesivas permite aumentar a absorção e a eficácia desses fármacos (LAI; WANG; HASNES, 2009).

Considerando o exposto, o desenvolvimento de um nanocarreador para administração da pranlintida com base na sua interação com polieletrólitos, avaliação biofarmacêutica *in vitro* e farmacológica em modelo animal da Doença de Alzheimer foram articulados neste trabalho. A fim de atingir os objetivos concebidos, diferentes etapas foram estabelecidas e nortearam a

execução dos experimentos e redação de três manuscritos. Assim, o primeiro capítulo desta tese compreende o *Manuscrito 1* e descreve o desenvolvimento de nanopartículas de sulfato de dextrana/pranlintida e a avaliação das interações envolvidas na formação dos nanocomplexos. No segundo capítulo (*Manuscritos 2*) foi proposta uma nova estratégia para estabilização dos complexos de sulfato de dextrana/pranlintida por sua associação às gotículas de uma nanoemulsão, para administração nasal. A influência do sistema desenvolvido na difusão em gel fluido de mucina, estabilidade contra degradação enzimática e permeação da pranlintida em mucosa nasal suína foram avaliadas e reportadas. Finalmente, as propriedades neuroprotetoras e a potencial aplicação terapêutica da pranlintida associada ao nanocarreador para administração nasal, foram investigadas, e os resultados foram descritos no terceiro capítulo (*Manuscrito 3*) desta tese.

2 OBJETIVOS

2.1 OBJETIVO GERAL

Desenvolver um nanocarreador para a pranlintida que possibilite sua administração nasal, preservando sua estabilidade, tanto durante o armazenamento quanto em meio biológico, e avaliar a sua atividade neuroprotetora em modelo animal de Doença de Alzheimer, induzido pela injeção intracerebroventricular de oligômeros do peptídeo $A\beta_{1-42}$.

2.2 OBJETIVOS ESPECÍFICOS

- Desenvolver nanocarreadores baseados na complexação da pranlintida com o sulfato de dextrana;
- Caracterizar os nanocarreadores quanto tamanho, índice de polidispersão, potencial zeta, morfologia, teor e associação da pranlintida;
- Avaliar as interações supramoleculares envolvidas na formação do complexo sulfato de dextrana/pranlintida;
- Avaliar as características estruturais da pranlintida livre e no complexo sulfato de dextrana/pranlintida;
- Avaliar a estabilidade dos nanocarreadores em meios com diferentes forças iônicas;
- Investigar estratégias para estabilização de complexos polieletrólito/peptídeos em meio fisiológico;
- Avaliar as propriedades mucodifusivas dos nanocarreadores obtidos;
- Avaliar o perfil de permeação do peptídeo livre e associado a nanocarreadores em modelo bicompartimental de células de Franz usando mucosa nasal suína como membrana;
- Avaliar a atividade neutroprotetora da pranlintida livre e associada ao nanocarreador, após administração nasal, em modelo animal de Alzheimer.

3 REVISÃO DA LITERATURA

3.1 DOENÇA DE ALZHEIMER

A doença de Alzheimer (DA), caracterizada por perda irreversível de memória e cognição, é a principal causa de incapacitação e dependência entre pessoas idosas no mundo. Os tratamentos atualmente disponíveis para a DA são apenas sintomáticos e não previnem o avanço da doença. Mecanismos moleculares complexos estão envolvidos na fisiopatologia do Alzheimer, dificultando o estabelecimento da sua etiologia (DE LA TORRE *et al.*, 2018).

A deposição de proteína β-amiloide (Aβ) e a formação de emaranhados neurofibrilares (*NFT*, *neurofibrilary tangles*) (Figura 1), ricos em proteína tau associada a microtúbulos e placas neuríticas, são considerados biomarcadores da DA, mas sua correlação com aparecimento dos sintomas cognitivos ainda não é completamente compreendida. O diagnóstico precoce é dificultado pelo aparecimento insidioso dos sintomas cognitivos, que ocorre apenas em estágios tardios, quando os danos e morte celular já são extensos. Fatores genômicos, como impressão genética hereditária, mecanismos oxidativos e mecanismos envolvendo a Apolipoproteína E têm sido relacionados com o aparecimento dos biomarcadores da DA e com o processo neurodegenerativo, contribuindo para a disfunção do circuito neural e a afetando a conectividade entre as redes de neurônios. Devido à deposição amiloide em pequenos vasos cerebrais, muitos dos indivíduos com DA tem angiopatia cerebral (Figura 1) (CANTER; PENNEY; TSAI, 2016; DOS SANTOS PICANCO *et al.*, 2018). A diminuição da neurogênese em pacientes com DA, comparados a indivíduos saudáveis da mesma faixa etária, é provavelmente causada pelo estresse oxidativo crônico e contribui para o agravamento e irreversibilidade da DA (POLIS; SAMSON, 2021).

A DA apresenta vários subtipos, com diferentes fenótipos clínicos, níveis de comprometimento e prognóstico. Menos comum do que a DA de início tardio, também existem a DA autossômica dominante, que corresponde a cerca de 1% dos casos, além de outros tipos de DA de início precoce. A DA autossômica dominante, ou familiar é causada por mutações em genes que codificam a proteína amiloide precursora (*APP*), presenelina-1 e presenelina-2. A coexistência de doenças sistêmicas, como cardiopatias, diabetes, corpos de Lewy e isquemia cerebral influenciam o curso da DA de modo desconhecido. Os testes clínicos para novos medicamentos geralmente desconsideram a heterogeneidade da DA, o que impede o desenvolvimento de medicamentos mais efetivos (DEVI; SCHELTENS, 2018; NIKOLAC PERKOVIC; PIVAC, 2019).

Figura 1 – Seção do córtex temporal marcada com Thioflavina S, uma sonda fluorescente, mostrando placas amiloides, emaranhados neurofibrilares e amiloide cerebrovascular.

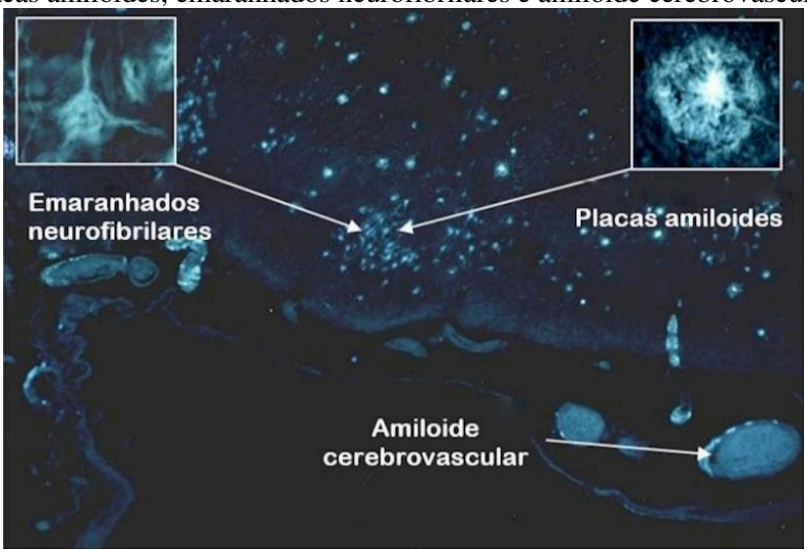

Insertos destacam placa amiloide (superior esquerdo) e emaranhados neurofibrilares (superior direito), ambos em maior magnificação. Fonte: Adaptado de ALLEN-BIRT (2017).

Com o avanço da DA ocorre diminuição geral do cérebro, especialmente do hipocampo e do lobo temporal, onde giros se tornam mais finos, enquanto sulcos mais espessos (Figura 2). Danos em rotas neurotransmissoras podem causar sintomas como depressão, agressão e disfunção de memória. O sistema cortical glutamatérgico e as projeções serotoninérgicas do núcleo dorsal da rafe, noradrenérgicas do locus coerulos e colinérgicas do núcleo basal, são particularmente vulneráveis. Pode ocorrer extensa gliose, com produção de astrócitos hipertróficos com fibras nas placas neuríticas e elevada expressão da proteína ácida glial fibrilar (*GFAP, glial fibrillary acid protein*), além de aumento das células microgliais na matéria cinzenta, nas placas neuríticas e nos emaranhados neurofibrilares, com maior expressão de antígenos MHC (*major histocompatibility complex*) de classe 2, receptores do complemento e receptores de produtos finais da glicação avançada (*RAGE, receptor for advanced glication end-products*), os quais se ligam prontamente a Aβ, mediando seus efeitos. O terceiro ventrículo e o ventrículo lateral podem aumentar, devido à extensa perda celular. As áreas motora, sensorial e visual primária são geralmente poupadas até os estágios mais tardios (ALLEN-BIRT, 2017).

Figura 2 – Placas amiloides e emaranhados neurofibrilares distribuídos no cérebro com progresso do Alzheimer.

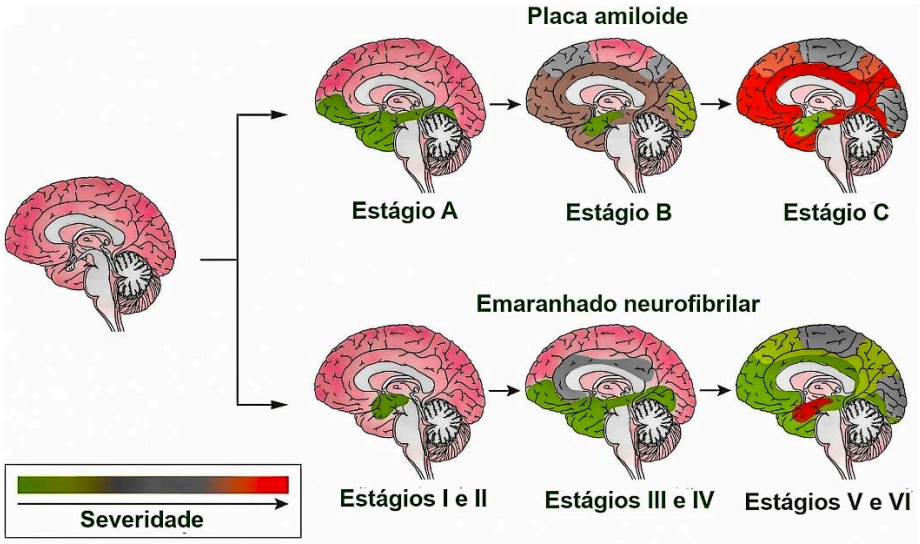

Deposição de Aβ (estágios A, B e C) e os emaranhados neurofibrilares (estágios I-VI). A deposição de Aβ comumente precede as alterações neurofibrilares e neuríticas com uma origem aparente nos lobos frontal e temporal, hipocampo e sistema límbico (linha superior). Mais raramente, a doença parece emergir de outras regiões do neocortex (lobos parietal e occipital) com comprometimento relativo do hipocampo. Os emaranhados neurofibrilares e a degeneração neurítica começam no lobo temporal medial e hipocampo e progressivamente se espalham para outras áreas do neocortex (linha inferior). Fonte: Adaptado de MASTERS *et al.* (2015).

Avanços na compreensão de como as funções cerebrais são perturbadas na DA e avanços tecnológicos que melhorem a liberação cerebral de fármacos são necessários para obtenção de um tratamento efetivo para o Alzheimer. Nesse contexto, o uso de nanocarreadores tem se revelado promissor para facilitar a transposição de fármacos e agentes diagnósticos através da barreira hematoencefálica (DE LA TORRE *et al.*, 2018).

3.3 AMILINA

A desregulação de vias biológicas ativadas por peptídeos pode causar várias doenças, instigando a descoberta e desenvolvimento clínico de fármacos peptídicos. Muitos peptídeos endógenos ativam receptores acoplados a proteína G (GPCRs), e cerca de 50 deste foram aprovados para uso clínico até o momento, com aplicação principalmente no tratamento de doenças metabólicas e oncológicas. Os GPCRs são agrupados em famílias, com base em seus ligantes: calcitonina, fator de liberação da corticotrofina, glucagon, hormônio da paratireoide, peptídeo intestinal vasoativo ou peptídeo ativador da adenilato ciclase, incluindo também alguns peptídeos órfãos. Os peptídeos endógenos que se ligam aos GPCRs na superfície das

células abrangem espaço temporalmente a sinalização parácrina e autócrina de hormônios com ação de longa duração a mediadores de funções celulares liberados localmente e neurotransmissores (DAVENPORT et al., 2020).

A amilina é um hormônio neuroendócrino peptídico, formado por 37 aminoácidos, produzido pelas células β-pancreáticas e secretado com a insulina, o qual ativa GPCRs específicos, formados por receptores de calcitonina $CalcR_{\alpha}$ e $CalcR_{\beta}$ heterodimerizados com proteínas modificadoras da atividade de receptores (RAMPs 1, 2 e 3), gerando seis tipos de receptores ($Amy_R\alpha$ e $Amy_R\beta$, 1 - 3), e exerce efeitos em diversos órgãos e sistemas, atuando principalmente na regulação da glicemia e do metabolismo energético. Em uma quantidade muito menor, a amilina também é produzida por células de regiões discretas do cérebro (neurônios do núcleo medial pré-óptico, área medial pré-óptica, múltiplos núcleos do hipotálamo, núcleo arqueado do hipotálamo e área postrema, AP), o que é estimulado pela leptina e aumentado em lactantes. O principal local de ligação da amilina periférica é a AP, que propaga o sinal para o núcleo do trato solitário e para o núcleo parabraquial lateral (NPBL), que é então transmitido para regiões do prosoencéfalo como a amígdala central e núcleo leito da estria terminal. A ativação dessas diferentes regiões cerebrais pela amilina medeia a alimentação e outras vias metabólicas, controlando o gasto energético e a homeostase da glicose. A amilina periférica também pode se ligar no núcleo arqueado do hipotálamo, onde atua independentemente da área postrema, ativando neurônios que expressam pró-opiomelanocortina (POMC), afetando o balanço energético e a atividade locomotora, e neurônios que expressam o neuropeptídeo Y, com transmissão sequencial para o NPBL e ação na alimentação, ativação de neurônios da área tegmental ventral e a via de recompensa dopaminérgica (BOCCIA; LE FOLL; LUTZ, 2020).

Baixas concentrações de amilina e pranlintida causam um aumento sutil dos níveis intracelulares de cálcio, mediado pelos receptores Amy_R. Enquanto isso, elevadas concentrações de amilina, que formam agregados invaginantes nas membranas celulares, conduzem a uma resposta muito maior do cálcio, mediada por um canal de cátions não seletivo, o receptor TPRV4, podendo resultar em morte celular pela sobrecarga dos mecanismos regulatórios do cálcio. Além disso, estudos em roedores mostraram que oligômeros de amilina humana estimulam a secreção de citocinas pró-inflamatórias (TNF-α, IL-6, IL-8, IL-1β e proteínas inflamatórias de macrófagos 1-α e 1-β), enquanto diminuem a secreção de citocinas anti-inflamatórias (IL-10) por macrófagos da medula óssea e ativam o inflamossoma NLRP3,

que participa na conversão de agregados pré-fibrilares em amiloides, levando a ruptura dos lisossomos (SERVIZI; CORRIGAN; CASADESUS, 2020).

3.4 PRANLINTIDA

A pranlintida (Figura 3) é um análogo da amilina humana, aprovado pelo FDA em 2005 para tratamento de pacientes com DM dos tipos 1 e 2, em combinação com a insulina. A substituição dos aminoácidos alanina na posição 25 (Ala25) e serinas nas posições 28 e 29 (Ser28 e Ser29) por prolinas faz com que a pranlintida se assemelhe a amilina murina, com menor potencial amiloidogênico. A prolina (Pro) é um aminoácido que desfavorece o enovelamento peptídico em β-folha, relacionado a formação de fibrilas amiloides (WANG, HUI *et al.*, 2015). A pranlintida auxilia a absorção da glicose, diminuindo velocidade de esvaziamento gástrico, promovendo a saciedade pela interação com receptores hipotalâmicos e diminuindo a secreção pós-prandial de glucagon (HAY *et al.*, 2015; YUAN *et al.*, 2017).

O acetato de pranlintida é um pó branco, solúvel em água, com fórmula $C_{171}H_{267}N_{51}O_{53}S_2$ e peso molecular de 3949,4 $g.mol^{-1}$. Nos países onde seu uso clínico é aprovado, a pranlintida é disponibilizada comercialmente na forma de canetas para injeção, contendo as doses de 60 μg (*SymlinPen* 60) ou 120 μg (*SymlinPen* 120), que substituíram as ampolas simples em solução límpida, estéril e isotônica, com pH 4,0 (TRAINA; KANE, 2011; YOUNK; MIKELADZE; DAVIS, 2011).

A pranlintida é obtida principalmente por síntese química em fase sólida (*solid phase peptide synthesis*, SPPS) (KHAZAEI-POUL *et al.*, 2020). A formação da ligação dissulfeto ocorre através da oxidação dos aminoácidos contendo enxofre, e é uma etapa crítica da síntese. O uso de nanopartículas de sílica com complexos de platina (Pt IV) como oxidantes de fase sólida reutilizáveis já foi avaliado para uma série de peptídeos, incluindo a pranlintida (HOU *et al.*, 2017). A expressão em organismos procarióticos (ex. *Escherichia coli*), tradicionalmente utilizada na engenharia genética, geralmente não possibilita modificações pós-translacionais, como a amidação da carbonila terminal, e a utilização de sistemas eucarióticos capazes de realizar essa modificação *in vivo* não é custo-efetiva. A síntese de um precursor recombinante da pranlintida, com um resíduo glicina adicionado a carbonila terminal (PAG), já foi proposta, considerando que a enzima mono-oxigenase α-amidadora é abundante nos tecidos humanos e animais. O PAG desempenhou a mesma atividade *in vivo* que a pranlintida em modelo de

esvaziamento gástrico (HU *et al.*, 2014). A produção da pranlintida recombinante (*r*-Pranlintida) em *E. colli* em meio quimicamente definido, com reposição de aminoácidos foi recentemente estudada. O organismo hospedeiro (*E. colli* BL21 D3) foi utilizado para expressão de um multímero de *r*-Pranlintida de 13,57 kDa, como um corpo de inclusão. O gene da pranlintida foi clonado em um vetor expresso em *E. colli*, entre pontos de restrição com uma *tag* C-terminal 6×His, o que levou a diminuição do estresse celular e aumento de produtividade (KUMAR, JASHWANT *et al.*, 2020).

Figura 3 – (a) Sequência de aminoácidos e (b) estrutura química da pranlintida.

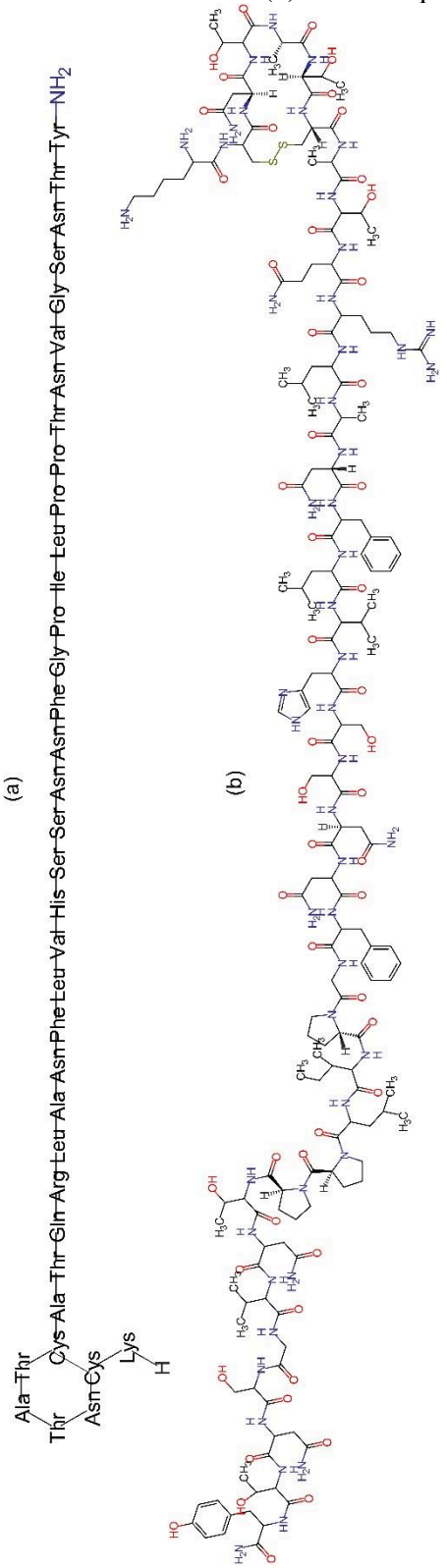

Fonte: (a) Elaborada pela autora, utilizando o software Marvin Sketch (b) ChemSpider.

A utilização da pranlintida é recomendada para pacientes diabéticos, que mesmo com o ajuste da terapia com insulina não atingiram um controle glicêmico satisfatório, (YUAN *et al.*, 2017). Apesar de ser geralmente bem tolerada e proporcionar uma elevada satisfação terapêutica no tratamento do DM, as propriedades farmacocinéticas da pranlintida não são ideais. Ela apresenta um curto tempo de meia-vida (c.a. 48 minutos) e uma rápida eliminação (2 h – 3 h após o término da infusão i.v.). Além disso, sua forma comercial deve ser administrada duas a três vezes ao dia por via subcutânea, não podendo ser associada à insulina, devido a incompatibilidades relacionadas ao pH das formulações. Esta forma de administração, juntamente com o efeito de indução de náuseas, representam inconvenientes para os pacientes (RUBIN; PEYROT, 2007). Mesmo com as diferenças estruturais em relação à amilina humana, alguns trabalhos têm demonstrado que a pranlintida ainda pode formar agregados amiloides em determinadas condições (DA SILVA *et al.*, 2016; ŁOBODA; ROWIŃSKA-ŻYREK, 2017). Estratégias como peguilação (GUERREIRO *et al.*, 2013), glicosilação (TOMABECHI *et al.*, 2013; YULE *et al.*, 2016) ou modificações na estrutura da amilina e da pranlintida para obtenção de um análogo com características melhoradas (FRIGORI, 2017; ALVES; DIAS; FRIGORI, 2019) ou para possibilitar a associação com a insulina (SINÉSIA *et al.*, 2019; MAIKAWA *et al.*, 2020) têm sido sugeridas.

Além de ser utilizada no tratamento de DM, estudos clínicos e pré-clínicos vêm demonstrando a potencialidade do uso da pranlintida no tratamento de obesidade, principalmente em combinação com a metreleptina, prevenção e tratamento de danos cardiovasculares em diabéticos, tumores sólidos e Alzheimer (Quadro 1).

Quadro 1 – Avaliação clínica e pré-clínica do acetato de pranlintida .

Doença ou condição	Tipo de estudo	Referências
DM1	Estudos clínicos e estudos de utilização pós-comercialização	(LEE, NANCY J.; NORRIS; THAKURTA, 2010; SINGH-FRANCO; PEREZ; HARRINGTON, 2011; HERRMANN *et al.*, 2014; QIAO *et al.*, 2017)
DM2	Estudos clínicos e estudos de utilização pós-comercialização	(LEE, NANCY J.; NORRIS; THAKURTA, 2010; SINGH-FRANCO; PEREZ; HARRINGTON, 2011; HERRMANN *et al.*, 2014).
Obesidade	Estudos clínicos	(ARONNE *et al.*, 2007; SMITH *et al.*, 2008; RAVUSSIN *et al.*, 2009; TAM; LECOULTRE; RAVUSSIN, 2011)
Danos cardiovasculares associados ao DM	Estudos pré-clínicos *in vitro* e *in vivo*	(LIU, XIAOYONG *et al.*, 2020; SAFAEIAN *et al.*, 2020)
Tumores sólidos	Estudos pré-clínicos *in vitro* e *in vivo*	(VENKATANARAYAN *et al.*, 2015; AL-KEILANI *et al.*, 2018)
Alzheimer	Estudos pré-clínicos *in vitro* e *in vivo*	(ADLER *et al.*, 2014; ZHU, H. *et al.*, 2015; KIMURA *et al.*, 2017; MOHAMED *et al.*, 2017; PATRICK *et al.*, 2019; MOUSA *et al.*, 2020).

Fonte: elaborado pela autora.

Os efeitos da amilina e da pranlintida na DA (Quadro 2) têm sido avaliados em diversos modelos *in vitro, in vivo e ex-vivo*. Entre os modelos animais utilizados nos estudos *in vivo*, o SAMP-8 tem senescência acelerada, aumento espontâneo dos níveis de *APP*, placas de Aβ no cérebro e déficit cognitivo aos 8-9 meses de idade (MORLEY, 2002). Os demais camundongos transgênicos têm mutações na *APP*, entre outras. O início e gravidade dos sintomas cognitivos, formação de placas e emaranhados amiloides, gliose (proliferação e hipertrofia das células gliais), perdas em sinapses, neurônios e plasticidade sináptica variam entre as linhagens. O 5xFAD, com 5 mutações, apresenta placas de Aβ aos 1,5 meses, gliose aos 2 meses, déficit cognitivo aos 4-5 meses e perda neuronal e sináptica aos 9 meses. O 3xTgAD, com 3 mutações, tem déficit cognitivo aos 4 meses, placas de Aβ e perda na plasticidade sináptica aos 6 meses, gliose aos 7 meses e emaranhados neurofibrilares no cérebro aos 12 meses. O Tg2576, com 2 mutações, tem perda nas sinapses e na plasticidade sináptica aos 4,5-5 meses, perda na cognição aos 6 meses, formação de placas de Aβ aos 7 meses e gliose aos 10 meses. O TgCRND8, com 2 mutações, tem déficit cognitivo e placas de Aβ evidentes

aos 3 meses, perda nas sinapses e na plasticidade sináptica entre 6-12 meses e fenótipo moderado a agressivo de DA aos 7 meses. O APP/PS1 têm 2 mutações, déficit cognitivo e sináptico aos 3 meses, placas de Aβ e gliose aos 6 meses e perda neuronal aos 22 meses. O TgSwDI tem 2 mutações, acúmulo vascular de Aβ no cérebro (angiopatia) e alterações cognitivas aos 3 meses (LEE, JEONG HYUN; BACSKAI; AYATA, 2012; AMRAM; FRENKEL, 2017).

Quadro 2 – Estudos avaliando o tratamento com pranlintida (Pram) ou amilina (Amy) em vários modelos de doença de Alzheimer em roedores.

Autores/ Ano	**Espécie/ modelo animal**	**Idade no início do protocolo/ Gênero**	**Dose/ via/ duração**	**Avaliações**	**Respostas**
(ADLER *et al.*, 2014)	SAMP-8 (senescência acelerada)	6m, ambos	Pram, 240 µg/kg/dia; i.p., 5 semanas	Reconhecimento de objeto (OR), marcadores sinápticos, de estresse oxidativo e de inflamação	Melhorou a performance dos animais no teste de OR; ↑sinaptofisina e CDK5, ↓HO-1 e COX-2 no hipocampo
(ZHU *et al.*, 2017); (WANG *et al.*, 2017)	5xFAD (APP/PS1 Tg); Apresenta depósitos de amiloide desde 1,5m e déficit cognitivo desde os 4m	3,5m; fêmeas	Amy, i.p., 200 µg/kg/dia, 10 semanas	MWM, Y-*maze,* (labirinto em Y), *p*-tau, Iba-1, CD68, Aβ (FCE, cérebro, soro)	Melhorou a performance nos testes de MWM e Y-*maze* e ↓marcadores da DA (estresse oxidativo e inflamação)
(GAN *et al.*, 2019)		4m, fêmeas	Amy, i.p., 200, 400 e 800 µg/kg/dia, 6 semanas	MWM, Aβ cerebral, marcadores sinápticos	Melhorou a performance de memória (em doses baixas e altas), melhorou o aprendizado (tanto em doses altas como baixas), ↓*p*-tau e depósitos amiloides (perfil dose-resposta em *U*); ↑PSD95 (apenas na menor dose).
(ZHU *et al.*, 2017)	3xTgAD (APP/tau/PS1 Tg); Apresenta emaranhados neurofibrilares a partir de 6 – 12m	9m, fêmeas	Amy, i.p.; 200 µg/kg/ dia, 10 semanas	Y-*maze*, *f*-tau, Iba-1, CD68, IL-1β, Aβ (FCE, cérebro, soro)	↑alternação no Y-*maze*, ↓tauopatia cerebral e marcadores relacionados a DA
(MOHAMED *et al.*, 2017)	Tg2576 (APP Tg); Apresenta emaranhados neurofibrilares a partir dos 7m	9m, fêmeas	Amy, i.p.; 200 µg/kg, dose única	Níveis Aβ no soro	↑Aβ no soro, como demonstrado *in vivo,* em consequência da ↓Aβ no cérebro, o que foi demonstrado em modelo *in vitro* de BHE
(KIMURA *et al.*, 2017)	TgCRND8 (APP Tg); Placas de Aβ e déficit cognitivo a partir dos 3m, perda na plasticidade sináptica e perda nas sinapses a partir dos 12m	10m e 12m, ambos	Pram, 1mg perfundido no cérebro dos animais	Potenciação do hipocampo de longa duração	↑níveis basais de potenciação do hipocampo de longa duração

Quadro 2 – Estudos avaliando o tratamento com pranlintida (Pram) ou amilina (Amy) em vários modelos de doença de Alzheimer em roedores (cont.).

Autores/ Ano	Espécie/ modelo animal	Idade no início do protocolo/ Gênero	Dose/ via/ duração	Avaliações	Respostas
(PATRICK *et al.*, 2019)	APP/PS1 (APP Tg) Déficits cognitivos e sinápticos a partir dos 3m e placas de Aβ a partir dos 6m	5,5m (antes da evolução da doença), ambos	Pram, 6µg/dia administrado por bomba osmótica; 18 semanas	MWM e marcadores do estresse oxidativo, enzimas que clivam a APP	Melhorou a performance no MWM; ↓Aβ cerebral, ↑enzimas antioxidantes no hipocampo (HO-1, ↑GP-x, MnSOD); ↑ADAM-10 no hipocampo e córtex e ↑BACE-1 e no hipocampo

Fonte: elaborado pela autora.

Com o objetivo de investigar os mecanismos envolvidos nos efeitos da amilina no cérebro, a pranlintida foi administrada em camundongos SAMP8 na dose de 0,24 µg/kg/dia, por 5 semanas, por via subcutânea. Neste estudo, a pranlintida melhorou o desempenho dos animais, no teste do reconhecimento objeto, um teste que avalia memória e cognição. Os animais tratados com pranlintida apresentaram o aumento da expressão do marcador sináptico sinapsina I e a da quinase-5 dependente de ciclina (CDK5) no hipocampo, bem como a redução dos marcadores do estresse oxidativo e inflamação. O aumento na CDK5 e ativação das quinases 1/2 reguladas por sinal extracelular (ERK1/2), após tratamento da pranlintida, em estudos *in vitro,* indicou a funcionalidade do receptor da amilina (Amy_R) nos neurônios. Os resultados mostraram que a pranlintida exibe propriedades neuroprotetoras e pode ser benéfica para o tratamento da DA (ADLER *et al.*, 2014).

Zhu e colaboradores (2017) propuseram que o acúmulo da Aβ no cérebro de indivíduos com DA poderia competir com a amilina pelo Amy_R. Os autores avaliaram se a administração periférica de peptídeos análogos da amilina poderia levar a uma competição com a Aβ e assim reduzir a cascata patológica da DA. Neste estudo, os autores verificaram que o tratamento com amilina humana por 10 semanas em camundongos 5xFAD e 3xTgAD, reduziu significativamente diferentes marcadores associados à DA, incluindo os níveis de tau fosforilada na fração insolúvel, os dois marcadores inflamatórios Iba1 (molécula adaptadora de ligação ao cálcio ionizado-1) e CD68 (proteína altamente expressa por monócitos), e a Aβ cerebral. O tratamento com a amilina também levou a melhorias no aprendizado e memória. Os autores mostraram que a administração do antagonista do receptor da amilina AC253 bloqueou alguns dos efeitos protetores da amilina *in vivo*, sugerindo que o efeito protetor da amilina requer a interação com o receptor cognato. Os autores sugeriram que a amilina suprime

a ativação da rota CDK5 pela Aβ, reduzindo dramaticamente os níveis da p25, que corresponde ao produto da clivagem da p35 (subunidade regulatória neuronal específica, requerida para ativação da CDK5) e causa ativação aberrante da CDK5 e aumento da fosforilação de substratos patológicos – com correspondente redução da fosforilação da tau. Considerando estes resultados, os autores sugeriram que o uso clínico do análogo da amilina, a pranlintida, poderia ser útil no tratamento da DA e de outras doenças neurodegenerativas.

Em outro estudo, o tratamento com amilina durante 10 semanas, por via intraperitoneal, segundo o mesmo protocolo descrito por Zhu *et al.* (2015), reduziu os níveis de marcadores inflamatórios CD68 e Iba1 em camundongos 5xFAD, por interação com receptores cognatos de amilina. Já o silenciamento dos receptores de amilina bloqueou esse efeito. O tratamento restaurou a expressão de vários genes no córtex dos animais, incluindo CD68 e ATP5b (que codifica a enzima mitocondrial subunidade β de ATP-sintase F1), relacionados respectivamente, a pró-inflamação, transporte vesicular e a função mitocondrial, e envolvidos na cascata do Alzheimer. Os autores concluíram que a amilina atua amplamente na cascata do Alzheimer e apontam seus derivados como potenciais alternativas para o tratamento da doença (WANG, ERMING *et al.*, 2017).

Uma única injeção de amilina (200 µg/kg) já foi suficiente para elevar os níveis plasmáticos de Aβ em camundongos fêmeos Tg2576. Esse efeito foi abolido pela ação de um antagonista do receptor de amilina (AC253). Em modelo celular de barreira hematoencefálica (BHE) antagonistas de amilina e siRNA do receptor de amilina RAMP3 aboliram a ação da amilina no transporte da Aβ. Um modelo celular de BHE com expressão de transportadores da Aβ foi utilizado para investigar o mecanismo desta ação. As células tratadas com amilina expressaram o LRP1 (proteína-1 relacionada ao receptor de lipoproteína de baixa densidade), um transportador envolvido no efluxo da Aβ na membrana, sugerindo sua translocação a partir do citoplasma, o que ao menos parcialmente explica o aumento dos níveis plasmáticos de Aβ identificado *in vivo*, pelo efluxo da BHE para o sangue (MOHAMED *et al.*, 2017).

Como demonstrado por Kimura *et al.* (2017), o pré-tratamento com pranlintida (250 nM, ou 1 mg) reverteu o efeito depressor da amilina na potenciação de sinapses de longa duração, em fatias do hipocampo de camundongos 129/SvEv, sem afetar a transmissão basal dela. Além disso, em camundongos TgCRND8 (derivados congênitos dos camundongos 129/SvEv), foi detectado menor atividade de potenciação de longa duração no hipocampo, e a administração de pranlintida causou o aumento dos níveis basais dela. Os autores sugeriram

que a pranlintida atua como um antagonista funcional da amilina, revertendo os efeitos tóxicos da $A\beta_{1-42}$ e da amilina (KIMURA *et al.*, 2017).

Nassar, Badae e Issa (2020) induziram o modelo DA pela injeção intracerebroventricular de estreptozotocina em ratos albinos machos. Esses animais foram tratados com pranlintida (200 µg/kg/dia) ou metformina (30 mg/kg/dia) por 5 semanas e apresentaram aumento da sinalização da insulina, comparados ao grupo controle, tratado com tampão fosfato salino (PBS). A expressão de receptor de insulina fosforilado (*p-IR*) e fosfatidilinositol 3-quinase fosforilada (*p-PI3K*) aumentou nesses animais, o que levou à redução da glicose no fluido cerebrospinal e da expressão de proteína tau fosforilada (*p-tau*) e Aβ no hipocampo. Além disso, os animais tratados com pranlintida, mas não os animais tratados com metformina, mostraram melhor desempenho nos testes de reconhecimento de objeto e labirinto aquático de Morris comparados ao controle. Os autores sugeriram que a amilina (ou a pranlintida) melhora o aprendizado e a memória por outro mecanismo específico além da ressensibilização à insulina.

Camundongos de linhagem transgênica *APP/PS1*, com 5,5 meses (antes do aparecimento dos sinais de DA), foram tratados com pranlintida na dose de 6 µg/dia, por 18 semanas. O objetivo dos pesquisadores (PATRICK *et al.*, 2019) foi verificar o papel do estresse oxidativo nos efeitos da pranlintida em modelos de DA. Nos testes realizados, os camundongos tratados tiveram melhor desempenho no labirinto aquático de Morris e menor acúmulo de Aβ no hipocampo. Os níveis de enzimas que clivam a proteína precursora amiloide (*APP*) foram avaliados no córtex e no hipocampo dos animais tratados. Ocorreu aumento da α-secretase (*ADAM 10*) no córtex e no hipocampo e β-secretase (*BACE-1*), no hipocampo, mas não no córtex. Os marcadores de estresse oxidativo alteraram de modo complexo com o tratamento, nas duas regiões cerebrais avaliadas (*teste t* para amostras independentes, $p < 0,05$). No córtex houve redução da heme-oxigenase (HO-1), enquanto os demais marcadores não alteraram significativamente (glutationa peroxidase, GP-x; manganês superóxido dismutase, MnSOD), apesar da GP-x ter mostrado uma tendência ao aumento ($p = 0,07$) e no hipocampo houve aumento de todos os marcadores (HO-1, GP-x e MnSOD). Em modelo de cultura de células neuronais (SH-SY5Y, diferenciadas com ácido retinóico) a pranlintida reduziu de forma dose-dependente a produção de marcadores do estresse oxidativo endógena induzida por peróxido de hidrogênio e a peroxidação lipídica, nos ensaios da diclorofluoresceína, (DCF) e de espécies reativas do ácido tiobarbitúrico, (*TBARs*). Os autores concluíram que os efeitos da pranlintida

na cognição e memória podem envolver suas propriedades antioxidantes (PATRICK *et al.*, 2019).

Gan *et al.* (2019) demonstraram em cultura primária de células de neurônios corticais de roedores que o tratamento unicamente com amilina em concentrações elevadas (~10 µM) causou taupatia, detectada por microscopia de fluorescência após incubação dos neurônios com o anticorpo contra *p-tau*, PHF-1. Nas células neuronais tratadas com $A\beta_{1-42}$ o tratamento com amilina (ou pranlintida ~5 nM) reduziu a proteína *p-tau* e a perda sináptica em regiões da cultura celular de co-localização da PSD95 e da sinaptofisina, em perfil de dose *U*, aumentou a expressão de PSD95, porém não de sinaptofisina e reverteu o encurtamento das neurites causado pela $A\beta_{1-42,}$ em perfil de dose *U* invertido. Nos camundongos 5xFAD (fêmeas, 4 meses) o tratamento com amilina intraperitoneal (200, 400 e 800 µg/kg/dia, por 6 semanas) diminuiu a *p*-tau e os depósitos de Aβ no córtex, em perfil de dose *U*, e aumentou a expressão de PSD95 na menor dose, corroborando com os resultados obtidos *in vitro*. No labirinto aquático de Morris, os animais treinaram a memória referencial, durante 10 dias (4 tentativas por dia), com a inserção de uma plataforma oculta em um dos quadrantes da piscina, e a latência para o escape foi monitorada. Na última tentativa do 10° dia a plataforma foi removida e o nado dos animais foi observado por 60 s. Os animais tratados com ambas as doses de amilina (200 vs. 800 µg/kg/dia) demonstraram melhora no aspecto de memória em relação ao controle (tratado com PBS), mas apenas os tratados com a menor dose demonstraram melhora no aspecto cognitivo. Os autores concluíram que a amilina em concentrações fisiológicas possui efeito neuroprotetor, porém a elevação das concentrações de ambas, amilina e Aβ, pode contribuir para a patogênese da DA.

Em um recente estudo, o efeito da amilina e da pranlintida sobre a patogênese da Aβ foi investigado em camundongos TgSwDI. Os estudos mostraram que a administração intraperitoneal de amilina ou pranlintida, na dose de 200 µg/kg/dia, durante 30 dias, aumentou a carga de Aβ no cérebro. Ambos os peptídeos alteraram a rota amiloidogênica e aumentaram a produção de Aβ pela modulação da *APP* e dos níveis de □-secretase nos microdomínios de lipídios (*lipid rafts*). Adicionalmente, ambos peptídeos aumentaram os níveis da enzima β-1,4 galactosaminil transferase-1 (B4GALNT1, envolvida na biossíntese de gangliosídeos complexos) e do gangliosídeo GM1, enquanto unicamente a pranlintida aumentou os níveis do gangliosídeo GM2, os quais atuam na regulação de proteínas da rota amiloidogênica. No teste do labirinto aquático de Morris, o tratamento com amilina ou pranlintida não conduziu a

alterações significativas nos parâmetros avaliados, sugerindo que não alteram a função de memória. Com estes resultados, os autores sugeriram que o uso clínico da pranlintida no tratamento da DM poderia aumentar o risco de desenvolvimento da Doença de Alzheimer (MOUSA *et al.*, 2020).

3.5 VIA NASAL PARA ADMINISTRAÇÃO DE FÁRMACOS PEPTÍDICOS

Os primeiros medicamentos peptídicos aprovados para uso clínico, a partir da década de 1920, foram a insulina, o hormônio tireoidiano e o fator VII. O desenvolvimento de técnicas de biologia molecular na década de 1960 permitiu a substituição de processos de extração e purificação de proteínas de tecidos animais ou humanos pela sua síntese por técnicas recombinantes em nível do gene (VAN DER WALLE; OLEJNIK, 2011). A partir de então, peptídeos e proteínas vêm se tornando uma classe muito importante de agentes terapêuticos e em um futuro próximo podem vir a substituir muitos medicamentos baseados em moléculas orgânicas atualmente disponíveis (SACHDEVA, 2017). No entanto, os fármacos peptídicos representam desafios para a indústria farmacêutica, devido ao alto custo e maior tempo de produção em comparação com moléculas menores, a baixa biodisponibilidade oral, o rápido metabolismo e, em alguns casos, a imunogenicidade (EDWARDS; LAPLANTE, 2011). A produção de medicamentos comerciais baseados em peptídeos ou proteínas recombinantes exige ainda um controle rigoroso dos processos de fermentação, cultura celular e purificação, além de proteção da proteína contra várias fontes de instabilidade coloidal ou conformacional e degradação, e posterior caracterização, envolvendo ferramentas analíticas complexas. Vários processos ou condições de armazenamento podem levar a agregação de moléculas peptídicas. Os agregados podem possuir atividade farmacológica menor ou ausente, e elevadas imunogenicidade e citotoxicidade (WANG, WEI; ROBERTS, 2010).

A maioria dos fármacos peptídicos são administrados por vias parenterais (intramuscular ou subcutânea), e a necessidade de múltiplas injeções diárias, devido ao curto tempo de meia-vida desses fármacos, dificulta a adesão dos pacientes ao tratamento e pode causar dor, reações alérgicas, infecções e danos aos nervos (SARMENTO; FERREIRA; VASCONCELOS, 2009; LAKSHMI; KUMAR, 2010). Apesar de a administração oral ser mais confortável e conveniente, os peptídeos terapêuticos geralmente apresentam instabilidade e baixa permeação no trato gastrointestinal, resultando em baixa biodisponibilidade (WANG, JIEMIN *et al.*, 2020).

No passado a via nasal era utilizada restritamente para administração de medicamentos para o tratamento tópico ou de doenças locais, como gripe e hipersensibilidade. Porém, a permeabilidade relativamente elevada, a resposta imunogênica da mucosa, a abundante vascularização, que favorece um rápido início de ação, aliadas à aceitação pelos pacientes impulsionaram o interesse na utilização da via nasal para administração de fármacos com efeitos sistêmicos e de vacinas, como alternativa às vias oral e parenteral (CHONKAR; NAYAK; UDUPA, 2015).

A via nasal se destaca por oportunizar a veiculação de fármacos para o sistema nervoso central, pela presença de terminações nervosas olfatórias e trigeminais na cavidade (YUBA; KONO, 2014). A mucosa nasal humana possui uma área superficial de cerca de 150 cm^2 e é formada por quatro regiões com características anátomo-histológicas distintas: vestíbulo e átrio, recobertos por células epiteliais, escamosas estratificadas e não-ciliadas de transição; região respiratória, recoberta por epitélio respiratório pseudoestratificado (células colunares, células basais e células de globet) e região olfatória, que apresenta células epiteliais ciliadas pseudoestratificadas especializadas, interespaçadas por terminações neuronais (Figura 4) (YUBA; KONO, 2014; CHONKAR; NAYAK; UDUPA, 2015).

A região anterior, formada pelo vestíbulo e pelo átrio não possui características atrativas para administração de fármacos, pois possui vibrissas (pelos nasais, responsáveis por filtrar o ar inalado), pequena área superficial, pobre vascularização e baixa permeabilidade. A maior parte da cavidade nasal, representada pela região respiratória, possui área superficial elevada pela presença de estruturas chamadas cornetos e por microvilosidades que recobrem as células colunares da região apical; alta permeabilidade e rica vascularização; que a tornam interessante para administração/liberação de fármacos. As células colunares da região posterior da cavidade nasal apresentam cílios (estruturas semelhantes à pelos), que se movimentam. A fina camada de muco (cerca de 5 μm de espessura) que recobre as células epiteliais é transportada em direção a nasofaringe pelo movimento mucociliar, o que auxilia na remoção de substâncias estranhas da mucosa nasal superior. A região olfatória, localizada na porção superior da cavidade nasal, apesar de apresentar uma pequena área, desperta interesse para liberação de fármacos devido a possibilidade única de veiculação para o sistema nervoso central (THWALA; PRÉAT; CSABA, 2017).

Figura 4 – Possíveis rotas de distribuição de fármacos administrados pela via nasal.

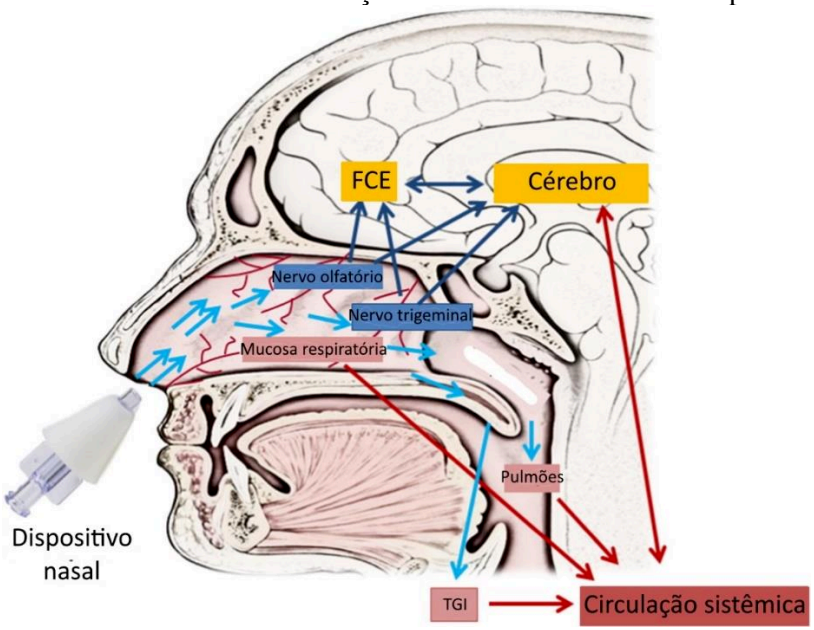

O fármaco (azul claro) pode se distribuir para o cérebro diretamente pelas vias neuronais olfatória e trigêmea (azul escuro) ou indiretamente pela circulação sistêmica (vermelho). TGI: trato gastrointestinal, FCE: fluido cerebrospinal. Fonte: KAPOOR; CLOYD; SIEGEL (2016).

Assim como em outras mucosas, a penetração de fármacos na barreira epitelial ocorre por vias transcelular (através das células epiteliais, por difusão passiva, transporte mediado por carreador ou endocitose) e paracelular (entre as células adjacentes, por difusão passiva ou carreados pelo solvente), porém a mucosa nasal é comparativamente mais fina e porosa do que as demais. A via transcelular é utilizada no transporte de moléculas hidrofóbicas, de moléculas grandes (com peso molecular acima de 1 kDa) por endocitose e de moléculas transportadas, por carreadores como transportadores de cátions e de aminoácidos. Já a via paracelular está principalmente envolvida no transporte de moléculas polares pequenas, por poros hidrofílicos ou pelas junções intercelulares. As moléculas pequenas e hidrofílicas são absorvidas pela mucosa nasal em um fluxo quase comparável a administração intravenosa, já as moléculas grandes têm sua absorção limitada pela barreira epitelial (WHATELEY, 2002; CHONKAR; NAYAK; UDUPA, 2015). Apesar disso, a mucosa nasal se destaca entre as vias de administração não invasivas, obtendo maior sucesso para liberação sistêmica de peptídeos como, por exemplo, buserelina, oxitocina e calcitonina, disponíveis comercialmente na forma de sprays (WHATELEY, 2002; YUBA; KONO, 2014).

Por outro lado, a via nasal não é isenta de limitações. A formulação pode sofrer rápida drenagem em direção a nasofaringe, promovida pela depuração mucociliar. Além disso, fármacos peptídicos podem interagir com a mucina, sendo retidos na camada de muco, ou degradados por enzimas proteolíticas, presentes na cavidade nasal, mesmo em menor

quantidade do que no trato gastrointestinal. O pequeno volume de administração tolerado, de cerca de 200 – 300 μL por narina, limita a utilização da via nasal para ação sistêmica de fármacos potentes. Finalmente, a biodisponibilidade é influenciada por condições patológicas comuns, como resfriados e gripes, e muitas substâncias podem causar irritação ou sensibilização da mucosa nasal, devido à fragilidade do seu epitélio (JALLOUK *et al.*, 2015).

3.6 NANOPARTÍCULAS DE POLIELETRÓLITOS PARA VEICULAÇÃO DE PEPTÍDEOS

São denominados "nanomedicamentos" formulações constituídas por estruturas nanométricas que permitem melhorar as propriedade biofarmacêuticas, farmacocinéticas e terapêuticas dos fármacos (JALLOUK *et al.*, 2015). As nanopartículas mais estudadas para a veiculação de fármacos, incluindo peptídeos, são as de composições polimérica e lipídica (FRÈRE; DANICHER; MULLER, 2013). O uso de sistemas nanotecnológicos constitui uma estratégia para aumentar a absorção de peptídeos terapêuticos por vias não invasivas, contornando as limitações e aumentando a eficácia desses fármacos (BOBO *et al.*, 2016). Uma revisão sobre o uso de sistemas nanotecnológicos para liberação nasal de peptídeos é apresentada no Apêndice A.

Sistemas nanoestruturados compostos por polissacarídeos são considerados interessantes para a veiculação de peptídeos terapêuticos, devido a abundância de grupos funcionais presentes nos polissacarídeos que são capazes de interagir com peptídeos, aliadas à outras propriedades das nanopartículas poliméricas. Além disso, características dos polissacarídeos, como capacidade de vetorização ativa e propriedades mucoadesivas, podem ser exploradas no desenvolvimento dos nanocarreadores (ZHANG, LIN *et al.*, 2017; BADWAIK *et al.*, 2018; WANG, KAILI; LIU; MO, 2020).

A complexação de polieletrólitos (PEs) com cargas opostas pode originar várias estruturas como complexos hidrossolúveis, complexos coloidais, precipitados amorfos, coacervados etc., dependendo do mecanismo de formação guiado pela difusão entre as cadeias e das características dos PEs envolvidos (peso molecular, flexibilidade das cadeias, densidade eletrônica etc.), do meio (pH, força iônica etc.) e do padrão de mistura. A formação de nanopartículas de polieletrólitos, que envolvem duas ou mais espécies multivalentes, também chamadas de nanopartículas de PEs, complexos de PEs ou nanocomplexos, ocorre basicamente em três etapas: (I) formação do complexo primário, guiada por interações eletrostáticas; (II)

rearranjo do complexo primário, incluindo ligações de hidrogênio, que pode levar à ocorrência de mudanças conformacionais nas cadeias dos PEs; (III) agregação dos complexos secundários, por interações hidrofóbicas, formando várias estruturas como agregados emaranhados, fibrilas, redes ordenadas, entre outros (ZHAO; SKWARCZYNSKI; TOTH, 2019; WU, DANJUN *et al.*, 2020).

O método mais utilizado para preparação de nanopartículas envolvendo peptídeos e proteínas terapêuticas e PEs solúveis é a titulação coloidal (titulação de PEs ou complexação de PEs), no qual a solução de uma das espécies de PE é adicionada lentamente à solução da outra espécie com carga oposta, sob agitação. A complexação eletrostática de PEs naturais ou sintéticos pode levar a obtenção de nanogéis, que são estruturas tridimensionais capazes de absorver elevadas quantidades de água ou intumescer, sem se dissolverem (SANT *et al.*, 2017; MAURI; PERALE; ROSSI, 2018). Além disso, copolímeros formados por blocos neutro e poli-iônico podem ser utilizados para a produção de nanopartículas do tipo micela, que também têm sido frequentemente propostas para associação de peptídeos e proteínas terapêuticas (MARRAS; VIEREGG; TIRRELL, 2019).

Outros métodos para obtenção de nanopartículas de PEs incluem a auto-complexação ou deposição em camadas sob partícula sólida (ou superfície) carregada, que leva à formação de nanopartículas de PEs multicamadas, a mistura a jato na qual os PEs são misturados confinados em um misturador de modo rápido (em tempos com duração de milissegundos) e a geleificação iônica, na qual um reticulador iônico é adicionado a uma solução ou mistura de PEs (BOURGANIS *et al.*, 2017).

As nanopartículas de polieletrólitos são reconhecidas por proporcionar uma maior associação de peptídeos terapêuticos em comparação aos outros tipos de nanopartículas, além de serem geralmente obtidas por condições brandas que são favoráveis para a preservação da estabilidade das (bio)macromoléculas. Por outro lado, em meios biológicos essas nanopartículas, formadas principalmente por interações eletrostáticas, apresentam elevada sensibilidade às variações na força iônica e no pH, podendo ocasionar a liberação imediata dos fármacos associados. Dessa forma, as propriedades biológicas diferenciadas atribuídas à nano-escala, incluindo a liberação controlada, a interação com membranas e a capacidade de veiculação, são precocemente perdidas. Para contornar esse problema o uso de tensoativos, reticuladores ou um terceiro polieletrólito são estratégias frequentemente propostas na literatura (SANTALICES *et al.*, 2017).

Alguns estudos encontrados na literatura que propõe o desenvolvimento de nanopartículas de polieletrólitos para associação de peptídeos são apresentados no *Quadro 3*.

Quadro 3 – Estudos envolvendo a preparação de nanopartículas do tipo polieletrólito/peptídeo para veiculação de peptídeos/proteínas terapêuticas descritos na literatura .

Peptídeo/polieletrólito, denominação empregada	Proposta do estudo	Autores, ano
Calcitonina de salmão/gliol quitosana conjugada ao ácido taurocólico/sulfato de dextrana, nanocomplexo ternário	Aumentar a biodisponibilidade oral da calcitonina	(SUN, LILONG *et al.*, 2020)
Insulina/quitosana/Dz13Scr, coacervado	Aumentar a biodisponibilidade oral da insulina	(WONG *et al.*, 2020)
Octreotide/quitosana/heparina, complexo de polieletrólitos	Contornar o curto tempo de meia vida e a baixa estabilidade do octreotide pelo desenvolvimento de nanopartículas de heparina peguiladas	(GHOFRANI *et al.*, 2019)
Nisina/sulfato de condroitina, nanogel auto-organizado	Proteção da nisina contra a degradação proteolítica, controle da liberação	(MOHTASHAMIAN; BODDOHI; HOSSEINKHANI, 2018)
Insulina/goma tragacanto, (nano)hidrogel	Obtenção de uma formulação para administração oral para tratamento do diabetes	(NUR; VASILJEVIC, 2018)
Polimixina B/poliestirenosulfonato de sódio, complexo de polieletrólitos	Avaliação da influência do tamanho da cadeia do PE na atividade antimicrobiana e estabilidade das nanopartículas	(INSUA *et al.*, 2017)
Calcitonina de salmão/sulfato de condroitina, nanoplexos	Produção e caracterização de nanopartículas para a veiculação da calcitonina	(UMERSKA; CORRIGAN; TAJBER, 2017)
Tigapotide/PVBTMAC-POEGMA, nanocomplexo de polieletrólitos	Obtenção de uma formulação com liberação modificada e propriedadese biológicas melhoradas	(PIPPA *et al.*, 2017)
α-galactosidase (GLA) /quitosana, nanocomplexo de polieletrólitos	Vetorização da GLA, proteína ausente na doença de Fabry, pela funcionalização das nanopartículas com o peptídeo RGD	(GIANNOTTI *et al.*, 2016)
Insulina/QNPHOSEO, nanocomplexo de polieletrólitos do tipo micela	Controle da liberação da insulina e melhora das propriedades farmacocinéticas.	(PIPPA *et al.*, 2015)

Fonte: elaborado pela autora.

Nanopartículas multicomponentes foram desenvolvidas por Lopes *et al.* (2016) para aumentar a biodisponibilidade oral da insulina, com fase interna inicialmente composta por

insulina, sulfato de dextrana, alginato e carbonato de cálcio, formando uma emulsão água em óleo pelo uso dos surfactantes monooleato de sorbitana e poloxamer 188. A diminuição do pH pela adição de ácido acético levou a formação de estruturas tipo caixa de ovo, correspondentes ao gel de cálcio/alginato. Além do cálcio incialmente presente, cloreto de cálcio, quitosana e polietilenoglicol e, sequencialmente albumina foram adicionados gota a gota, formando um revestimento duplo de quitosana e albumina nas nanopartículas.

A complexação com polieletrólitos pode ser uma forma de proteção e modulação da associação e liberação de proteínas e peptídeos em sistemas híbridos, protegendo as proteínas da desnaturação e mudanças estruturais que poderiam ocorrer pelo seu contato com a interface óleo/água (MCCLEMENTS, 2018). A formação de complexo insolúvel liofilizado de octreotida com sulfato de dextrana foi utilizada para aumentar a afinidade do peptídeo pela fase orgânica, na obtenção de microesferas poliméricas por emulsificação múltipla sólido-em-óleo-em-água (LIU, JIWEI *et al.*, 2019). Nanopartículas poliméricas contendo complexos de sulfato de dextrana/albumina (GAUDANA *et al.*, 2011) e sulfato de dextrana/IgG Fab (PATEL; GAUDANA; MITRA, 2014) foram obtidas por este mesmo método.

A adsorção de polieletrólitos nas gotículas de uma emulsão pode ocorrer em nível molecular, originando sistemas revestidos mono- ou multicamadas de composição homogênea ou heterogênea (LI, MOTING *et al.*, 2020). Surfactantes lipofílicos podem ser utilizados para estabilização de peptídeos/proteínas nas gotículas de óleo, na forma de micelas reversas, através de emulsificação múltipla. A emulsificação água-em-óleo-em-água foi utilizada para a obtenção de micro- e nanoemulsões de insulina revestidas com quitosana e quitosana e alginato, respectivamente (LI, XIAOYANG *et al.*, 2012; FAGHMOUS *et al.*, 2020), além de microesferas de PLGA contendo complexos de sulfato de condroitina/insulina (JUNG; NA, 2011). Nanocomplexos formados por biopolímeros, como proteínas e polissacarídeos, podem atuar como estabilizantes interfaciais, originando emulsões de Pickering biocompatíveis (WHITBY, 2019). Emulsões de Pickering com interfaces funcionalizadas compostas por conjugados de ácido gálico-ovotransferrina (antioxidante e aporte proteico) complexados com a carboximetil-dextrana, e por lisozima (antimicrobiana) complexada com ácido γ-glutamico modificado com dopamina (AAPG-DA) foram propostas para aplicações na área alimentícia e farmacêutica (WEI; ZHANG; HUANG, 2019; ZHANG, CUIGE *et al.*, 2020).

REFERÊNCIAS

ABHILASH, M.; AUGUSTINE, R. Diabetes and Health Care: an Overview. In: GEORGE, A.; AUGUSTINE, R.; SEBASTIAN, M. (Ed.). **Diabetes Mellitus and Human Health Care: A holistic approach to diagnosis and treatment**. Oakville: CRC Press, 2014. p. 273–314.

ADLER, B. L. *et al.* Neuroprotective Effects of the Amylin Analogue Pramlintide on Alzheimer's Disease Pathogenesis and Cognition. **Neurobiology of Aging**, v. 35, n. 4, p. 793–801, Apr. 2014.

AL-KEILANI, M. S. *et al.* Pramlintide, an Antidiabetic, Is Antineoplastic in Colorectal Cancer and Synergizes with Conventional Chemotherapy. **Clinical pharmacology : advances and applications**, v. 10, p. 23–29, Mar. 2018.

ALLEN-BIRT, S. Pathophysiology of Alzheimer's disease. In: WALDEMAR, G.; BURNS, A. (Ed.). **Alzheimer's Disease**. 2. ed. Oxford: Oxford University Press, 2017. p. 7–15.

ALVES, N. A.; DIAS, L. G.; FRIGORI, R. B. Synergistic Long-Range Effects of Mutations Underlie Aggregation Propensities of Amylin Analogues. **Journal of Molecular Modeling**, v. 25, n. 9, p. 263, Sep. 2019.

AMRAM, S.; FRENKEL, D. Animal Models of Alzheimer's Disease. In: GOZES, I. (Ed.). **Neuroprotection in Alzheimer's Disease**. London: Elsevier Inc., 2017. p. 31–58.

ANDRADE, F. *et al.* Chitosan Formulations as Carriers for Therapeutic Proteins. **Current Drug Discovery Technologies**, v. 8, n. 3, p. 157–172, Aug. 2011.

AREOSA SASTRE, A. *et al.* Effect of the treatment of Type 2 diabetes mellitus on the development of cognitive impairment and dementia. **Cochrane Database of Systematic Reviews,** n. 6, p. 1-60, 2017.

ARNOLD, S. E. *et al.* Brain Insulin Resistance in Type 2 Diabetes and Alzheimer Disease: Concepts and Conundrums. **Nature Reviews Neurology**, v. 14, n. 3, p. 168–181, Jan. 2018.

ARONNE, L. *et al.* Progressive Reduction in Body Weight after Treatment with the Amylin Analog Pramlintide in Obese Subjects: A Phase 2, Randomized, Placebo-Controlled, Dose-Escalation Study. **Journal of Clinical Endocrinology and Metabolism**, v. 92, n. 8, p. 2977–2983, 2007.

AVILA-VAZQUEZ, M. F.; ALTAMIRANO-BUSTAMANTE, N. F.; ALTAMIRANO-BUSTAMANTE, M. M. Amyloid Biomarkers in Conformational Diseases at Face Value: A Systematic Review. **Molecules**, v. 23, n. 1, p. 79, Dec. 2018.

BADWAIK, H. R. *et al.* Oral Delivery of Proteins and Polypeptides through Polysaccharide Nanocarriers. In: KUMAR, G. T.; BIJAYA, G. (Ed.). **Polysaccharide-based Nano-Biocarrier in Drug Delivery**. Boca Raton: CRC Press, 2018. p. 1–24.

BERRILL, A.; BIDDLECOMBE, J.; BRACEWELL, D. Product Quality During Manufacture

and Supply. In: VAN DER WALLE, C. F. (Ed.). **Peptide and Protein Delivery**. London: Academic Press, 2011. p. 313–339.

BOBO, D. *et al.* Nanoparticle-Based Medicines: A Review of FDA-Approved Materials and Clinical Trials to Date. **Pharmaceutical Research**, v. 33, n. 10, p. 2373–2387, Oct. 2016.

BOCCIA, L.; LE FOLL, C.; LUTZ, T. A. Noradrenaline Signaling in the LPBN Mediates Amylin's and Salmon Calcitonin's Hypophagic Effect in Male Rats. **The FASEB Journal**, v. 34, n. 11, p. 15448–15461, Nov. 2020.

BOURGANIS, V. *et al.* Polyelectrolyte complexes as prospective carriers for the oral delivery of protein therapeutics. **European Journal of Pharmaceutics and Biopharmaceutics**, v. 111, p. 44-60, Feb. 2017.

BRAGA, R. R. *et al.* Molecular Confinement of Human Amylin in Lipidic Nanoparticles. **Journal of Liposome Research**, v. 26, n. 3, p. 188–198, 2016.

CANTER, R. G.; PENNEY, J.; TSAI, L.-H. The Road to Restoring Neural Circuits for the Treatment of Alzheimer's Disease. **Nature**, v. 539, n. 7628, p. 187–196, Nov. 2016.

CHONKAR, A.; NAYAK, U.; UDUPA, N. Smart Polymers in Nasal Drug Delivery. **Indian journal of pharmaceutical sciences**, v. 77, n. 4, p. 367–375, 2015.

DA SILVA, D. C. *et al.* Amyloidogenesis of the Amylin Analogue Pramlintide. **Biophysical Chemistry**, v. 219, p. 1–8, Dec. 2016.

DE LA TORRE, C. *et al.* The Delivery Challenge in Neurodegenerative Disorders: The Nanoparticles Role in Alzheimer's Disease Therapeutics and Diagnostics. **Pharmaceutics**, v. 10, n. 4, p. 190, Oct. 2018.

DEVI, G.; SCHELTENS, P. Heterogeneity of Alzheimer's Disease: Consequence for Drug Trials? **Alzheimer's Research and Therapy**, v. 10, n. 1, p. 122, Dec. 2018.

DOS SANTOS PICANCO, L. C. *et al.* Alzheimer's Disease: A Review from the Pathophysiology to Diagnosis, New Perspectives for Pharmacological Treatment. **Current Medicinal Chemistry**, v. 25, n. 26, p. 3141–3159, Sep. 2018.

EDWARDS, P. J.; LAPLANTE, S. R. Peptides as Leads for Drug Discovery. In: CASTANHO, M.; SANTOS, N. (Ed.). **Peptide Drug Discovery and Development: Translational Research in Academia and Industry**. Wheinhein: Wiley, 2011. p. 1–55.

FAGHMOUS, N. *et al.* Optimization of Chitosan-Coated W/O/W Multiple Emulsion Stabilized with Span 80 and Tween 80 Using Box–Behnken Design. **Journal of Dispersion Science and Technology**, p. 1–13, 2020.

FRÈRE, Y.; DANICHER, L.; MULLER, S. Peptide Nanostructured Conjugates for Therapeutics: The Example of P140 Peptide for the Treatment of Systemic Lupus Erythematosus. In: ALEMÁN, C.; BIANCO, A.; VENANZI, M. (Ed.). **Peptide Materials: From Nanostructures to Applications**. Chinchester: John Wiley & Sons, 2013. p. 385–415.

FRIGORI, R. B. Be Positive: Optimizing Pramlintide from Microcanonical Analysis of Amylin Isoforms. **Physical Chemistry Chemical Physics**, v. 19, n. 37, p. 25617–25633, Sep. 2017.

GAN, Q. *et al.* Effects of Amylin Against Amyloid-β-Induced Tauopathy and Synapse Loss in Primary Neurons. **Journal of Alzheimer's Disease**, v. 70, n. 4, p. 1–16, Aug. 2019.

GAO *et al.* Sustained and Extended Release with Structural and Activity Recovery of Lysozyme from Complexes with Sodium (Sulfamate Carboxylate) Isoprene/Ethylene Oxide Block Copolymer. **Macromolecular Bioscience**, v. 10, n. 2, p. 139–146, 2010.

GAUDANA, R. *et al.* Encapsulation of Protein-Polysaccharide HIP Complex in Polymeric Nanoparticles. **Journal of Drug Delivery**, v. 2011, p. 1–7, 2011.

GHOFRANI, M. *et al.* Development of Octreotide-Loaded Chitosan and Heparin Nanoparticles: Evaluation of Surface Modification Effect on Physicochemical Properties and Macrophage Uptake. **Journal of Pharmaceutical Sciences**, v. 108, n. 9, p. 3036–3045, 1 Sep. 2019.

GIANNOTTI, M. I. I. *et al.* Highly Versatile Polyelectrolyte Complexes for Improving the Enzyme Replacement Therapy of Lysosomal Storage Disorders. **ACS Applied Materials and Interfaces**, v. 8, n. 39, p. 25741–25752, Oct. 2016.

GUERREIRO, L. H. *et al.* Polymeric Particles for the Controlled Release of Human Amylin. **Colloids and Surfaces B: Biointerfaces**, v. 94, p. 101–106, 2012.

GUERREIRO, L. H. *et al.* Preparation and Characterization of PEGylated Amylin. **AAPS PharmSciTech**, v. 14, n. 3, p. 1083–1097, Sep. 2013.

HAY, D. L. *et al.* Amylin: Pharmacology, Physiology, and Clinical Potential. **Pharmacological Reviews**, v. 67, n. 3, p. 564–600, 2015.

HERRMANN, K. *et al.* Effects of Pramlintide in Patients with Type 2 Diabetes Mellitus: An Analysis Using Daily Insulin Dose Tertiles. **Endocrine Practice**, v. 20, n. 10, p. 1070–1075, 2014.

HOU, X. *et al.* Synthesis of Reusable Silica Nanosphere-Supported Pt(IV) Complex for Formation of Disulfide Bonds in Peptides. **Molecules**, v. 22, n. 2, p. 338, Feb. 2017.

HU, H. *et al.* Expression, Purification, and Biological Activity of the Recombinant Pramlintide Precursor. **Applied Microbiology and Biotechnology**, v. 98, n. 18, p. 7837–7844, Apr. 2014.

INSUA, I. *et al.* Polymyxin B Containing Polyion Complex (PIC) Nanoparticles: Improving the Antimicrobial Activity by Tailoring the Degree of Polymerisation of the Inert Component. **Scientific Reports**, v. 7, n. 1, p. 9396, Dec. 2017.

JALLOUK, A. P. *et al.* Modifications of Natural Peptides for Nanoparticle and Drug Design. **Advances in Protein Chemistry and Structural Biology**, v. 98, p. 57–91, 2015.

JUNG, Y.-S.; NA, K. Protein Delivery System Based on Various Polysaccharides. **Journal of**

Pharmaceutical Investigation, v. 41, n. 4, p. 197–204, Aug. 2011.

KAPOOR, M.; CLOYD, J. C.; SIEGEL, R. A. A Review of Intranasal Formulations for the Treatment of Seizure Emergencies. **Journal of Controlled Release**, v. 237, p. 147–159, Sep. 2016.

KHAZAEI-POUL, Y. *et al.* Monocyclic Peptides: Types, Synthesis and Applications. **Current Pharmaceutical Biotechnology**, v. 21, Jan. 2020.

KIMURA, R. *et al.* Pramlintide Antagonizes Beta Amyloid (Aβ)- and Human Amylin-Induced Depression of Hippocampal Long-Term Potentiation. **Molecular Neurobiology**, v. 54, n. 1, p. 748–754, 2017.

KUMAR, A.; PANDEY, A. N.; JAIN, S. K. Nasal-Nanotechnology: Revolution for Efficient Therapeutics Delivery. **Drug Delivery**, v. 23, n. 3, p. 681–693, 2016.

KUMAR, J. *et al.* Amino Acid Supplementation for Enhancing Recombinant Protein Production in *E. Coli*. **Biotechnology and Bioengineering**, v. 117, n. 8, p. 2420–2433, Aug. 2020a.

KUMAR, P. *et al.* Neurotransmitters and Their Receptors—State of the Art. In: **Frontiers in Pharmacology of Neurotransmitters**. Singapore: Springer, 2020b. p. 1–29.

LAI, S. K.; WANG, Y. Y.; HASNES, J. Mucus-Penetrating Nanoparticles for Drug and Gene Delivery to Mucosal Tissues. **Advanced Drug Delivery Reviews**, v. 61, n. 2, p. 158–171, Feb. 2009.

LAKSHMI, P.; KUMAR, G. A. Nanosuspension Technology: A Review. **International Journal of Pharmacy and Pharmaceutical Sciences**, v. 2, n. SUPPL. 4, p. 35–40, 2010.

LEE, J. H.; BACSKAI, B. J.; AYATA, C. Genetic animal models of cerebral vasculopathies. In: CONN, P. M. (Ed.). **Progress in Molecular Biology and Translational Science**. London: Elsevier, 2012. 105p. 25–55.

LEE, N. J.; NORRIS, S. L.; THAKURTA, S. Efficacy and Harms of the Hypoglycemic Agent Pramlintide in Diabetes Mellitus. **Annals of Family Medicine**, v. 8, n. 6, p. 542–549, 2010.

LI, M. *et al.* Design Principles of Oil-in-Water Emulsions with Functionalized Interfaces: Mixed, Multilayer, and Covalent Complex Structures. **Comprehensive Reviews in Food Science and Food Safety**, v. 19, n. 6, p. 3159–3190, Nov. 2020.

LI, X. *et al.* Nanoemulsions Coated with Alginate/Chitosan as Oral Insulin Delivery Systems: Preparation, Characterization, and Hypoglycemic Effect in Rats. **International Journal of Nanomedicine**, v. 8, n. 8, p. 23–32, Dec. 2012.

LIU, J. *et al.* A Modified Hydrophobic Ion-Pairing Complex Strategy for Long-Term Peptide Delivery with High Drug Encapsulation and Reduced Burst Release from PLGA Microspheres. **European Journal of Pharmaceutics and Biopharmaceutics**, v. 144, p. 217–229, Nov. 2019.

LIU, X. *et al.* Involvement of Amylin B-H2S-Connexin 43 Signaling Pathway in Vascular Dysfunction and Enhanced Ischemia–Reperfusion-Induced Myocardial Injury in Diabetic Rats. **Bioscience Reports**, v. 40, n. 6, Jun. 2020.

ŁOBODA, D.; ROWIŃSKA-ŻYREK, M. Zn(II) - Pramlintide: Stability, Binding Sites and Unexpected Aggregation. **Journal of Inorganic Biochemistry**, v. 174, p. 150–155, Sep. 2017.

MAGLIANO, D. J.; ZIMMET, P.; SHAW, J. E. Classification of Diabetes Mellitus and Other Categories of Glucose Intolerance. **International Textbook of Diabetes Mellitus**, p. 1–16, 2015.

MAIKAWA, C. L. *et al.* A Co-Formulation of Supramolecularly Stabilized Insulin and Pramlintide Enhances Mealtime Glucagon Suppression in Diabetic Pigs. **Nature Biomedical Engineering**, v. 4, n. 5, p. 507–517, May 2020.

MARRAS, A.; VIEREGG, J.; TIRRELL, M. Assembly and Characterization of Polyelectrolyte Complex Micelles. **Journal of Visualized Experiments**, v. 157, Dec. 2020.

MASTERS, C. L. *et al.* Alzheimer's Disease. **Nature Reviews Disease Primers**, v. 1, n. 1, p. 1–18, Oct. 2015.

MAURI, E.; PERALE, G.; ROSSI, F. Nanogel Functionalization: A Versatile Approach to Meet the Challenges of Drug and Gene Delivery. **ACS Applied Nano Materials**, v. 1, n. 12, p. 6525–6541, Dec. 2018.

MCCLEMENTS, D. J. Encapsulation, Protection, and Delivery of Bioactive Proteins and Peptides Using Nanoparticle and Microparticle Systems: A Review. **Advances in Colloid and Interface Science**, v. 253, p. 1–22, Mar. 2018.

MOHAMED, L. A. *et al.* Amylin Enhances Amyloid-β Peptide Brain to Blood Efflux Across the Blood-Brain Barrier. **Journal of Alzheimer's Disease**, v. 56, n. 3, p. 1087–1099, Jan. 2017.

MOHTASHAMIAN, S.; BODDOHI, S.; HOSSEINKHANI, S. Preparation and Optimization of Self-Assembled Chondroitin Sulfate-Nisin Nanogel Based on Quality by Design Concept. **International Journal of Biological Macromolecules**, v. 107, p. 2730–2739, Feb. 2018.

MORLEY, J. E. The SAMP8 Mouse: A Model of Alzheimer Disease? **Biogerontology**, v. 3, n. 1–2, p. 57–60, 2002.

MOUSA, Y. M. *et al.* Amylin and Pramlintide Modulate γ-Secretase Level and APP Processing in Lipid Rafts. **Scientific Reports**, v. 10, n. 1, p. 1–14, Dec. 2020.

NIKOLAC PERKOVIC, M.; PIVAC, N. Genetic Markers of Alzheimer's Disease. In: **Advances in Experimental Medicine and Biology**. New York: Springer, 2019. 1192p. 27–52.

NUR, M.; VASILJEVIC, T. Insulin Inclusion into a Tragacanth Hydrogel: An Oral Delivery System for Insulin. **Materials**, v. 11, n. 1, p. 79, Jan. 2018.

PATEL, A.; GAUDANA, R.; MITRA, A. K. A Novel Approach for Antibody Nanocarriers Development through Hydrophobic Ion-Pairing Complexation. **Journal of Microencapsulation**, v. 31, n. 6, p. 542–550, 2014.

PATRICK, S. *et al.* Neuroprotective Effects of the Amylin Analog, Pramlintide, on Alzheimer's Disease Are Associated with Oxidative Stress Regulation Mechanisms. **Journal of Alzheimer's Disease**, v. 69, n. 1, p. 1–12, Apr. 2019.

PIPPA, N. *et al.* Complexation of Cationic-Neutral Block Polyelectrolyte with Insulin and in Vitro Release Studies. **International Journal of Pharmaceutics**, v. 491, n. 1–2, p. 136–143, 2015.

PIPPA, N. *et al.* Preparation and Physicochemical Characterization of Polyelectrolyte Complexes Incorporating Antitumor Peptide. **Journal of Nanoscience and Nanotechnology**, v. 17, n. 7, p. 4901–4906, Jul. 2017.

POLIS, B.; SAMSON, A. Neurogenesis versus Neurodegeneration: The Broken Balance in Alzheimer's Disease. **Neural Regeneration Research**, v. 16, n. 3, p. 496, Mar. 2021.

PONCE-LÓPEZ, T. *et al.* Diabetes Mellitus and Amyloid Beta Protein Pathology in Dementia. In: KUROUSKI, D. (Ed.). **Amyloid Diseases**. London: IntechOpen, 2019.

QIAO, Y.-C. *et al.* Efficacy and Safety of Pramlintide Injection Adjunct to Insulin Therapy in Patients with Type 1 Diabetes Mellitus: A Systematic Review and Meta-Analysis. **Oncotarget**, v. 8, n. 39, p. 66504–66515, Sep. 2017.

RAVUSSIN, E. *et al.* Enhanced Weight Loss With Pramlintide/Metreleptin: An Integrated Neurohormonal Approach to Obesity Pharmacotherapy. **Obesity**, v. 17, n. 9, p. 1736–1743, Sep. 2009.

RIDDLE, M. C. Basal Glucose Can Be Controlled, but the Prandial Problem Persistsdit's Thenext Target. **Diabetes Care**, v. 40, n. 3, p. 291–300, 2017.

RUBIN, R. R.; PEYROT, M. Assessing Treatment Satisfaction in Patients Treated with Pramlintide as an Adjunct to Insulin Therapy. **Current Medical Research and Opinion**, v. 23, n. 8, p. 1919–1929, 2007.

SACHDEVA, S. Peptides as 'Drugs': The Journey so Far. **International Journal of Peptide Research and Therapeutics**, v. 23, n. 1, p. 49–60, 2017.

SAFAEIAN, L. *et al.* The Effect of Pramlintide, an Antidiabetic Amylin Analogue, on Angiogenesis-Related Markers in Vitro. **Research in Pharmaceutical Sciences**, v. 15, n. 4, p. 323, Aug. 2020.

SANT, S. *et al.* Self-Assembled Hydrogel Fiber Bundles from Oppositely Charged Polyelectrolytes Mimic Micro-/Nanoscale Hierarchy of Collagen. **Advanced Functional Materials**, v. 27, n. 36, p. 1606273, Sep. 2017.

SANTALICES, I. *et al.* Advances on the Formulation of Proteins Using Nanotechnologies.

Journal of Drug Delivery Science and Technology, v. 42, p. 155–180, Dec. 2017.

SARMENTO, B.; FERREIRA, D.; VASCONCELOS, T. Polymer-Based Delivery Systems for Oral Delivery of Peptides and Proteins. **Delivery technologies for biopharmaceuticals: peptides, proteins, nucleic acids and vaccines.**, p. 207–226, 2009.

SEN, S.; CHAKRABORTY, R.; DE, B. Diabetes Mellitus: General Consideration. In: SEN, S.; CHAKRABORTY, R.; DE, B. (Ed.). **Diabetes Mellitus in 21st Century**. New York: Springer, 2016. p. 13–22.

SERVIZI, S.; CORRIGAN, R. R.; CASADESUS, G. The Importance of Understanding Amylin Signaling Mechanisms for Therapeutic Development in the Treatment of Alzheimer's Disease. **Current Pharmaceutical Design**, v. 26, n. 12, p. 1345–1355, 2020.

SHIMADA, N. *et al.* Inter-Polyelectrolyte Nano-Assembly Induces Folding and Activation of Functional Peptides. **Journal of Controlled Release**, v. 218, p. 45–52, 2015.

SINÉSIA, C. *et al.* Physico-Chemical Stability of Co-Formulation of PEGylated Human Amylin with Insulin. **Pharmaceutical Development and Technology**, v. 24, n. 8, p. 975–981, 14 Sep. 2019.

SINGH-FRANCO, D.; PEREZ, A.; HARRINGTON, C. The Effect of Pramlintide Acetate on Glycemic Control and Weight in Patients with Type 2 Diabetes Mellitus and in Obese Patients without Diabetes: A Systematic Review and Meta-Analysis. **Diabetes, Obesity and Metabolism**, v. 13, n. 2, p. 169–180, 2011.

SMITH, S. R. *et al.* Sustained Weight Loss Following 12-Month Pramlintide Treatment as an Adjunct to Lifestyle Intervention in Obesity. **Diabetes Care**, v. 31, n. 9, p. 1816–1823, Sep. 2008.

SUN, L. *et al.* Flash Fabrication of Orally Targeted Nanocomplexes for Improved Transport of Salmon Calcitonin across the Intestine. **Molecular Pharmaceutics**, v. 17, n. 3, p. 757–768, Mar. 2020.

SUTHERLAND, G. T. *et al.* Epidemiological Approaches to Understanding the Link between Type 2 Diabetes and Dementia. **Journal of Alzheimer's Disease**, v. 59, n. 2, p. 393–403, 2017.

TAM, C. S.; LECOULTRE, V.; RAVUSSIN, E. Novel Strategy for the Use of Leptin for Obesity Therapy. **Expert opinion on biological therapy**, v. 11, n. 12, p. 1677–85, 2011.

THWALA, L. N.; PRÉAT, V.; CSABA, N. S. Emerging Delivery Platforms for Mucosal Administration of Biopharmaceuticals: A Critical Update on Nasal, Pulmonary and Oral Routes. **Expert Opinion on Drug Delivery**, v. 14, n. 1, p. 23–36, Jan. 2017.

TOMABECHI, Y. *et al.* Glycosylation of Pramlintide: Synthetic Glycopeptides That Display In Vitro and In Vivo Activities as Amylin Receptor Agonists. **Chemistry - A European Journal**, v. 19, n. 45, p. 15084–15088, 4 Nov. 2013.

TRAINA, A. N.; KANE, M. P. Primer on Pramlintide, an Amylin Analog. **The Diabetes EDUCATOR**, v. 37, n. 3, 2011.

TRIPATHI, A. S. *et al.* Amylin Dual Action: A Second Gluco Regulatory ??-Cell Hormone, Treatment and Cause for the Diabetes. **International Journal of Diabetes in Developing Countries**, v. 34, n. 3, p. 125–129, 2014.

UMERSKA, A.; CORRIGAN, O. I.; TAJBER, L. Design of Chondroitin Sulfate-Based Polyelectrolyte Nanoplexes: Formation of Nanocarriers with Chitosan and a Case Study of Salmon Calcitonin. **Carbohydrate Polymers**, v. 156, p. 276–284, 2017.

VAN DER WALLE, C. F.; OLEJNIK, O. An Overview of the Field of Peptide and Protein Delivery. In: VAN DER WALLE, C. (Ed.). **Peptide and Protein Delivery**. Boston: Academic Press, 2011. p. 1–22.

VENKATANARAYAN, A. *et al.* IAPP-Driven Metabolic Reprogramming Induces Regression of P53-Deficient Tumours in Vivo. **Nature**, v. 517, n. 7536, p. 626–630, Nov. 2015.

WANG, E. *et al.* Amylin Treatment Reduces Neuroinflammation and Ameliorates Abnormal Patterns of Gene Expression in the Cerebral Cortex of an Alzheimer's Disease Mouse Model. **Journal of Alzheimer's Disease**, v. 56, n. 1, p. 47–61, 2017.

WANG, H. *et al.* Analysis of the Ability of Pramlintide to Inhibit Amyloid Formation by Human Islet Amyloid Polypeptide Reveals a Balance between Optimal Recognition and Reduced Amyloidogenicity. **Biochemistry**, v. 54, n. 44, p. 6704–6711, 2015.

WANG, J. *et al.* The Brief Analysis of Peptide-Combined Nanoparticle: Nanomedicine's Unique Value. **Current Protein & Peptide Science**, v. 21, n. 4, p. 334–343, Feb. 2020.

WANG, K.; LIU, M.; MO, R. Polysaccharide-Based Biomaterials for Protein Delivery. **Medicine in Drug Discovery**, p. 100031, Apr. 2020.

WANG, W.; ROBERTS, C. J. **Aggregation of Therapeutic Proteins**. Hoboken: John Wiley & Sons, 2010.

WEI, Z.; ZHANG, H.; HUANG, Q. Curcumin-Loaded Pickering Emulsion Stabilized by Insoluble Complexes Involving Ovotransferrin-Gallic Acid Conjugates and Carboxymethyldextran. **Food and Function**, v. 10, n. 8, p. 4911–4923, Aug. 2019.

WHATELEY, T. L. Drug Delivery and Targeting; for Pharmacists and Pharmaceutical Scientists. **Journal of Drug Targeting**, v. 10, n. 8, p. 637–637, 2002.

WHITBY, C. P. Nanoparticles at Fluid Interfaces: From Surface Properties to Biomedical Applications. In: NANN, T. (Ed.). **Comprehensive Nanoscience and Nanothechnology**. 2. ed. New York: Academic Press, 2019.

WONG, C. Y. *et al.* Development of Orally Administered Insulin-Loaded Polymeric-Oligonucleotide Nanoparticles: Statistical Optimization and Physicochemical Characterization. **Drug Development and Industrial Pharmacy**, p. 1–15, 2020.

WU, D. *et al.* Chitosan-based Colloidal Polyelectrolyte Complexes for Drug Delivery: A

Review. **Carbohdrate Polymers,** v. 238, p. 116-126, Jun. 2020.

WU, F.-G. G. *et al.* Folding Behaviors of Protein (Lysozyme) Confined in Polyelectrolyte Complex Micelle. **Langmuir**, v. 32, n. 15, p. 3655–3664, 2016.

YOUNK, L. M.; MIKELADZE, M.; DAVIS, S. N. Pramlintide and the Treatment of Diabetes: A Review of the Data since Its Introduction. **Expert Opinion on Pharmacotherapy**, v. 12, n. 9, p. 1439–1451, 2011.

YUAN, Y. *et al.* Study of Forced Degradation Behavior of Pramlintide Acetate by HPLC and LC-MS. **Journal of Food and Drug Analysis**, v. 26, n. 1, p. 409–415, 2017.

YUBA, E.; KONO, K. Nasal Delivery of Biopharmaceuticals. In: DAS NEVES, J.; SARMENTO, B. (Ed.). **Mucosal Delivery of Biopharmaceuticals**. New York: Springer, 2014. p. 197–220.

YULE, L. R. *et al.* Synthesis and Amylin Receptor Activity of Glycomimetics of Pramlintide Using Click Chemistry. **Organic & Biomolecular Chemistry**, v. 14, n. 23, p. 5238–5245, Jun. 2016.

ZHANG, C. *et al.* Influence of Ionic Strength on Gel-like Pickering Emulsions Stabilized by Self-Assembled Colloidal Nanoparticles Containing Lysozyme. **Colloid and Polymer Science**, v. 298, n. 9, p. 1249–1262, Sep. 2020.

ZHANG, L. *et al.* The Application of Polysaccharide-Based Nanogels in Peptides/Proteins and Anticancer Drugs Delivery. **Journal of Drug Targeting**, v. 25, n. 8, p. 673–684, Sep. 2017.

ZHAO, L.; SKWARCZYNSKI, M.; TOTH, I. Polyelectrolyte-Based Platforms for the Delivery of Peptides and Proteins. **ACS Biomaterials Science and Engineering**, v. 5, n. 10, p. 4937–4950, Oct. 2019.

ZHU, H. *et al.* Intraperitoneal Injection of the Pancreatic Peptide Amylin Potently Reduces Behavioral Impairment and Brain Amyloid Pathology in Murine Models of Alzheimer's Disease. **Molecular Psychiatry**, v. 20, n. 2, p. 252–262, Feb. 2015.

ZHU, H. *et al.* Amylin Receptor Ligands Reduce the Pathological Cascade of Alzheimer's Disease. **Neuropharmacology**, v. 119, p. 170–181, Jun. 2017.

CAPÍTULO I – NANOPARTÍCULAS DE SULFATO DE DEXTRANA/PRANLINTIDA COMO UM SISTEMA DE LIBERAÇÃO PROMISSOR: OTIMIZAÇÃO, AVALIAÇÃO DAS INTERAÇÕES SUPRAMOLECULARES E EFEITO SOBRE A ESTABILIDADE CONFORMACIONAL DO FÁRMACO PEPTÍDICO

O sulfato de dextrana (Figura 5) é um polissacarídeo, considerado análogo de glicosaminoglicano (GAG) polianiônico, biocompatível e altamente ramificado, formado por ligações glicosídicas α 1-6 e α 1-4, com cerca de 2,3 grupos sulfato de sódio associados a cada unidade glicosil. É produzido pela esterificação da dextrana (sintetizada por espécies fúngicas como *Leuconostoc spp.*) com o ácido cloro-sulfônico. O sulfato de dextrana é utilizado nos segmentos industriais alimentício, biotecnológico, cosmético e farmacêutico, como agente de purificação, de revestimento, condicionante e possui atividade anticoagulante (HOLBAN *et al.*, 2016; TAZI; JAYAWICKREME, 2016).

Figura 5 – Estrutura molecular do sulfato de dextrana.

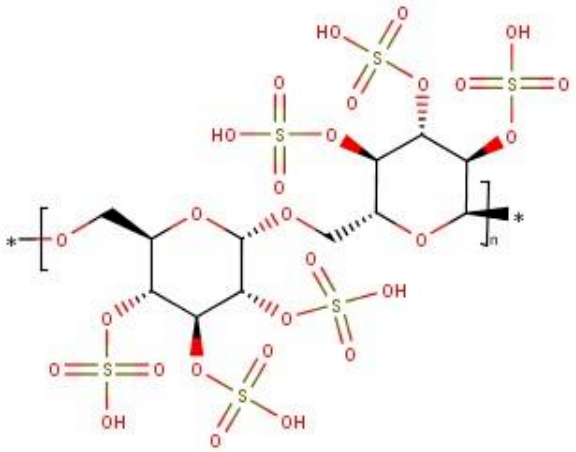

Fonte: ChEBI.

Os GAGs possuem funções fisiológicas importantes, como componentes estruturais da matriz extracelular e na diferenciação, morfogênese e migração celular. São reconhecidos por promover e estabilizar fibrilas amiloides pela forte interação com peptídeos que carregam domínios de ligação à heparina. A complexação com o sulfato de dextrana, que possui estrutura similar a heparina, também já foi proposta para aumentar a incorporação e a estabilidade de peptídeos terapêuticos em sistemas de liberação (KUMAR, AMRISH; PANDEY; JAIN, 2016; ZAMAN *et al.*, 2016; AGEITOS *et al.*, 2019; SUN, CHANGYE *et al.*, 2019). As propriedades do sulfato de dextrana parecem favorecer a formação de nanopartículas com a pranlintida, que é um peptídeo de natureza catiônica. Dessa forma, a complexação com o sulfato de dextrana foi avaliada como estratégia para a produção de nanopartículas com elevada associação da pranlintida. A concentração teórica do fármaco adicionada para formação das suspensões de

nanopartículas foi definida com base na concentração presente no produto comercial (Symlin®) (RIDDLE, 2017).

Assim, neste primeiro capítulo, buscou-se responder se a complexação com um polieletrólito com alta densidade eletrônica, o sulfato de dextrana, seria uma alternativa viável para a obtenção de nanopartículas de polieletrólitos de pranlintida com elevada associação do fármaco. As interações entre a pranlintida e o sulfato de dextrana foram estudadas por diversas técnicas como supressão da fluorescência, espectroscopia no infravermelho, microcalorimetria de titulação isotérmica e dicroísmo circular. Os resultados obtidos foram apresentados na forma de um artigo científico, o qual foi submetido para publicação no periódico *Journal of the Brazilian Chemical Society.*

Manuscrito 1 – ***Dextran Sulfate/Pramlintide Polyelectrolyte Nanoparticles as a Promising Delivery System: Optimization, Evaluation of Supramolecular Interactions and Effect on Conformational Stability of the Peptide Drug***

Manuscript submission to the

Journal of the Brazilian Chemical Society

Graphical Abstract (GA)

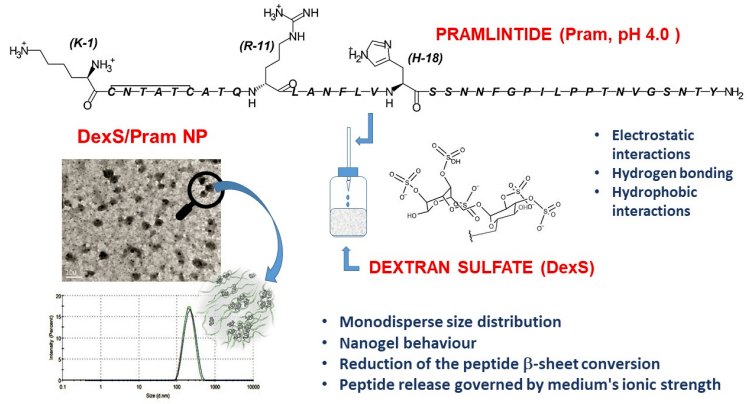

DexS/Pram polyelectrolyte nanoparticles diminished Pram conversion to β-sheet and controlled Pram release, depending on ionic strength.

Dextran Sulfate/Pramlintide Polyelectrolyte Nanoparticles as a Promising Delivery System: Optimization, Evaluation of Supramolecular Interactions and Effect on Conformational Stability of the Peptide Drug

Carine Zuglianello[a], Andrés F. Chamorro[b], Vanessa A. de Oliveira[c], Francisco H. Xavier Júnior[d], Elenara Lemos-Senna[e]*

[a,e]Departamento de Ciências Farmacêuticas, Programa de Pós-graduação em Nanotecnologia Farmacêutica, Universidade Federal de Santa Catarina, Campus Trindade, Florianópolis, SC, 88040-900, Brasil.

[b]Departamento de Química, Programa de Pós-graduação em Química, Universidade Federal de Santa Catarina, Campus Trindade, Florianópolis, SC, 88040-900, Brasil.

[c]Laboratório Central de Biologia Molecular e Estrutural, Universidade Federal de Santa Catarina, Campus Trindade, Florianópolis, SC, 88040-900, Brasil.

[d]Laboratório de Imunopatologia Keizo Asami, Universidade Federal de Pernambuco, Recife, Pernambuco, PE, 50670-901, Brasil.

email: lemos.senna@ufsc.br

*ORCID ID: https://orcid.org/0000-0002-3642-4468.

Abstract

In this study we investigated the feasibility to obtain nanoparticles (NPs) by assembling pramlintide (Pram) with dextran sulfate (DexS), as a new approach for mucosal peptide delivery. DexS/Pram NPs were prepared by dropwise addition of a Pram solution to a DexS solution under magnetic stirring. The physicochemical characteristics of the NPs and molecular interactions involved in the co-assembling were evaluated by dynamic light scattering, transmission electronic microscopy, isothermal titration microcalorimetry, FTIR spectroscopy, fluorescence quenching and circular dichroism. DexS/Pram NPs displayed a narrow size distribution (~ 200 nm), negative zeta potential (about −40 mV), association efficiency close to 100% and nanogel behavior. The assembling with DexS increased the Pram α-helical content, stabilizing the peptide in its bioactive form. The colloidal stability of nanoparticles was dependent on the salt concentration and it could be assumed that peptide release from nanoparticles occurs by dissociation of the complex at physiological conditions.

Keywords: Pramlintide, dextran sulfate, polyelectrolyte nanoparticles, supramolecular interactions, peptide drug delivery.

Introduction

Pramlintide acetate (Pram) is an analog peptide drug of amylin (also known as human islet amyloid polypeptide), which has been approved for clinical use for the treatment of Type 1 and Type 2 diabetes in patients who did not reach a satisfactory glycemic control, even though insulin therapy was thoroughly adjusted.[1] Pram differs from human amylin by the replacement of amino acids alanine, serine, and serine at positions 25, 26 and 27, respectively, by proline. It retains its biological potency but prevents self-aggregation and provides a higher aqueous solubility than human amylin. These changes were inspired by the discovery of lesser amyloidogenic murine amylin.[2] The advantageous property of Pram for therapeutic applications is that it avoids the formation of extracellular amyloid deposits that lead to the development of pancreatic β-cell disfunction and death, which is characteristic of the pathogenesis of Type 2 diabetes.[3] Pram acts by lowering postprandial glucagon secretion, inhibiting gastric emptying and giving a sensation of satiety by interacting with the hypothalamic receptors in the brain.[4] In addition, anti-obesity,[5] antitumoral,[6,7] and neuroprotectant activities[8,9] have also been described for this peptide drug.

Despite retaining all of the beneficial actions of native amylin without the disadvantages of amyloid formation and cytotoxicity, pramlintide still has solubility issues, particularly at physiological pH, exhibiting a higher solubility at acidic pH where the N-terminus and His-18 are fully protonated. This property prevents coformulation with insulin, which is formulated at near neutral pH, leading to increased cost in combination therapies and potentially reducing patient compliance due to the need for multiple injections.[10,11] In this regard, the development of dosage forms intended to deliver pramlintide across the epithelial mucosa, e.g., buccal, nasal, and pulmonary mucosae, may represent an alternative approach to avoid the use of invasive parenteral routes.[12] However, the development and production of peptide and protein drug products is also a challenge, since aggregation can take place in several industrial processes or storage conditions, leading to the formation of larger species consisting of multiple polypeptide chains. The reduction of the physical stability of peptide drugs leads not only to a loss in activity, but also to increases in toxicity and immunogenicity.[12,13] With this respect, the use of strategies to stabilize peptides in the helical conformation may reduce their conformational heterogeneity, increasing their resistance to enzymatic degradation and maintaining their therapeutic functionality.[13,14]

A variety of nanocarrier delivery systems has been proposed to overcome the limitations of delivering therapeutic peptides. However, the eligibility of a nanocarrier for association of a peptide drug depends on several peptide characteristics such as molecular dimension, electrostatic effects, stability, polarity, solubility and surface activity.[15] Moreover, an ideal delivery system should provide high peptide payload, optimal stability, batch reproducibility and scale up and tailorable release profile.[16] With this regard, polyelectrolytes have been successfully used to form nanocomplex assemblies with many peptides, playing an important role in various platforms relating to the delivery of peptide-based drugs.[17] The assembly occurs by weak and polyvalent interactions, rather than covalent bonds, bridging individual building blocks and guiding the formation of a thermodynamically stable nanocomplex.[18] In particular, polyelectrolyte nanoparticles may offer an interesting approach for delivering peptides by mucosal routes, since they could control the drug release, improve macromolecule stability, avoid enzymatic degradation, and improve retention and permeability by promoting intimate interaction with the mucosal epithelium.[19]

According previous studies, N-terminus and the side chains of Lys-1 (lysine -1, K-1), Arg-11 (arginine-11, R-11) and His-18 (histidine-18, H-18) (NH_3^+, Lys^+, Arg^+, and His^+) of Pram are protonated at acidic pH.[20,21] Also, computational simulation of its molecular structure indicated that Pram displays four positively charged amine groups at pH 4.0 (Figure 1). Then, we have hypothesized that polyeletrolyte nanoparticles can be obtained by interaction of pramlintide with negatively charged polysaccharides and that it can be exploited as new drug delivery system for delivery of this peptide through mucosal surfaces. Dextran sulfate (DexS) is a semisynthetic sulfated polysaccharide derived from dextran, in which sodium sulfate groups ($-OSO_3Na$) are attached to each (1→6)-α-linked anhydroglucose unit.[22] Interactions of DexS with proteins have been reported in the literature for both protein drug delivery and protein stabilization purposes.[23] The approach to obtain polyelectrolyte nanoparticles for delivery of Pram is described for the first time in the literature.

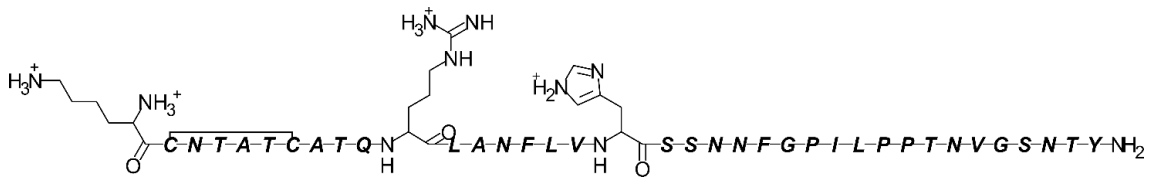

Figure 1. Fully protonated pramlintide sequence indicating the charged amino acids at low pH values (pH < 4; Drawn with Marvin Sketch 20.3.0, Chemaxon).[24]

Experimental

Materials

Pramlintide acetate (Pram, > 95.2% purity, MW 3,951.4) was obtained from Genemed Syn (lot #108695, Genemed Synthesis, Texas, USA). Dextran sodium sulfate (DexS) (M_r 40,000; with a sulfur content of 17.6%, according to the supplier specification sheet) and fluorescamine (Fluram, BioReagent, suitable for fluorescence, ≥ 99.0%) were supplied by Sigma-Aldrich (São Paulo, Brazil). Acetonitrile (HPLC grade, Honeywell) and trifluoroacetic acid (HPLC grade, Fisher Chemical) were purchased from Navelab (Curitiba, Brazil). All other solvents and reagents were of analytical grade and used without further purification. Stock solutions of Pram and DexS were prepared using acidified ultrapure water (Milli-Q).

Methods

Physicochemical characterization of DexS

DexS was characterized by high-performance size exclusion chromatography (HPSEC) using a Viscotek-HPSEC multidetector system (Malvern Instruments, Worcestershire, UK) equipped with a Shodex OHpak SB-806 HQ column (Showa Denko America, New York, NY, USA), connected in series and coupled to a differential refractometer (Viscoteck VE3580 RI detector), a viscometric detector and a laser light scattering detector (model 270 dual detector) with low angle 7° (LALLS) and right angle 90° (RALLS) lasers with λ 632.8 nm. The analyses were carried out at 40 ºC (313.15 K) using 0.1 mol L^{-1} $NaNO_3$ (sodium nitrate) with 200 parts per million (ppm) NaN_3 (sodium azide) as a mobile phase and a flow rate of 0.4 mL min^{-1}.

Preparation of DexS/Pram polyelectrolyte nanoparticles

DexS/Pram NPs were prepared by dropwise addition of different volumes of a Pram solution (2.50×10^{-4} mol L^{-1}, in acetic acid 1.00×10^{-3} mol L^{-1}, pH ~ 4.0) to a DexS solution (1.20×10^{-5} mol L^{-1}) under constant magnetic stirring (~600 revolutions per minute, rpm, Multistirrer 15, Velp Scientifica, Italy) at room temperature. DexS/Pram NPs were produced at molar ratios (MRs) from 2.40×10^{-2} to 5.30×10^{-2}. The colloidal dispersions were stored at 8 °C at least for 12 h (281.15 K, for 43, 200 s) before analysis. All DexS/Pram NPs were prepared in triplicate.

Characterization of DexS/Pram polyelectrolyte NPs

Hydrodynamic particle size

The size distribution, mean particle size, and polydispersity index were determined by dynamic light scattering (DLS) using Zetasizer Nano ZS equipment (Malvern Instruments, Worcestershire, UK). The measurements were made after appropriate dilution of the DexS/Pram NPs in ultrapure water at fixed scattering angle of 173°. Size distribution was also analyzed at scattering angles varying from 30 to 145°, using an ALV laser goniometer (AVL-Laser, Germany) equipped with a 35 megawatts (mW) red helium-neon linearly polarized laser (wavelength, λ = 632.8 nm) and multiple tau digital correlator (LSE-5004). ALV-correlator software V.3.0 was used to obtain the DLS autocorrelation functions $g^{(1)}(q,t)$.[25] The distribution function of the decay time A(t) and the distribution function of size $A(R_h)$ were obtained by CONTIN analysis of the $g^{(1)}(q,t)$ function. The hydrodynamic radii of the nanoparticles (R_h^{NP}) were calculated using the Einstein−Stokes equation (Equation 1).

$$R_h^{NP} = \frac{kT}{6\pi\eta\, D^{NP}} \quad (1)$$

where T is absolute temperature, k is the Boltzmann constant, D^{NP} is the diffusion coefficient of the aggregate and η is the water viscosity.[26] Analyses were conducted in triplicate.

Zeta potential

Zeta potential was determined by laser-doppler anemometry using a Zetasizer Nanoseriers (Malvern Instruments, Worcestershire, UK). The DexS/Pram NPs were diluted in ultrapure water and placed in an electrophoretic cell where a potential of ±150 millivolts (mV) was established. The zeta potential values were obtained by the equipment software from the mean electrophoretic mobility using Smoluchowski's equation.[27]

Nanoparticle morphology

The morphological examination of the DexS/Pram NPs was performed using a JEM-1011 transmission electron microscope (Jeol, Japan), operating at 100 kilovolts (kV). Drops of the colloidal dispersions were deposited in formvar/carbon copper grids and left to dry for 10 min (600 s). The samples were then negatively stained with 1.0% phosphotungstic acid (weigh by volume, w/v) and left to dry overnight under vacuum. TEM images were obtained and ImageJ software was also used to measure particle size using the Image J software.[28]

Association efficiency

Free Pram was separated from the DexS/Pram NPs by ultracentrifugation at 40,000 g for 30 min at 4 °C (1,800 s, 277.15 K) using an Optima Max-XP ultracentrifuge (Beckman Counter, USA). The supernatants were collected and free Pram was determined by fluorescamine assay [29], using an analytical curve constructed with Pram at concentrations ranging from 8.00×10^{-3} to 4.80×10^{-2} mg mL^{-1}, ($y = 0.057x + 0.367$, r > 0.999). Free Pram was used as control. The association efficiency (%) was estimated as the mass percentage of Pram that formed polyelectrolyte nanoparticles relative to the initial amount of peptide added. The analyses were performed in triplicate.

Investigation of DexS/Pram interactions

Fluorescence quenching

Fluorescamine assay was used to investigate the molecular interactions between DexS and Pram in the DexS/Pram NPs. Briefly, DexS/Pram complexes corresponding to a constant Pram concentration of 7.25×10^{-5} mol L^{-1} and DexS concentrations ranging from 0 to 3.25×10^{-6} mol L^{-1} were both prepared in 1.00×10^{-3} mol L^{-1} acetic acid (pH ~ 4.0) in a 96-well black microplate and incubated for 60 minutes (final volume 0.15 mL, 3,600 s). Then, 0.05 mL of a 0.50 mg mL^{-1} fluorescamine solution in dimethyl sulfoxide (DMSO) was added to each well and left to react for 10 min (600 s). The fluorescence emission was recorded using a Tecan Infinite M200 microplate reader in the wavelength interval 430–600 nm, with excitation settled at 390 nm. Fluorescence suppression was fitted in the Stern–Volmer model, described by Equation (2).

$$\frac{F_0}{F} = 1 + K_{SV}[Q] = 1 + K_q\tau_0[Q] \quad (2)$$

where F_0 and F are the fluorescence intensity in the absence and presence of several concentrations of the DexS (fluorescence suppressor), respectively, K_{SV} is the Stern–Volmer constant, [Q] is the molar concentration of suppressor agent, K_q is the suppression rate constant, and τ_0 is the polypeptide half-life in the absence of suppressor. DexS solutions at respective concentrations were used as control. Experiments were carried out in triplicate.

Isothermal calorimetry titration (ITC)

The affinity experiments used ITC200 equipment (GE Healthcare Life Sciences, Uppsala, Sweden). The titrations were performed by filling the ITC cell with a 1.20×10^{-5} mol L^{-1} DexS solution and the syringe with a 2.50×10^{-4} mol L^{-1} Pram solution. The first injection of 4.00×10^{-4} mL was discarded to eliminate diffusion effects of material from the syringe to the sample cell. Experiments were set up with 19 consecutive injections (2.00×10^{-3} mL) with a duration of 5 s each and intervals of 150 s, at a stirring speed of 400 rpm, and temperature fixed at 25 °C (298.15 K). Blank titrations were performed by adding Pram solution into the cell filled with 1.00×10^{-3} mol L^{-1} acetic acid. Data analysis was performed by Origin 7.0 MicroCal iTC200 provided by MicroCal. The isotherm was established based on the integration of the obtained peaks by plotting the resulting heat values from each injection against the DexS/Pram molar ratio. In addition, heat of dilution was subtracted from the data considering the final points of the ITC experiments, where no significant heat changes were observed. The thermodynamic parameters were determined using the One Set of Sites model that adjusts the curve by nonlinear regression (least-squares method). The thermodynamic relationships considered for this experiment are described in Equation (3).

$$\Delta G = -RT \ln Ka = RT \ln Kd \quad (3)$$

Fourier-transform infrared (FTIR) spectroscopy

FTIR analyses were performed on the dry powder of DexS/Pram NPs, obtained by isolation of the pellet by ultracentrifugation of the formulations at 40,000 g for 30 min at 4 °C (Optima Max-XP, Beckman Counter, USA) (1,800 s, 277.15 K). Before analysis, the pellet was completely dried under vacuum for 24 h (86,400 s). Spectra of Pram, DexS, and DexS/Pram NPs were obtained using an FTIR spectrophotometer (Frontier, PerkinElmer, Waltham, USA) in the scanning region of 1,000–1,800 cm^{-1} at a resolution of 2 cm^{-1}. Second-derivative FTIR spectra were plotted.

Circular dichroism (CD)

Changes in Pram structure after its association with DexS (at DexS concentrations ranging from 4.00×10^{-7} to 1.70×10^{-6} mol L^{-1} and constant pramlintide concentration of 2.90×10^{-5} mol L^{-1}) were evaluated by CD using ultrapure water adjusted to pH 4.0 as diluent, when freshly prepared samples were analyzed, and to pH 7.0 for samples incubated for 24 h at 37 °C (86,400 s, 310.15 K). Free Pram was used as control. Measurements were performed in a Jasco

J-815 spectropolarimeter at 25 °C (298.15 K), at wavelength range 260–185 nm and cell length of 10 mm, bandwidth of 1.0 nm and scan rate of 0.8 nm s^{-1}. Analyses were performed in triplicate. Predictions of secondary structures from molar ellipticity in the wavelength range 240–190 nm were obtained using k2d3 webserver.[30]

Colloidal stability and drug release

The effect of the ionic strength of the medium on aggregation of the nanoparticles and Pram dissociation was evaluated by diluting the colloidal dispersions in ultrapure water or NaCl solution at concentrations ranging from 1.00×10^{-2} to 2.00×10^{-1} mol L^{-1}. The samples were analyzed according to size, polydispersity index (PdI) and zeta potential as described above. Pram dissociation was evaluated by incubating DexS/Pram NPs or free Pram at 1:10 (volume by volume, v/v) dilution in saline solutions for 60 minutes (3,600 s). The Pram release kinetics from nanoparticles was also evaluated after dilution of the samples in simulated nasal fluid (SNF, pH 5.5)[31] or ultrapure water at 1:50 (v/v). Samples were then submitted to ultracentrifugation at 40,000 g, 4 °C for 30 min (277.15 K, 1,800 s) in an Optima Max-XP ultracentrifuge (Beckman Counter, USA). Supernatants were withdrawn and analyzed for Pram concentration by liquid chromatography with ultraviolet detection (LC-UV), using a PerkinElmer Series 200 LC system (equipped with degasser, pump, autosampler and UV-Vis detector). The analyses were performed using a C18 column (Zorbax Eclipse Plus, 150 × 4.6 mm, 5 µm) and a mobile phase consisting of acetonitrile with trifluoracetic acid 0.1% (v/v) (A) and water with trifluoracetic acid 0.1% (v/v) (B). The mobile phase was eluted at a flow rate of 1.0 mL min^{-1} using a linear gradient program of 10% to 65% (A) over 25 min (1,500 s). The injection volume of the samples was 2.00×10^{-3} mL and detection was at 205 nm. The Pram concentration was determined using an analytical curve constructed with Pram at concentrations ranging from 1.13×10^{-2} to 4.52×10^{-2} mg mL^{-1} ($y = 26794x - 36790$, r = 0.999).

Results and Discussion

Physicochemical characterization of the DexS

Since the properties of the polymers, specially the molecular weight, affect the formation of polyelectrolyte nanoparticles, DexS was characterized by HPSEC. According to the analysis, DexS presented a number average molecular weight (M_n) and a weight average molecular weight (M_w) of 30,302 and 50,191 g mol^{-1}, respectively, a dispersity (M_n/M_w) of 1.656, and intrinsic viscosity of 0.3003 dL g^{-1}. The degree of sulfation was calculated from the sulfur content (17.6%) provided by the supplier and it was found to be 2.24. The DexS weight average molecular weight (M_w) was used for calculating the DexS to Pram molar ratio in the nanoparticles.

Preparation and characterization of polyelectrolyte nanoparticles

In this study, a suitable concentration range for spontaneous formation of nanoparticles was previously identified by varying the concentration of DexS between 4.00×10^{-6} and 2.00×10^{-5} mol L^{-1} and keeping the concentration of Pram at constant 1.25×10^{-4} mol L^{-1}, which corresponds to a DexS/Pram molar ratio varying from 3.20×10^{-2} to 1.60×10^{-1}. The Tyndall effect, characteristic of nanoparticle dispersions, was observed at a DexS concentration of 1.20×10^{-5} mol L^{-1}, whereas macroscopic aggregates were formed at lower DexS concentrations (4.00×10^{-6} and 8.00×10^{-6} mol L^{-1}) and transparent solutions were obtained at higher DexS concentrations (1.60×10^{-5} and 2.00×10^{-5} mol L^{-1}). Formation of macroscopic aggregates occurred due to the presence of an excess of peptide. It is most likely that intrapolymer complexes are firstly formed by complexation of a single dextran molecule with several peptide molecules. Aggregation of these primary complexes by the formation interpolymer complexes then takes place, causing in turn precipitation of the complexes from the colloidal dispersion.[32] Once the DexS and Pram concentrations were established, the polyelectrolyte nanoparticles were prepared at a DexS/Pram molar ratio varying from 2.40×10^{-2} to 5.30×10^{-2}, which corresponds to a charge ratio varying from 1.63 to 3.66. Charge ratio was calculated from the molar charge densities of DexS and Pram, which were equal to 5.50×10^{-3} (~275.5 negative residues mol^{-1}, sulfur content of 17.6%) and 1.01×10^{-6} mol charge mg^{-1} (~4 positive residues mol^{-1} at pH 4.0), respectively. These polyelectrolyte nanoparticle dispersions displayed mean particle sizes between 200 and 400 nm, PdI between 0.20 and 0.25, and zeta potential ranging from –30 to –40 mV (Table 1). Negative zeta potential indicated the presence of the DexS

polyanion at the particle surface, and the net surface charge obtained can be considered sufficient to provide physically stable colloidal dispersions. The theoretical Pram concentration in the nanodispersions varied from 1.19×10^{-4} to 1.69×10^{-4} mol L^{-1}, and the association efficiency, evaluated by fluorescamine assay (SI, Figure S1), was near 100% for all DexS/Pram ratios tested. Neither zeta potential nor Pram association efficiency was affected by increasing charge ratio, which can be related to the narrow range of DexS/Pram molar ratios in which nanoparticles were obtained in this study.

Table 1. Composition, physicochemical properties and drug association of DexS/Pram polyelectrolyte NPs.

Pram (mol. L^{-1}) $\times 10^{-4}$ [a]	DexS (mol. L^{-1}) $\times 10^{-6}$	DexS/Pram MR[b] $\times 10^{-2}$	DexS/Pram charge ratio	Particle diameter (PdI)[c] (nm)	Zeta potential (mV)	Pram AE[d] (%)
1.69	3.98	2.36	1.63	281 ± 113 (0.23)	–36 ± 4	> 99
1.56	4.60	2.95	2.03	262 ± 31 (0.23)	–31 ± 2	> 99
1.45	5.13	3.54	2.44	208 ± 20 (0.22)	–33 ± 1	> 99
1.35	5.58	4.13	2.85	210 ± 11 (0.22)	–41 ± 2	> 99
1.27	5.98	4.72	3.25	229 ± 10 (0.23)	–33 ± 3	> 99
1.19	6.33	5.31	3.66	236 ± 5 (0.23)	–40 ± 2	> 99

[a] Theoretical concentration; [b] molar ratio, [c] PdI: polydispersion index; [d] AE: pramlintide association efficiency.

Considering the monodisperse distribution of particle size obtained by backscattering analysis, which is required to ensure a reproductive absorption of the peptide through the absorptive mucosa, further characterization studies were carried out using polyelectrolyte NPs prepared at a DexS/Pram molar ratio of 3.54×10^{-2} (SI, Figure S2). The charge ratio in this case of 2.44 was away from charge stochiometric conditions, as described to be required to form stable polyelectrolyte nanoparticles. [33–35] The hydrodynamic radius of the nanoparticles (R_h^{NP}) was determined by multi-angle DLS at scattering angles between 30° and 140°. Figure 2a shows the correlation function $g^{(1)}(q,t)$ and the decay time distribution A(t) of the nanoparticles obtained at scattering angle of 90°. A bimodal distribution can be seen, with fast and slow relaxation modes attributed to the dispersity of DexS/Pram nanoparticles. The multi-angle DLS analysis showed a consistent diameter with the backscattering analysis (208.4 ± 20.4 nm against 194.8 ± 5.8 nm). From the CONTIN analysis of each correlation function, the relaxation time τ

was obtained and the angular dependency of the relation frequency Γ (Γ= τ^{-1}) estimated and plotted against q^2 function (Figure 2b). The linear fitting in multi-angle to size correlation suggests that polyelectrolyte nanoparticles have a spherical form and a homogeneous size distribution, maintaining their size constant independent of settled angle. The R_h^{NP} value of the nanoparticles was found to be 97.4 ± 2.91 nm. Similar results were found by Frère et al.,[34] whose described the formation of spherical polyelectrolyte nanoparticles by interaction of the P140 peptide with a polyelectrolyte presenting approximately a 10-fold higher molecular weight.

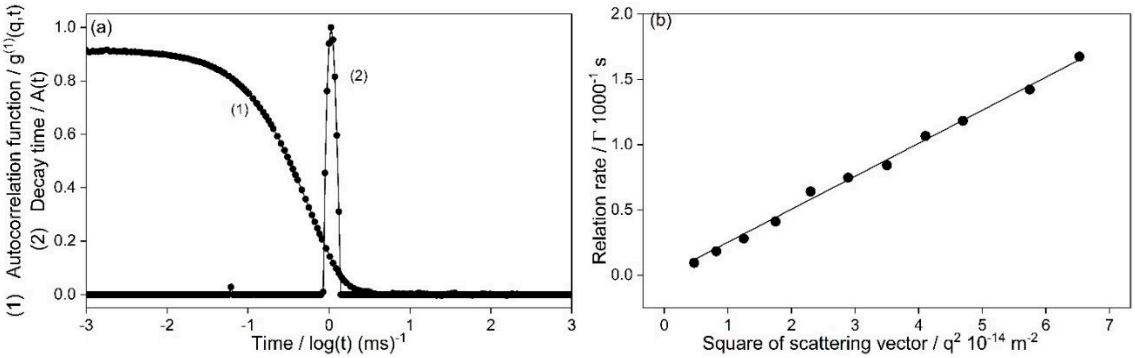

Figure 2. (a) (1) Autocorrelation function $g^{(1)}(q,t)$ and (2) distribution function of decay time A(t) obtained by CONTIN method at scattering angle 90° and 298.15 K for DexS/Pram NPs in water. The slow modes represent 99% of the population. (b) Dependence of the relation rate on the square of scattering vector q^2 for DexS/Pram NPs at different scattering angles (varying from 30° to 140°). Continuous lines correspond to linear fits with intercept at the origin and a correlation coefficient of 0.9994.

TEM images of polyelectrolyte DexS/Pram NPs revealed the presence of spherical particles displaying homogeneous size distribution, corroborating data obtained by multi-angle DLS analysis (Figure 3). However, particle size obtained by ImageJ software was 43.4 ± 7.3 nm. This smaller particle size may be attributed to the nanogel character of the DexS/Pram colloidal dispersions, as described elsewhere[33,36,37] and to the slower mode viewed in the multi-angle light scattering, that might represents a large portion of the particles population by number. Moreover, when analyzed by TEM, nanogel particles are expected to be smaller than those observed in hydrated conditions, due to the water loss during the sample drying.

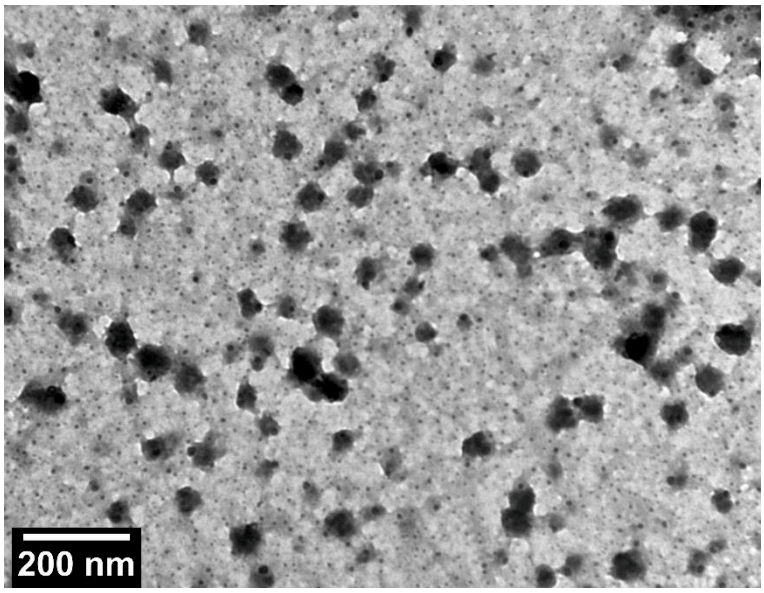

Figure 3. TEM image of DexS/Pram nanoparticles negatively stained with phosphotungstic acid solution 1.0% (w/v); bar 200 nm.

Study of supramolecular interactions

Fluorescence quenching

Supramolecular interactions between DexS and Pram were investigated by fluorescamine assay. Fluorescamine, a heterocyclic dione, reacts with primary amines to form a fluorescent product. Pram has a single primary amine, located in its Lys-1 amino acid. Since negatively charged DexS is thought to interact with the positively charged Lys of the Pram molecule, the effect of DexS addition on the fluorescence of the Pram–fluorescamine product was investigated. As can be seen in Figure 4a, the fluorescence of the samples decreased linearly upon addition of increasing concentrations of DexS, from 1.00×10^{-6} to 2.80×10^{-6} mol L^{-1}. Higher DexS concentrations were also tested, but its effect in fluorescence quenching was negligible, probably because the Pram binding sites were already occupied (data not shown). Quenching data were fitted to the Stern–Volmer equation to give a linear curve ($F_0\ F^{-1} = 5.60 \times 10^6(Q) - 3.20$) with correlation coefficient of 0.9978 (Figure 4b). Assuming the binding of DexS to Pram is a static rather than a dynamic process, the binding constant was found to be 5.60×10^6 L mol^{-1}, which is comparable with values reported in the literature for other polysaccharide–peptide complexes.[38,39]

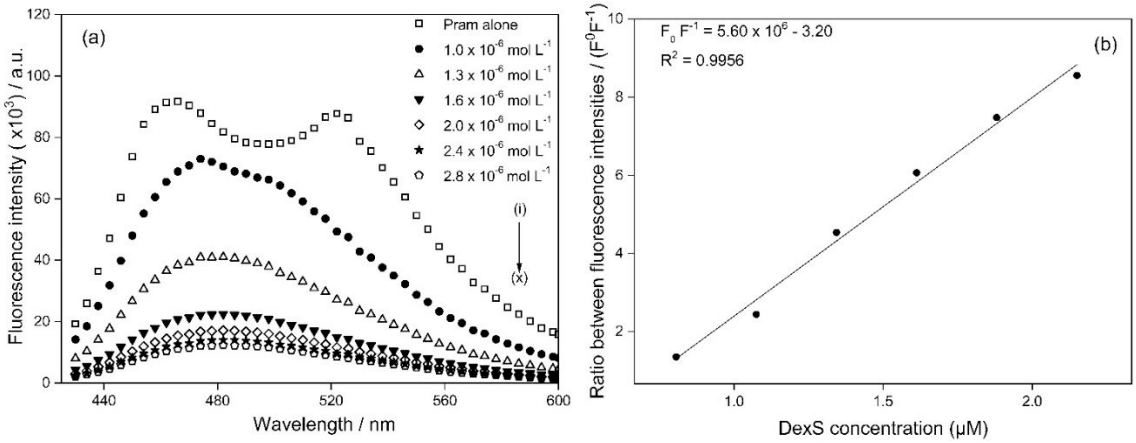

Figure 4. (a) Fluorescence quenching of pramlintide with several concentrations of DexS. Spectra from (i) to (x) correspond to DexS concentrations of 1.00×10^{-6} to 2.80×10^{-6} mol L^{-1}, at a constant pramlintide concentration of 7.25×10^{-5} mol L^{-1} (1.45×10^{-4} mol L^{-1} diluted 1:2 v/v, with ultrapure water). (b) Stern–Volmer plot of fluorescence quenching of pramlintide with DexS. Stern–Volmer constant K_{SV} or binding constant K= 5.60×10^{6} L mol^{-1}.

Isothermal titration calorimetry

The ITC technique has emerged as an important tool for the examination of the thermodynamic properties of biomacromolecule binding interactions and synthetic polyelectrolyte aggregation by determining the equilibrium constants, stoichiometry, and binding partners under defined experimental conditions. Here, the thermodynamic parameters of the DexS–Pram interactions in the polyelectrolyte nanoparticles were obtained by fitting the binding isotherms (integrated titration peaks corrected for the heats of dilution) to the one-site binding model (Figure 5). Binding affinity constant (K) obtained by titrating the peptide into a DexS solution was 2.45×10^{5} L mol^{-1}, similar to that obtained in other mechanistic studies of polysaccharide–peptide complex formation, e.g., for dextran sulfate–parathyroid hormone (1.90×10^{6} L mol^{-1}),[40] and fucoidan–protamine polypeptide (2.07×10^{6} L mol^{-1}) complexes.[41] The titrations indicated an exothermic interaction process as expected for an electrostatic interaction of oppositely charged compounds (Figure 5a). Polyelectrolyte nanoparticle formation was produced with spontaneous energy ($\Delta G = -30.85$ kJ mol^{-1}), in a process driven by an enthalpic contribution ($\Delta H = -82.43$ kJ mol^{-1}).[40,42] Favorable enthalpic binding is characteristic of non-covalent electrostatic interactions as well as of hydrogen bonding formed by attractive dipole–dipole interactions between Pram and DexS. In addition, DexS/Pram NP formation involves more conformational changes, as indicated by the unfavorable entropy ($-T\Delta S = +51.58$ kJ mol^{-1}, Figure 5b). This effect could originate from the loss in biopolymer conformational freedom after complexation, or that the peptide is very flexible and undergoes a conformational change in the binding process.[42,43]

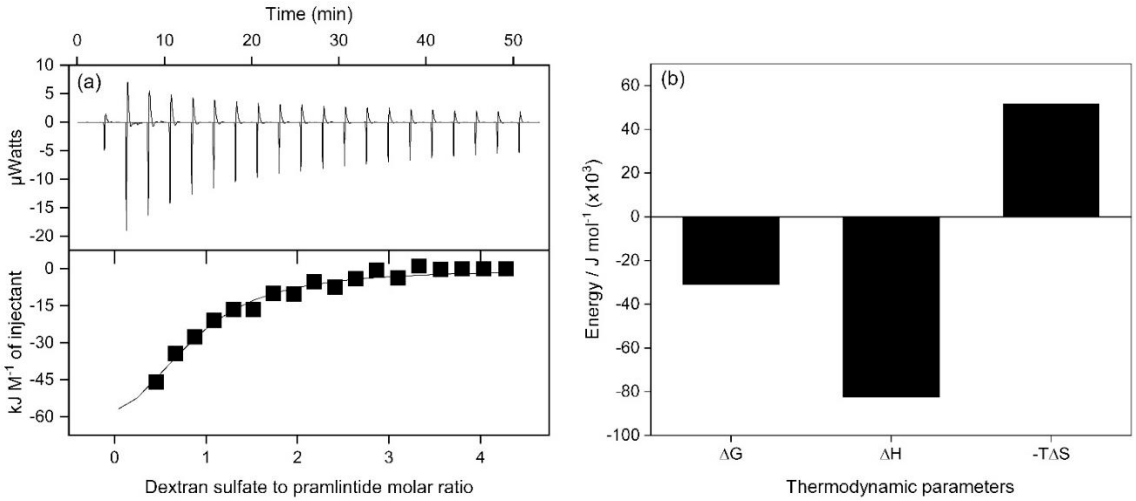

Figure 5. (a) Isothermal titration calorimetry profile of Pram (2.50×10^{-4} mol L^{-1} solution) titrated with DexS solution (1.20×10^{-5} mol L^{-1} solution) at temperature of 298.15 K. (b) Thermodynamic parameters of interactions in the DexS/Pram nanoparticles obtained by fitting the binding isotherms to the one-site binding model.

Fourier-transform infrared (FTIR) spectroscopy and circular dichroism

FTIR spectrum was obtained for Pram, DexS and DexS/Pram NPs at wavelengths ranging from 1,800 to 1,000 cm^{-1}, but overlapping peaks of DexS and Pram in FTIR spectra hampered the analysis of the secondary structure of the peptide in higher wavenumber (data not shown). However, in the amide III region (Figure 6) it was possible to identify peaks that can be related to the Tyr ring vibration (1,265–1,270 cm^{-1} and 1,180 cm^{-1}) or to turn peptide structure (between 1,260 and 1,280 cm^{-1}) in the both spectra of Pram and DexS/Pram NPs (Figs 6a and 6c, respectively). Also, a small negative peak at 1,315 cm^{-1} in that of DexS/Pram NPs (Fig. 6c) can be related to the α-helix peptide structure.

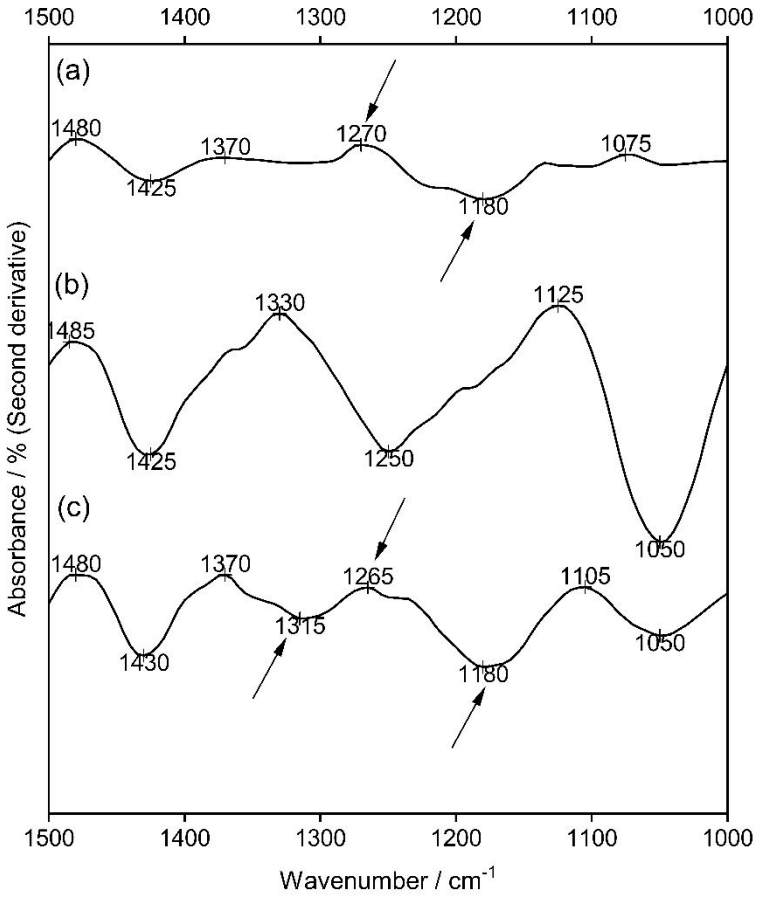

Figure 6. FTIR spectra of (a) pramlintide (Pram) (b) dextran sulfate (DexS) and (c) DexS/Pram polyelectrolyte nanoparticles (DexS/Pram NPs). Peaks related to Tyr ring vibration (1,265–1,270 cm–1 and 1,180 cm–1) or to turn peptide structure (between 1,260 and 1,280 cm–1) are indicated by arrows in Fig. 6a and 6c. A small negative peak at 1,315 cm–1 that can be related to the α-helix peptide structure in that of DexS/Pram NPs is also indicated by an arrow in Fig. 6c.

Circular dichroism (CD) experiments give information about the three-dimensional structure of macromolecules containing chiral centers, using circular polarized light, and it have been considered a powerful technique for studying the secondary structure of peptides. The CD spectrum of unordered peptides is usually characterized by a single band below 200 nm, while α-helices structures usually display large CD bands with negative ellipticity at 222 and 208 nm along with a positive ellipticity at 193 nm, and β-sheets exhibit a broad negative band near 218 nm and a large positive band near 195 nm.

The CD spectra obtained for the Pram solution and DexS/Pram complexes (pH 4.0) are depicted in Figure 7. Pram CD spectrum exhibited a negative peak near 200 nm, which is a characteristic of unordered structures. Unlike the Pram alone, the assembly of the peptide with DexS seemed to lead to formation of hybrid coiled–coil-like structures, thus promoting an increase in ellipticity. Based on the analysis carried out using the k2D3 method, Pram in

solution contains 5.16% α-helical structure and 11.63% β-sheets. This predicted secondary structure content obtained for Pram is in accordance with that reported elsewhere, where 68% disordered structure, 4% α-helix, 13% β-sheet and 11% turn was found.[44] When DexS/Pram nanoparticles were evaluated (at dilution of 1:5), the content of α-helical structure increased to 36.25%, while β-sheet reduced to 6.70% (Table 2). This pattern was maintained after of incubation of the samples previously adjusted to pH 7.0 for 24 hours at 37° C (1,400 s, 310.15 K) (Figure S3), suggesting that assembling with DexS stabilizes the peptide in physiological conditions by inducing its helical conformation, which could preclude the amyloids formation,[45] already described to occur when Pram is submitted to extreme conditions.[29] An increase in ellipticity has been reported to occur in interactions of polysaccharides with other peptides/proteins, enhancing their colloidal stability and maintaining peptide biological activity.[40,46] Similar patterns were found in a novicidin–hyaluronic acid nanocomplex, and its complexation was shown to maintain its antimicrobial properties while improving its security profile in cell culture experiments.[47] Likewise, glycosaminoglycans located at the cell membrane or in the extracellular matrix are thought to induce helical conformations in GAG-binding peptides and proteins, which may enhance the peptide/protein activity and receptor affinity.[40] Both inhibition and overstabilization of α-helix (between approximately 15 to 30% of α-helix over the time) were already described as alternatives to reduce the amylin proteotoxicity, being the partial helix more prone to amyloid formation.[45,48,49]

Considering the results described here, we can assume that Pram acts by physically crosslinking DexS chains by electrostatic interactions, inducing phase separation and leading the formation of a coacervate.[50–52] The macromolecular environment led the peptide to reduce its conformational freedom and to adopt a more compact structure (α-helix instead of a random coil), which is stabilized by electrostatic interactions between Dexs and Pram and by inter and intramolecular hydrogen bonds.

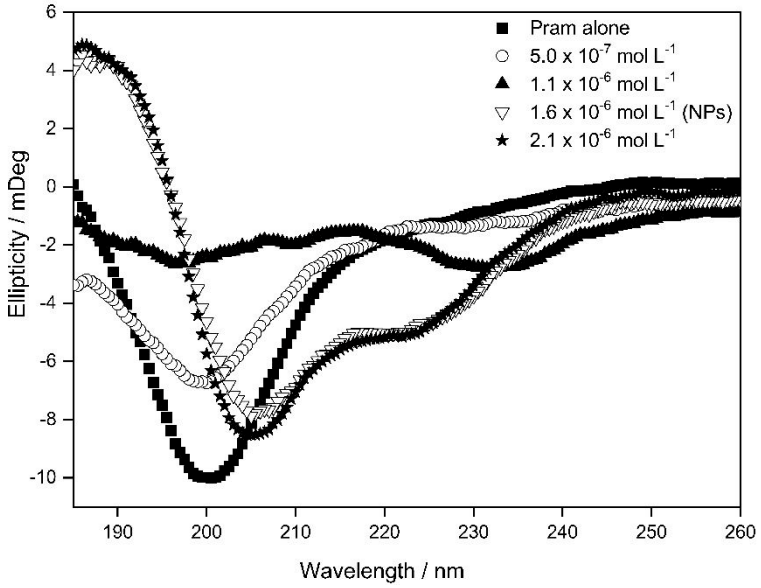

Figure 7. Circular dichroism of DexS/Pram complexes corresponding to a DexS concentration of 5.00 × 10−7 – 2.10 × 10-6 mol L-1, at constant Pram concentration of 2.90 × 10-5 mol L-1 (DexS/Pram NPs diluted 1:5, 1.60 × 10-6 mol L-1 / 2.90 × 10-5 mol L-1).

Table 2. Secondary structure of Pram predicted by k2d3 web server from Far-UV CD data.

Secondary structure	Pram alone (in solution)		DexS/Pram NPs	
	pH 4.0	after incubation at 37º C, pH 7.0	pH 4.0	after incubation at 37º C, pH 7.0
α-helix (%)	5.16 ± 0.10	1.09 ± 0.21	36.25 ± 1.84	40.09 ± 4.29
β-sheet (%)	11.63 ± 0.15	26.97 ± 0.62	6.70 ± 0.15	7.22 ± 3.73

Colloidal behavior of DexS/Pram NPs in aqueous saline media

The colloidal stability of DexS/Pram NPs was assessed by evaluating the parameters of size, PdI and zeta potential after dilution with NaCl solution at concentrations of 1.00×10^{-2}, 5.00×10^{-2}, 1.00×10^{-1} and 2.00×10^{-1} mol L^{-1} (1:10, v/v, Figure 8a). Ionic strength was expected to affect these physicochemical properties of DexS/Pram NPs by causing charge shielding and resulting in larger particle sizes. Salt may interact electrostatically with the peptide and the polyelectrolyte favoring swelling and dissociation of the particles. This hypothesis was confirmed by dissociation studies (Figure 8b), where free Pram concentrations, evaluated by liquid chromatography with ultraviolet detection (Figure S4), were higher in stronger ionic diluents, from NaCl 1.00×10^{-2} mol L^{-1} to 2.00×10^{-1} mol L^{-1} . This result indicated that the peptide release from the nanocomplex will be triggered by the body´s natural ionic strength, as related elsewhere.[53] In this case, salts in the surrounding medium are able to access the complex and outcompete the ionic interaction formed between DexS and Pram, leading to dissociation. This feature dramatically affects the Pram release rate from

nanoparticles. As can be seen in Fig. 9, about 80% of Pram is released after 48 h when diluted in ultrapure water, whereas the same amount of the drug is released in the first 2 h, after diluting the samples in SNF. Then, the drug release is governed by drug dissociation from DexS/Pram NPs in biological fluids, where saline concentration is around 1.50×10^{-1} mol L^{-1}, and it is considered essential for reaching therapeutically effective concentrations of the peptide after mucosal administration.

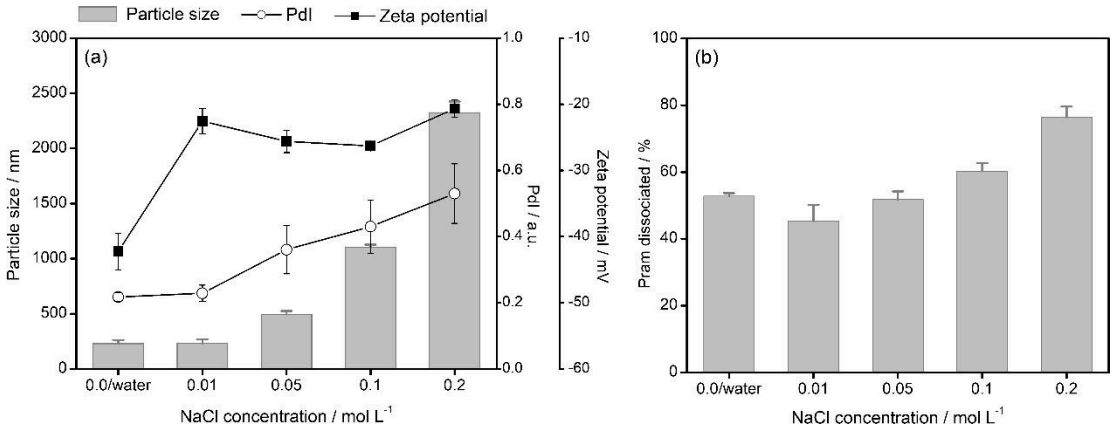

Figure 8. (a) Particle size, PdI, and zeta potential values obtained for DexS/Pram NPs and (b) Pram dissociation (%) as a function of the NaCl concentration of the medium.

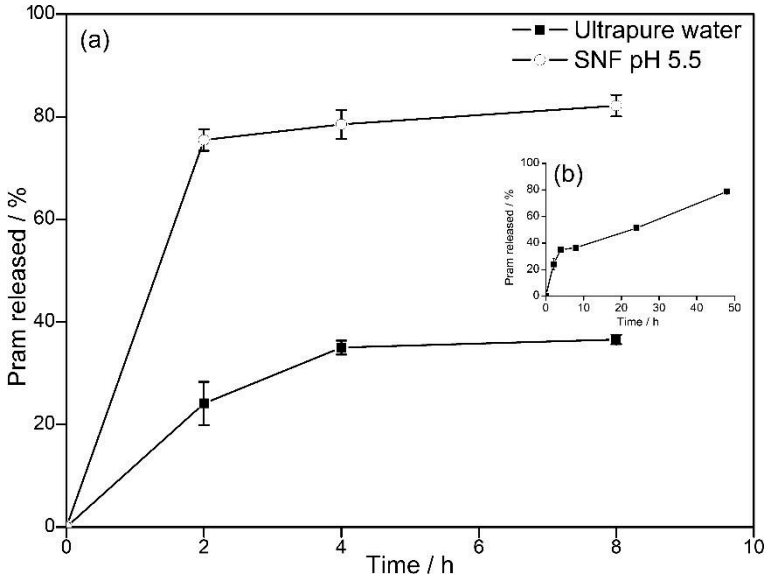

Figure 9. (a) Release profile of Pram from DexS/Pram NPs after dilution of the sample in ultrapure water or SNF pH 5.5 (1: 50, v/v) during the first 8 h. (b) Inset shows the Pram release profile from NPs in ultrapure during 48 h.

Conclusions

This study showed for the first time the feasibility of obtaining DexS/Pram polyelectrolyte nanoparticles with high drug payload, nanometric size and monodisperse particle size distribution. The formation and the physicochemical properties of the DexS/Pram NPs were dependent on the DexS/Pram molar ratio. Supramolecular interactions involved in the DexS/Pram binding were evidenced by different experimental techniques. The high affinity between DexS and Pram, characterized by favorable enthalpic binding, was demonstrated by the fluorescence quenching and ITC experiments. Considering the results described here, we can assume that Pram acts by physically crosslinking DexS chains by electrostatic interactions. In addition, the assembling of the peptide with DexS induced the conformational change of the peptide to the bioactive α-helical structure. However, colloidal stability was dependent on the ionic strength of the medium, causing nanoparticle aggregation and peptide dissociation at higher salt concentrations. In this regard, peptide release from the nanocomplex is more likely to occur by dissociation of the complex caused by the body´s natural ionic strength. Taken all together, this study brings valuable information about the physicochemical behavior of DexS/Pram polyelectrolyte nanoparticles that can be useful for developing transmucosal delivery systems for Pram.

Supplementary Information

Supplementary Information with respect to calibration curves, obtained to pramlintide by fluorescamine assay and liquid chromatography with ultraviolet detection, size distribution profile of dextran sulfate/pramlintide nanoparticles obtained by backscattering analysis and circular dichroism of pramlintide and dextran sulfate/pramlintide nanoparticles submitted to incubation for 24 h, at temperature of 37 °C (1,440 s, 330.15 K) and pH 7.0 are available free of charge at http://jbcs.sbq.org.br.

Acknowledgments

This study is part of the National Institute of Science and Technology in Pharmaceutical Nanotechnology: a transdisciplinary approach INCT-NANOFARMA, which is supported by São Paulo Research Foundation (FAPESP), Brazil (Grant #2014/50928-2), and

by National Council for Scientific and Technological (CNPq), Brazil (Grant # 465687/2014-8). The study was also received financial support from National Council for Scientific and Technological (Grant # 425448/2016-2). Carine Zuglianello received a doctoral scholarship from Coordination for the Improvement of Higher Education Personnel (CAPES), Brazil. The authors would like to thank the CEBIME/UFSC and LCME/UFSC for technical support in the circular dichroism and electron microscopy analysis, respectively.

Author Contributions

Carine Zuglianello conceived the ideas and performed all the experiments, data analysis, and writing of the original draft. Andrés Felipe Chamorro participated of the performance, analysis, and interpretation of DLS and fluorescence quenching studies. Vanessa Almeida de Oliveira participated of the performance, analysis, and interpretation of the circular dichroism experiments. Francisco H. Xavier participated of the performance, analysis, and interpretation of the ITC experiments. Elenara Lemos-Senna conceived the ideas. She was responsible for the project administration and funding acquisition.

References

1. Yuan, Y.; Li, Y.-B.; Tai, Z.-F.; Xie, Y.-P.; Pu, X.-F.; Gao, J.; *J. Food Drug Anal.* **2018**, *26*, 409.

2. Guerreiro, L. H.; Guterres, M. F. A. N.; Melo-Ferreira, B.; Erthal, L. C. S.; Rosa, M. da S.; Lourenço, D.; Tinoco, P.; Lima, L. M. T. R.; *AAPS PharmSciTech* **2013**, *14*, 1083.

3. Bader, A. R.; Li, T.; Wang, W.; Kohane, D. S.; Loscalzo, J.; Zhang, Y.-Y.; *J. Vis. Exp.* **2015**, *e52323*, 1.

4. Hay, D. L.; Chen, S.; Lutz, T. A.; Parkes, D. G.; Roth, J. D.; *Pharmacol. Rev.* **2015**, *67*, 564.

5. Tam, C. S.; Lecoultre, V.; Ravussin, E.; *Expert Opin. Biol. Ther.* **2011**, *11*, 1677.

6. Al-Keilani, M.; Alsmadi, D.; Darweesh, R.; Alzoubi, K.; *Clin. Pharmacol. Adv. Appl.* **2018**, *Volume 10*, 23.

7. Venkatanarayan, A.; Raulji, P.; Norton, W.; Chakravarti, D.; Coarfa, C.; Su, X.; Sandur, S. K.; Ramirez, M. S.; Lee, J.; Kingsley, C. V.; Sananikone, E. F.; Rajapakshe, K.; Naff, K.; Parker-Thornburg, J.; Bankson, J. A.; Tsai, K. Y.; Gunaratne, P. H.; Flores, E. R.;

Nature **2015**, *517*, 626.

8. Kimura, R.; MacTavish, D.; Yang, J.; Westaway, D.; Jhamandas, J. H.; *Mol. Neurobiol.* **2017**, *54*, 748.

9. Tao, Q.; Zhu, H.; Chen, X.; Stern, R. A.; Kowall, N.; Au, R.; Blusztajn, J. K.; Qiu, W. Q.; *J. Alzheimer's Dis.* **2018**, *62*, 597.

10. Bower, R. L.; Hay, D. L.; *Br. J. Pharmacol.* **2016**, *173*, 1883.

11. Wang, H.; Abedini, A.; Ruzsicska, B.; Raleigh, D. P.; *Biochemistry* **2014**, *53*, 5876.

12. Anselmo, A. C.; Gokarn, Y.; Mitragotri, S.; *Nat. Rev. Drug Discov.* **2019**, *18*, 19.

13. Henchey, L. K.; Jochim, A. L.; Arora, P. S.; *Curr. Opin. Chem. Biol.* **2008**, *12*, 692.

14. Zapadka, K. L.; Becher, F. J.; Gomes dos Santos, A. L.; Jackson, S. E.; *Interface Focus* **2017**, *7*, 20170030.

15. Perry, S. L.; McClements, D. J.; *Molecules* **2020**, *25*, 1161.

16. Yang, M.; Frokjaer, S.; In *Delivery Technologies for Biopharmaceuticals: Peptides, Proteins, Nucleic Acids and Vaccines*; John Wiley & Sons, Ltd: Chichester, UK, 2009; pp. 9–28.

17. Zhao, L.; Skwarczynski, M.; Toth, I.; *ACS Biomater. Sci. Eng.* **2019**, *5*, 4937.

18. Li, Y.; Wang, Y.; Huang, G.; Gao, J.; *Chem. Rev.* **2018**, *118*, 5359.

19. de la Fuente, M.; Csaba, N.; Garcia-Fuentes, M.; Alonso, M. J.; *Nanomedicine* **2008**, *3*, 845.

20. Kenley, R. A.; Tracht, S.; Stepanenko, A.; Townsend, M.; L'Italien, J.; *AAPS PharmSciTech* **2000**, *1*, 1.

21. Bai, C.; Lao, Z.; Chen, Y.; Tang, Y.; Wei, G.; *Front. Chem.* **2020**, *8*, 51.

22. Yu, M.; Every, H. A.; Jiskoot, W.; Witkamp, G.-J.; Buijs, W.; *J. Mol. Struct.* **2018**, *1156*, 320.

23. Wu, F.; Zhou, Z.; Su, J.; Wei, L.; Yuan, W.; Jin, T.; *Nanoscale Res. Lett.* **2013**, *8*, 197.

24. Csizmadia, P.; In *Proceedings of The 3rd International Electronic Conference on Synthetic Organic Chemistry*; MDPI: Basel, Switzerland, 1999; p. 1775.

25. ALV-Laser Vertriebsgesellschaft mbH; *ALV correlator software*; V.3.0.0.17 10/2002: Langen, DE, 2002.

26. Korchagina, E. V.; Philippova, O. E.; *Macromolecules* **2015**, *48*, 8622.

27. Sze, A.; Erickson, D.; Ren, L.; Li, D.; *J. Colloid Interface Sci.* **2003**, *261*, 402.

28. Collins, T. J.; *Biotechniques* **2007**, *43*, S25.

29. da Silva, D. C.; Fontes, G. N.; Erthal, L. C. S.; Lima, L. M. T. R.; *Biophys. Chem.* **2016**, *219*, 1.

30. Louis-Jeune, C.; Andrade-Navarro, M. A.; Perez-Iratxeta, C.; *Proteins Struct. Funct. Bioinforma.* **2012**, *80*, 374.

31. Jug, M.; Hafner, A.; Lovrić, J.; Kregar, M. L.; Pepić, I.; Vanić, Ž.; Cetina-Čižmek, B.; Filipović-Grčić, J.; *J. Pharm. Biomed. Anal.* **2018**, *147*, 350.

32. Xia, J.; Dubin, P. L.; In *Macromolecular Complexes in Chemistry and Biology*; Springer Berlin Heidelberg: Berlin, Heidelberg, 1994; pp. 247–271.

33. Mohtashamian, S.; Boddohi, S.; Hosseinkhani, S.; *Int. J. Biol. Macromol.* **2018**, *107*, 2730.

34. Frère, Y.; Danicher, L.; Muller, S.; In *Peptide Materials*; Alemán, C.; Bianco, A.; Venanzi, M., Eds.; John Wiley & Sons: Chichester (UK), 2013; pp. 385–415.

35. Umerska, A.; Corrigan, O. I.; Tajber, L.; *Carbohydr. Polym.* **2017**, *156*, 276.

36. Xia, L.-W.; Xie, R.; Ju, X.-J.; Wang, W.; Chen, Q.; Chu, L.-Y.; *Nat. Commun.* **2013**, *4*, 2226.

37. Khan, A.; El-Toni, A. M.; Alam, J.; Aldalbahi, A.; Ahmed, M.; Labis, J. P.; Ahamad, T.; Hezam, M.; *J. Nanomater.* **2018**, *2018*, 1.

38. Xu, A. Y.; Melton, L. D.; Jameson, G. B.; Williams, M. A. K.; McGillivray, D. J.; *Soft Matter* **2015**, *11*, 6790.

39. Hu, B.; Wang, S. S.; Li, J.; Zeng, X. X.; Huang, Q. R.; *J. Phys. Chem. B* **2011**, *115*, 7515.

40. Kamerzell, T. J.; Joshi, S. B.; McClean, D.; Peplinskie, L.; Toney, K.; Papac, D.; Li, M.; Middaugh, C. R.; *Protein Sci.* **2007**, *16*, 1193.

41. Lu, K.-Y.; Li, R.; Hsu, C.-H.; Lin, C.-W.; Chou, S.-C.; Tsai, M.-L.; Mi, F.-L.; *Carbohydr. Polym.* **2017**, *165*, 410.

42. Hadian, M.; Hosseini, S. M. H.; Farahnaky, A.; Mesbahi, G. R.; Yousefi, G. H.; Saboury, A. A.; *Food Hydrocoll.* **2016**, *55*, 108.

43. Cao, Y.; Fang, Y.; Nishinari, K.; Phillips, G. O.; *Sci. Rep.* **2016**, *6*, 23739.

44. Nonoyama, A.; Laurence, J. S.; Garriques, L.; Qi, H.; Le, T.; Middaugh, C. R.; *J. Pharm. Sci.* **2008**, *97*, 2552.

45. Bhattacharya, S.; Xu, L.; Thompson, D.; *ACS Chem. Neurosci.* **2019**, *10*, 2830.

46. Antonov, Y. A.; Zhuravleva, I. L.; Cardinaels, R.; Moldenaers, P.; *Food Hydrocoll.* **2018**,

74, 227.

47. Water, J. J.; Kim, Y.; Maltesen, M. J.; Franzyk, H.; Foged, C.; Nielsen, H. M.; *Pharm. Res.* **2015**, *32*, 2727.

48. Cort, J. R.; Liu, Z.; Lee, G. M.; Huggins, K. N. L.; Janes, S.; Prickett, K.; Andersen, N. H.; *Protein Eng. Des. Sel.* **2009**, *22*, 497.

49. Raimundo, A. F.; Ferreira, S.; Martins, I. C.; Menezes, R.; *Front. Mol. Neurosci.* **2020**, *13*, 35.

50. Zhang, L.; Furst, E. M.; Kiick, K. L.; *J. Control. Release* **2006**, *114*, 130.

51. Pechar, M.; Pola, R.; Laga, R.; Braunová, A.; Filippov, S. K.; Bogomolova, A.; Bednárová, L.; Vaněk, O.; Ulbrich, K.; *Biomacromolecules* **2014**, *15*, 2590.

52. Ristroph, K. D.; Prud'homme, R. K.; *Nanoscale Adv.* **2019**, *1*, 4207.

53. Patel, A.; Gaudana, R.; Mitra, A. K.; *J. Microencapsul.* **2014**, *31*, 542.

Supplementary Information

Dextran Sulfate/Pramlintide Polyelectrolyte Nanoparticles as a promising Delivery System: Optimization, evaluation of Supramolecular Interactions and effect on Conformational Stability of the Peptide Drug

Carine Zuglianello[a], Andrés F. Chamorro[b], Vanessa A. de Oliveira[c], Francisco H. Xavier Júnior[d], Elenara Lemos-Senna[e]*

[a,e]Departamento de Ciências Farmacêuticas, Programa de Pós-graduação em Nanotecnologia Farmacêutica, Universidade Federal de Santa Catarina, Campus Trindade, Florianópolis, SC, 88040-900, Brasil.

[b]Departamento de Química, Programa de Pós-graduação em Química, Universidade Federal de Santa Catarina, Campus Trindade, Florianópolis, SC, 88040-900, Brasil.

[c]Laboratório Central de Biologia Molecular e Estrutural, Universidade Federal de Santa Catarina, Campus Trindade, Florianópolis, SC, 88040-900, Brasil.

[d]Laboratório de Imunopatologia Keizo Asami, Universidade Federal de Pernambuco, Recife, Pernambuco, PE, 50670-901, Brasil.

email: lemos.senna@ufsc.br

*ORCID ID: https://orcid.org/0000-0002-3642-4468.

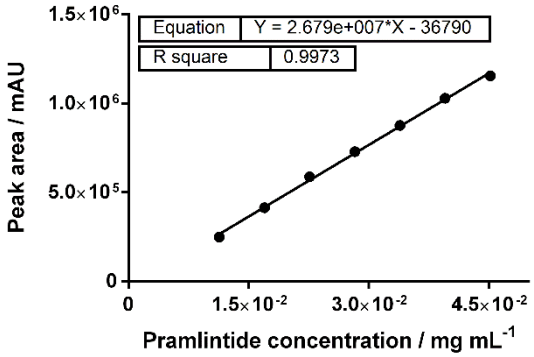

Figure S. 1. Calibration curve obtained to pramlintide by fluorescamine assay.

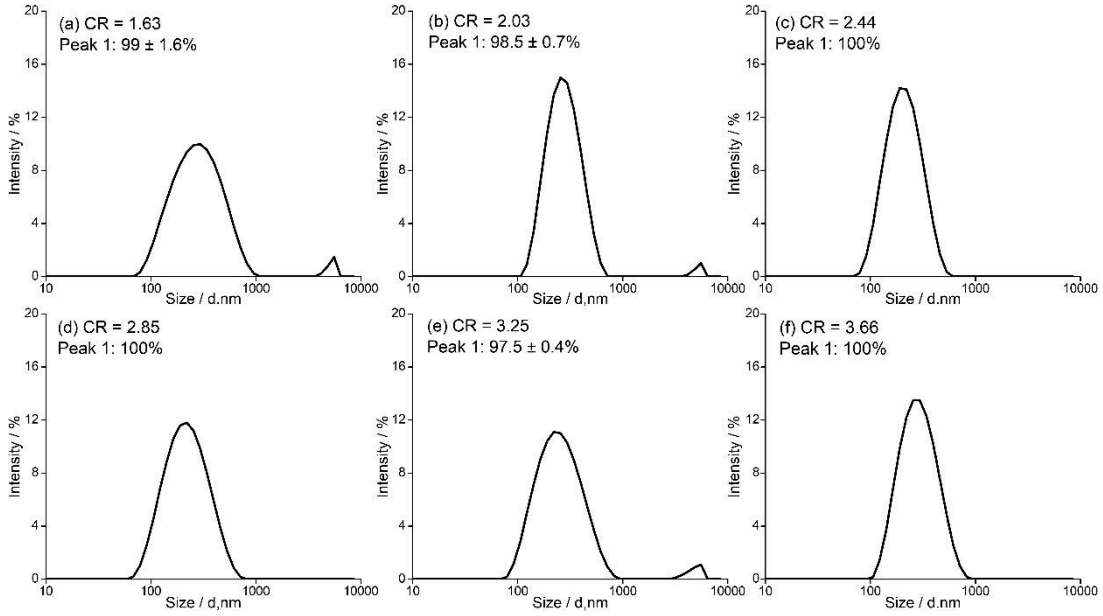

Figure S. 2. Intensity profile of particle size distribution obtained by dynamic light scattering at angle of 173° of three batches of DexS/Pram polyelectrolyte nanoparticles with a DexS to Pram charge ratio (CR) of of 1.63, 2.03, 2.44, 2.85, 3.25 and 3.66 DexS/Pram.

Investigation of DexS/Pram interactions

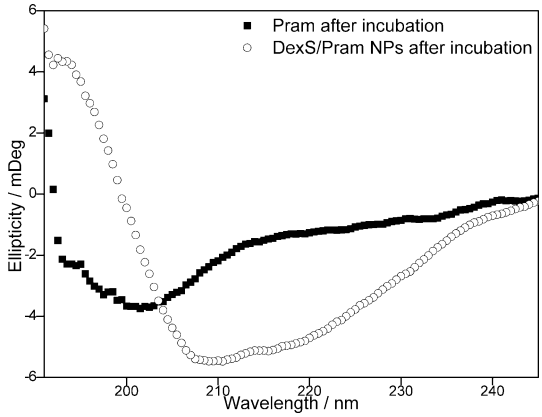

Figure S. 3. Circular dichroism profile of Pram and DexS/Pram NPs previously adjusted to pH 7.0 and incubated at 37° C for 24 hours (310.15 K, 86,400 s), diluted with ultrapure water (1:5, v/v) for analysis.

Colloidal behavior of DexS/Pram NPs in aqueous saline media

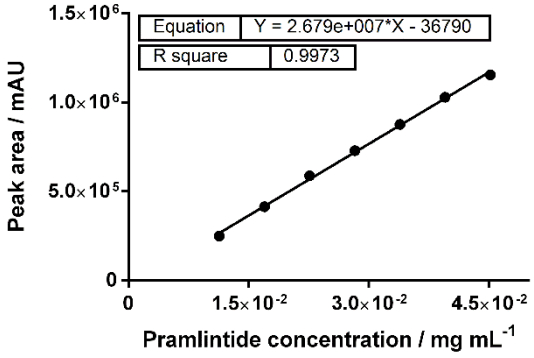

Figure S. 4. Calibration curve obtained to pramlintide by reversed phase liquid chromatography (Zorbax Eclipse Plus C18 column, 150 × 4.6 mm, 5 µm) with ultraviolet detection at 205 nm using linear gradient flux of 1.0 mL min^{-1} from 10 to 65% of A (acetonitrile:TFA 0.1%) in B (water:TFA 0.1%) over 25 minutes.

CAPÍTULO II – COMPLEXOS POLISSACARÍDEO/PEPTÍDEO ESTABILIZADOS AO REDOR DE GOTÍCULAS DE NANOEMULSÕES: UMA NOVA ESTRATÉGIA PARA ADMNISTRAÇÃO NASAL DA PRANLINTIDA

Nanopartículas de polieletrólitos permitem uma elevada associação de peptídeos terapêuticos, mas são geralmente pouco estáveis em fluidos biológicos (SANTALICES *et al.*, 2017). Como mostrado no Capítulo 1 desta tese, as nanopartículas de polieletrólitos constituídas de sulfato de dextrana e pranlintida foram instáveis em meio com força iônica semelhante aos fluidos biológicos. Conforme descrito na literatura, a adição de um terceiro componente carregado pode ser usada como estratégia para aumentar a estabilidade coloidal de nanopartículas de polieletrólitos em meios com elevada força iônica (MOTIEI *et al.*, 2020). (MOTIEI *et al.*, 2020). Então, duas espécies catiônicas, mono- e polivalente foram testadas nesse sentido, o brometo de cetiltrimetilamonio e o lactato de quitosana oligossacarídeo, para estabilização dos complexos de sulfato de dextrana/pranlintida em fluido nasal simulado (FNS). A utilização de tensoativo não-iônico, hidrossolúvel e combinação de tensoativos não-iônicos hidro/lipossolúvel foram igualmente testados com o intuito de estabilizar o complexo (*Apêndice A*). No entanto, a estratégia que se mostrou mais promissora foi a associação do complexo à superfície de nanoemulsões. Assim, este segundo capítulo descreve o uso desta estratégia para o aprimoramento das formulações com vistas à obtenção de um nanocarreador estável em condições fisiológicas para administração nasal da pranlintida. As formulações contendo pranlintida constituídas pelos complexos polieletrólito/peptídeo estabilizados ao redor de nanogotículas de uma emulsão foram preparadas, caracterizadas e avaliadas quanto as suas propriedades biofarmacêuticas. Os resultados obtidos são apresentados na forma de um artigo científico a ser submetido no *Journal of Drug Delivery Sciences and Technology*.

Manuscrito 2 – ***Polysaccharide/peptide complexes stabilized around nanoemulsion droplets: an application for nasal administration of pramlintide***

Polysaccharide/peptide complexes stabilized around nanoemulsion droplets: an application for nasal administration of pramlintide

Carine Zuglianello[a]; Nícolas G. M. Silva[b]; Elenara Lemos-Senna[a,b*]

[a]Pharmaceutical Nanotechnology Postgraduate Program, Federal University of Santa Catarina, Campus Trindade, Florianópolis, SC, 88040-900, Brazil

[b]Department of Pharmaceutical Sciences, Federal University of Santa Catarina, Campus Trindade, Florianópolis, SC, 88040-900, Brazil

[*]email*:* lemos.senna@ufsc.br; *ORCID ID: https://orcid.org/0000-0002-3642-4468*.

Abstract

Pramlintide (Pram) is a peptide drug approved by the FDA for the treatment of diabetes, used in combination with insulin. It has shown several potentialities in the treatment of obesity, Alzheimer´s disease, and cancer. Its complexation with dextran sulfate has previously shown to enable high drug payload in the obtention of dextran sulfate/pramlintide polyelectrolyte nanoparticles. However, these nanoparticles were not stable in biological fluids, losing their colloidal properties. Herein we proposed the development of a nanostructured system for intranasal administration in which the dextran sulfate/pramlintide complex was stabilized on the surface of the droplets of a nanoemulsion. The polyelectrolyte complexes-coated nanoemulsions (PEC-NEs) were prepared by spontaneous emulsification and characterized according to the particle size, zeta potential, and Pram content and association efficiency. Polyelectrolyte complexes were found to be adsorbed onto the o/w interface, displaying a particle size of about 150 nm and negative zeta potential. The PEC-NEs were stable after incubation with simulated nasal fluid (SNF) and after storage for 30 days. Nanostructured systems improved pramlintide mucus-diffusion and stability against trypsin degradation and provide a sustained permeation of the peptide drug across the nasal mucosa, which was probably dependent on the peptide release.

Keywords: pramlintide, polyelectrolyte complexes, nanoemulsions, nasal route, mucosa permeation

Introduction

Peptides of natural and synthetic sources are compounds involved in a wide range of biological functions. The interest of using peptides in therapeutics is mostly due to their advantageous biocompatibility and target selectivity over conventional drugs for the management of serious human diseases. However, even though their potential application in therapeutics, the clinical use of peptides has some drawbacks as their metabolic instability via protease degradation and undesirable pharmacokinetic properties. These drawbacks have motivated many researchers to pursue new approaches for administrating peptide drugs [1,2].

Pramlintide acetate is an antidiabetic drug commonly recommended as an adjunctive to patients who did not reach satisfactory glycemic control with insulin therapy. Pramlintide is

an analog of the human neuroendocrine peptide amylin, which is produced and secreted with insulin by the pancreatic β-cells. Pram differs from human amylin by the replacement of amino acids alanine, serine, and serine at positions 25, 28, and 29, respectively, by proline [3]. It mimics the glucoregulatory effects of amylin, which collectively limit postprandial glucose excursions. Clinical studies have demonstrated that pramlintide reduces postprandial glucose concentrations by modulating gastric emptying, preventing abnormal postprandial glucagon secretion, and increasing satiety which leads to a reduction in caloric intake [4,5]. Besides its antidiabetic properties, neuroprotective activities have also been described for this peptide drug [6,7].

Besides its antidiabetic activity, pramlintide also has shown other potentialities as anti-obesity [8], antitumoral [9,10], and anti-Alzheimer drug [6,7]. There are amylin receptors in various human organs, including the stomach and the brain [11]. Regulation of oxidative stress has already been reported for pramlintide and may contribute to its therapeutic activities [12]. Like most peptide or protein drugs, pramlintide is administrated by the parenteral route, twice, or three times a day, which represents an inconvenience for patients [13].

The nasal mucosa is an interesting alternative drug delivery route, especially for peptide drugs. The nose has a more permeable mucosal epithelium compared to other mucosal sites and offers the unique possibility of direct brain delivery due to the presence of trigeminal and olfactory nervous terminations in the nasal cavity [14,15]. To reach an efficient nasal absorption, drug delivery systems should provide a balance between bioadhesion and muco-diffusion, permeation, and distribution to a specific region, which may be tailored by the drug delivery system physicochemical characteristics like stability, lipophilicity, size, osmolarity, pH, viscosity and so on [16]. It was showed that nasal administration targets higher peptide amounts to the brain than intravenous administration, probably due to the comparable contribution of direct (nose-to-brain) and indirect (mucosal) transport pathways [17].

The use of nanoparticles as drug delivery systems has the potential to enhance peptide physicochemical and biological stabilities, control release, and improve mucosal permeation, allowing its administration by needle-free routes [18,19]. The use of organic solvents is a drawback of encapsulation methods to maintain peptide stability. Further, achieving a high drug payload is also difficult, contrasting to the natural ability to compartmentalize and stabilize the peptide in cellular cytosol. In this context, polysaccharides nanoparticles have a highlighted position compared to other systems [20]. Polysaccharides are complex biopolymers with several functionalities in drug delivery, including protection of the drug from the recognition

by the reticuloendothelial system, stabilization of macromolecules, increase in bioavailability and transport throw the binding mucosa [21]. Although the polysaccharide nanoparticles obtained by colloidal complexation generally enable utilization of brander processes and achievement of a satisfactory peptide loading, they are commonly overly labile to biological conditions, like pH and ionic strength. The strategies proposed in the literature to enhance the polysaccharide polyelectrolyte nanoparticles stability in biological medium commonly involve the addition of a crosslinker or another polyelectrolyte, which could lead to peptide displacement [22].

In a previous study, we developed dextran sulfate/pramlintide polyelectrolyte nanoparticles, assembled by non-covalent interactions between the cationic peptide and the polyanionic polysaccharide. Here we studied the association to a nanoemulsion as a strategy to the colloidal stabilization of peptide/polysaccharide complexes in nasal fluid and its influence on the mucus-interaction, enzymatic stability, and mucosal permeation of pramlintide.

Materials and methods

Materials

Pramlintide acetate (> 95.2%), was obtained from Genemed Syn (lot # 108695, Genemed Synthesis, Texas, USA). Dextran sodium sulfate (MW 40.000 Da, sulfur content between 15 – 19%), mucin from porcine stomach, fluorescamine (Fluram, BioReagent, suitable for fluorescence, ≥ 99.0%), medium-chain triglycerides (NEOBEE® 1053, Stepan, Illinois, USA), sorbitan monooleate (Span 80®), and polysorbate 80 (Tween 80®) were obtained from Sigma-Aldrich (São Paulo, Brazil). Acetonitrile (Honeywell) and trifluoroacetic acid HPLC grade was purchased from Navelab (Curitiba, Brazil). Glacial acetic acid, sodium acetate, sodium chloride, sodium hydroxide, monobasic and dibasic potassium phosphate, and all other solvents and reagents were analytical grade and were used without further purification. Stock solutions of pramlintide and dextran sulfate were prepared using ultrapure water (Milli-Q).

Preparation of DexS/Pram-coated nanoemulsions (PEC-NEs)

The polyelectrolyte complexes-coated nanoemulsions (PEC-NEs) were prepared by spontaneous emulsification, by vortexing for 3 minutes the polysaccharide/peptide complex (1.0 mL, obtained as previously described) with a mixture containing 26 µL of glycerol, 5.0 µL of medium-chain triglycerides, 1.0 µL of sorbitan monooleate, and 3.0 µL of polysorbate 80,

preheated at 37 °C. Finally, the pH of the PEC-NEs was adjusted to 4.5 ± 0.3, using NaOH or HCl 0.1 M. The PEC-$NE_{DexS/Pram}$ were prepared in triplicate and were stored at about 8 °C. For comparison purposes, uncoated nanoemulsions (uncoated-NE) and dextran sulfate-coated nanoemulsions (NE_{DexS}) were also prepared using the same conditions.

Particle size, pH and zeta potential

The hydrodynamic diameter and zeta potential of the PEC-NEs were determined by dynamic light scattering (DLS) and laser-Doppler anemometry, respectively, using a Zetasizer Nano Series (Malvern Instruments, Worcestershire, UK). The size analyses were performed at a scattering angle of 173°, after dilution of the samples in ultrapure water. For zeta potential analyses, the samples were placed in electrophoretic cells, where a potential of ±150 mV was established. Zeta potential values were calculated from the measured electrophoretic mobility using Smoluchowski's equation [23]. All samples were analyzed in triplicate. The pH of the nanoparticles was measured using an MS Tecnopon potentiometer previously calibrated with buffer solutions pH 4.0 and 7.0. The measurements were carried out in triplicate at a temperature of 25 °C.

Peptide content and association efficiency

The peptide content (mg/mL) in the PEC-NE was determined after complete dissolution of samples with DMSO (1:10, v/v), in an ultrasonic bath for 20 minutes. The samples were filtered through 0.22 μm PVDF syringe filters (Millipore, USA) prior to HPLC/UV analysis. The association efficiency (%) of Pram was estimated as being the difference between the total peptide concentration and free drug found in the dispersant phase of the PEC-NE. For that, the samples were submitted to ultrafiltration/centrifugation at 6000 rpm, using an Amicon Centrifugal Filter Device with Ultracel-100 membrane (100 kDa, Millipore Corp., USA). Pram was then quantified in the samples using an HPLC system equipped with an LC-20AD binary pump, CTO-20A oven, SPD-M20A 206 photodiode array detector (DAD), and software LC Solution 1.2 (Shimadzu, Japan). The analyses were performed in reverse-phase mode using a C18 column (Zorbax Eclipse Plus; 150 x 4.6 mm, 5 μm). The mobile phase consisted of an 0.1 % (v/v) trifluoroacetic acid solution (buffer A) and acetonitrile containing 0.1% (v/v) of trifluoroacetic acid (buffer B) eluted at a flow rate of 1.0 mL min^{-1} using the following gradient program: aqueous trifluoracetic acid 0.1 % (v/v) (buffer A) and acetonitrile-trifluoroacetic acid 0.1% (v/v) (buffer B), which was eluted at a linear

gradient from 10% to 65% of buffer B over 25 minutes. The injection volume was 20 µL and detection was achieved at the wavelength of 205 nm. The calibration plots for Pram were linear over the concentration range of 13.6 to 60.0 µg mL^{-1} (y = 5247.5x – 28475, r = 0.999). Limits of detection and quantification for Pram were 2.92 and 9.74 µg/mL, respectively. The HPLC/UV method demonstrated to be specific, precise, and accurate for determining Pram in the samples (R.S.D. < 5%).

Stability in simulated nasal electrolyte solution (SNES)

The stability of PEC-NE was evaluated by incubating the formulations in a simulated nasal electrolyte solution (SNES, 1:1, v/v) for 30 min at 37° C [24]. The samples were analyzed according to the particle size, zeta potential, and peptide content as described above.

Transmission electronic microscopy

PEC-NEs morphological characteristics were evaluated by transmission electron microscopy (TEM) in a JEM-1011 electron microscope (Jeol, Japan), operating at 100 kV. The nanoparticles were diluted in ultrapure water (1:5, v/v), dropped onto carbon-coated copper grids, which were left to dry for 10 minutes and negatively stained with 1% (w/v) phosphotungstic acid. The grids were left to dry under room temperature overnight before TEM visualization. The analysis was performed only on the selected nanodispersion.

Stability during storage and conformational drug stability

The stability of PEC-NE was evaluated after storage of the samples at a temperature of 8 °C for 30 days. The samples were analyzed according to the particle size, zeta potential, and peptide content as described above. Changes in the peptide structure after its association with the PEC- were evaluated by Fourier transformed infrared spectroscopy (FTIR) and circular dichroism (CD). FTIR analyses were performed on the PEC-NE previously freeze-dried, the powder raw materials were analyzed directly without any preparation process. Measurements were performed in an Agilent Cary 660 infrared spectrometer at the wavenumber range from 1000 to 2000 cm^{-1}. Second-derivative FTIR spectra were plotted. For CD analysis, PEC-NE was diluted in ultrapure water at 1:5 (v/v). Measurements were performed in a Jasco J-815 spectropolarimeter at 25 °C, at wavelength range 260–185 nm and cell length of 10 mm, a bandwidth of 1.0 nm, and a scan rate of 50 nm min^{-1}. Free Pram was used as controls and the data were expressed in terms of ellipticity (mDeg).

Mucus interaction and enzymatic degradation

The PEC-NE interaction with the mucin was evaluated by measuring the particle size after the addition of 100 µL of mucin suspension (1.0 mg/mL in SNES) to 10 µL of the nanoemulsions or respective drug solution. Samples were diluted in ultrapure water at 1: 10, v/v for the analysis. Mucus-diffusion studies were performed to evaluate the penetration ability of PEC-$NE_{DexS/Pram}$ by a mucus layer. This study was performed using an adapted microfilter device composed of a cell strainer (donor compartment) inserted in a well of a 6-well cell culture microplate (acceptor compartment) separated by a 0.45 µm cellulose ester membrane [25]. A 0.5 mg/mL mucin dispersion in SNES (pH 5.5) was deposited into the cell strainer, forming a mucus layer. The microplate well was prefilled with 5 mL of the SNES. Then, 200 µL the PEC-$NE_{DexS/Pram}$ or the free drug were carefully added to the devices and left to diffuse for 20 minutes, in a water bath at 37 °C. The enzymatic degradation was evaluated by incubating the Pram solution or the PEC-$NE_{DexS/Pram}$ in SNES added of trypsin (at 1:5, v/v, trypsin final concentration of 50 µg/mL) [26] for 15, 30, and 60 minutes. Samples were withdrawn, diluted with acetonitrile containing 0.1% of trifluoroacetic acid (1:1, v/v), centrifuged, filtered, and analyzed for peptide content by HPLC/UV as described previously. The results were expressed as a percentage of the total amount of peptide initially added (40 µg/mL and 60 µg/mL, respectively for mucus-diffusion and enzymatic degradation studies) and statistical analysis was performed by unpaired t-test and two-way ANOVA, followed by Sidak post-hoc, respectively, with a significance level of 5 %.

Permeation studies and histological examination of the porcine nasal mucosa

In vitro permeation studies were performed using a Franz vertical diffusion cell apparatus using porcine nasal mucosa as a membrane model. Porcine heads were obtained from a local slaughterhouse (Antonio Carlos, Brazil), sawed longitudinally, and soaked on phosphate saline buffer (PBS) for transportation to the laboratory. Fresh porcine nasal mucosa from the respiratory region was carefully removed, cleaned with PBS, and mounted on Franz diffusion cells with a diffusion area of 1.76 cm^2. The receptor compartment (11 mL) was filled with simulated nasal electrolyte solution (SNES, pH 5.5) and maintained under magnetic stirring and temperature of 37 °C during the experiments. The Franz cell system could equilibrate during 30 minutes prior to the running of the diffusion experiment. Following, 1000 µL of PEC-$NE_{DexS/Pram}$ or the respective peptide solution previously prepared at the same concentration and pH were applied at the donor compartment, which was further covered with an aluminum foil

cap. Samples were then withdrawn from the receptor compartment at periods of up to 10 h (2, 4, 6, 8 and 10 hours). The volume of the receptor compartment was immediately replaced by an equivalent volume of fresh medium. The samples were filtered through 0.22 µm cellulose acetate membrane (Allcrom®, USA) and analyzed by HPLC/UV. At the end of the permeation study, the mucosa was removed from the Franz cells, cleaned with gauze, and washed in distilled water, and weighed. The pramlintide retained in the mucosa was extracted by adding 3.0 mL of a mixture of acetonitrile:water:trifluoroacetic acid (65:35:1, v/v/v) followed sonication for 1 minute using an Ultrasonic Processor UP200S (Hielscher, Germany). The samples were filtered through 0.22 µm cellulose acetate membrane (Allcrom®, USA) and analyzed. The amount of peptide retained in the mucosa by surface area was then estimated. The HPLC/UV method was previously validated and demonstrated to be specific, precise, and accurate for determining Pram in the receptor medium and porcine mucosa (R.S.D. < 5%). All experiments were carried out in sextuplicate. The cumulative amount of the peptide permeated ($\mu g/cm^2$) through the nasal mucosa was plotted against time. Linear profiles (showing non-significant deviation from the linearity) were analyzed by linear regression to check their slope deviation from zero, corresponding to the flux. The results obtained for peptide retention were statistically analyzed by unpaired t-test with a significance level of 5%.

To evaluate the integrity of the porcine mucosa after the permeation studies, additional Franz cells were mounted with porcine nasal mucosa. Following, PEC-$NE_{DexS/Pram}$ and free Pram were applied at the donor compartment. After 4 h of permeation experiment, the mucosa was removed from the Franz cells. The tissue was embedded in paraffin and cut at 5 µm using a rotary microtome (RM 2145, Leica Co., Nussloch Germany). Sections were stained with hematoxylin and eosin and examined by light microscope (Olympus BX-51, Tokyo, Japan).

Results and discussion

Nanoparticles physicochemical characterization

DexS/Pram coated nanoemulsion (PEC-$NE_{DexS/Pram}$) showed a mean particle size of 130 ± 2 nm, potential zeta of -40 ± 1 mV, and drug association efficiency of 89 ± 4.9%. The NE-coating is found to occur by the non-competitive interaction between the amphiphilic peptide-helix and the oil droplet interface. Pram also interacts with the anionic DexS leading to the formation of the negatively charged particles. DexS-coated nanoemulsion (DexS-NE) and uncoated-NE showed mean sizes of 154 ± 2 nm and 162 ± 9 nm, and zeta potential of -28 ± 4

mV and -11 ± 1 mV, respectively. Some extent of coating might occur in the DexS-NE due to the presence of sodium ions (from dextran sulfate sodium salt) and the surface activity of DexS, despite the lack of electrostatic interactions. Sodium deoxycholate-polysorbate 80 interaction was already described to occur similarly, by the counterion binding [27]. The PEC-NE was obtained by a simple procedure, without toxic solvents or requirement of final steps of concentration.

PEC-NE was characterized according to its morphological properties by transmission electronic microscopy and compared with uncoated-NE (Fig. 1). Stability during 30 days of storage and conformational peptide stability was also evaluated (Table 1, Fig. 2).

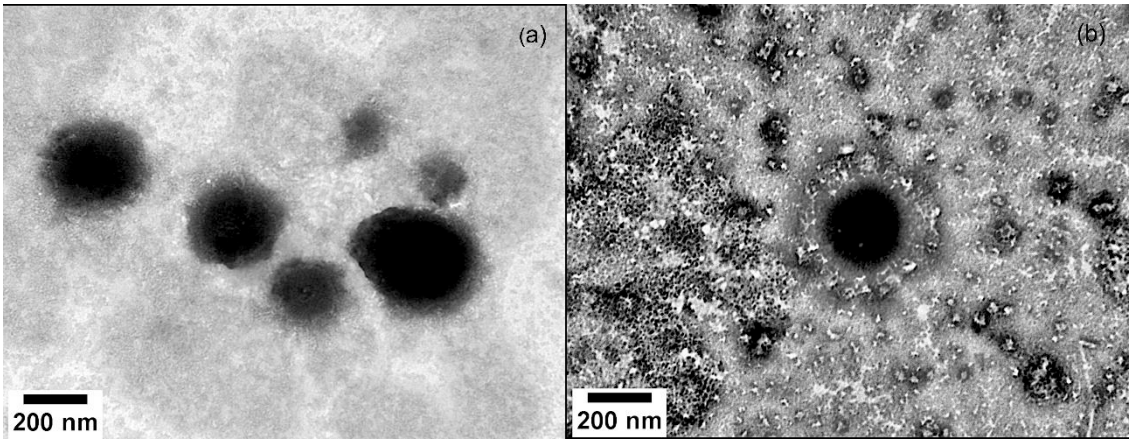

Fig. 1. Transmission electron microscopy of (a) uncoated-nanoemulsion (uncoated-NE, (b) Dextran sulfate/pramlintide coated-nanoemulsion (PEC-NEDexS/Pram). Scale bars are 200 nm.

Table 1 Storage stability of the nanodispersions in terms of size (nm), zeta potential (mV), and drug content (mg/mL) evaluated at 30th day.

NP ID[a]	Size (PdI[b]) nm		Zeta potential mV		Drug content mg/mL	
	1st day	30th day	1st day	30th day	1st day	30th day
Uncoated-NE	162 ± 9 (0.38)	Out of range	-11 ± 1	n.a[c].	n.a.	n.a.
DexS-NE	154 ± 2 (0.26)	154 ± 11 (0.32)	-28 ± 4	-41 ± 6	n.a.	n.a.
DexS/Pram NP	208 ± 20 (0.22)	Out of range	-33 ± 1	n.a.	n.a.	n.a.
PEC-NE$_{DexS/Pram}$	130 ± 19 (0.22)	156 ± 28 (0.36)	-40 ± 1	-45 ± 2	0.63 ± 0.03	0.52 ± 0.01

[a] NP ID: nanoparticle identification, [b] in parenthesis: polydispersion index, [c] n.a.: not applicable.

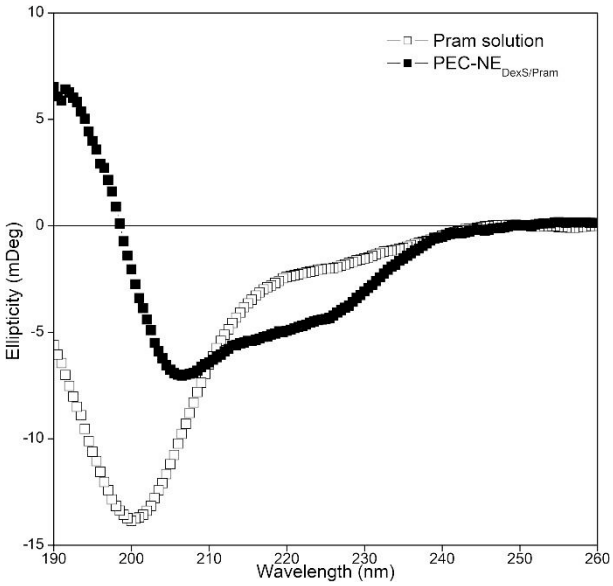

Fig. 2. Circular dichroism profiles obtained for the pramlintide solution (white squares) and the polyelectrolyte-coated nanoemulsion (PEC-NEDexS/Pram, black squares).

As observed in Figure 2, Pram changed its structure from a majorly random coil to α-helix in PEC-NE$_{DexS/Pram}$, as previously found to the DexS/Pram complex (see *Manuscript 1*). This result was expected for Pram, since it is known that amylin, which has an intrinsically disordered structure, folds as a helix at the cell membrane surface. This conformational change is not expected to affect Pram activity, since it corresponds to an amylin biological-like folding and its overstabilization was already suggested to inhibit the peptide misfolding [30].

Interactions of the formulations with mucin were evaluated by the particle size method and mucus-diffusion experiment (Table 2, Fig. 3a). A water-soluble fraction of the mucin dispersion (1.0 mg/mL in SNES, diluted 1:10 in ultrapure water) and its mixtures displayed bi- or trimodal particle size distribution profiles. Mean diameters obtained to mucin were 401 ± 124 nm (peak 1) and 60 ± 11 nm (peak 2), while to Pram/mucin mixture (1: 10, v/v) were of 700 ± 117 nm (peak 1) and 36 ± 12 nm (peak 2) and to Pram NE/mucin mixture (1: 10, v/v) were of 132 ± 21 nm (peak 1), 500 ± 174 nm (peak 2) and 62 ± 8 nm. Pram/mucin peak 1 value increased compared to mucin alone peak value, showing that Pram (positively charged) probably interacted with mucin (negatively charged), while PEC-NE/mucin peak 1 value might be related to the PEC-NE itself (negatively charged) or to the peak 2 of the mucin, showing lower interaction. Negatively charged nanoparticles as PEC-NE$_{DexS/Pram}$ were not expected to interact in a large extent with mucin, which is also negatively charged (net charge at pH 4.5), favoring their diffusion. DexS is also known to alter the thickness of the mucus layer, allowing the particles to penetrate [31]. Mucin carries positive patches in its chain, besides reactive

functional groups sialic acid, that can interact with the sulfate residues in the dextran sulfate chain by hydrogen-bonding. These interactions help to explain the mucoadhesive properties attributed to dextran sulfate in some studies. The mucoadhesive capacity was found to be influenced by the molecular weight and by the zeta potential, being more prominent to the high molecular weight-dextran sulfate (~500 kDa versus 40 kDa) and at more negative zeta potential [32].

On the other hand, Pram in solution is positively charged at pH 5.5 and may have been entrapped by the mucin gel or undergone aggregation in SNES-mucin, as verified by dynamic light scattering analyses. As the entire nasal mucus blanket is changed in about 20 minutes [33], a muco-diffusion capacity might favor the systemic and brain drug delivery after nasal administration [34]. Association to the PEC-NE protected Pram from trypsin degradation after 60 minutes incubation (Fig. 4b). However, degradation of the amino acid constituents is described to occur mainly in proline-containing peptides rather than by peptidase digestion [17].

Table 2 Interactions of PEC-NE and free Pram with mucin suspension evaluated by the particle size analysis.

Samples	**Peak 1 (nm)**	**Other peaks (nm)**
Mucin alone (control)	401 ± 124 [a]	60 ± 11 [b, c]
Mucin + Pram solution	700 ± 117	36 ± 12 [b, c]
Mucin + PEC-$NE_{DexS/Pram}$	132 ± 21 [b, c]	500 ± 174 [a] / 62 ± 8 [b, c]
PEC-$NE_{DexS/Pram}$ alone	130 ± 19 [(b), c]	absent

At the significance level of 0.05, the same letter-attributed means were NOT statistically different (two-way ANOVA, followed by Tukey post-hoc).

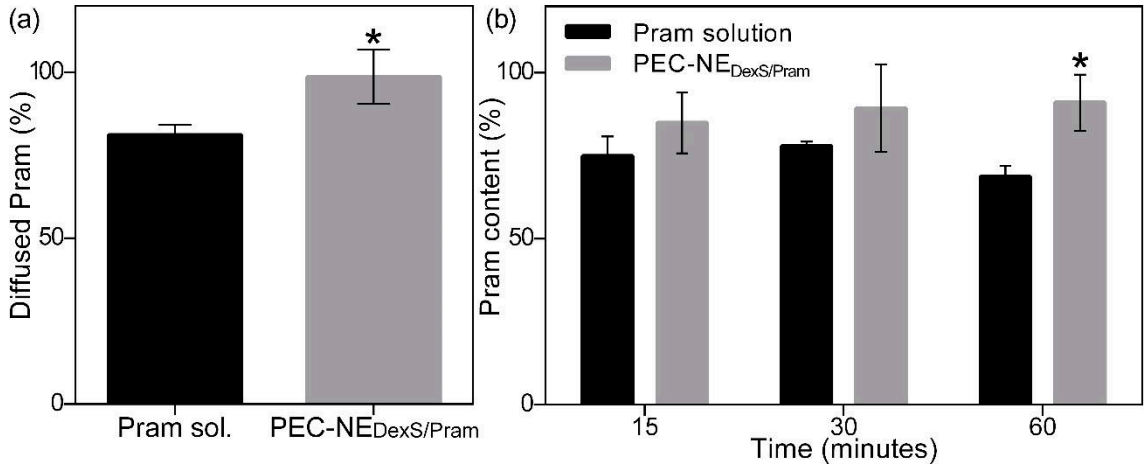

Fig. 3. (a) Mucus-diffusion percentual of pramlintide after application of the peptide solution and the polyelectrolyte-coated nanoemulsion (PEC-NEDexS/Pram). *At the significance level of 0.05, the Pram solution and PEC-NEDexS/Pram means were statistically different (unpaired t-test, $p < 0.05$). (b) Pramlintide percentual content after incubation with trypsin (at 0.5 mg/mL) for 15, 30 and 60 minutes. *At the significance level of 0.05 Pram sol. and PEC-$NE_{DexS/Pram}$ were statistically different at 60 minutes (two-way ANOVA, followed by Sidak post-hoc).

Permeation and retention results obtained for the free peptides and associated to PEC-NEs are shown in *Fig. 4*. The HPLC analytical method showed to be accurate and precise for the determination of Pram the receptor medium and nasal mucosa (data not shown). Earlier time points of the permeation study were out of range of the quantification method, then steady-state flux (J) and latency time (T_{lag}) could not be obtained. A suitable mathematical model could help to better understand the initial portion of these profiles and to obtain permeation parameters. While for free Pram (charge ≈ 3.9, log D ≈ -35 in the pH of the study) the permeation occurred in the first hours, for PEC-$NE_{DexS/Pram}$ a sustained permeation profile was observed (Fig. 4a, with a non-zero slope). Apparent permeability was higher for free Pram than for PEC-$NE_{DexS/Pram}$ in the first hours, although the total permeated amounts were similar (51.0 ± 2.0 and 58.5 ± 2.6 μg/cm^2, respectively from Pram solution and PEC-$NE_{DexS/Pram}$). Pram sustained permeation could be useful for maintaining the biological activity of this drug along the time, since it has a short half-life, and to give an opportunity to the peptide to reach the olfactory epithelium, in the roof of nasal cavity. Pram retention was not significantly affected by using the $PEC_{DexS/Pram}$ after 10 h of permeation study (10.6 ± 2.2 μg/cm^2 and 12.0 ± 0.9 μg/cm^2 for Pram solution and PEC-$NE_{DexS/Pram}$, respectively) (Fig. 4b). We suggest that although PEC-$NE_{DexS/Pram}$ can diffuse across the mucus reaching the nasal epithelium. Pram needs to be released from its complex and from the nanoemulsion to be absorbed through the tight junctions. DexS chain rigidity may have contributed to the subtle difference between the permeation profiles, but the bioavailability is expected to be influenced by the mucus-diffusion

and enzymatic stability, which were both improved by Pram association to the PEC-NE. H&E-stained microscopy images of nasal mucosal tissues exposed to Pram solution and PEC-$NE_{DexS/Pram}$ for 4 hours are shown in Fig. 6. While the mucosa treated with Pram solution appeared to be dry and damaged, the mucosa treated with PEC-$NE_{DexS/Pram}$ was hydrated and undamaged. Nanoemulsions formed a film under the mucosa, reducing water loss and dryness. No apparent toxic effect was observed.

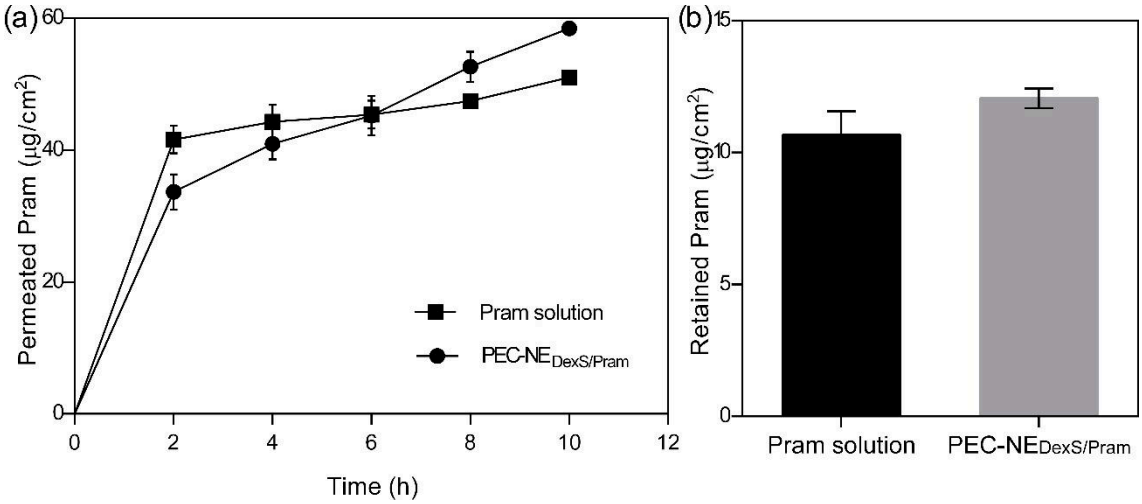

Fig. 4. Pramlintide (a) permeation and (b) retention profile in nasal swine mucosa, evaluated utilizing Franz diffusion cell and acceptor medium composed by simulated nasal electrolyte solution (SNES, pH 5.5), for 10 hours. Statistical analysis indicated a linear profile for PEC-$NE_{DexS/Pram}$ with a slope significantly different from zero, while for Pram solution the slope was not significantly different from zero. Analysis by unpaired t-test did not indicate any difference between retained to solution or PEC-NE_{DexS}/Pram (p-value > 0.05).

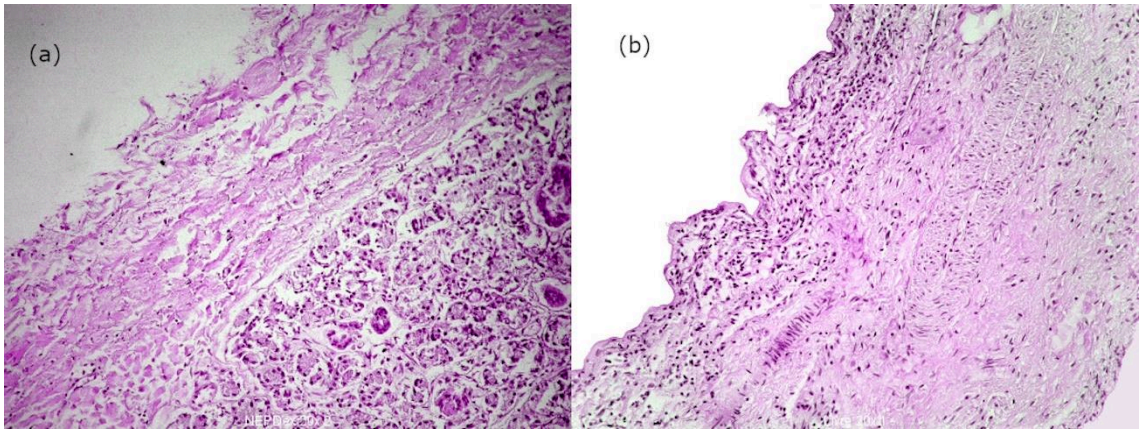

Fig. 5. Images of hematoxylin-eosin-stained nasal porcine mucosa obtained in 4 h of permeation studies after applying (a) PEC-NEDexS/Pram and (b) free Pram and at the donor compartment.

Conclusion

Polysaccharide/peptide polyelectrolyte complexes were successfully stabilized around nanoemulsion droplets by using green solvents and a low energy process. The association to a nanoemulsion improved the colloidal stability in biological fluids and during storage, favored pramlintide mucus-diffusion and stability against trypsin digestion. Furthermore, it tailored a slight sustained pramlintide permeation in the nasal mucosa, showing to be a potential system for intranasal pramlintide administration.

References

[1] D. Tesauro, A. Accardo, C. Diaferia, V. Milano, J. Guillon, L. Ronga, F. Rossi, Peptide-based drug-delivery systems in biotechnological applications: Recent advances and perspectives, Molecules. 24 (2019) 351. https://doi.org/10.3390/molecules24020351.

[2] L.Y. Filatova, D.M. Donovan, S.C. Becker, D.N. Lebedev, A.D. Priyma, H. V Koudriachova, A. V Kabanov, N.L. Klyachko, Physicochemical characterization of the staphylolytic LysK enzyme in complexes with polycationic polymers as a potent antimicrobial., Biochimie. 95 (2013) 1689–96. https://doi.org/10.1016/j.biochi.2013.04.013.

[3] L.H. Guerreiro, M.F.A.N. Guterres, B. Melo-Ferreira, L.C.S. Erthal, M. da S. Rosa, D. Lourenço, P. Tinoco, L.M.T.R. Lima, Preparation and characterization of PEGylated amylin., AAPS PharmSciTech. 14 (2013) 1083–97. https://doi.org/10.1208/s12249-013-9987-4.

[4] J. Pullman, T. Darsow, J.P. Frias, Pramlintide in the management of insulin-using patients with type 2 and type 1 diabetes, Vasc. Health Risk Manag. 2 (2006) 203–212. https://doi.org/10.2147/vhrm.2006.2.3.203.

[5] M.C. Riddle, Basal glucose can be controlled, but the prandial problem persists—it's the next target!, Diabetes Care. 40 (2017) 291–300. https://doi.org/10.2337/dc16-2380.

[6] R. Kimura, D. MacTavish, J. Yang, D. Westaway, J.H. Jhamandas, Pramlintide Antagonizes Beta Amyloid (Aβ)- and Human Amylin-Induced Depression of Hippocampal Long-Term Potentiation, Mol. Neurobiol. 54 (2017) 748–754. https://doi.org/10.1007/s12035-016-9684-x.

[7] Q. Tao, H. Zhu, X. Chen, R.A. Stern, N. Kowall, R. Au, J.K. Blusztajn, W.Q. Qiu, Pramlintide: The Effects of a Single Drug Injection on Blood Phosphatidylcholine Profile for Alzheimer's Disease, J. Alzheimer's Dis. 62 (2018) 597–609. https://doi.org/10.3233/JAD-170948.

[8] C.S. Tam, V. Lecoultre, E. Ravussin, Novel strategy for the use of leptin for obesity

therapy, Expert Opin. Biol. Ther. 11 (2011) 1677–1685. https://doi.org/10.1517/14712598.2011.619974.

[9] M. Al-Keilani, D. Alsmadi, R. Darweesh, K. Alzoubi, Pramlintide, an antidiabetic, is antineoplastic in colorectal cancer and synergizes with conventional chemotherapy, Clin. Pharmacol. Adv. Appl. Volume 10 (2018) 23–29. https://doi.org/10.2147/CPAA.S153780.

[10] A. Venkatanarayan, P. Raulji, W. Norton, D. Chakravarti, C. Coarfa, X. Su, S.K. Sandur, M.S. Ramirez, J. Lee, C. V. Kingsley, E.F. Sananikone, K. Rajapakshe, K. Naff, J. Parker-Thornburg, J.A. Bankson, K.Y. Tsai, P.H. Gunaratne, E.R. Flores, IAPP-driven metabolic reprogramming induces regression of p53-deficient tumours in vivo, Nature. 517 (2015) 626–630. https://doi.org/10.1038/nature13910.

[11] D.L. Hay, S. Chen, T.A. Lutz, D.G. Parkes, J.D. Roth, Amylin: Pharmacology, physiology, and clinical potential, Pharmacol. Rev. 67 (2015) 564–600. https://doi.org/10.1124/pr.115.010629.

[12] S. Patrick, R. Corrigan, J. Grizzanti, M. Mey, J. Blair, M. Pallas, A. Camins, H. Lee, G. Casadesus, Neuroprotective Effects of the Amylin Analog, Pramlintide, on Alzheimer's Disease Are Associated with Oxidative Stress Regulation Mechanisms, J. Alzheimer's Dis. 69 (2019) 157–168. https://doi.org/10.3233/JAD-180421.

[13] R.R. Rubin, M. Peyrot, Assessing treatment satisfaction in patients treated with pramlintide as an adjunct to insulin therapy, Curr. Med. Res. Opin. 23 (2007) 1919–1929. https://doi.org/10.1185/030079907X210804.

[14] T.L. Whateley, Drug delivery and targeting; for pharmacists and pharmaceutical scientists, J. Drug Target. 10 (2002) 637–637. https://doi.org/10.1080/1061186021000040848.

[15] E. Yuba, K. Kono, Nasal delivery of biopharmaceuticals, in: J. Das Neves, B. Sarmento (Eds.), Mucosal Deliv. Biopharm., Springer US, Boston (MA), 2014: pp. 197–220. https://doi.org/10.1007/978-1-4614-9524-6_8.

[16] F. Rodriguez-Otormin, A. Duro-Castano, I. Conejos-Sánchez, M.J. Vicent, Envisioning the future of polymer therapeutics for brain disorders, Wiley Interdiscip. Rev. Nanomedicine Nanobiotechnology. 11 (2019) e1532. https://doi.org/10.1002/wnan.1532.

[17] K. V. Shevchenko, I.Y. Nagaev, L.A. Andreeva, V.P. Shevchenko, N.F. Myasoedov, Stability of Proline-Containing Peptides in Biological Media, Biochem. Suppl. Ser. B Biomed. Chem. 13 (2019) 179–201. https://doi.org/10.1134/S1990750819030089.

[18] A.P. Jallouk, R.U. Palekar, H. Pan, P.H. Schlesinger, S.A. Wickline, Modifications of natural peptides for nanoparticle and drug design, in: R. Donev (Ed.), Adv. Protein Chem. Struct. Biol., Waltham (MA), 2015: pp. 57–91. https://doi.org/10.1016/bs.apcsb.2014.12.001.

[19] D. Bobo, K.J. Robinson, J. Islam, K.J. Thurecht, S.R. Corrie, Nanoparticle-based medicines: a review of FDA-approved materials and clinical trials to date, Pharm. Res.

33 (2016) 2373–2387. https://doi.org/10.1007/s11095-016-1958-5.

[20] W.C. Blocher McTigue, S.L. Perry, Protein encapsulation using complex coacervates: what nature has to teach us, Small. 16 (2020) 1907671. https://doi.org/10.1002/smll.201907671.

[21] T.G. Barclay, C.M. Day, N. Petrovsky, S. Garg, Review of polysaccharide particle-based functional drug delivery, Carbohydr. Polym. 221 (2019) 94–112. https://doi.org/10.1016/j.carbpol.2019.05.067.

[22] I. Santalices, A. Gonella, D. Torres, M.J. Alonso, Advances on the formulation of proteins using nanotechnologies, J. Drug Deliv. Sci. Technol. 42 (2017) 155–180. https://doi.org/10.1016/j.jddst.2017.06.018.

[23] A. Sze, D. Erickson, L. Ren, D. Li, Zeta-potential measurement using the Smoluchowski equation and the slope of the current–time relationship in electroosmotic flow, J. Colloid Interface Sci. 261 (2003) 402–410. https://doi.org/10.1016/S0021-9797(03)00142-5.

[24] M. Jug, A. Hafner, J. Lovrić, M. Lusina Kregar, I. Pepić, Ž. Vanić, B. Cetina-Čižmek, J. Filipović-Grčić, In vitro dissolution/release methods for mucosal delivery systems, ADMET DMPK. 5 (2017) 173. https://doi.org/10.5599/admet.5.3.425.

[25] J. Grießinger, S. Dünnhaupt, B. Cattoz, P. Griffiths, S. Oh, S.B.I. Gómez, M. Wilcox, J. Pearson, M. Gumbleton, M. Abdulkarim, I. Pereira De Sousa, A. Bernkop-Schnürch, Methods to determine the interactions of micro- and nanoparticles with mucus, Eur. J. Pharm. Biopharm. 96 (2015) 464–476. https://doi.org/10.1016/j.ejpb.2015.01.005.

[26] K. Langer, M.G. Anhorn, I. Steinhauser, S. Dreis, D. Celebi, N. Schrickel, S. Faust, V. Vogel, Human serum albumin (HSA) nanoparticles: Reproducibility of preparation process and kinetics of enzymatic degradation, Int. J. Pharm. 347 (2008) 109–117. https://doi.org/10.1016/j.ijpharm.2007.06.028.

[27] M.E. Haque, A.R. Das, S.P. Moulik, Mixed micelles of sodium deoxycholate and polyoxyethylene sorbitan monooleate (Tween 80), J. Colloid Interface Sci. 217 (1999) 1–7. https://doi.org/10.1006/jcis.1999.6267.

[28] Y. Zhang, B. Newton, E. Lewis, P.P. Fu, R. Kafoury, P.C. Ray, H. Yu, Cytotoxicity of organic surface coating agents used for nanoparticles synthesis and stability, Toxicol. Vitr. 29 (2015) 762–768. https://doi.org/10.1016/j.tiv.2015.01.017.

[29] A. V. Filippov, G. Gröbner, O.N. Antzutkin, Aggregation of amyloid Aβ(1-40) peptide in perdeuterated 2,2,2-trifluoroethanol caused by ultrasound sonication, Magn. Reson. Chem. 48 (2010) 427–434. https://doi.org/10.1002/mrc.2596.

[30] R.W. Woody, Circular Dichroism of Intrinsically Disordered Proteins, in: Instrum. Anal. Intrinsically Disord. Proteins, John Wiley & Sons, Inc., Hoboken, NJ, USA, 2010: pp. 303–321. https://doi.org/10.1002/9780470602614.ch10.

[31] M.E. V. Johansson, J.K. Gustafsson, K.E. Sjöberg, J. Petersson, L. Holm, H. Sjövall, G.C. Hansson, Bacteria Penetrate the Inner Mucus Layer before Inflammation in the Dextran Sulfate Colitis Model, PLoS One. 5 (2010) e12238.

https://doi.org/10.1371/journal.pone.0012238.

[32] B. Menchicchi, J.P. Fuenzalida, A. Hensel, M.J. Swamy, L. David, C. Rochas, F.M. Goycoolea, Biophysical Analysis of the Molecular Interactions between Polysaccharides and Mucin, Biomacromolecules. 16 (2015) 924–935. https://doi.org/10.1021/bm501832y.

[33] X. Duan, S. Mao, New strategies to improve the intranasal absorption of insulin., Drug Discov. Today. 15 (2010) 416–27. https://doi.org/10.1016/j.drudis.2010.03.011.

[34] E. Samaridou, H. Walgrave, E. Salta, D.M. Álvarez, V. Castro-López, M. Loza, M.J. Alonso, Nose-to-brain delivery of enveloped RNA - cell permeating peptide nanocomplexes for the treatment of neurodegenerative diseases, Biomaterials. 230 (2020) 119657. https://doi.org/10.1016/j.biomaterials.2019.119657.

Supplementary information

Methods

Particle size by laser diffraction

The particle size of PEC-NEs was also measured by laser diffraction (Malvern Mastersizer 2000, Malvern Instruments Ltd., UK) using the Hydro SM dispersion unit after appropriated dilution of the samples with ultrapure water to achieve an obscuration value between 0.5% and 1%. Particle size and size distribution were obtained by applying the Mie scattering theory using refractive indexes supplied by the Mastersizer 2000 software´s database.

Fluorescence microscopy of PEC-NEs

PEC-$NE_{DexS/Pram}$ was also examined by fluorescence microscopy. For that, Nile Red and fluorescamine were added directly to the PEC-$NE_{DexS/Pram}$. The sample was vortex during 30 s and then left to rest to allow the excess of the stains to settle. A drop of the stained PEC-$NE_{DexS/Pram}$ was deposited on a glass slide and viewed under a BX-41 Olympus microscope at 400× magnification, using red and blue filters. Images were captured by a digital color camera (QImaging, 3.3 mpixel, QCapture Pro 5.1 software).

Results

Mean diameter sizes (*D 4,3*) obtained by laser diffraction were nearby to the values obtained by dynamic light scattering (*Z-average*), being respectively 142 nm (*Span* of 1.44) to PEC $NE_{DexS/Pram}$, showing a monomodal profile. DexS-coated NE and showed a mean diameter size of 141 nm (*Span* of 1.41). While uncoated NE showed a micrometric size value by this technique (*D 4,3* of 6880 nm with *Span* of 1.12). The laser diffraction technique is more sensitive to determine particle sizes at the micrometric range, which causes more laser obscuration, then nanometric particles are not detected. The monomodal particle size distribution at nanometric range obtained by laser diffraction is an indicative of the good quality of the samples.

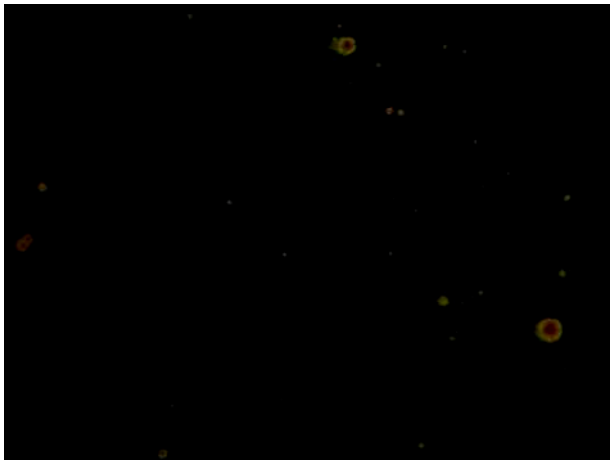

Fig. S. 1. Fluorescence microscopy of PEC-$NE_{DexS/Pram}$ added of Nile Red (oil droplet, red) and fluorescamine (green), which reacts with the primary amine of the peptide.

CAPÍTULO III – EFEITO NEUROPROTETOR DE NANOEMULSÕES REVESTIDAS COM COMPLEXOS DE SULFATO DE DEXTRANA/PRANLINTIDA ADMINISTRADAS POR VIA NASAL

A pranlintida têm demonstrado efeitos interessantes no tratamento do Alzheimer em estudos pré-clínicos, como melhora do desempenho em testes de memória e cognição, aumento de enzimas antioxidantes, diminuição de marcadores inflamatórios e diminuição do conteúdo cerebral de Aβ insolúvel (ADLER *et al.*, 2014; ZHU, H. *et al.*, 2015; KIMURA *et al.*, 2017; MOHAMED *et al.*, 2017; PATRICK *et al.*, 2019). Alguns efeitos aparentemente não desejáveis, que precisam ser melhor compreendidos foram demonstrados, como elevação da β-secretase (BACE-1) (PATRICK *et al.*, 2019) e ɣ-secretases e dos gangliosídeos 1 e 2, além de elevação do conteúdo de Aβ não-solúvel no cérebro de animais TgSwDI, modelo para angiopatia amiloide cerebral e DA (MOUSA *et al.*, 2020).

Neste estudo, diferentemente dos trabalhos que avaliaram a atividade da pranlintida no tratamento do Alzheimer anteriormente citados, propusemos a administração do fármaco veiculado em um nanocarreador, por via nasal. Com a administração nasal é sugestionado que a pranlintida diminua sua distribuição para os tecidos periféricos e aumente sua distribuição no cérebro. A associação ao nanocarreador foi planejada com a intenção de manter a integridade da molécula nos fluidos biológicos e na mucosa no local de administração, aumentar a mucodifusão pela presença do sulfato de dextrana, com atividade mucolítica (SUDO; BOYD; KING, 2000b), e aumentar a interação com a mucosa pelo aumento da área superficial, que é uma propriedade conferida pela nanoescala (NISTOR, 2014).

Assim, este terceiro capítulo é dedicado à avaliação dos efeitos do tratamento nasal com pranlintida livre e associada ao nanocarreador na dose de 100 µg/kg/dia, em camundongos com modelo de doença de Alzheimer, induzido pela administração intracerebroventricular (i.c.v.) do peptídeo $A\beta_{1-42}$. O estresse oxidativo foi avaliado em estruturas cerebrais de camundongos submetidos a um pré-tratamento nasal com pranlintida livre ou associada ao nanocarreador. Além disso, foram realizados testes comportamentais de desempenho de memória e aprendizado (a partir do 9° dia de tratamento), assim como a mensuração de proteínas sinápticas presentes no hipocampo e no córtex pré-frontal de camundongos tratados durante um período de 14 dias. Os resultados são apresentados na forma de um artigo em redação a ser submetido no *Journal of the Alzheimer's Disease*.

Manuscrito 3 – ***Intranasal administration of dextran sulfate/pramlintide polyelectrolyte complex-coated nanoemulsions restores cognitive impairment induced by β-Amyloid peptide oligomers in an animal model of Alzheimer´s disease***

Intranasal administration of dextran sulfate/pramlintide polyelectrolyte complex-coated nanoemulsions restores cognitive impairment induced by β-Amyloid peptide oligomers in an animal model of Alzheimer´s disease

Zuglianello, C.[a] França, A. P.[b] de Souza, B. S.[c], Agnes, J. P.[c], Zanotto-Filho[c], A. Prediger, R. D. S.[c], Lemos-Senna, E.[*a]

[a]Department of Pharmaceutical Sciences, Pharmaceutical Nanotechnology Postgraduate Program, Center of Health Sciences, Federal University of Santa Catarina, Florianópolis, SC, Brazil

[b]Pharmacy Postgraduate Program, Center of Health Sciences, Federal University of Santa Catarina, Florianópolis, SC, Brazil

[c]Department of Pharmacology, Pharmacology Postgraduate Program, Center of Biological Sciences, Federal University of Santa Catarina, Florianópolis, SC, Brazil

*email: lemos.senna@ufsc.br

*ORCID ID: https://orcid.org/0000-0002-3642-4468

Abstract

Pramlintide has shown potential benefits in the treatment of Alzheimer disease. Herein we investigated the effects of fourteen-days intranasal dextran sulfate/pramlintide complex coated-nanoemulsion against the damages caused by intracerebroventricular injection of $A\beta_{1-42}$ oligomers to swiss male mice. Behavioral tasks were checked from the ninth to the thirteenth days after the Aβ oligomers-injection. In the object relocation, modified Y-maze, and sucrose splash tests, the Aβ-oligomers´ injection provoked a reduction in the exploration of the relocated object, the number of the entries and time spent in the novel arm, and longer latency to start to grooming and reduction of the time spent for doing the grooming, respectively, compared to the control group. Their levels of the postsynaptic protein PSD-95 were diminished in the prefrontal cortex. The inspective activity was restored in the animals treated with the intranasal but not the intraperitoneal pramlintide solution. Neither the hedonic nor the self-caring patterns were influenced by the treatment. The PSD-95 levels in the prefrontal cortex did not change, regardless of the treatment. Animals that received the dextran sulfate/pramlintide coated-nanoemulsion intranasally had the spatial memory and inspective activity restored, besides had a trend in the restoring of the reference memory. Nanoemulsion might have acted by increasing the drug bioavailability in the brain. Evaluation of the biodistribution and chronic toxicity are essential to consider intranasal-administered pramlintide and pramlintide-loaded nanocarriers to the treatment of Alzheimer´s disease.

Keywords: pramlintide, dextran sulfate, nanocarrier, amyloid-β, Alzheimer

INTRODUCTION

Pramlintide is an amylin analog, approved by the FDA for the treatment of diabetes mellitus (DM) types 1 and 2. Its use is recommended to patients who did not reach a goal glycemic control with insulin therapy, mainly in the post-prandial period. Pramlintide solubility was increased and its amylogenesis was reduced, by changing the Ala-25, Ser-28 and Ser-29 amylin amino acids by proline [1]. It acts by decreasing the velocity of gastric emptying, decreasing the post-prandial secretion of glucagon, and inducing a satiety sense by interaction with amylin-neuropeptide hypothalamic receptors [2,3]. Due to the capacity of amylin and its derivatives to form amyloid aggregates its role in the Alzheimer´s disease (AD) was not

completely clear yet. However, both beneficial [4] and harmful [5] effects of pramlintide in AD were already suggested by researchers.

The increasing number of older people in the world is reflected by increasing cases of dementia. According to the World Health Organization (WHO), nowadays nearly 50 million people live with memory impairment. Alzheimer´s disease (AD) is the commoner form of dementia and usually causes poor health conditions in the elderly. The medicines currently available are not effective in prevent its progression, acting solely in the relief of the symptoms [6,7]. The deposition of Aβ and the appearance of neurofibrillary tangles are considered as the major AD biomarkers. Generally, extensive cell damage and cell death has already occurred before the diagnostic, because of the insidious emergence of the symptoms [8,9].

In preclinical researches, the treatment with pramlintide or amylin (usual dose of 200 µg/kg/day, during 4 – 10 weeks) has been showing to cause memory and cognitive improvements in several AD transgenic animal models like SAMP-8 [10], 5xFAD [11–13] and 3xTgAD [11] and in the albino rat, induced to AD symptomatology by the intracerebroventricular injection of streptozotocin [14], mainly on the object recognition [10,14], Morris-Water Maze (MWM) [11–13] and Y-maze [11] behavioral tests. Reduction of oxidative stress and inflammation biomarkers like as HO-1 and COX-2 in the hippocampus [10] and Iba-1 and CD68 [11,12], increase on synaptic protein synaptophysin [10] and post-synaptic protein PSD-95 [13], as like as reduction of cerebral levels of Aβ and *p*-tau [11–13] have been also reported. When different doses of amylin (200, 400 and 800 µg/kg/day) were evaluated in the 5xFAD mice [13], responses were found to be dose-dependent (*U-shaped* profile) and authors concluded that amylin has neuroprotective effects in physiological concentrations, but at higher concentrations, it might acquire some toxic activities.

A lower pramlintide daily dose (6 µg/day) [4], delivered by an osmotic mini-pump, by a longer time (18 weeks), in the transgenic APP/PS1 mice, led to memory improvement in the MWM, reduction of the brain Aβ levels and increase on antioxidant enzymes (HO-1, GP-x and MnSOD) in the hippocampus and also increase on ADAM-10 in the hippocampus and in the cortex. Furthermore, it was reported an unexpected increase in the BACE-1 (amyloidogenic β-secretase) in the hippocampus suggesting that pramlintide might act by a generalized enzymatic response, associated to efflux of Aβ only where it is actively depositing.

The intranasal route has been attracting attention for drug delivery due to the recognition of the nose-to-brain pathway by the olfactory neuroepithelium. The effectiveness

of the treatment of some central nervous diseases might be improved by the utilization of the intranasal route. Neuropeptides are involved in various regulatory mechanisms and biological activities, including neurotransmission, having a great potential to treat brain diseases. The major drawbacks are related to effectively deliver peptide drugs to the brain and circumvent systemic exposure. The abundance of peptidases in the nasal mucosa limits the peptide-drugs transport from the nose to distal brain regions. Furthermore, sustained release and enhanced bioavailability are required for the treatment of many diseases. Biodegradable nanoparticles those can attach and protect peptides from degradation the potential for improving the safety and efficacy of neuropeptide drugs. Nonetheless, large nanoparticles are less likely to be transported by the olfactory pathway [8,9,15].

In a previous study, we have developed a new drug delivery system based on self-assembling of dextran sulfate and pramlintide and this complex stabilization around nanoemulsion droplets (PEC-$NE_{DexS/Pram}$). The assembling with DexS increased the Pram α-helical content, stabilizing the peptide in a bioactive form, while the association of the complex to the nanoemulsion allowed to maintain the integrity of the complex in presence of physiological ionic strength conditions (see *manuscript 2*). Here, we evaluate the effect of 14-day treatment with pramlintide associated or not to the nanocarrier by the nasal route in an Alzheimer animal model induced by intracerebroventricular injection of Aβ oligomers to Swiss male mice. Behavioral tests were carried out from day 9 to 13, after Aβ intracerebroventricular injection. The neuroprotective effect of the pretreatment (15 min before the Aβ injection) was also evaluated by determining the oxidative stress biomarkers in the hippocampus and prefrontal cortex of the animals. Moreover, pre-synaptic (SNAP-25) and post-synaptic (PSD95) proteins involved on Alzheimer, were assayed in mice prefrontal cortex and hippocampus synaptosomes.

METHODS

Materials

Pramlintide acetate (> 95.2%) was obtained from Genemed Syn (lot # 108695, Genemed Synthesis, Texas, USA). Dextran sodium sulfate (MW 40.000 Da, sulfur content between 15 – 19%), fluorescamine (Fluram, BioReagent, suitable for fluorescence, ≥ 99.0%), sorbitan monooleate (Span 80®), polysorbate 80 (Tween 80), amyloid $Aβ_{1-42}$ peptide (lot #

SLBZ690), phenylmethylsulphonyl fluoride (PMSF), pepstatin, leupeptin, anti-mouse IgG HRP linked (1: 2,500, v/v), anti-rabbit IgG HRP linked (1: 2,500, v/v), anti-PSD95 clone 3H 4.3 (lot # MABN1194, 1: 2,000, v/v), anti-SNAP25 (lot # S9684, 1: 25,000), mouse anti-β-actin (1:50,000, v/v) and Immobilon® Forte were obtained from Merck (São Paulo, Brazil). Isoflurane (BioChimico, lot 008870) was obtained from a local hospital supplier. Acetonitrile (Honeywell®) and trifluoroacetic acid (JT Backer®) were HPLC grade. Ultra-purified water was obtained from the MilliQ® system. Glacial acetic acid, bovine serum albumin, sodium chloride, potassium chloride, calcium chloride, glycerin, Percoll®, polyacrylamide, Tris hydrochloride, Ponceau, methanol, isopropanol, sodium dodecyl sulfate, ammonium persulfate (APS), tetramethyl ethylenediamine (TEMED), bromophenol, copper sulfate, sodium potassium tartrate, sodium carbonate, Folin-Ciocalteu, and all other solvents and reagents were analytical grade and were used without further purification.

Preparation of Pram solutions

Pramlintide solution at 1.2 µg/mL was prepared in acetic acid 1.0 mM and maintained at -20 °C in microcentrifuge tubes until its use. For intranasal administration, Pram solution was diluted 1: 1, v/v in ultrapure water. For the intraperitoneal administration the prediluted solution (10 µL) was completed with 90 µL of saline to reach a volume of 100 µL.

Preparation and characterization of PEC-NE$_{DexS/Pram}$

Dextran sulfate/pramlintide polyelectrolyte complex (PEC$_{DexS/Pram}$) was obtained by polyelectrolyte titration, as previously described (manuscript 1 ref.). Briefly, a 500 µL of a Pram solution (1.2 µg/mL, pH ~ 4.0) was added dropwise to a 0.6 µg/mL DexS solution under constant magnetic stirring (Multistirrer 15, Velp Scientifica, Italy) at room temperature to obtain complex with a DexS/Pram molar ratio of 4.0×10^{-2}. The polyelectrolyte complex-coated nanoemulsion (PEC-NE$_{DexS/Pram}$) was prepared by spontaneous emulsification, by vortexing for 3 minutes the DexS/Pram complex (1.0 mL) with a mixture containing 26 µL of glycerol, 5.0 µL of medium-chain triglycerides, 1.0 µL of sorbitan monooleate, and 3.0 µL of polysorbate 80, preheated at 37 °C. Finally, the pH of the PEC-NE$_{DexS/Pram}$ was adjusted to 4.5 ± 0.3, using NaOH or HCl 0.1 M. A dextran sulfate-coated nanoemulsion (referred to as NE$_{DexS}$)

was prepared using the same procedure, but the drug was omitted, it was used as a control in the *in vivo* studies. The PEC-$NE_{DexS/Pram}$ and NE_{DexS} were characterized according to the particle size and zeta potential by dynamic light scattering (DLS) and laser-Doppler anemometry, respectively, using a Zetasizer Nano Series (Malvern Instruments, Worcestershire, UK), after appropriate dilution of the samples in ultrapure water (1:500, v/v). Particle size of PEC-NEs was also measured by laser diffraction (Malvern Mastersizer 2000, Malvern Instruments Ltd., UK) using the Hydro SM dispersion unit after appropriated dilution of the samples with ultrapure water to achieve an obscuration value between 0.5% and 1%. The particle size and size distribution were obtained by applying the Mie scattering theory using refractive indexes supplied by the Mastersizer 2000 software´s database.

Determination of Pram content and association efficiency

The Pram content (mg/mL) in the PEC-$NE_{DexS/Pram}$ was determined after the complete dissolution of samples with DMSO. The association efficiency (%) of Pram was estimated as being the difference between the total peptide concentration and free drug found in the dispersant phase of the formulations, obtained after ultrafiltration/centrifugation at 6000 rpm, using an Amicon Centrifugal Filter Device with Ultracel-100 membrane (100 kDa, Millipore Corp., USA). The Pram was quantified in the samples using a previously validated HPLC/UV method in a Shimadzu HPLC system (Shimadzu, Japan). The analyses were performed in reverse-phase mode using a C18 column (Zorbax Eclipse Plus; 150 × 4.6 mm, 5 µm). The mobile phase consisted of an 0.1 % (v/v) trifluoroacetic acid solution (buffer A) and acetonitrile containing 0.1% (v/v) of trifluoroacetic acid (buffer B) eluted at a flow rate of 1.0 mL/min using the following gradient program: aqueous trifluoracetic acid 0.1 % (v/v) (buffer A) and acetonitrile-trifluoroacetic acid 0.1% (v/v) (buffer B), which was eluted at a linear gradient from 10% to 65% of buffer B over 25 minutes. The injection volume was 20 µL and detection was achieved at the wavelength of 205 nm. The retention time of Pram using these conditions was 15.2 minutes.

Animals

Male Swiss three-month-old mice (45 - 50 g, N = 106) were supplied by the animal facility of the Federal University of Santa Catarina. The animals were kept in a light-controlled

room (12-hour-light-dark cycle) at a room temperature of 21 ± 1 °C and 60±10% humidity. Food and water were given *ad libitum*. All experimental procedures were performed in at least two independent groups. The experiments were carried out following the recommendations of the *Guide for the Care and Use of Laboratory Animals* of the National Institutes of Health and approved by the local Institutional Ethics Committee for Animal Research (CEUA/UFSC, protocol number PP00161/CEUA).

Aβ-oligomer preparation and administration

Aβ-oligomers were produced by incubating 0.1 mg of $A\beta_{1-42}$, dissolved in dimethyl sulfoxide (5.0 µL) and diluted with phosphate saline buffer pH 7.4 (PBS, 84.5 µL) for 4 days at 37 °C. At the administration time, Aβ dispersion was again diluted with PBS (84.5 µL) to reach a final concentration of 133 µM. A volume of 3 µL of the Aβ-oligomers or PBS were administrated to isoflurane anesthetized-animals by intracerebroventricular (i.c.v.) infusion (0.1 µL/s), utilizing an infusion syringe pump (Insight, EFF 311, Brazil) and a Hamilton syringe (25 µL) with its needle attached to a custom-made catheter. The needle was free-handedly inserted into a virtual point located at 1 mm right and 1 mm posterior from to the bregma (coordinates from bregma anteroposterior = −0.1 mm, mediolateral = 1 mm, and dorsoventral = −3 mm) and the infusion pump was started on [16].

Treatments

Animals were divided in six groups of 10 animals each, which received the following treatments:

(I) PBS (i.c.v) plus PBS (i.n.) (negative control);
(II) Aβ oligomers (i.c.v) PBS (i.n.) (positive control);
(III) Aβ oligomers (i.c.v.) plus pramlintide solution (i.n.);
(IV) Aβ oligomers (i.c.v.) plus pramlintide solution (i.p.);
(V) Aβ oligomers (i.c.v.) plus NE_{DexS} (i.n.); and
(VI) Aβ oligomers (i.c.v.) plus PEC-$NE_{DexS/Pram}$ (i.n.).

Intranasal treatments (pramlintide dose of 100 µg/kg/day) were administered to awakened and gently immobilized animals [17]. By using a micropipette with an extralong tip,

10 µL of Pram solution or nanoemulsions (NE_{DexS} and PEC-$NE_{DexS/Pram}$) were dripped to the animal's nostril letting to be spontaneously sucked. For intraperitoneal treatment, Pram solution (10 µL) was diluted in saline 0.9% (w/v) to reach a volume of 0.1 mL and administrated with an insulin syringe with a 30 G needle. For oxidative stress evaluation, treatments were proceeded 15 minutes before i.c.v. infusion to intranasally treated groups. For behavioral tests, treatments were administered immediately and 3 h after the i.c.v. infusion (two doses on the 1st day) and maintained once a day until the 13th day to each group (I to VII). These protocols were based on previous group publications [18,19]. Figure 1 summarizes the study timeline. Animals were euthanized on the 14th day.

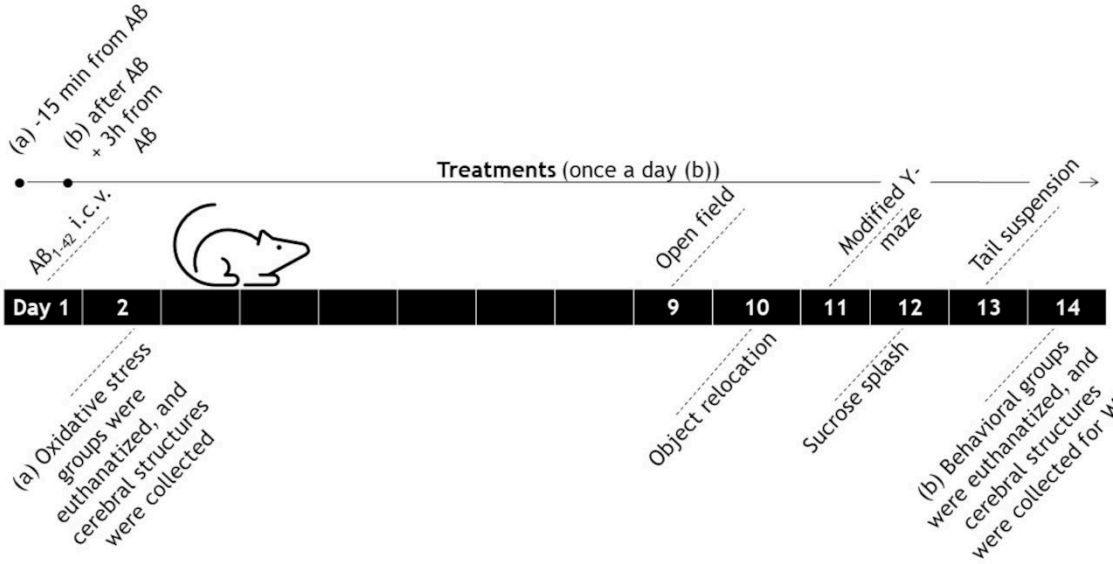

Fig. 1. Study timeline for oxidative stress (a) and behavioral (b) tests in animal Alzheimer model.

Evaluation of biochemical markers of the oxidative stress

After 24 h from Aβ infusion and intranasal treatment, animals (n = 6) were euthanized by decapitation under isoflurane sedation. The hippocampus and prefrontal cortex were dissected and immediately frozen in liquid nitrogen. Eppendorf tubes, containing the structures were maintained in an ultra-freezer (at -80 °C) until the analysis. For the analysis [20], brain structures were homogenized in 1.5 mL of 10 µL of PBS pH 7.4, containing 10 µL of PMSF and centrifuged at 10,000 × g for 15 min at 4 °C. The supernatant was withdrawn to different tubes, to avoid freezing and thawing cycles, and stored at -80 °C. Protein quantification was performed by the Lowry method.

Thiobarbituric acid reactive substances (TBARS)

Endogenous lipoperoxidation was estimated by TBARS assay, according to described by Draper and Hadley (1990). Protein was precipitated from the samples (~ 5 mg protein) by adding trichloroacetic acid at 10% (v/v) and centrifuging at 10,000 × g for 15 min. Obtained supernatants were reacted with thiobarbituric acid in an acid-heating medium. The pink Schiff base (malondialdehyde) formed was read spectrophotometrically at 532 nm. Lipid peroxidation was expressed as malondialdehyde levels (µg/mg protein).

Sulfhydryl (thiol)

Protein aliquot (0.1 to 0.2 mg) was diluted in 10 mM of PBS buffer (180 µL) added of 100 mM of boric acid buffer (35 µL, containing 0.2 mM EDTA, pH 8.5). Blank and sample were reacted with 10 µL of 5'5-dithiobis (2-nitrobenzoic acid) (DTNB) by 1 h at room temperature. Reading was performed spectrophotometrically at 412 nm [22]. Thiol content was calculated against n-acetylcysteine standard curves and expressed as nmol R-SH nM/mg protein.

Behavioral tests

Each group (n = 10 per group) was implied in the behavioral tests carried out and scored in an observation sound-attenuated room under low-intensity light (12 lx). Animals were previously habituated for at least 1 h in the testing room, between 9:00 and 14:00 h. A video camera positioned above the apparatuses was utilized to monitor the animal's behavior. The videos were analyzed with the ANY Maze video tracking system (Stoelting Co., Wood Dale, IL, USA). To avoid odor clues the apparatus was cleaned with a hydroethanolic solution (30% v/v) between each animal entry.

Open field: spontaneous locomotor activity (9th day)

Spontaneous locomotor activity was evaluated for 15 minutes in an open field square arena (50 × 50 × 40 cm). During the first 5 min, the total time spent in the center zone (aversive zone) and total distance traveled was recorded.

Object relocation: short term spatial memory (10th day)

Animals were subjected to a prior training section for 5 minutes, in the open field arena with two identical objects aligned in the center. For the testing section, 90 minutes after the training, one object was relocated toper or downer in the arena. Both during the training and the testing, the time that animals sniffed, whisked or looked to the objects from no more than 1 cm away were accounted within 5 minutes. Animals that did not explore more than 3 s total for both objects were excluded from the experiments. The discrimination index was calculated as follows:

$$DI = \frac{time\ exploring\ the\ relocated\ object\ -\ time\ exploring\ the\ unmoved\ object}{time\ exploring\ the\ relocated\ object\ +\ time\ exploring\ the\ unmoved\ object}$$

Modified Y-maze: short term spatial memory/learning (11th day)

Animals were subjected to a prior training section, for 8 minutes, in the Y-maze apparatus (composed of three arms at 120°, 41 cm long, 15 cm high, and having a 50-cm-wide floor). Mice were placed in one of the arms, facing to the center of the apparatus and left to explore this arm and another one opened arm. During the training, the third arm was closed with a removable door. The blocked arm varied between animals. For the testing section, 180 minutes from the training, every maze arm was opened. The number of entries and the time spent in each arm were recorded for 8 minutes. Entry into an arm was defined as the placement of all four paws into it.

Sucrose splash: anhedonic and self-care behavior (12th day)

Animals were placed individually in a Plexiglas box (9 × 7 × 11 cm) and a solution of sucrose 10% (w/v) was sprayed on the back coat of them. The time that mice take to start grooming (grooming latency) and the total time mice spent doing it (duration of grooming) were recorded.

Tail suspension: immobility and depression-like behavior (13th day)

Mice were suspended 50 cm above the floor by an adhesive tape glued 1 cm from the top of their tail. The time they stay immobile was recorded for 6 minutes.

Synaptic proteins analysis

On the 14th day, animals were euthanized by decapitation under isoflurane sedation. The hippocampus and prefrontal cortex were dissected and immediately frozen in liquid nitrogen. Eppendorf tubes, containing the structures were maintained at -80 °C until the analysis. The content of synaptic proteins in the prefrontal cortex and hippocampus of animals previously submitted to the behavioral tests were extracted [23,24].

Synaptosomes extraction

Samples of hippocampus and prefrontal cortex, maintained in an ice bath, were homogenized with cold sucrose solution – composed of sucrose (320 µM), sodium EDTA (1.0 mM), HEPES (10 mM), and BSA (1.00 mg mL^{-1}), to reach 10 mL. Then samples were centrifuged at 3,000 x g at 4 °C, the supernatants were maintained and centrifuged again at 14,000 × g for 12 min at 4 °C. Supernatants were discarded and pellets were resuspended in microcentrifuge tubes containing 1 mL of Percoll® at 45% (v/v, in Krebs-HEPES Ringer, KHR (140 mM NaCl, 1 mM EDTA, 10 mM HEPES, 5 mM KCl, 5 mM glucose) plus NaCl (67 mM). Samples were centrifuged at 16,000 × g for 2 min, at 4 °C. The top layer was collected and resuspended in 1.0 mL of KHR solution. Once again samples were centrifuged at the same conditions. Supernatants were discarded and pellets were resuspended in 50 µL of RIPA (10

mM Tris-HCl pH 7.4, 100 mM NaCl, sodium deoxycholate, 1%, Triton-X 100, 1%) added of proteases and phosphatase inhibitor cocktail (Sigma-Aldrich, Brazil) plus PMSF at 1.0 mM.

Protein assay and standardization

Total protein content in the samples was measured against an albumin analytical curve using the Peterson-modified Lowry method [25]. Protein standardization was proceeded by diluting the samples in ultrapure water and adding the sample buffer 6× (10.3% SDS, w/v, 30% glycerol, v/v, 500 mM Tris-HCl, pH 7.0, 0.012% bromophenol blue, w/v, 30% β-mercaptoethanol, v/v) at 1: 6. Samples were heated at 70 °C in a water bath, for 20 min, following instructions from the antibody's manufacturer before being added to the gels.

Electrophoresis in polyacrylamide gels

The resolving gel was prepared at 14% (v/v) of polyacrylamide (2.7 mL of ultrapure water, 4.7 mL of acrylamide/bis at 30% (w/v), 2.5 mL of 1.5 M Tris-HCl buffer, pH 8.8; 0.1 mL of SDS solution at 10% w/v, 0.1 mL of freshly prepared APS solution at 10% w/v and 5 µL of TEMED). This mixture was added between two glasses properly mounted on a specific device, to occupy a 1.5 mm thicker space and form a layer of about 7.5 cm in height. A thin layer of isopropanol was added to remove any air bubbles and the mixture was let to polymerize. Isopropanol was discarded and a layer of about 1 cm of the stacking gel (at 4% of polyacrylamide – 6.1 mL of ultrapure water, 1.3 mL of acrylamide/bis at 30% (w/v), 2.5 mL of Tris-HCl buffer at 0.5 M, pH 6.8; 0.1 mL of SDS solution at 10%, w/v, 0.1 mL of APS and 10 µL of TEMED) was added over the resolving gel. A 15-wells comb was inserted into the stacking gel mixture. After polymerization, four gels were immersed on the running buffer (Tris base 0.30% and glycine 1.44%, w/v, prepared from the Tris-glycine buffer at 10×) inside the electrophoretic unit. A standard molecular weight (Rainbow RPN800V, Amersham) was applied on the first well of each gel and samples were applied on the other wells (at a volume of 13.4 or 20 µL, depending on the protein concentration). The electrophoretic system was started on and the gel was let to run at 80 V for about 10 minutes and at 120 V for about 45 min. For the electro-transference, the nitrocellulose membranes were activated by immersion in ultrapure water for 2 min and then kept in the transfer solution (Tris-glycine/methanol buffer – prepared from the Tris-glycine buffer 10× added of methanol 10% v/v final concentration) for 30 min. The electro-transference unit was mounted as described following: the equipment

was wetted with distilled water, the inferior electrode was covered by two layers of wetted filter paper, the pre-wetted membranes were put over the filter paper and the gels were put over them and covered with more two layers of wetted filter paper and finally the unit was closed. The transference was proceeded at 180 mA, 30 mV for 90 min. Membranes were colored with Ponceau, for 2 – 5 min and washed with water. Membranes were let to dry and stored at -20 °C until the immunodetection assays.

Immunodetection

For the immunodetection membranes were incubated and washed under horizontal agitation with TBS-T-based solutions (Tris-buffered saline-Tween 0.1%, v/v, prepared from the TBS 10 × solution – 20 mM Tris-HCl, 137 mM NaCl, pH 7.6). The primary and secondary antibodies were diluted at the manufacturer-specified concentrations. Firstly, 5% BSA, w/v (blocking solution) was added and left for 1 h, primary antibody was left throughout the night (at 4 °C), pure TBS-T was cycling-exchanged for 15 min (three washing cycles) and finally, the secondary antibody was left for 2 h (at room temperature). Membranes were revealed by the enhanced chemiluminescence reactive (Immobilon® Forte, Sigma Aldrich), added for 5 – 10 min, 1.0 mL/membrane, and visualized in a ChemiDoc MP system (Bio-Rad). Membranes were reprobed and tested for β-actin immunoreactivity as a loading control. The optical density of Western blot bands was quantified using Image Lab™ software version 2.0.1 (Bio-Rad).

Statistical analysis

The experimental data were analyzed by descriptive statistics, unpaired t-test (between negative PBS i.c.v.: PBS i.n. (-) and positive Aβ i.c.v.: PBS i.n. (+) control groups), one sample t-test (discrimination index, entries in the novel arm and time spent in the novel arm) and one-way ANOVA with Dunnett post-hoc test whether applicable (against Aβ i.c.v.: PBS i.n. (+)). Outliers were identified and removed following the Grubbs test ($\alpha = 0.05$). Results were reported as statistically different at $\alpha = 0.05$ (*) in the figures and at $\alpha = 0.1$, only in the discussion. Some behavioral tasks had specific inclusion/exclusion rules, cited in the task description.

RESULTS

Nanoemulsions characterization

Physicochemical characteristics found to PEC-NEs in terms of mean particle size, zeta potential, drug loading, and association efficiency are described in *Table 1*. Further, the PEC-$NE_{DexS/Pram}$ showed a mean diameter of 142 ± 5.6 nm, by laser diffraction, while the diameter of 90% of the particles by number was below 112 ± 1 nm by this technique. DexS-coated nanoemulsion was named as NE_{DexS} (the drug is absent).

Table 1. Physicochemical characteristics of nanoemulsions in terms of mean particle size, zeta potential, drug loading, and association efficiency.

Nanoemulsion	Mean particle size (nm) (PdI)	Zeta potential (mV)	Drug loading (mg/mL)	Association efficiency (%)
PEC-$NE_{DexS/Pram}$	130 ± 19 (0.22)	-45 ± 2	0.63 ± 0.03	>99
NE_{DexS}	154 ± 2 (0.26)	-41 ± 6	n.a.	n.a.

n.a.: not applicable.

Oxidative stress

Data obtained in the oxidative stress analyses (sulfhydryl and TBARs, Figure 2a and 2b) did not show statistically significant differences between treated groups in the hippocampus. In the prefrontal cortex the $A\beta_{1-42}$ treated animals (positive control) showed lower MDA levels than animals that have received PBS, and treated groups did not show any significant difference compared to the positive or negative controls (one-way ANOVA).

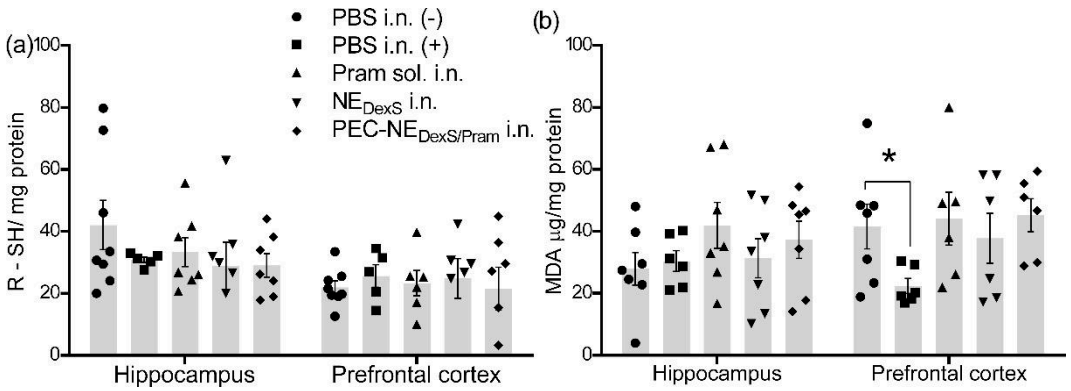

Fig. 2. (a) Sulfhydryl reactive species expressed as thiol/mg of protein (b) thiobarbituric acid reactive species converted in malondialdehyde, in the hippocampus and prefrontal cortex of Alzheimer model animals induced by intracerebroventricular injection of $A\beta_{1-42,}$ which received two doses of the treatments. Data are mean ± S.E.M (n=5-7/group). (a) At the 0.05 level the population means of [PBS i.c.v.: PBS i.n.] and [Aβ i.c.v.: PBS i.n.] are

NOT significantly different (unpaired t-test with two-tailed p value, $t_{(8)}$ = 0.2466 and 0.7475, p = 0.8115 and 0.4762). No significant difference was found between the treatment groups at the 0.05 level (one-way ANOVA), in the hippocampus, $F_{(4,23)}$ = 0.09566, p = 0.9828 or in prefrontal cortex, $F_{(4,21)}$ = 1.115, p = 0.3759.(b) At the 0.05 level population means of [PBS i.c.v.: PBS i.n.] and [Aβ i.c.v.: PBS i.n.] are NOT significantly different in the hippocampus (unpaired t-test with two-tailed p value, $t_{(8)}$ = 0.1064, p = 0.9179). At the 0.05 level population means of [PBS i.c.v.: PBS i.n.] and [Aβ i.c.v.: PBS i.n.] are significantly different in the prefrontal cortex (unpaired t-test with two-tailed p value, $t_{(11)}$ = 2.606, p = 0.0244). No significant difference was found between the treatment groups at the 0.05 level (one-way ANOVA), in the hippocampus ($F_{(4,25)}$ = 0.9117, p = 0.4724) or in the prefrontal cortex ($F_{(4,25)}$ = 1.905, p = 0.1409).

Behavioral tests

In the open field test, statistical analyses (unpaired t test, PBS i.c.v.: PBS i.n. *vs* Aβ i.c.v.: PBS i.n.) indicated that intracerebroventricular injection of $A\beta_{1-42}$ did not alter spontaneous locomotor activity ($t_{(15)}$ = 0.5795; p = 0.5708) and the time spent in the center zone of apparatus ($t_{(14)}$ = 0.8851; p = 3910). When evaluating the effect of different treatments after $A\beta_{1-42}$ injection, one-way ANOVA revealed no significant difference between the experimental groups neither in the total distance travelled [$F_{(4, 37)}$ = 0.41063; p = 0.79981] nor in the time spent in the center in the open field [$F_{(4, 35)}$ = 0.83783; p = 0.51053] (Figure 3).

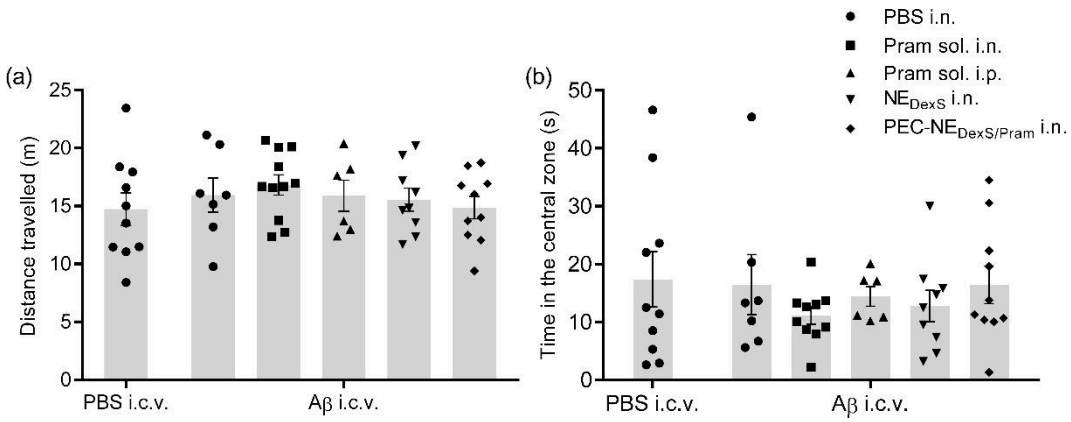

Fig. 3. (a) Total distance traveled (m) and (b) time in the center zone in the open field test by Alzheimer model animals induced by intracerebroventricular injection of $A\beta_{1-42}$ and submitted to intranasal treatments for 14 days. Data are means ± S.E.M (n=9-12/group). (a, b) At the 0.05 level the population means of [PBS i.c.v.: PBS i.n.] and [Aβ i.c.v.: PBS i.n.] are NOT significantly different (unpaired t-test). (a, b) No significant difference was found between the experimental groups submitted to the Aβ injection, neither in the total distance travelled [$F_{(4, 37)}$ = 0.4640; p = 0.7617] nor in the time spent in the center in the open field [$F_{(4, 41)}$ = 0.5325; p = 0.7126] (one-way ANOVA).

During the training session of the object relocation task (Figure 4a) the animals tested did not exhibit a preference for any object. In the test session (Figure 5a), one-sample t-test (compared to the theoretical value of zero) showed that negative control group [PBS i.c.v.: PBS i.n.] was able to recognize the relocated object ($t_{(5)}$ = 3.645, p < 0.05), as indicated by the

positive score (0.2950 ± 0.08094, mean ± S.E.M.). Intracerebroventricular injection of $A\beta_{1-42}$ lead to impairment in the short-term spatial memory, once animals from positive control group [Aβ i.c.v.: PBS i.n.] were unable to recognize the relocated object during the test session ($t_{(5)}$ = 0.1288, p = 0.9025). Our results demonstrated that pramlintide associated to the nanocarrier administrated intranasally restored the damage caused by the administration of Aβ, increasing the discrimination index ($t_{(8)}$ = 2.776; $p < 0.05$), while pramlintide solution administrated intranasally showed a tendency to restore the damage ($t_{(9)}$ = 2.161, p = 0.0590), being different at $\alpha = 0.1$ significance level, Figure 5a. One-way ANOVA applied to evaluate the effects of treatments after Aβ injection did not reveal significant differences between the analyzed groups [$F_{(4, 34)}$ = 0.96961, p = 0.43685].

Regarding modified Y-maze task (training section data in the Figure 4b and c and test data in the Figure 5b, c and d), intracerebroventricular injection of $A\beta_{1-42}$ did not alter the locomotor activity during the test session, indicated by the total entries in the arms (unpaired t test, PBS i.c.v.: PBS i.n. *vs* Aβ i.c.v.: PBS i.n.; $t_{(15)}$ = 0.8575; p = 0.4047). Subsequent one-way ANOVA demonstrated that animal groups did not differ by the total number of entries in the maze arms [$F_{(4, 39)}$ = 0.58535; p = 0.67511], showing that every group had similar chances to choose the "novel" arm in the test. When evaluating the inspective behavior (Figure 5c), one-sample t-test (compared to theoretical value of 33.33%) showed that the animals from negative control group [PBS i.c.v.: PBS i.n.] spent more time investigating the novel arm ($t_{(8)}$ = 2.259; $p < 0.05$). Intracerebroventricular injection of $A\beta_{1-42}$ led to impairment in the inspective behavior, as evidenced by the diminishing number of entries in the novel arm ($t_{(6)}$ = 2.115; p = 0.0789), Figure 5c. In addition, one-sample t-test indicated that administration of pramlintide solution i.n. ($t_{(10)}$ = 3.243; $p < 0.05$), NE_{DexS} i.n. ($t_{(8)}$ = 2.550; $p < 0.05$) and PEC-$NE_{DexS/Pram}$ i.n.($t_{(10)}$ = 6.387; $p < 0.05$), restored the inspective behavior in the modified Y maze task test session, increasing the entries in the novel arm (%).

Considering the time spent in the novel arm (Figure 5d), the negative control group [PBS i.c.v.: PBS i.n] recognized the novel arm during the test session ($t_{(7)}$ = 2.984; $p < 0.05$), while the intracerebroventricular injection of $A\beta_{1-42}$ led to an impairment in the spatial reference memory ($t_{(6)}$ = 0.9264; p = 0.3900), since the animals from Aβ i.c.v.: PBS i.n. group were unable to recognize the novel arm. After $A\beta_{1-42}$ injection, the treatment with Pram sol. i.n. ($t_{(10)}$ = 1.599; p = 0.1408), Pram sol. i.p. ($t_{(5)}$ = 0.7862; p = 0.4674), NE_{DexS} i.n.($t_{(7)}$ =2.029; p = 0.0820) and PEC-$NE_{DexS/Pram}$ i.n. ($t_{(9)}$ = 2.077; p = 0.0676) did not alter this behavioral parameter statistically

($\alpha = 0.05$). However, a trend to improve spatial reference memory was observed after PEC-$NE_{DexS/Pram}$ i.n. ($t_{(9)} = 2.077$; $p = 0.0676$) administration.

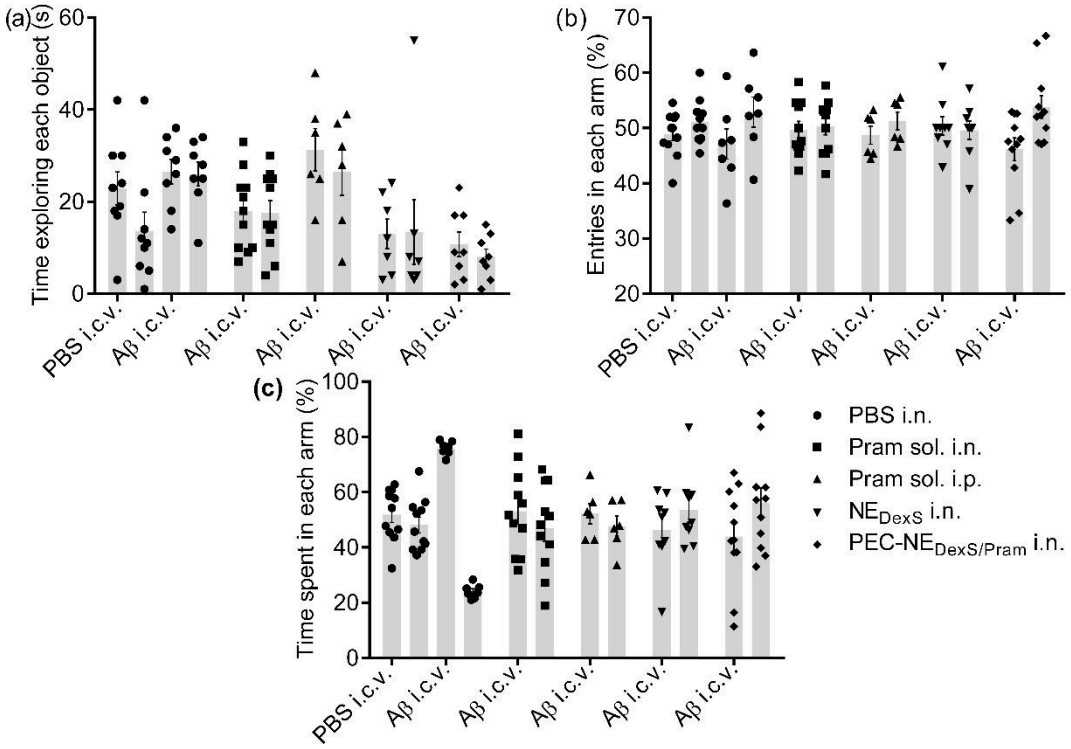

Fig. 4. Data obtained in the training sections of (a) the object relocation test, (b, c) the modified Y-maze test. (a) Time exploring each object, (b) percentual of entries in each arm, (c) percentual of time spent in each arm. (a, b) At the 0.05 level the means one and two (to the object/arm 1 and object/arm 2) were NOT significantly different to each group (unpaired t-test). (c) At the 0.05 level, the means one and two of [Aβ i.c.v. + PBS i.n.] (to arm 1 and arm 2) were significantly different ($p < 0.05$, unpaired t-test).

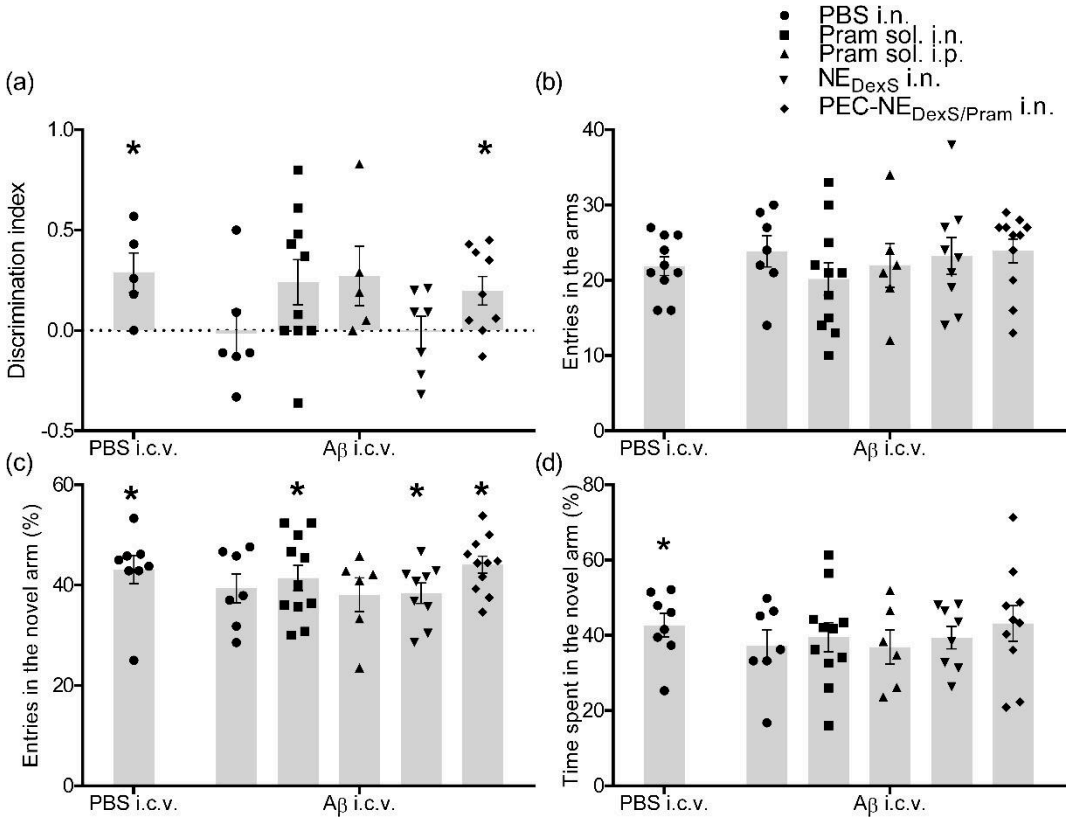

Fig. 5. (a) Discrimination index calculated from exploration times, (b) the total number of entries in the Y-maze, (c) percentual of entries in the novel arm and (d) percentual of time spent in the novel arm, by Alzheimer animal model-animals, induced by intracerebroventricular injection of $A\beta_{1-42}$, submitted to the treatments for 14 days. Data are means ± S.E.M [n=6-10/group; 7-12/group; 6-11/group, respectively for a, (b and c) and d]. (a) * $p < 0.05$ when compared to theoretical value of zero (one-sample t-test). At the 0.05 level the population means of treated groups were NOT significantly different (one-way ANOVA), [$F_{(4, 32)} = 1.592$; $p = 0.2004$]. (b) At the 0.05 level population means of [PBS i.c.v.: PBS and Aβ i.c.v.: PBS] are NOT significantly different (unpaired t-test). There was no a significant difference between the groups treated after Aβ injection (one-way ANOVA). (c) * $p < 0.05$ when compared to theoretical value of 33.33% (one-sample t-test). (d) (* $p < 0.05$ when compared to theoretical value of 33.33%) (one-sample t-test).

In the sucrose splash test (Figure 6a, b), intracerebroventricular injection of $A\beta_{1-42}$ caused a reduction in the hedonic response and in the self-care behavior, as indicated by increased latency for the first grooming behavior ($t_{(14)} = 2.242$; $p < 0.05$, PBS i.c.v.: PBS i.n. *vs* Aβ i.c.v.: PBS i.n) and decrease in the total grooming time ($t_{(14)} = 3.538$; $p < 0.05$; PBS i.c.v.: PBS i.n. *vs* Aβ i.c.v.: PBS i.n). After $A\beta_{1-42}$ administration, one-way ANOVA indicated that pharmacological treatment did not alter the latency for the first grooming behavior [$F_{(4, 38)} = 0.89005$; $p = 0.47926$], Figure 6a. For the total grooming time, one-way ANOVA showed a main effect for treatment [$F_{(4, 38)} = 2.6014$; $p < 0.05$], indicating an effect *per se* for the NE_{DexS} i.n. treated group in self-care behavior (Figure 6b).

Regarding the immobility time evaluated in the tail suspension test (Figure 6c), the intracerebroventricular injection of $A\beta_{1-42}$ did not cause any effect ($t_{(16)} = 0.04930$; $p = 0,9613$;

PBS i.c.v.: PBS i.n. *vs* Aβ i.c.v.: PBS i.n.; unpaired t-test). One-way ANOVA demonstrated that no significant difference was observed between the treated groups after Aβ1-42 injection [$F_{(4, 39)}$ = 1.1833; p = 0.33325].

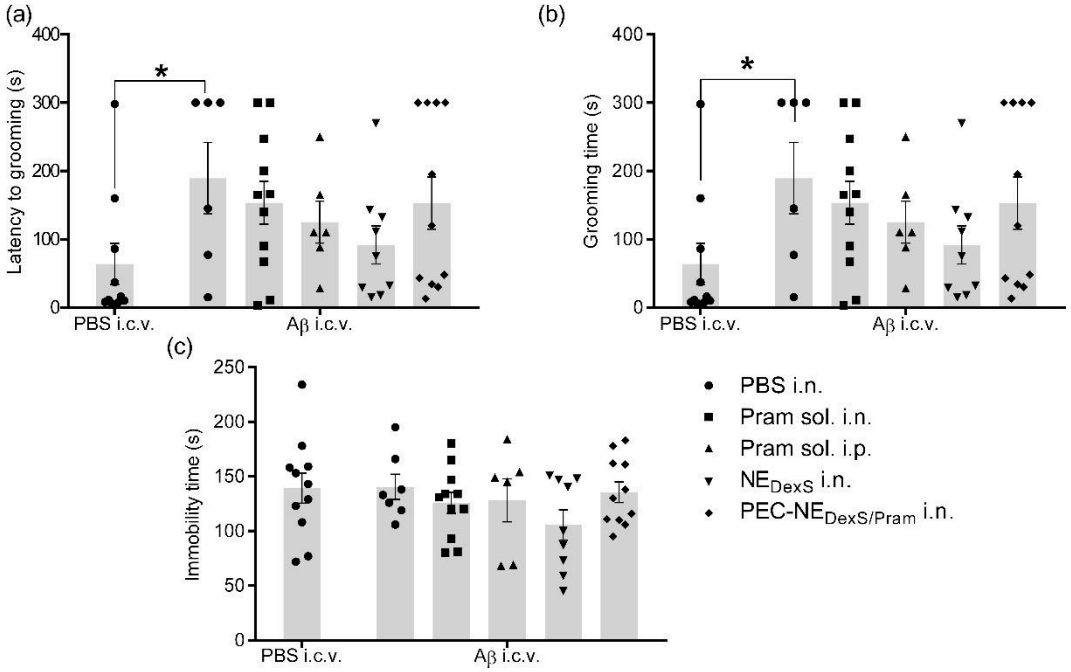

Fig. 6. Latency to grooming (a) and grooming time (b) in the sucrose splash task and immobility time in the tail suspension test (c) by Alzheimer animal model-animals, induced by intracerebroventricular injection of $A\beta_{1-42}$, submitted to the treatments for 14 days. Data are means ± S.E.M (n=6-11/group, a, b and c). (a, b) * $p < 0.05$ when compared PBS i.c.v.: PBS i.n. vs Aβ i.c.v.: PBS i.n. (unpaired t-test). (a) At the 0.05 level the population means are NOT significantly different (one-way ANOVA) [$F_{(4, 38)} = 0.89005$; $p = 0.47926$]. (b) # $p < 0.05$ when compared to positive control group [Aβ i.c.v.: PBS i.n.] (one-way ANOVA followed by Dunett's post-hoc test) [$F_{(4, 38)} = 2.6014$; $p < 0.05$]. (c) At the 0.05 level the population means of [PBS i.c.v.: PBS i.n. and Aβ i.c.v.: PBS] are NOT significantly different (unpaired t-test). At the 0.05 level the population means are NOT significantly different (one-way ANOVA) [$F_{(4, 39)} = 1.1833$; $p = 0.33325$].

For the levels of the presynaptic protein SNAP-25 (Figure 7a, b, c), the Alzheimer model induction showed a tendency to decrease the immunocontent in the hippocampus ($t_{(8)}$ = 1.958; p = 0.0860; PBS i.c.v.: PBS i.n. *vs* Aβ i.c.v.: PBS i.n.; unpaired t-test), that is different at α = 0.1 significance level, but did not in the prefrontal cortex ($t_{(8)} = 0.4698$; p = 0.6511; PBS i.c.v.: PBS i.n. *vs* Aβ i.c.v.: PBS i.n.; unpaired t-test). One-way ANOVA demonstrated that no significant difference was observed between the treated groups after $A\beta_{1-42}$ injection {hippocampus [[$F_{(4, 22)}$ = 1.2896; p = 0.30449] and prefrontal cortex [[$F_{(4, 17)}$ = 1.3687; p = 0.28617]}, as showed in the Figure 7.

Regarding the post-synaptic protein PSD-95 (Figure 7 d, e, f) it was not found a significant alteration in its levels in the hippocampus caused by the model ($t_{(8)} = 0.3398$; p =

0.7427; PBS i.c.v.: PBS i.n. *vs* Aβ i.c.v.: PBS i.n.; unpaired t-test) or by the treatment [$F_{(4, 18)}$ = 0.44228; p = 0.77650, One-way ANOVA]. But there was a significant reduction of PSD-95 on the prefrontal cortex of the animals that received $A\beta_{1-42}$ injection ($t_{(9)}$ = 2.430; $p < 0.05$) when compared to the negative control group [PBS i.c.v.: PBS i.n.]. After $A\beta_{1-42}$ injection, the PSD-95 immunocontent in the prefrontal cortex did not change [$F_{(4, 20)}$ = 1.2355; p = 0.32763], regardless of the treatment applied (Figure 7d).

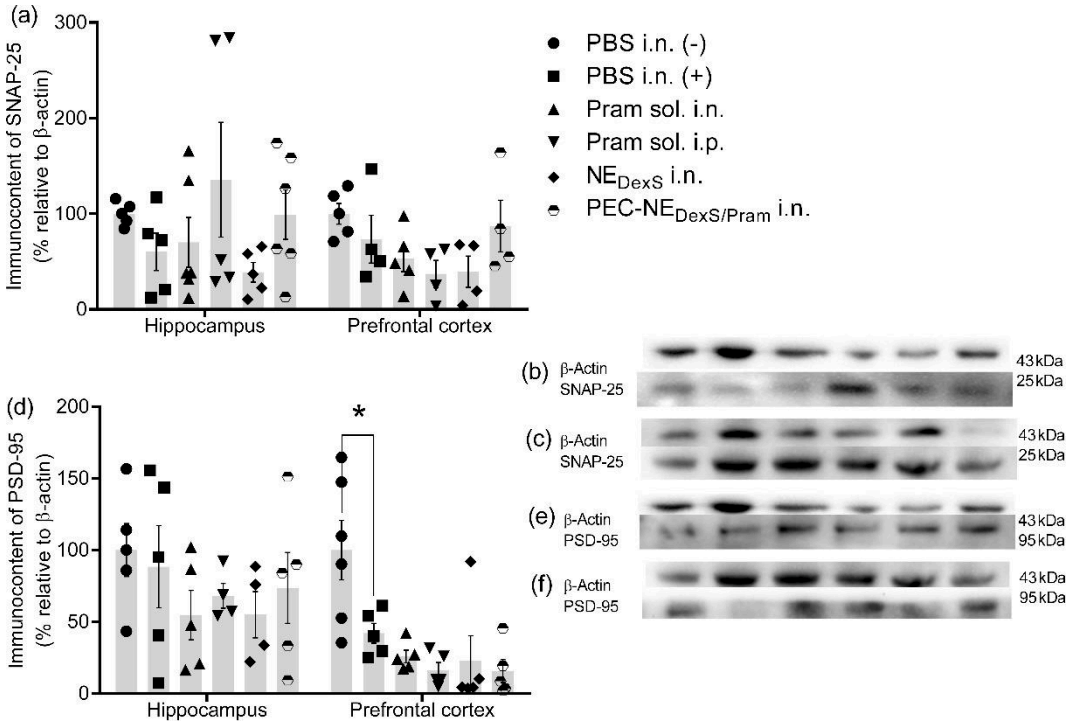

Fig. 7. Immunocontent of (a) the presynaptic protein SNAP-25 and (d) the post-synaptic protein PSD-95 relative to the β-actin content (%) in the synaptosomes obtained from the hippocampus (b, e) and prefrontal cortex (c, f) of Alzheimer animal model-animals, induced by intracerebroventricular injection of $A\beta_{1-42}$, submitted to the treatments for 14 days. Data are mean ± S.E.M (n=4-6/group). At the 0.05 level the population means of [PBS i.c.v.: PBS i.n. and Aβ i.c.v.: PBS i.n.] were not significantly different in the hippocampus and in the prefrontal cortex to SNAP-25 (a) and to PSD95 in the hippocampus (d). At 0.05 level the population means of treated groups were NOT significantly different in the hippocampus nor in the prefrontal cortex (one-way ANOVA), [$F_{(4, 22)}$ = 1.2896; p = 0.30449], [$F_{(4, 17)}$ = 1.3687; p = 0.28617]] to SNAP-25 (a). At 0.05 level the population means of [PBS i.c.v.: PBS i.n. and Aβ i.c.v.: PBS i.n.] were significantly different in the prefrontal cortex to PSD-95 (d) (unpaired t-test). At the 0.05 level the population means of treated groups were NOT significantly different in the hippocampus nor in the prefrontal cortex (one-way ANOVA), [$F_{(4, 18)}$ = 0.44228; p = 0.77650], [$F_{(4, 20)}$ = 1.2355; p = 0.32763] to PSD-95.

DISCUSSION

Nanoemulsions showed physicochemical characteristics (Table 1) in agreement with was already reported to PEC-NE$_{DexS/Pram}$ and NE$_{Dex}$ and similar systems. They are expected to be stable in the nasal fluid and mucosa, as reported elsewhere (*manuscript 2*), favoring the pramlintide nasal administration. Moreover, as 90% of the nanoparticles by number showed a

diameter below 112 nm, the PEC-NEs might be eligible to some extend by intact transport by the olfactory pathway, which is restricted to nanoparticles smaller than 100 nm. Dextran sulfate-coating is described to improve the mucus-penetration [26] and inhibit the phagocytic system [27].

Although a bigger oxidative injury was expected to occur in the animals that received the i.c.v. injection of $A\beta_{1-42}$ (Figure 2) variable results have been reported in the literature to this model [28,29]. Differences in rodent specie, strain, and protocol, beyond the inherent circadian oscillation of oxidative markers [30] may explain these results. The pramlintide potential benefits on Alzheimer´s disease were related to its antioxidant properties besides its insulin sensibility restoring capacity [14], and its effects were not studied in $A\beta_{1-42}$ oligomers injected animal model yet.

The locomotor activity was not altered in these animals regardless the model induction or the treatments. They traveled similar distances and did not show increased thigmotaxis, which could be caused by anxiety or stress [31]. It was reported that the amylin receptor mediates the extracellular-signal-regulated kinase (ERK) signaling in the pro-opiomelanocortin (POMC)-neurons increasing the locomotor activity in chow-fed male mice [32]. This effect was not observed in pramlintide-treated animals herein.

Animals that received the Aβ-oligomers [Aβ i.c.v. + PBS i.n.] had impairments in the spatial recognition- and spatial reference memories, inspective activity, and hedonic and self-caring activities in comparison to their controls [PBS i.c.v., PBS i.n.], showing that this model reassembles characteristics of the Alzheimer disease [18, 33]. Furthermore, alteration in a post-synaptic protein level (PSD-95) in the prefrontal cortex area, which was verified in the animals treated with Aβ-oligomers, corroborates these results.

In the object relocation test animals that received the Aβ-oligomers were not able to discriminate the novelty while their controls were. Interesting, animals that were treated with intranasal PEC-$NE_{DexS/Pram}$ also had positive discrimination indexes, showing that the spatial recognition memory was restored. In the modified Y-maze test, the Aβ-received animals did not increase their inspective activity when the novel arm was opened. On the other hand, their controls increased the entries and the time spent in the novel arm in relation to the other arms or to the total time spent in the arena. Meanwhile, animals that were treated with the intranasal PEC-$NE_{DexS/Pram}$ or with the intranasal but not the intraperitoneal Pram solution rescued the inspective pattern and entered more times in the novel arm. A per se effect of the NE_{DexS} in the

inspective activity and the reference memory, increasing the entries and the time spent in the novel arm was observed. Animals that received the PEC-$NE_{DexS/Pram}$ showed a trend to increase the time spent in the novel arm (one-sample t-test, $p = 0.0676$) and other treatments [Pram sol. i.n. or Pram sol. i.p.] did not influence it. The intranasal route probably favored the drug interaction with the amylin receptors in the brain and trigged its central actions. In this context, the nanocarrier might have had a role in increasing the drug bioavailability. The nanocarrier effects may occur in several ways like favoring the contact of the drug with the mucosa, improving the mucus-diffusion, due to the mucolytic activity of dextran sulfate, maintaining the peptide stability, tailoring the drug tissue's permeation, and increasing the nose-to-brain transport.

Animals that received Aβ-oligomers showed changes in the hedonic and self-caring activities, expressed as longer latency to start and shorter duration of the grooming in comparison to their controls. These changes were not accompanied by depressive-like animus as showed by the tail suspension test. Possibly, pramlintide did not reduce the Aβ effects in this case, due to its proper activities in suppressing appetite and preference by sucrose as well as causing nausea, as an adverse effect [34,35], or even by interfering with gonadotropin hormone release, as like do amylin [36].

Regarding the synaptic proteins, a trend in reducing the SNAP-25 (a pre-synaptic marker) in the hippocampus and a reduction of the PSD-95 (post-synaptic marker) in the prefrontal-cortex occurred to in animals that received the Aβ-oligomers. The hippocampus and the prefrontal areas are recognized to be directly involved in memory and cognition. SNAP-25 is a synaptosome-associated protein involved in the synaptic vesicle exocytosis, whereas PSD-95 is an important scaffold protein that regulates the distribution and activity of glutamate receptors (NMDA and AMPA). These proteins are largely expressed on the synapses and a reduction in their content is indicative of synapses loss, which characterizes the Alzheimer´s disease, and has been described to occur in many animal models of this disease [33,37]. The described synaptic alterations persisted regarding the treatments, showing that the pramlintide beneficial effects in the behavioral tasks probably occurred by other mechanisms than by synaptic restoration. Besides by degenerative stimulus, the expression of PSD-95 is also regulated by reactive or compensatory mechanisms [38]. It was already proposed that interactions between the dopamine receptor D1, PSD-95, and receptors glutamatergic NMDA acting by simultaneously regulating the surface expression and preventing the excessive positive feedback generated by the two receptors, so balancing the glutamatergic/dopaminergic

signaling [39,40]. It is important to remark that in our experiments the animals did not show metabolic decompensation. Perhaps the proposed treatment would show even more enthusiastic results in a model combining metabolic and cognitive impairments.

CONCLUSIONS

The intranasal administration of dextran-sulfate/pramlintide-coated nanoemulsion showed promising effects in treating impairments caused by Aβ in the swiss male mice model, on the behavioral tasks. However, the treatment did not restore the post-synaptic marker PSD-95, which was reduced by $A\beta_{1-42}$ oligomers nor affected the hedonic and self-caring behaviors. The intranasal route and the nanocarrier showed promising results for the treatment of memory and cognitive impairs. Future studies evaluating the biodistribution and the chronic toxicity are essential to consider intranasal pramlintide and its nano(systems) to the treatment of the Alzheimer´s disease.

References

[1] Wang H, Ridgway Z, Cao P, Ruzsicska B, Raleigh DP (2015) Analysis of the Ability of Pramlintide To Inhibit Amyloid Formation by Human Islet Amyloid Polypeptide Reveals a Balance between Optimal Recognition and Reduced Amyloidogenicity. *Biochemistry* **54**, 6704–6711.

[2] Hay DL, Chen S, Lutz TA, Parkes DG, Roth JD (2015) Amylin: Pharmacology, physiology, and clinical potential. *Pharmacol Rev* **67**, 564–600.

[3] Yuan Y, Li Y-B, Tai Z-F, Xie Y-P, Pu X-F, Gao J (2018) Study of forced degradation behavior of pramlintide acetate by HPLC and LC–MS. *J Food Drug Anal* **26**, 409–415.

[4] Patrick S, Corrigan R, Grizzanti J, Mey M, Blair J, Pallas M, Camins A, Lee H, Casadesus G (2019) Neuroprotective Effects of the Amylin Analog, Pramlintide, on Alzheimer's Disease Are Associated with Oxidative Stress Regulation Mechanisms. *J Alzheimer's Dis* **69**, 157–168.

[5] Mousa YM, Abdallah IM, Hwang M, Martin DR, Kaddoumi A (2020) Amylin and pramlintide modulate γ-secretase level and APP processing in lipid rafts. *Sci Rep* **10**, 3751.

[6] de la Torre C, Ceña V (2018) The Delivery Challenge in Neurodegenerative Disorders: The Nanoparticles Role in Alzheimer's Disease Therapeutics and Diagnostics. *Pharmaceutics* **10**, 190.

[7] Gorain B, Rajeswary DC, Pandey M, Kesharwani P, Kumbhar SA, Choudhury H (2020) Nose to Brain Delivery of Nanocarriers Towards Attenuation of Demented Condition. *Curr Pharm Des* **26**, 2233–2246.

[8] Nimer NA, Ismael NS, Abdo RW, Taha Alkhammas SY, Alkhames Aga QA (2020) Pharmacology of neuropeptides: substance P, vasoactive intestinal peptides, neuropeptide Y, calcitonin peptides and their receptors. In *Frontiers in Pharmacology of Neurotransmitters*, Kumar P, Deb PK, eds. Springer Singapore, Singapore, pp. 503–551.

[9] Shevchenko K V., Nagaev IY, Andreeva LA, Shevchenko VP, Myasoedov NF (2019) Prospects for Intranasal Delivery of Neuropeptides to the Brain. *Pharm Chem J* **53**, 89–100.

[10] Adler BL, Yarchoan M, Hwang HM, Louneva N, Blair JA, Palm R, Smith MA, Lee H, Arnold SE, Casadesus G (2014) Neuroprotective effects of the amylin analogue pramlintide on Alzheimer's disease pathogenesis and cognition. *Neurobiol Aging* **35**, 793–801.

[11] Zhu H, Xue X, Wang E, Wallack M, Na H, Hooker JM, Kowall N, Tao Q, Stein TD, Wolozin B, Qiu WQ (2017) Amylin receptor ligands reduce the pathological cascade of Alzheimer's disease. *Neuropharmacology* **119**, 170–181.

[12] Wang E, Zhu H, Wang X, Gower AC, Wallack M, Blusztajn JK, Kowall N, Qiu WQ (2017) Amylin treatment reduces neuroinflammation and ameliorates abnormal patterns of gene expression in the cerebral cortex of an Alzheimer's disease mouse model. *J Alzheimer's Dis* **56**, 47–61.

[13] Gan Q, Yao H, Na H, Ballance H, Tao Q, Leung L, Tian H, Zhu H, Wolozin B, Qiu WQ (2019) Effects of Amylin Against Amyloid-β-Induced Tauopathy and Synapse Loss in Primary Neurons. *J Alzheimer's Dis* **70**, 1025–1040.

[14] Nassar SZ, Badae NM, Issa YA (2020) Effect of amylin on memory and central insulin resistance in a rat model of Alzheimer's disease. *Arch Physiol Biochem* **126**, 326–334.

[15] Martins PP, Smyth HDC, Cui Z (2019) Strategies to facilitate or block nose-to-brain drug delivery. *Int J Pharm* **570**, 118635.

[16] Pardridge WM (1997) Drug Delivery to the Brain. *J Cereb Blood Flow Metab* **17**, 713–731.

[17] Hanson LR, Fine JM, Svitak AL, Faltesek KA (2013) Intranasal administration of CNS therapeutics to awake mice. *J Vis Exp*.

[18] Lanznaster D, Mack JM, Coelho V, Ganzella M, Almeida RF, Dal-Cim T, Hansel G, Zimmer ER, Souza DO, Prediger RD, Tasca CI (2017) Guanosine prevents anhedonic-like behavior and impairment in hippocampal glutamate transport following amyloid-β1–40 administration in mice. *Mol Neurobiol* **54**, 5482–5496.

[19] dos Santos V V., Santos DB, Lach G, Rodrigues ALS, Farina M, De Lima TCM, Prediger RD (2013) Neuropeptide Y (NPY) prevents depressive-like behavior, spatial memory deficits and oxidative stress following amyloid-β (Aβ1–40) administration in mice.

Behav Brain Res **244**, 107–115.

[20] Delgobo M, Agnes JP, Gonçalves RM, dos Santos VW, Parisotto EB, Zamoner A, Zanotto-Filho A (2019) N-acetylcysteine and alpha-lipoic acid improve antioxidant defenses and decrease oxidative stress, inflammation and serum lipid levels in ovariectomized rats via estrogen-independent mechanisms. *J Nutr Biochem* **67**, 190–200.

[21] Draper HH, Hadley M (1990) [43] Malondialdehyde determination as index of lipid Peroxidation. In *Methods in Enzymology* Methods Enzymol, pp. 421–431.

[22] Ellman GL (1959) Tissue sulfhydryl groups. *Arch Biochem Biophys* **82**, 70–77.

[23] Canas PM, Porciuncula LO, Cunha GMA, Silva CG, Machado NJ, Oliveira JMA, Oliveira CR, Cunha RA (2009) Adenosine A2A Receptor Blockade Prevents Synaptotoxicity and Memory Dysfunction Caused by -Amyloid Peptides via p38 Mitogen-Activated Protein Kinase Pathway. *J Neurosci* **29**, 14741–14751.

[24] França AP, Schamne MG, de Souza BS, da Luz Scheffer D, Bernardelli AK, Corrêa T, de Souza Izídio G, Latini A, da Silva-Santos JE, Canas PM, Cunha RA, Prediger RD (2020) Caffeine consumption plus physical exercise improves behavioral impairments and stimulates neuroplasticity in spontaneously hypertensive rats (SHR): an animal model of attention deficit hyperactivity disorder. *Mol Neurobiol* **57**, 3902–3919.

[25] Peterson GL (1977) A simplification of the protein assay method of Lowry et al. which is more generally applicable. *Anal Biochem* **83**, 346–356.

[26] Ferreira LMB, Alonso JD, Kiill CP, Ferreira NN, Buzzá HH, Martins de Godoi DR, de Britto D, Assis OBG, Seraphim T V., Borges JC, Gremião MPD (2018) Exploiting supramolecular interactions to produce bevacizumab-loaded nanoparticles for potential mucosal delivery. *Eur Polym J* **103**, 238–250.

[27] Hult A, Toss F, Malm C, Oldenborg P (2020) In vitro phagocytosis of liquid-stored red blood cells requires serum and can be inhibited with fucoidan and dextran sulphate. *Vox Sang* **115**, 647–654.

[28] Cetin F, Yazihan N, Dincer S, Akbulut G (2012) The effect of intracerebroventricular injection of beta amyloid peptide (1-42) on caspase-3 activity, lipid peroxidation, nitric oxide and nos expression in young adult and aged rat brain. *Turk Neurosurg* **23**, 144–150.

[29] Sharma S, Verma S, Kapoor M, Saini A, Nehru B (2016) Alzheimer's disease like pathology induced six weeks after aggregated amyloid-beta injection in rats: increased oxidative stress and impaired long-term memory with anxiety-like behavior. *Neurol Res* **38**, 838–850.

[30] Ledezma C, Coria-Lucero C, Delsouc MB, Casais M, Della Vedova C, Ramirez D, Devia CM, Delgado SM, Navigatore-Fonzo L, Anzulovich AC (2021) Effect of an Intracerebroventricular Injection of Aggregated Beta-amyloid (1–42) on Daily Rhythms of Oxidative Stress Parameters in the Prefrontal Cortex. *Neuroscience* **458**, 99–107.

[31] Pierce RC, Kalivas PW (2007) Locomotor Behavior. *Curr Protoc Neurosci* **40**, 8.1.1-8.1.9.

[32] Coester B, Koester-Hegmann C, Lutz TA, Le Foll C (2020) Amylin/Calcitonin Receptor–Mediated Signaling in POMC Neurons Influences Energy Balance and Locomotor Activity in Chow-Fed Male Mice. *Diabetes* **69**, 1110–1125.

[33] Canas PM, Porciuncula LO, Cunha GMA, Silva CG, Machado NJ, Oliveira JMA, Oliveira CR, Cunha RA (2009) Adenosine A2A Receptor Blockade Prevents Synaptotoxicity and Memory Dysfunction Caused by -Amyloid Peptides via p38 Mitogen-Activated Protein Kinase Pathway. *J Neurosci* **29**, 14741–14751.

[34] Mietlicki-Baase EG, Rupprecht LE, Olivos DR, Zimmer DJ, Alter MD, Pierce RC, Schmidt HD, Hayes MR (2013) Amylin Receptor Signaling in the Ventral Tegmental Area is Physiologically Relevant for the Control of Food Intake. *Neuropsychopharmacology* **38**, 1685–1697.

[35] Smith SR, Aronne LJ, Burns CM, Kesty NC, Halseth AE, Weyer C (2008) Sustained Weight Loss Following 12-Month Pramlintide Treatment as an Adjunct to Lifestyle Intervention in Obesity. *Diabetes Care* **31**, 1816–1823.

[36] Kitagawa Y, Sasaki T, Suzumura R, Morishima A, Tatebayashi R, Assadullah, Ieda N, Morita Y, Matsuyama S, Inoue N, Uenoyama Y, Tsukamura H, Ohkura S (2020) Facilitatory and inhibitory role of central amylin administration in the regulation of the gonadotropin-releasing hormone pulse generator activity in goats. *Neurosci Lett* **736**, 135276.

[37] Tu S, Okamoto S, Lipton SA, Xu H (2014) Oligomeric Aβ-induced synaptic dysfunction in Alzheimer's disease. *Mol Neurodegener* **9**, 48.

[38] Savioz A, Leuba G, Vallet PG (2014) A framework to understand the variations of PSD-95 expression in brain aging and in Alzheimer's disease. *Ageing Res Rev* **18**, 86–94.

[39] Zhang J, Vinuela A, Neely MH, Hallett PJ, Grant SGN, Miller GM, Isacson O, Caron MG, Yao W-D (2007) Inhibition of the Dopamine D1 Receptor Signaling by PSD-95. *J Biol Chem* **282**, 15778–15789.

[40] Keith D (2008) Excitation control: balancing PSD-95 function at the synapse. *Front Mol Neurosci* **1**, 4.

4 DISCUSSÃO GERAL

A via nasal é reconhecidamente promissora para a veiculação cerebral de peptídeos terapêuticos. Mas apesar de permitir contornar a barreira hematoencefálica, os peptídeos/proteínas administrados por via nasal podem sofrer proteólise pelos componentes do epitélio olfatório (SHEVCHENKO *et al.*, 2019). Aliado a isso, o crescente número de trabalhos avaliando a atividade da pranlintida no tratamento da doença de Alzheimer (ADLER *et al.*, 2014; ZHU, H. *et al.*, 2015; KIMURA *et al.*, 2017; MOHAMED *et al.*, 2017; PATRICK *et al.*, 2019) foi encorajador para que propuséssemos o desenvolvimento de um nanocarreador para permitir sua vetorização direta para o cérebro por esta via. Muitos dos métodos tradicionalmente utilizados para a produção de nanopartículas envolvem a utilização de solventes orgânicos e processos agressivos, o que foi considerado para a escolha do método de titulação coloidal para a obtenção das partículas (SANTALICES *et al.*, 2017). O sulfato de dextrana foi selecionado por possuir uma elevada densidade aniônica (KUMAR, AMRISH; PANDEY; JAIN, 2016; ZAMAN *et al.*, 2016; AGEITOS *et al.*, 2019; SUN, CHANGYE *et al.*, 2019), sendo favorável para a associação da pranlintida, que possui natureza catiônica (TRAINA; KANE, 2011; YOUNK; MIKELADZE; DAVIS, 2011). No entanto, o uso de baixas concentrações do polissacarídeo na preparação das nanopartículas causaram a agregação das cadeias peptídicas, formando uma suspensão grosseira com tendência à precipitação. Em estudos de formulação foi identificada uma faixa estreita de concentração dos polieletrólitos onde ocorria a formação de uma suspensão coloidal monodispersa e tamanho nanométrico, com comportamento de um nanogel. Além de interações eletrostáticas e ligações de hidrogênio, também foram constatadas interações hidrofóbicas, que levaram a mudança da conformação do peptídeo intrinsicamente desordenado para α-hélice, fenômeno que é descrito para a amilina em ambiente biológico, pela interação com as membranas e durante a liberação pelas células β-pancreáticas (ZHANG, XIAO-XI *et al.*, 2016).

Apesar das fortes interações identificadas, a suspensão coloidal formada não foi estável em fluido nasal simulado, ocorrendo sua dissociação. Então, diversas estratégias de estabilização foram testadas, seguindo os relatos da literatura para a estabilização de nanopartículas de polieletrólitos em fluidos biológicos (SANTALICES *et al.*, 2017). Inicialmente um terceiro componente com cargas foi adicionado à suspensão. A quitosana oligossarídeo (polivalente) demonstrou em baixas concentrações causar o deslocamento da pranlintida, competindo pelos sítios de ligação com o sulfato de dextrana. Em concentrações mais elevadas não foi possível a obtenção de nanopartículas, ocorrendo agregação. O brometo

de cetrimônio (monovalente) também causou o deslocamento da pranlintida em baixas concentrações, e a utilização de concentrações altas foi limitada pela sua toxicidade. Apenas pela produção de uma emulsão muito diluída e posterior concentração da mesma, por evaporação sob pressão reduzida foi possível obter uma suspensão de nanopartículas estável em fluido nasal simulado, com moderada associação do fármaco (cerca de 60 %).

A adição de tensoativos não-iônicos à suspensão de nanopartículas de polieletrólitos sulfato de dextrana/pranlintida também foi testada. O polissorbato 80, hidrossolúvel, não interferiu na dissociação das nanopartículas em soluções com maior força iônica. O monooleato de sorbitano, lipossolúvel, precisou ser dispersado na suspensão com auxílio de sonda ultrassom. Apesar de ter possibilitado a obtenção de nanopartículas moderadamente estáveis no fluido nasal simulado, a utilização da sonda de ultrassom é um método considerado agressivo e pode levar a precipitação e agregação do peptídeo (TIAN *et al.*, 2020). Por isso optamos por adicionar um óleo, capaz de solubilizar o tensoativo lipofílico na composição das nanopartículas. A incorporação do peptídeo em um sistema mais deformável também poderia favorecer sua penetração na mucosa. Assim, obtivemos as nanoemulsões revestidas pelo complexo sulfato de dextrana/pranlintida em que o complexo pode se restabilizado na interface óleo/água.

As nanoemulsões finais foram constituídas de triglicerídeos de cadeia média e dos tensoativos não iônicos polissorbato 80 e monooleato de sorbitano. A estabilização de complexos de polieletrólitos na interface das gotículas e a água ocorreu provavelmente por interações eletrostáticas e hidrofóbicas, semelhante aos sistemas denominados emulsões de Pickering (WEI; ZHANG; HUANG, 2019; ZHANG, CUIGE *et al.*, 2020). Emulsões de Pickering são estabilizados unicamente por nanopartículas sólidas ou nanogéis de polissacarídeo/proteína. Alguns estudos relatam à associação de complexos iônicos hidrofóbicos às nanopartículas lipídicas e poliméricas com a diferença que, neste caso, uma molécula de baixo peso (fármaco) e um polieletrólito ou uma macromolécula (peptídeo terapêutico) e um surfactante iônico se inserem no interior do núcleo hidrofóbico da partícula (PATEL; GAUDANA; MITRA, 2014). Nas emulsões de Pickering os complexos de polissacarídeo/proteína são usados para estabilizar as gotículas da (nano)emulsão, que podem conter moléculas lipofílicas (fármacos ou geralmente nutrientes) solubilizadas (WHITBY, 2019). No contexto da estabilização coloidal de nanopartículas de polieletrólitos, não é de nosso conhecimento a descrição prévia dessa proposta na literatura. Esta estratégia se mostrou vantajosa em relação as demais por não utilizar componentes reconhecidamente tóxicos, nem

de processos vigorosos para a sua formação, além de não necessitar da remoção da água por evaporação para a obtenção de uma suspensão com concentração de fármaco desejável. Estudos de permeação através da mucosa nasal *in vitro* foram realizados para as nanoemulsões desenvolvidas, usando o modelo bicompartimental de células de Franz. O tecido epitelial da mucosa nasal suína foi utilizado como membrana. O método de quantificação da pranlintida por cromatografia líquida de alta eficiência, com detecção no ultravioleta foi previamente validado (*Apêndice B*). A pranlintida foi quantificada no meio receptor, composto por fluido nasal simulado, e nas mucosas, após processo de extração. A permeação da pranlintida associada ao nanocarreador ocorreu de forma sustentada ao longo do experimento, sendo menor nas primeiras horas do que a permeação do peptídeo livre. Na mucosa o nanocarredor não interferiu na quantidade de peptídeo retida. O efeito mucolítico, atribuído ao sulfato de dextrana (SUDO; BOYD; KING, 2000a) não influenciou a permeação da pranlintida de modo relevante nesses experimentos.

Os processos coleta, transporte e limpeza da mucosa nasal podem ter contribuído para a remoção da camada de muco. Por isso propusemos a avaliação da difusão das nanopartículas por uma camada de muco artificial, constituída por uma dispersão de mucina em fluido nasal simulado. Essa camada foi depositada sobre um *strainer* celular, inserido em um poço de uma microplaca, com uma membrana entre o compartimento superior (*strainer*) e o poço, o qual foi preenchido com fluido nasal simulado (compartimento inferior). Ao final do experimento o *strainer* e a membrana foram removidos, e o fluido nasal foi coletado, diluído 1:1, v/v com acetonitrila, centrifugado e a pranlintida foi quantificada. Os resultados demonstraram que as nanoemulsões de sulfato de dextrana/pranlintida tiveram uma maior capacidade de difusão na camada de muco em comparação com o fármaco livre, como era esperado. As cargas positivas da pranlintida possivelmente interagiram com a mucina formando agregados, o que dificultou sua difusão. Na presença de muco e viabilidade tecidual (*in vivo*), a permeação através da mucosa nasal possivelmente será influenciada pelas propriedades do sulfato de dextrana e do nanocarreador.

Uma vez tendo sido obtido uma formulação em que o complexo DexS/Pram manteve-se estável no fluido nasal simulado, o trabalho foi continuado em estudos *in vivo* com o intuito de investigar os efeitos da pranlintida após administração nasal em modelos comportamentais da DA. No estudo em modelo de DA induzido pela injeção intracerebroventricular de oligômeros da proteína $A\beta_{1-42}$, as nanoemulsões revestidas por complexos de polieletrólitos

melhoraram o desempenho dos animais em relação ao controle (DA induzido, tratado com PBS nasal), enquanto a solução do peptídeo, administrada por via nasal ou intraperitonial não apresentou diferença em relação ao controle, principalmente em testes comportamentais específicos para memória e cognição. Alguns efeitos da $A\beta_{1-42}$ (redução do grooming e da PSD-95 no córtex) não foram impedidos ou suprimidos pelo tratamento, independente da via de administração, no caso da solução de pranlintida e independente de estar associada ou não ao nanocarreador no caso da administração nasal. Isso pode ter ocorrido tanto pela ineficácia do tratamento em prevenir ou reverter parte dos danos provocados pela $A\beta_{1-42}$, ou pelos mecanismos neuroprotetores da Aβ solúvel e da pranlintida atuarem no mesmo sentido, para evitar a excitotoxicidade glutamatérgica, provocada pelos oligômeros de Aβ. Em geral a pranlintida associada ao nanocarreador exerceu efeitos mais bem-definidos (diferentes estaticamente ou não do grupo controle) em relação aos efeitos observados para solução de pranlintida, independente da via de administração, para qual foram observadas menores diferenças em relação ao grupo controle (com ou sem significância estatística). Esses resultados estão de acordo com as propriedades esperadas para as nanoemulsões, que foram formuladas para manter a estabilidade nos fluidos biológicos e mucosa nasal, aumentar a área superficial de contato com a mucosa e se difundir através do obstáculo representado pela camada de muco.

Com o uso de nanotecnologia, um sistema provavelmente capaz de melhorar a distribuição ou vetorização da pranlintida, em nível cerebral ou sistêmico, após administração nasal, permitindo o exercício de seus efeitos terapêuticos, foi desenvolvido nesta tese. Porém, tanto os alvos para as ações da pranlintida no tratamento do Alzheimer, quanto a influência da nanoemulsão proposta, e dos nanocarreadores em geral, na distribuição de fármacos administrados por via nasal, são questões que merecem ser mais bem compreendidas. A toxicidade crônica e o desempenho desses sistemas como carreadores de peptídeos terapêuticos no tratamento do Diabetes mellitus e da obesidade também são questões bastante instigantes.

5 CONCLUSÕES

A adição de uma solução de pranlintida a uma solução de sulfato de dextrana, em uma estreita faixa de concentrações e razão molar, permitiu a obtenção de nanopartículas de polieletrólitos de tamanho nanométrico e com baixa dispersão de tamanho.

Os nanocomplexos foram formados por interações eletrostáticas e ligações de hidrogênio espontâneas, além de interações hidrofóbicas, que levaram a modificações estruturais na pranlintida, permitindo a sua estabilização na forma bioativa de alfa-hélice.

Apesar de apresentarem características intencionadas, como distribuição de tamanho estreita e homogênea e potencial zeta negativo, devido à maior proporção de grupamentos aniônicos do sulfato de dextrana, em relação aos grupamentos catiônicos da pranlintida, os complexos não foram estáveis em fluido nasal simulado, ocorrendo completa dissociação e precipitação.

Nos complexos a pranlintida modificou sua estrutura secundária, majoritariamente intrinsicamente desordenada para α-helice, que corresponde ao tipo de enovelamento encontrado para a amilina em associação às membranas celulares, e na pró-amilina durante sua secreção pelas células β-pancreáticas.

A adição de um terceiro componente carregado permitiu a estabilização dos nanocomplexos em fluido nasal simulado, porém ocorreu competição pelos sítios de ligação ao sulfato de dextrana, reduzindo a associação do fármaco. Além disso, a concentração final por evaporação foi necessária para a obtenção de uma suspensão de nanopartículas com concentração de fármaco pretendida.

Das estratégias para a estabilização do complexo DexS/Pram, a associação às gotículas de uma nanoemulsão mostrou ser mais promissora por não utilizar compostos tóxicos e permitir a obtenção de concentrações desejáveis do peptídeo para a realização de estudos *in vivo*.

A associação do complexo sulfato de dextrana/pranlintida às nanoemulsões levou à estabilização do complexo em fluido nasal simulado, mantendo o tamanho nanométrico das partículas após à incubação.

O método de quantificação para pranlintida por cromatografia líquida de alta eficiência, com detecção no ultravioleta foi validado e apresentou os requisitos necessários de especificidade, precisão e exatidão para quantificação dos peptídeos em amostras de fluido nasal simulado e extrato da mucosa nasal oriundos de estudos de permeação através da mucosa nasal *in vitro*.

Nos estudos de permeação *in vitro*, utilizando célula de difusão de Franz e mucosa nasal suína como modelo de membrana, a pranlintida associada ao nanocarreador, demonstrou uma permeação sustentada ao longo do tempo e mais lenta nas primeiras horas, em comparação com o peptídeo em solução. As propriedades mucolíticas do sulfato de dextrana não aumentaram a permeação do peptídeo na mucosa nasal, possivelmente devido à remoção significativa do muco, causada pelos processos de transporte e preparação das membranas.

Nos estudos de retenção dos peptídeos na mucosa nasal *in vitro*, a associação da pranlintida ao nanocarreador não modificou seu perfil de retenção na mucosa.

Nos estudos de mucodifusão, a associação ao nanocarreador aumentou a difusão da pranlintida através do gel fluido de mucina. Esse resultado está de acordo com as propriedades mucolíticas atribuídas ao sulfato de dextrana.

Nos estudos *in vivo*, em modelo animal de doença de Alzheimer, a associação da pranlintida ao nanocarreador levou à obtenção de resultados mais bem-definidos estatisticamente diferentes do grupo controle (correspondente ao grupo com indução do modelo e tratado com tampão fosfato), especialmente nos testes comportamentais que envolvem memória e cognição, impedindo ou prevenindo alguns efeitos dos oligômeros de Aβ. Os grupos tratados com solução de pranlintida mostraram menores diferenças em relação ao controle, com ou sem significância estatística.

Alguns parâmetros (PSD-95 no córtex, latência para o grooming e tempo de grooming) foram alterados pela indução pela injeção intracerebroventricular de Aβ, e não foram impedidos ou prevenidos pelo tratamento com pranlintida em solução, por via nasal ou intraperitoneal, nem pelo tratamento com pranlintida associada ao nanocarreador, por via nasal. Isso pode ter sido causado pela inefetividade do tratamento (100 µg/kg/dia, durante 14 dias) contra determinados danos causados pelos oligômeros de Aβ ou pela ação da pranlintida na prevenção da excitotoxidade glutamatérgica ocorrer no mesmo sentido da ação da proteína Aβ solúvel.

A nanoemulsão proposta pareceu favorecer a chegada da pranlintida em níveis terapêuticos nos seus alvos de ação, após a administração nasal. Estudos de biodistribuição e toxicidade crônica precisam ser realizados para afirmar os possíveis benefícios do fármaco livre e nanocarreado no tratamento do Alzheimer. Outras aplicações que podem ser futuramente investigadas para os sistemas contendo pranlintida incluem o tratamento do Diabetes mellitus e da obesidade.

REFERÊNCIAS BIBLIOGRÁFICAS

ABHILASH, M.; AUGUSTINE, R. Diabetes and Health Care: an Overview. In: GEORGE, A.; AUGUSTINE, R.; SEBASTIAN, M. (Ed.). **Diabetes Mellitus and Human Health Care: A holistic approach to diagnosis and treatment**. Oakville: CRC Press, 2014. p. 273–314.

ADLER, B. L. *et al.* Neuroprotective Effects of the Amylin Analogue Pramlintide on Alzheimer's Disease Pathogenesis and Cognition. **Neurobiology of Aging**, v. 35, n. 4, p. 793–801, 1 Apr. 2014.

AGEITOS, J. M. *et al.* Study of Nanostructured Fibroin/Dextran Matrixes for Controlled Protein Release. **European Polymer Journal**, v. 114, p. 197–205, 1 May 2019.

AL-KEILANI, M. S. *et al*. Pramlintide, an Antidiabetic, Is Antineoplastic in Colorectal Cancer and Synergizes with Conventional Chemotherapy. **Clinical pharmacology : advances and applications**, v. 10, p. 23–29, Mar. 2018.

ALLEN-BIRT, S. Pathophysiology of Alzheimer's disease. In: WALDEMAR, G.; BURNS, A. (Ed.). **Alzheimer's Disease**. 2. ed. Oxford: Oxford University Press, 2017. p. 7–15.

ALVES, N. A.; DIAS, L. G.; FRIGORI, R. B. Synergistic Long-Range Effects of Mutations Underlie Aggregation Propensities of Amylin Analogues. **Journal of Molecular Modeling**, v. 25, n. 9, p. 263, 19 Sep. 2019.

AMRAM, S.; FRENKEL, D. Animal Models of Alzheimer's Disease. In: GOZES, I. (Ed.). **Neuroprotection in Alzheimer's Disease**. London: Elsevier Inc., 2017. p. 31–58.

ANDRADE, F. *et al.* Chitosan Formulations as Carriers for Therapeutic Proteins. **Current Drug Discovery Technologies**, v. 8, n. 3, p. 157–172, 8 Aug. 2011.

AREOSA SASTRE, A. *et al.* Effect of the treatment of Type 2 diabetes mellitus on the development of cognitive impairment and dementia. **Cochrane Database of Systematic Reviews**, n. 6, p. 1-60, 2017.

ARNOLD, S. E. *et al.* Brain Insulin Resistance in Type 2 Diabetes and Alzheimer Disease: Concepts and Conundrums. **Nature Reviews Neurology**, v. 14, n. 3, p. 168–181, Jan. 2018.

ARONNE, L. *et al.* Progressive Reduction in Body Weight after Treatment with the Amylin Analog Pramlintide in Obese Subjects: A Phase 2, Randomized, Placebo-Controlled, Dose-Escalation Study. **Journal of Clinical Endocrinology and Metabolism**, v. 92, n. 8, p. 2977–2983, 2007.

AVILA-VAZQUEZ, M. F.; ALTAMIRANO-BUSTAMANTE, N. F.; ALTAMIRANO-BUSTAMANTE, M. M. Amyloid Biomarkers in Conformational Diseases at Face Value: A Systematic Review. **Molecules**, v. 23, n. 1, p. 79, Dec. 2018.

BADWAIK, H. R. *et al.* Oral Delivery of Proteins and Polypeptides through Polysaccharide Nanocarriers. In: KUMAR, G. T.; BIJAYA, G. (Ed.). **Polysaccharide-based Nano-Biocarrier in Drug Delivery**. Boca Raton: CRC Press, 2018. p. 1–24.

BERRILL, A.; BIDDLECOMBE, J.; BRACEWELL, D. Product Quality During Manufacture

and Supply. In: VAN DER WALLE, C. F. (Ed.). **Peptide and Protein Delivery**. London: Academic Press, 2011. p. 313–339.

BOBO, D. *et al.* Nanoparticle-Based Medicines: A Review of FDA-Approved Materials and Clinical Trials to Date. **Pharmaceutical Research**, v. 33, n. 10, p. 2373–2387, Oct. 2016.

BOCCIA, L.; LE FOLL, C.; LUTZ, T. A. Noradrenaline Signaling in the LPBN Mediates Amylin's and Salmon Calcitonin's Hypophagic Effect in Male Rats. **The FASEB Journal**, v. 34, n. 11, p. 15448–15461, Nov. 2020.

BOURGANIS, V. *et al.* Polyelectrolyte complexes as prospective carriers for the oral delivery of protein therapeutics. **European Journal of Pharmaceutics and Biopharmaceutics,** v. 111, p. 44-60, Feb. 2017.

BRAGA, R. R. *et al.* Molecular Confinement of Human Amylin in Lipidic Nanoparticles. **Journal of Liposome Research**, v. 26, n. 3, p. 188–198, 2016.

CANTER, R. G.; PENNEY, J.; TSAI, L.-H. The Road to Restoring Neural Circuits for the Treatment of Alzheimer's Disease. **Nature**, v. 539, n. 7628, p. 187–196, Nov. 2016.

CHONKAR, A.; NAYAK, U.; UDUPA, N. Smart Polymers in Nasal Drug Delivery. **Indian journal of pharmaceutical sciences**, v. 77, n. 4, p. 367–375, 2015.

CRAFT, S. *et al.* Intranasal Insulin Therapy for Alzheimer Disease and Amnestic Mild Cognitive Impairment: A Pilot Clinical Trial. **Archives of Neurology**, v. 69, n. 1, p. 29–38, Jan. 2012.

DA SILVA, D. C. *et al.* Amyloidogenesis of the Amylin Analogue Pramlintide. **Biophysical Chemistry**, v. 219, p. 1–8, Dec. 2016.

DE LA TORRE, C. *et al.* The Delivery Challenge in Neurodegenerative Disorders: The Nanoparticles Role in Alzheimer's Disease Therapeutics and Diagnostics. **Pharmaceutics**, v. 10, n. 4, p. 190, Oct. 2018.

DEVI, G.; SCHELTENS, P. Heterogeneity of Alzheimer's Disease: Consequence for Drug Trials? **Alzheimer's Research and Therapy**, v. 10, n. 1, p. 122, Dec. 2018.

DIOP, M. *et al.* Design, Characterisation, and Bioefficiency of Insulin-Chitosan Nanoparticles after Stabilisation by Freeze-Drying or Cross-Linking. **International Journal of Pharmaceutics**, v. 491, n. 1–2, p. 402–408, Jul. 2015.

DOS SANTOS PICANCO, L. C. *et al.* Alzheimer's Disease: A Review from the Pathophysiology to Diagnosis, New Perspectives for Pharmacological Treatment. **Current Medicinal Chemistry**, v. 25, n. 26, p. 3141–3159, Sep. 2018.

EDWARDS, P. J.; LAPLANTE, S. R. Peptides as Leads for Drug Discovery. In: CASTANHO, M.; SANTOS, N. (Ed.). **Peptide Drug Discovery and Development: Translational Research in Academia and Industry**. Wheinhein: Wiley, 2011. p. 1–55.

FAGHMOUS, N. *et al.* Optimization of Chitosan-Coated W/O/W Multiple Emulsion Stabilized with Span 80 and Tween 80 Using Box–Behnken Design. **Journal of Dispersion**

Science and Technology, p. 1–13, 2020.

FRÈRE, Y.; DANICHER, L.; MULLER, S. Peptide Nanostructured Conjugates for Therapeutics: The Example of P140 Peptide for the Treatment of Systemic Lupus Erythematosus. In: ALEMÁN, C.; BIANCO, A.; VENANZI, M. (Ed.). **Peptide Materials: From Nanostructures to Applications**. Chinchester: John Wiley & Sons, 2013. p. 385–415.

FRIGORI, R. B. Be Positive: Optimizing Pramlintide from Microcanonical Analysis of Amylin Isoforms. **Physical Chemistry Chemical Physics**, v. 19, n. 37, p. 25617–25633, Sep. 2017.

GAN, Q. *et al.* Effects of Amylin Against Amyloid-β-Induced Tauopathy and Synapse Loss in Primary Neurons. **Journal of Alzheimer's Disease**, v. 70, n. 4, p. 1–16, Aug. 2019.

GAO *et al.* Sustained and Extended Release with Structural and Activity Recovery of Lysozyme from Complexes with Sodium (Sulfamate Carboxylate) Isoprene/Ethylene Oxide Block Copolymer. **Macromolecular Bioscience**, v. 10, n. 2, p. 139–146, 2010.

GAUDANA, R. *et al.* Encapsulation of Protein-Polysaccharide HIP Complex in Polymeric Nanoparticles. **Journal of Drug Delivery**, v. 2011, p. 1–7, 2011.

GHOFRANI, M. *et al.* Development of Octreotide-Loaded Chitosan and Heparin Nanoparticles: Evaluation of Surface Modification Effect on Physicochemical Properties and Macrophage Uptake. **Journal of Pharmaceutical Sciences**, v. 108, n. 9, p. 3036–3045, Sep. 2019.

GIANNOTTI, M. I. I. *et al.* Highly Versatile Polyelectrolyte Complexes for Improving the Enzyme Replacement Therapy of Lysosomal Storage Disorders. **ACS Applied Materials and Interfaces**, v. 8, n. 39, p. 25741–25752, Oct. 2016.

GUERREIRO, L. H. *et al.* Polymeric Particles for the Controlled Release of Human Amylin. **Colloids and Surfaces B: Biointerfaces**, v. 94, p. 101–106, 2012.

GUERREIRO, L. H. *et al.* Preparation and Characterization of PEGylated Amylin. **AAPS PharmSciTech**, v. 14, n. 3, p. 1083–1097, Sep. 2013.

HAY, D. L. *et al.* Amylin: Pharmacology, Physiology, and Clinical Potential. **Pharmacological Reviews**, v. 67, n. 3, p. 564–600, 2015.

HERRMANN, K. *et al.* Effects of Pramlintide in Patients with Type 2 Diabetes Mellitus: An Analysis Using Daily Insulin Dose Tertiles. **Endocrine Practice**, v. 20, n. 10, p. 1070–1075, 2014.

HOLBAN, A. M. *et al.* Smart Nanopolysaccharides for the Delivery of Bioactives. **Nanoarchitectonics for Smart Delivery and Drug Targeting**, p. 67–94, Jan. 2016.

HOU, X. *et al.* Synthesis of Reusable Silica Nanosphere-Supported Pt(IV) Complex for Formation of Disulfide Bonds in Peptides. **Molecules**, v. 22, n. 2, p. 338, Feb. 2017.

HU, H. *et al.* Expression, Purification, and Biological Activity of the Recombinant

Pramlintide Precursor. **Applied Microbiology and Biotechnology**, v. 98, n. 18, p. 7837–7844, Apr. 2014.

INSUA, I. *et al.* Polymyxin B Containing Polyion Complex (PIC) Nanoparticles: Improving the Antimicrobial Activity by Tailoring the Degree of Polymerisation of the Inert Component. **Scientific Reports**, v. 7, n. 1, p. 9396, Dec. 2017.

JALLOUK, A. P. *et al.* Modifications of Natural Peptides for Nanoparticle and Drug Design. **Advances in Protein Chemistry and Structural Biology**, v. 98, p. 57–91, 2015.

JUNG, Y.-S.; NA, K. Protein Delivery System Based on Various Polysaccharides. **Journal of Pharmaceutical Investigation**, v. 41, n. 4, p. 197–204, Aug. 2011.

KAPOOR, M.; CLOYD, J. C.; SIEGEL, R. A. A Review of Intranasal Formulations for the Treatment of Seizure Emergencies. **Journal of Controlled Release**, v. 237, p. 147–159, Sep. 2016.

KHAZAEI-POUL, Y. *et al.* Monocyclic Peptides: Types, Synthesis and Applications. **Current Pharmaceutical Biotechnology**, v. 21, Jan. 2020.

KIMURA, R. *et al.* Pramlintide Antagonizes Beta Amyloid (Aβ)- and Human Amylin-Induced Depression of Hippocampal Long-Term Potentiation. **Molecular Neurobiology**, v. 54, n. 1, p. 748–754, 2017.

KUMAR, A.; PANDEY, A. N.; JAIN, S. K. Nasal-Nanotechnology: Revolution for Efficient Therapeutics Delivery. **Drug Delivery**, v. 23, n. 3, p. 681–693, 2016.

KUMAR, J. *et al.* Amino Acid Supplementation for Enhancing Recombinant Protein Production in *E. Coli*. **Biotechnology and Bioengineering**, v. 117, n. 8, p. 2420–2433, Aug. 2020a.

KUMAR, P. *et al.* Neurotransmitters and Their Receptors—State of the Art. In: Kumar, P.; Deb, P. K. **Frontiers in Pharmacology of Neurotransmitters**. Singapore: Springer, 2020b. p. 1–29.

LAI, S. K.; WANG, Y. Y.; HASNES, J. Mucus-Penetrating Nanoparticles for Drug and Gene Delivery to Mucosal Tissues. **Advanced Drug Delivery Reviews**, v. 61, n. 2, p. 158–171, Feb. 2009.

LAKSHMI, P.; KUMAR, G. A. Nanosuspension Technology: A Review. **International Journal of Pharmacy and Pharmaceutical Sciences**, v. 2, n. SUPPL. 4, p. 35–40, 2010.

LEE, J. H.; BACSKAI, B. J.; AYATA, C. Genetic animal models of cerebral vasculopathies. In: CONN, P. M. (Ed.). **Progress in Molecular Biology and Translational Science**. London: Elsevier B.V., 2012. 105p. 25–55.

LEE, N. J.; NORRIS, S. L.; THAKURTA, S. Efficacy and Harms of the Hypoglycemic Agent Pramlintide in Diabetes Mellitus. **Annals of Family Medicine**, v. 8, n. 6, p. 542–549, 2010.

LI, M. *et al.* Design Principles of Oil-in-Water Emulsions with Functionalized Interfaces: Mixed, Multilayer, and Covalent Complex Structures. **Comprehensive Reviews in Food**

Science and Food Safety, v. 19, n. 6, p. 3159–3190, Nov. 2020.

LI, X. *et al.* Nanoemulsions Coated with Alginate/Chitosan as Oral Insulin Delivery Systems: Preparation, Characterization, and Hypoglycemic Effect in Rats. **International Journal of Nanomedicine**, v. 8, n. 8, p. 23–32, Dec. 2012.

LIU, J. *et al.* A Modified Hydrophobic Ion-Pairing Complex Strategy for Long-Term Peptide Delivery with High Drug Encapsulation and Reduced Burst Release from PLGA Microspheres. **European Journal of Pharmaceutics and Biopharmaceutics**, v. 144, p. 217–229, Nov. 2019.

LIU, X. *et al.* Involvement of Amylin B-H2S-Connexin 43 Signaling Pathway in Vascular Dysfunction and Enhanced Ischemia–Reperfusion-Induced Myocardial Injury in Diabetic Rats. **Bioscience Reports**, v. 40, n. 6, Jun. 2020.

ŁOBODA, D.; ROWIŃSKA-ŻYREK, M. Zn(II) - Pramlintide: Stability, Binding Sites and Unexpected Aggregation. **Journal of Inorganic Biochemistry**, v. 174, p. 150–155, Sep. 2017.

M. WAYS, T.; LAU, W.; KHUTORYANSKIY, V. Chitosan and Its Derivatives for Application in Mucoadhesive Drug Delivery Systems. **Polymers**, v. 10, n. 3, p. 267, Mar. 2018.

MAGLIANO, D. J.; ZIMMET, P.; SHAW, J. E. Classification of Diabetes Mellitus and Other Categories of Glucose Intolerance. **International Textbook of Diabetes Mellitus**, p. 1–16, 2015.

MAIKAWA, C. L. *et al.* A Co-Formulation of Supramolecularly Stabilized Insulin and Pramlintide Enhances Mealtime Glucagon Suppression in Diabetic Pigs. **Nature Biomedical Engineering**, v. 4, n. 5, p. 507–517, May 2020.

MARRAS, A.; VIEREGG, J.; TIRRELL, M. Assembly and Characterization of Polyelectrolyte Complex Micelles. **Journal of Visualized Experiments**, v. 157, Dec. 2020.

MASTERS, C. L. *et al.* Alzheimer's Disease. **Nature Reviews Disease Primers**, v. 1, n. 1, p. 1–18, Oct. 2015.

MAURI, E.; PERALE, G.; ROSSI, F. Nanogel Functionalization: A Versatile Approach to Meet the Challenges of Drug and Gene Delivery. **ACS Applied Nano Materials**, v. 1, n. 12, p. 6525–6541, Dec. 2018.

MCCLEMENTS, D. J. Encapsulation, Protection, and Delivery of Bioactive Proteins and Peptides Using Nanoparticle and Microparticle Systems: A Review. **Advances in Colloid and Interface Science**, v. 253, p. 1–22, Mar. 2018.

MOHAMED, L. A. *et al.* Amylin Enhances Amyloid-β Peptide Brain to Blood Efflux Across the Blood-Brain Barrier. **Journal of Alzheimer's Disease**, v. 56, n. 3, p. 1087–1099, Jan. 2017.

MOHTASHAMIAN, S.; BODDOHI, S.; HOSSEINKHANI, S. Preparation and Optimization of Self-Assembled Chondroitin Sulfate-Nisin Nanogel Based on Quality by Design Concept. **International Journal of Biological Macromolecules**, v. 107, p. 2730–2739, 1 Feb. 2018.

MORLEY, J. E. The SAMP8 Mouse: A Model of Alzheimer Disease? **Biogerontology**, v. 3, n. 1–2, p. 57–60, 2002.

MOTIEI, M. *et al.* Stabilization of Chitosan-Based Polyelectrolyte Nanoparticle Cargo Delivery Biomaterials by a Multiple Ionic Cross-Linking Strategy. **Carbohydrate Polymers**, v. 231, p. 115709, Mar. 2020.

MOUSA, Y. M. *et al.* Amylin and Pramlintide Modulate γ-Secretase Level and APP Processing in Lipid Rafts. **Scientific Reports**, v. 10, n. 1, p. 1–14, Dec. 2020.

NADENDLA, K.; FRIEDMAN, S. H. Light Control of Protein Solubility Through Isoelectric Point Modulation. **Journal of the American Chemical Society**, v. 139, n. 49, p. 17861–17869, Dec. 2017.

NIKOLAC PERKOVIC, M.; PIVAC, N. Genetic Markers of Alzheimer's Disease. In: Kim, Y (Ed.)**Advances in Experimental Medicine and Biology**. New York: Springer, 2019. 1192p. 27–52.

NISTOR, M. T. Drug Delivery and Release from Polymeric Nanomaterials. In: Arias, J. (Ed.) **Nanotechnology and Drug Delivery, Volume One**. Boca Raton: CRC Press, 2014. p. 40–92.

NUR, M.; VASILJEVIC, T. Insulin Inclusion into a Tragacanth Hydrogel: An Oral Delivery System for Insulin. **Materials**, v. 11, n. 1, p. 79, Jan. 2018.

PATEL, A.; GAUDANA, R.; MITRA, A. K. A Novel Approach for Antibody Nanocarriers Development through Hydrophobic Ion-Pairing Complexation. **Journal of Microencapsulation**, v. 31, n. 6, p. 542–550, 2014.

PATRICK, S. *et al.* Neuroprotective Effects of the Amylin Analog, Pramlintide, on Alzheimer's Disease Are Associated with Oxidative Stress Regulation Mechanisms. **Journal of Alzheimer's Disease**, v. 69, n. 1, p. 1–12, Apr. 2019.

PIPPA, N. *et al.* Complexation of Cationic-Neutral Block Polyelectrolyte with Insulin and in Vitro Release Studies. **International Journal of Pharmaceutics**, v. 491, n. 1–2, p. 136–143, 2015.

PIPPA, N. *et al.* Preparation and Physicochemical Characterization of Polyelectrolyte Complexes Incorporating Antitumor Peptide. **Journal of Nanoscience and Nanotechnology**, v. 17, n. 7, p. 4901–4906, Jul. 2017.

POLIS, B.; SAMSON, A. Neurogenesis versus Neurodegeneration: The Broken Balance in Alzheimer's Disease. **Neural Regeneration Research**, v. 16, n. 3, p. 496, Mar. 2021.

PONCE-LÓPEZ, T. *et al.* Diabetes Mellitus and Amyloid Beta Protein Pathology in Dementia. In: KUROUSKI, D. (Ed.). **Amyloid Diseases**. London: IntechOpen, 2019.

QIAO, Y.-C. *et al.* Efficacy and Safety of Pramlintide Injection Adjunct to Insulin Therapy in

Patients with Type 1 Diabetes Mellitus: A Systematic Review and Meta-Analysis. **Oncotarget**, v. 8, n. 39, p. 66504–66515, Sep. 2017.

RAVUSSIN, E. *et al.* Enhanced Weight Loss With Pramlintide/Metreleptin: An Integrated Neurohormonal Approach to Obesity Pharmacotherapy. **Obesity**, v. 17, n. 9, p. 1736–1743, Sep. 2009.

RIDDLE, M. C. Basal Glucose Can Be Controlled, but the Prandial Problem Persistsdit's Thenext Target. **Diabetes Care**, v. 40, n. 3, p. 291–300, 2017.

RUBIN, R. R.; PEYROT, M. Assessing Treatment Satisfaction in Patients Treated with Pramlintide as an Adjunct to Insulin Therapy. **Current Medical Research and Opinion**, v. 23, n. 8, p. 1919–1929, 2007. Disponível em: <http://www.tandfonline.com/doi/full/10.1185/030079907X210804>.

SACHDEVA, S. Peptides as 'Drugs': The Journey so Far. **International Journal of Peptide Research and Therapeutics**, v. 23, n. 1, p. 49–60, 2017.

SAFAEIAN, L. *et al.* The Effect of Pramlintide, an Antidiabetic Amylin Analogue, on Angiogenesis-Related Markers in Vitro. **Research in Pharmaceutical Sciences**, v. 15, n. 4, p. 323, 1 Aug. 2020. Disponível em: <http://www.rpsjournal.net/text.asp?2020/15/4/323/293510>. Acesso em: 2 nov. 2020.

SANT, S. *et al.* Self-Assembled Hydrogel Fiber Bundles from Oppositely Charged Polyelectrolytes Mimic Micro-/Nanoscale Hierarchy of Collagen. **Advanced Functional Materials**, v. 27, n. 36, p. 1606273, 26 Sep. 2017. Disponível em: <http://doi.wiley.com/10.1002/adfm.201606273>. Acesso em: 18 apr. 2020.

SANTALICES, I. *et al.* Advances on the Formulation of Proteins Using Nanotechnologies. **Journal of Drug Delivery Science and Technology**, v. 42, p. 155–180, 1 Dec. 2017.

SARMENTO, B.; FERREIRA, D.; VASCONCELOS, T. Polymer-Based Delivery Systems for Oral Delivery of Peptides and Proteins. **Delivery technologies for biopharmaceuticals: peptides, proteins, nucleic acids and vaccines.**, p. 207–226, 2009.

SEN, S.; CHAKRABORTY, R.; DE, B. Diabetes Mellitus: General Consideration. In: SEN, S.; CHAKRABORTY, R.; DE, B. (Ed.). **Diabetes Mellitus in 21st Century**. New York: Springer, 2016. p. 13–22.

SERVIZI, S.; CORRIGAN, R. R.; CASADESUS, G. The Importance of Understanding Amylin Signaling Mechanisms for Therapeutic Development in the Treatment of Alzheimer's Disease. **Current Pharmaceutical Design**, v. 26, n. 12, p. 1345–1355, 2020.

SHEVCHENKO, K. V. *et al.* Prospects for Intranasal Delivery of Neuropeptides to the Brain. **Pharmaceutical Chemistry Journal**, v. 53, n. 2, p. 89–100, 15 May 2019. Disponível em: <https://link.springer.com/article/10.1007/s11094-019-01960-x>. Acesso em: 21 dec. 2020.

SHIMADA, N. *et al.* Inter-Polyelectrolyte Nano-Assembly Induces Folding and Activation of Functional Peptides. **Journal of Controlled Release**, v. 218, p. 45–52, 2015.

SINÉSIA, C. *et al.* Physico-Chemical Stability of Co-Formulation of PEGylated Human Amylin with Insulin. **Pharmaceutical Development and Technology**, v. 24, n. 8, p. 975–981, 14 Sep. 2019.

SINGH-FRANCO, D.; PEREZ, A.; HARRINGTON, C. The Effect of Pramlintide Acetate on Glycemic Control and Weight in Patients with Type 2 Diabetes Mellitus and in Obese Patients without Diabetes: A Systematic Review and Meta-Analysis. **Diabetes, Obesity and Metabolism**, v. 13, n. 2, p. 169–180, 2011.

SMITH, S. R. *et al.* Sustained Weight Loss Following 12-Month Pramlintide Treatment as an Adjunct to Lifestyle Intervention in Obesity. **Diabetes Care**, v. 31, n. 9, p. 1816–1823, Sep. 2008. Disponível em: </pmc/articles/PMC2518351/?report=abstract>. Acesso em: 21 dec. 2020.

SUDO, E.; BOYD, W. A.; KING, M. Effects of Dextran Sulfate on Tracheal Mucociliary Velocity in Dogs. **Journal of Aerosol Medicine: Deposition, Clearance, and Effects in the Lung**, v. 13, n. 2, p. 87–96, 7 Jul. 2000.

SUN, C. *et al.* Sulfated Polysaccharides Interact with Fibroblast Growth Factors and Protect from Denaturation. **FEBS Open Bio**, v. 9, n. 8, p. 1477–1487, 16 Aug. 2019. Disponível em: <https://onlinelibrary.wiley.com/doi/abs/10.1002/2211-5463.12696>. Acesso em: 1 oct. 2019.

SUN, L. *et al.* Flash Fabrication of Orally Targeted Nanocomplexes for Improved Transport of Salmon Calcitonin across the Intestine. **Molecular Pharmaceutics**, v. 17, n. 3, p. 757–768, 2 Mar. 2020. Disponível em: <https://dx.doi.org/10.1021/acs.molpharmaceut.9b00827>. Acesso em: 22 nov. 2020.

SUTHERLAND, G. T. *et al.* Epidemiological Approaches to Understanding the Link between Type 2 Diabetes and Dementia. **Journal of Alzheimer's Disease**, v. 59, n. 2, p. 393–403, 2017.

TAM, C. S.; LECOULTRE, V.; RAVUSSIN, E. Novel Strategy for the Use of Leptin for Obesity Therapy. **Expert opinion on biological therapy**, v. 11, n. 12, p. 1677–85, 2011.

TAZI, L. M.; JAYAWICKREME, S. Determination of Residual Dextran Sulfate in Protein Products by SEC–HPLC. **Journal of Chromatography B**, v. 1011, p. 89–93, Feb. 2016.

THWALA, L. N.; PRÉAT, V.; CSABA, N. S. Emerging Delivery Platforms for Mucosal Administration of Biopharmaceuticals: A Critical Update on Nasal, Pulmonary and Oral Routes. **Expert Opinion on Drug Delivery**, v. 14, n. 1, p. 23–36, 2 Jan. 2017.

TIAN, R. *et al.* Ultrasound Driven Conformational and Physicochemical Changes of Soy Protein Hydrolysates. **Ultrasonics Sonochemistry**, v. 68, p. 105202, 1 Nov. 2020.

TOMABECHI, Y. *et al.* Glycosylation of Pramlintide: Synthetic Glycopeptides That Display In Vitro and In Vivo Activities as Amylin Receptor Agonists. **Chemistry - A European Journal**, v. 19, n. 45, p. 15084–15088, Nov. 2013.

TRAINA, A. N.; KANE, M. P. Primer on Pramlintide, an Amylin Analog. **The Diabetes EDUCATOR**, v. 37, n. 3, 2011.

TRIPATHI, A. S. *et al.* Amylin Dual Action: A Second Gluco Regulatory β-Cell Hormone, Treatment and Cause for the Diabetes. **International Journal of Diabetes in Developing Countries**, v. 34, n. 3, p. 125–129, 2014.

UMERSKA, A.; CORRIGAN, O. I.; TAJBER, L. Design of Chondroitin Sulfate-Based Polyelectrolyte Nanoplexes: Formation of Nanocarriers with Chitosan and a Case Study of Salmon Calcitonin. **Carbohydrate Polymers**, v. 156, p. 276–284, 2017.

VAN DER WALLE, C. F.; OLEJNIK, O. An Overview of the Field of Peptide and Protein Delivery. In: VAN DER WALLE, C. (Ed.). **Peptide and Protein Delivery**. Boston: Academic Press, 2011. p. 1–22.

VENKATANARAYAN, A. *et al.* IAPP-Driven Metabolic Reprogramming Induces Regression of P53-Deficient Tumours in Vivo. **Nature**, v. 517, n. 7536, p. 626–630, Nov. 2015.

WANG, E. *et al.* Amylin Treatment Reduces Neuroinflammation and Ameliorates Abnormal Patterns of Gene Expression in the Cerebral Cortex of an Alzheimer's Disease Mouse Model. **Journal of Alzheimer's Disease**, v. 56, n. 1, p. 47–61, 2017.

WANG, H. *et al.* Analysis of the Ability of Pramlintide to Inhibit Amyloid Formation by Human Islet Amyloid Polypeptide Reveals a Balance between Optimal Recognition and Reduced Amyloidogenicity. **Biochemistry**, v. 54, n. 44, p. 6704–6711, 2015.

WANG, J. *et al.* The Brief Analysis of Peptide-Combined Nanoparticle: Nanomedicine's Unique Value. **Current Protein & Peptide Science**, v. 21, n. 4, p. 334–343, Feb. 2020.

WANG, K.; LIU, M.; MO, R. Polysaccharide-Based Biomaterials for Protein Delivery. **Medicine in Drug Discovery**, p. 100031, Apr. 2020.

WANG, W.; ROBERTS, C. J. **Aggregation of Therapeutic Proteins**. Hoboken: John Wiley & Sons, 2010.

WEI, Z.; ZHANG, H.; HUANG, Q. Curcumin-Loaded Pickering Emulsion Stabilized by Insoluble Complexes Involving Ovotransferrin-Gallic Acid Conjugates and Carboxymethyldextran. **Food and Function**, v. 10, n. 8, p. 4911–4923, Aug. 2019.

WHATELEY, T. L. Drug Delivery and Targeting; for Pharmacists and Pharmaceutical Scientists. **Journal of Drug Targeting**, v. 10, n. 8, p. 637–637, 2002.

WHITBY, C. P. Nanoparticles at Fluid Interfaces: From Surface Properties to Biomedical Applications. In: NANN, T. (Ed.). **Comprehensive Nanoscience and Nanothechnology**. 2. ed. New York: Academic Press, 2019.

WONG, C. Y. *et al.* Development of Orally Administered Insulin-Loaded Polymeric-Oligonucleotide Nanoparticles: Statistical Optimization and Physicochemical Characterization. **Drug Development and Industrial Pharmacy**, p. 1–15, 2020.

WU, D. *et al.* Chitosan-based Colloidal Polyelectrolyte Complexes for Drug Delivery: A

Review. **Carbohydrate Polymers,** v. 238, p. 116-126, Jun. 2020.

WU, F.-G. G. *et al.* Folding Behaviors of Protein (Lysozyme) Confined in Polyelectrolyte Complex Micelle. **Langmuir**, v. 32, n. 15, p. 3655–3664, 2016.

YOUNK, L. M.; MIKELADZE, M.; DAVIS, S. N. Pramlintide and the Treatment of Diabetes: A Review of the Data since Its Introduction. **Expert Opinion on Pharmacotherapy**, v. 12, n. 9, p. 1439–1451, 2011.

YUAN, Y. *et al.* Study of Forced Degradation Behavior of Pramlintide Acetate by HPLC and LC-MS. **Journal of Food and Drug Analysis**, v. 26, n. 1, p. 409–415, 2017.

YUBA, E.; KONO, K. Nasal Delivery of Biopharmaceuticals. In: DAS NEVES, J.; SARMENTO, B. (Ed.). **Mucosal Delivery of Biopharmaceuticals**. New York: Springer, 2014. p. 197–220.

YULE, L. R. *et al.* Synthesis and Amylin Receptor Activity of Glycomimetics of Pramlintide Using Click Chemistry. **Organic & Biomolecular Chemistry**, v. 14, n. 23, p. 5238–5245, Jun. 2016.

ZAMAN, P. *et al.* Incorporation of Heparin-Binding Proteins into Preformed Dextran Sulfate-Chitosan Nanoparticles. **International journal of nanomedicine**, v. Volume 11, p. 6149–6159, Nov. 2016.

ZHANG, C. *et al.* Influence of Ionic Strength on Gel-like Pickering Emulsions Stabilized by Self-Assembled Colloidal Nanoparticles Containing Lysozyme. **Colloid and Polymer Science**, v. 298, n. 9, p. 1249–1262, Sep. 2020.

ZHANG, L. *et al.* The Application of Polysaccharide-Based Nanogels in Peptides/Proteins and Anticancer Drugs Delivery. **Journal of Drug Targeting**, v. 25, n. 8, p. 673–684, Sep. 2017.

ZHANG, X.-X. *et al.* Neuroendocrine Hormone Amylin in Diabetes. **World Journal of Diabetes**, v. 7, n. 9, p. 189, 2016.

ZHAO, L.; SKWARCZYNSKI, M.; TOTH, I. Polyelectrolyte-Based Platforms for the Delivery of Peptides and Proteins. **ACS Biomaterials Science and Engineering**, v. 5, n. 10, p. 4937–4950, Oct. 2019.

ZHU, H. *et al.* Intraperitoneal Injection of the Pancreatic Peptide Amylin Potently Reduces Behavioral Impairment and Brain Amyloid Pathology in Murine Models of Alzheimer's Disease. **Molecular Psychiatry**, v. 20, n. 2, p. 252–262, Feb. 2015.

ZHU, H. *et al.* Amylin Receptor Ligands Reduce the Pathological Cascade of Alzheimer's Disease. **Neuropharmacology**, v. 119, p. 170–181, Jun. 2017.

APÊNDICE A – ESTRATÉGIAS PARA ESTABILIZAÇÃO DE NANOPARTÍCULAS DE POLIELETRÓLITOS EM MEIOS COM FORÇA IÔNICA COMPATÍVEL A DOS MEIOS BIOLÓGICOS

APRESENTAÇÃO

Este apêndice é constituído por texto no qual são apresentadas as alternativas testadas para estabilização das nanopartículas de polieletrólitos sulfato de dextrana/pranlintida em meios com elevada força iônica, como o fluido nasal simulado. A adição de um terceiro componente catiônico (quitosana oligossacarídeo ou brometo de cetrilamônio), assim como a adição de tensoativos não iônicos, hidro- e lipofílicos foram avaliadas. Essas alternativas, apesar de terem permitido a obtenção de sistemas moderadamente estáveis, levaram a uma dissociação do peptídeo, por competição pelos sítios de interação com o sulfato dextrana, ou a necessidade de incluir tratamentos agressivos durante a preparação (ex.: tratamento com sonda ultrassom) ou uso de concentrações elevadas de componentes reconhecidamente tóxicos. Assim, neste apêndice são mostrados os resultados não apresentados no Capítulo 2 da tese.

ESTRATÉGIAS PARA ESTABILIZAÇÃO DE NANOPARTÍCULAS DE POLIELETRÓLITOS EM MEIOS COM FORÇA IÔNICA COMPATÍVEL A DOS MEIOS BIOLÓGICOS

1 INTRODUÇÃO

A complexidade dos sistemas biológicos, incluindo as propriedades físico-químicas dos fluidos biológicos, a bioquímica e a fisiologia dos organismos vivos, não possibilitou o completo sucesso esperado para os nano-medicamentos nas últimas décadas. Como o revestimento é a primeira parte da partícula que entra em contato com o meio biológico, além de definir a biocompatibilidade ele também define a estabilidade coloidal e a depuração das nanopartículas em sistemas biológicos (SCHUBERT; CHANANA, 2018).

As nanopartículas de polissacarídeos são reconhecidas por proporcionarem uma maior associação de peptídeos terapêuticos em relação aos outros tipos de nanopartículas. O principal desafio para esses sistemas é o controle de sua dissociação precoce em meios biologicamente relevantes. A combinação de diferentes biomateriais e surfactantes é uma alternativa para lidar com esse problema (SANTALICES et al., 2017).

Duas espécies catiônicas, mono- e polivalente foram testadas como terceiro componente, para melhorar a estabilidade das nanopartículas de sulfato de dextrana/pramlintida ($PEC_{DexS/Pram}$), o brometo de cetiltrimetilamonio (CTAB, com carga 1+ por molécula, Figura 1) e o lactato de quitosana oligossacarídeo (COS, com carga 2+ por monômero, Figura 2), originando as PEC_{CTAB} e PEC_{QOS}, respectivamente.

Figura 1 – Estrutura química do brometo de cetiltrimetilamonio.

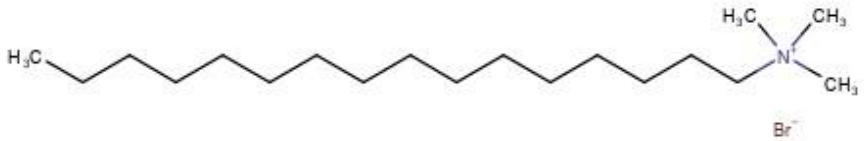

Fonte: ChemSpider.

Figura 2 – Estrutura química do monômero do lactato de quitosana oligossacarídeo, com peso molecular de 340 g/mol.

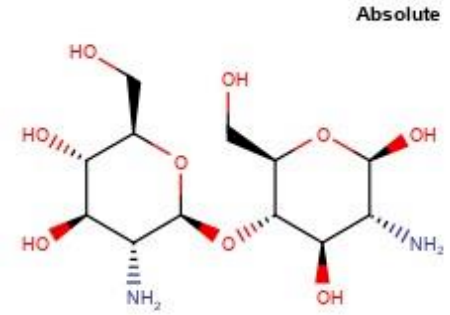

Fonte: ChemSpider.

Figura 3 – Estrutura química do polioxietileno (20) monooleato de sorbitana (polissorbato 80).

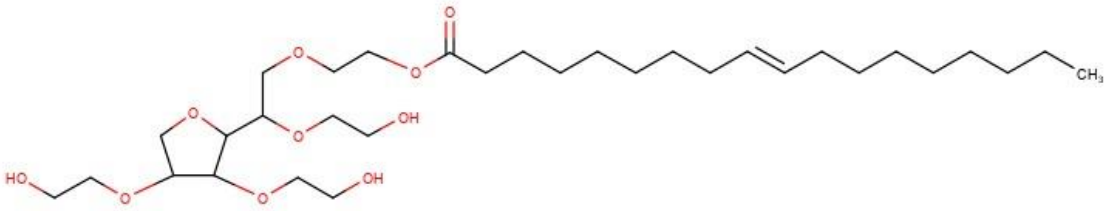

Fonte: ChemSpider.

Figura 4 – Estrutura química do monooleato de sorbitana.

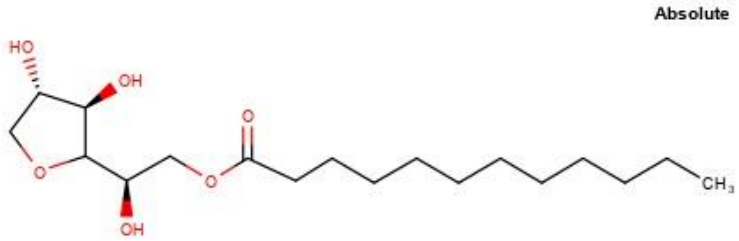

Fonte: ChemSpider.

2 MATERIAIS E MÉTODOS

2.1 Matérias-primas, reagentes e solventes

Acetato de pramlintida (Genemed Syn, EUA), sulfato de dextrana Mn 40 kDa, grau de sulfonação entre 17 e 19 % (Sigma Aldrich, EUA), quitosana de baixo peso molecular, Mw 50 – 190 kDa, desacetilação entre 75 e 85 % (Sigma Aldrich, EUA), triglicerídeos de cadeia média (NEOBEE® 1053, Stepan, Illinois, EUA), monooleato de sorbitana (Span 80®, Sigma Aldrich, EUA), polissorbato 80 (Tween 80®, Sigma Aldrich, EUA), brometo de cetiltrimetilamonio (CTAB, Sigma Aldrich, EUA), ácido fosfotúngstico, ácido trifluoroacético grau CLAE,

acetonitrila grau CLAE, água Milli-Q (Millipore, Merk, EUA), ácido acético, glicerina, cloreto de sódio, cloreto de potássio e cloreto de cálcio grau reagente. Demais solventes e reagentes utilizados com grau reagente e sem purificação prévia.

2.2 Equipamentos

Zetasizer Nano ZS (Malvern, EUA), agitador magnético multiponto, evaporador rotatório (Büchi, R-300), microscópio de transmissão eletrônica 100 kV (JEM/1011, Japão), cromatógrafo Shimadzu com detector de arranjo de diodos/UV, microcentrifuga (MiniStar, Bélgica).

2.3 Metodologia

2.3.1 Preparação das nanopartículas de pramlintida estabilizadas com quitosana oligossacarídeo ou brometo de cetiltrimetil amônio

As nanopartículas foram preparadas adicionando gota-a-gota a solução de pramlintida (1,2 mg/mL) à solução de sulfato de dextrana (0,5 mg/mL) sob agitação magnética moderada, em volumes iguais. Para a inclusão de um terceiro componente, o volume da solução de dextrana foi reduzido para $^{3}/_{4}$, mantendo-se a concentração final. Uma solução do terceiro componente (COS ou CTAB), com volume correspondente a $^{1}/_{4}$ da solução de sulfato de dextrana da formulação inicial, em diferentes concentrações, foi adicionada e homogeneizada com pipeta. Volumes correspondentes a $^{2}/_{4}$ e $^{3}/_{4}$ do volume da solução sulfato de dextrana da formulação inicial também foram testados, mantendo-se o volume da solução de sulfato de dextrana fixo, essas formulações foram concentradas em evaporador rotatório (Buchi, R-300, Alemanha), em banho maria, na temperatura de 40 °C, para o ajuste das concentrações finais.

2.3.2 Preparação das nanopartículas de pramlintida estabilizadas com polissorbato 80 e associação de polissorbato 80 e monooleato de sorbitana

As nanopartículas poli-iônicas de pramlintida foram preparadas como descrito no item 5.2.3.1 e no *Artigo 1*. O polissorbato 80 (concentração final de 3,0 mg/mL) foi previamente adicionado na solução de sulfato de dextrana, mantendo-se as concentrações de

polieletrólito/peptídeo das formulações iniciais. O monooleato de sorbitana (concentração final de 1,0 mg/mL) foi disperso na emulsão por aplicação de sonda ultrassom (amplitude de 30 %, por 30 segundos), quando aplicável.

2.3.3 Caracterização físico-química das nanopartículas

As nanopartículas foram caracterizadas quanto ao tamanho de partícula, por espalhamento de luz dinâmico e potencial zeta, por mobilidade eletroforética – antes e após tratamento com fluido nasal simulado, pH 5,5 (JUG et al., 2017) (FNS, diluição 1:1, v/v e incubação por 30 min a 37 °C). As amostras (n= 3) foram preparadas pela diluição das formulações em água ultrapura (1:10 e 1:5, v/v respectivamente) e analisadas em equipamento Zetasizer Nano ZS na temperatura de 25 °C para as nanopartículas não tratadas e de 37 °C para as nanopartículas tratadas com FNS.

Aspectos morfológicos das nanopartículas estabilizadas com quitosana ou CTAB foram observados por microscopia eletrônica de transmissão (MET). Um volume de 10 µL da suspensão de nanopartículas (n= 1) foi depositado em um grid de formvar/carbono 200 mesh e após 10 minutos o mesmo volume de uma solução aquosa de ácido fosfotúngstico 1 %, m/v foi adicionado sob o grid (contraste negativo). Após 10 minutos um papel absorvente foi utilizado para remoção do excesso de amostra, pelo contato com a lateral do grid. O grid foi armazenado sob um papel absorvente, coberto com uma placa de Petri, em temperatura ambiente, por 24 horas, para secagem. As análises foram realizadas em microscópio eletrônico JEM/1011 (100 kV) no LCME/UFSC. Análises de espectroscopia de absorção no infravermelho (Cary 660, Agilent) também foram realizadas para essas nanopartículas, preliminarmente liofilizadas, no intervalo de número de onda de 1200 a 1700 cm^{-1}.

A eficiência de associação foi determinada por ultrafiltração-centrifugação utilizando dispositivos Amicon 100 kD (Merk, Millipore), para as nanopartículas estabilizadas com quitosana, CTAB e polissorbato 80/monooleato de sorbitana com características mais apropriadas (menor tamanho de partícula, maior associação de fármaco, estabilidade coloidal após tratamento com FNS). Um volume de 400 µL das suspensões de nanopartículas (n=1) foi adicionado no dispositivo, o qual foi inserido em um microtubo e submetido à centrifugação na velocidade de 6.000 r.p.m. por 15 minutos (MiniStar, Bélgica). A pramlintida foi quantificada no ultrafiltrado por cromatografia líquida com detecção ultravioleta (CLAE/UV) em cromatógrafo Shimatzu no comprimento de onda de 205 nm, utilizando coluna de fase reversa C18 (Zorbax Eclipse Plus, 150 x 4,6 mM x 5 µM) e fase móvel composta por ácido

trifluoroacético 0,1% (v/v) (solução A) e acetonitrila: ácido trifluoroacético 0,1% (v/v) (solução B), em gradiente de eluição linear, por 25 minutos (de 20 % a 65% da solução B). Esse método demonstrou previamente ser linear, preciso e exato para quantificação da pramlintida ($Y = 26794x - 36790$ e r = 0,999), conforme descrito no *Capítulo 2*.

3 RESULTADOS E DISCUSSÃO

Os resultados obtidos pela caracterização das nanopartículas estabilizadas com CTAB ou quitosana oligossacarídeo (PEC_{CTAB} e PEC_{QOS}) são mostrados na Tabela 1. As nanopartículas estabilizadas com quitosana produzidas com volumes maiores da solução deste componente e concentradas em evaporador rotatório (1 ou 2 vezes) não estão descritas na tabela, porque mostraram características inadequadas (elevado tamanho de partícula e polidispersão) para a análise por espalhamento de luz dinâmico.

Tabela 1 – Composição e caracterização físico-química dos nanocomplexos de polieletrólitos (PECs) de sulfato de dextrana/pramlintida estabilizados com componentes catiônicos.

PEC ID	CTAB mg/ mL	QOS mg/ mL	Tamanho (nm)		PdI		Potencial zeta (mV)		EA (%)
			Água	FNS	Água	FNS	Água	FNS	
PEC_{CTAB1}	0,10	-	296 ± 2	>4000	0,38	muito elevado	-44 ± 1	-26±1	100±14
PEC_{CTAB2}	0,50	-	precipitou	-	-	-	-	-	-
PEC_{CTAB3}	0,75	-	-34 ± 59	330 ± 25	0,56	0,23	35 ± 1	23 ± 5	86 ± 16
PEC_{CTAB4}	1,00	-	179 ± 5	213 ± 22	0,26	0,15	40 ± 2	33 ± 2	7 ± 3
PEC_{CTAB5}	1,00 (1×)	-	136 ± 5	207 ± 30	0,25	0,24	28 ± 2	39 ± 4	37 ± 5
PEC_{CTAB6}	1,00 (2×)	-	138 ± 2	132 ± 1	0,20	0,22	22 ± 1	30 ± 1	69 ± 3
PEC_{COS1}	-	0,10	433 ± 42	>4000	0,43	muito elevado	-34 ± 1	-16±1	100±14
PEC_{COS2}	-	0,50	227 ± 17	270 ± 21	0,35	0,18	28 ± 2	17 ± 2	10 ± 2
PEC_{COS3}	-	0,75	174 ± 22	213 ± 18	0,25	0,23	38 ± 3	21 ± 6	39 ± 3
PEC_{COS4}	-	1,00	612 ± 38	>4000	0,47	muito elevado	60 ± 3	29 ± 2	60 ± 1

PEC ID: identificação dos (nano)complexos de polieletrólitos; CTAB: brometo de cetrimônio, QOS: quitosana oligossacarídeo; PdI: índice de polidispersão; EA: eficiência de associação. Fonte: elaborada pela autora.

Figura 5 – Nanopartículas de polieletrólitos DexS/Pram revestidas por componentes catiônicos.

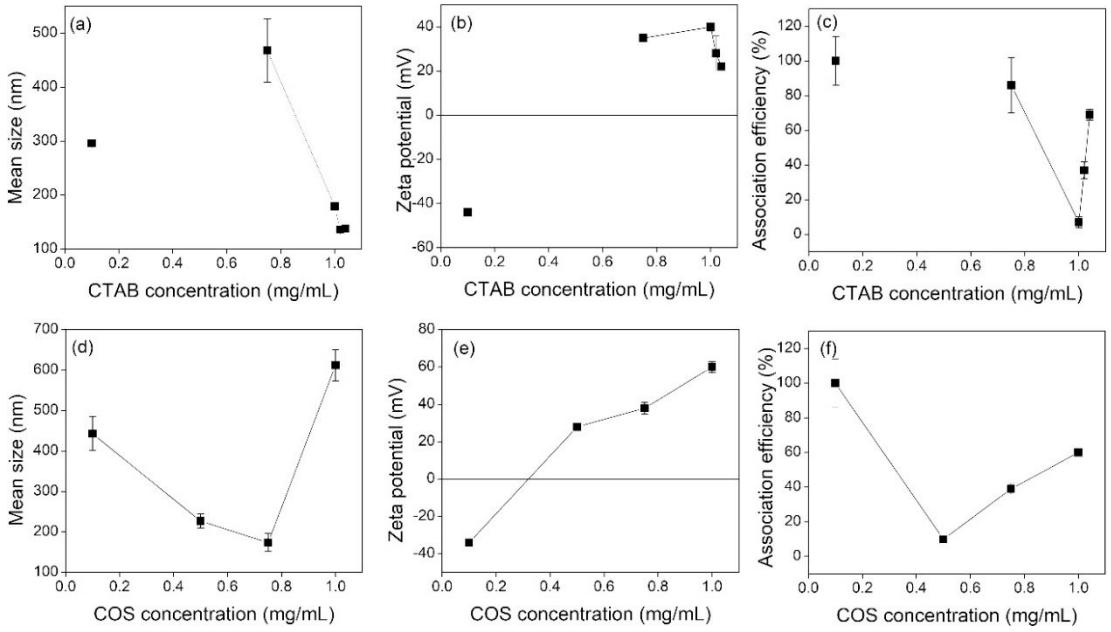

Linha superior (a, b, c): nanopartículas revestidas com CTAB, obtidas diretamente nas concentrações de 0,1; 0,75 e 1,0 mg/mL ou concentradas para 1,0 mg/mL a partir de suspensões diluídas (+1/4 ou +1/2 do volume, plotadas respectivamente em 1.02 e 1.04 no eixo x). Linha inferior (d, e, f): nanopartículas revestidas com COS nas concentrações de 0,1; 0,5; 0,75 e 1,0 mg/mL. Caracterizações quanto ao tamanho das partículas (a *e* d); potencial zeta (b *e* e) e eficiência de associação (c *e* f).

A adição de componentes catiônicos, CTAB ou quitosana oligossacarídeo, na concentração final de 0,10 mg/mL não foi suficiente para causar reversão do potencial zeta ou estabilização em FNS das PECs. Para o CTAB uma concentração final de 0,50 mg/mL causou precipitação visível, possivelmente devido a neutralização das cargas entre os componentes, enquanto uma concentração final de 0,75 mg/mL foi capaz de reverter o potencial zeta (de cerca de -40 mV para cerca de 35 mV), porém as partículas obtidas apresentaram um maior tamanho e índice de polidispersão em comparação com as $PEC_{DexS/Pram}$ originais. A utilização da concentração final de CTAB de 1,0 mg/mL apresentou respostas variáveis, dependendo da diluição da fase catiônica no momento de sua adição na suspensão de nanopartículas. O aumento direto da concentração de CTAB (0,75 para 1,00 mg/mL) causou um maior deslocamento de Pram (15 < 93 % de Pram nas PEC_{CTAB3} e PEC_{CTAB4}, respectivamente), devido a competição pelos sítios de ligação negativos da DexS. Já quando a fase catiônica foi previamente diluída (1: 1 ou 1: 2, v/v, PEC_{CTAB5} e PEC_{CTAB6}, respectivamente) e a nanosuspensão final concentrada por rotaevaporação para o volume original, o deslocamento da Pram foi menor (93 > 63 > 31 % nas PEC_{CTAB4}, PEC_{CTAB5} e PEC_{CTAB6}, respectivamente),

assim como o potencial zeta (40 > 28 > 22 mV, respectivamente) e todas demonstraram manutenção do tamanho das partículas após tratamento com FNS.

Para as PEC_{QOS} o aumento da concentração de quitosana (0,50; 0,75 e 1,00 mg/mL) produziu um efeito inverso no deslocamento da Pram (90 > 61 > 40 % de Pram nas PEC_{QOS2}, PEC_{QOS3} e PEC_{QOS4} respectivamente), aumento no potencial zeta (17 < 21 < 29 mV, respectivamente) e manutenção da estabilidade coloidal para PEC_{COS2} e PEC_{COS3}. O aumento da concentração de quitosana provavelmente favoreceu sua interação com os domínios negativos existentes nas moléculas de Pram, devido aos diversos grupos funcionais presentes na quitosana e no peptídeo. As imagens de MET das PEC_{CTAB} e PEC_{QOS}, que apresentaram resultados mais adequados na caracterização em relação ao tamanho de partículas, estabilidade coloidal e associação do fármaco, respectivamente PEC_{CTAB6} e PEC_{COS3} estão apresentadas na Figura 6. Na Figura 7 os perfis de FTIR dessas nanopartículas são apresentados. Devida a elevada sobreposição dos perfis a análise de modificações na estrutura secundária do peptídeo é dificultada. O aparecimento do pico negativo em 1.315 cm^{-1} (região amida III) para o PEC_{CTAB6} pode indicar o aumento do conteúdo de α-hélice da pramlintida nesse complexo.

Figura 6 – Microscopia eletrônica de transmissão das nanopartículas de DexS/Pram estabilizadas com CTAB 1,0 mg/mL (concentrada 2 x) (a) ou quitosana 0,75 mg/mL (b), contrastadas com ácido fosfotúngstico 1,0 % (m/v), barras de 100 nm.

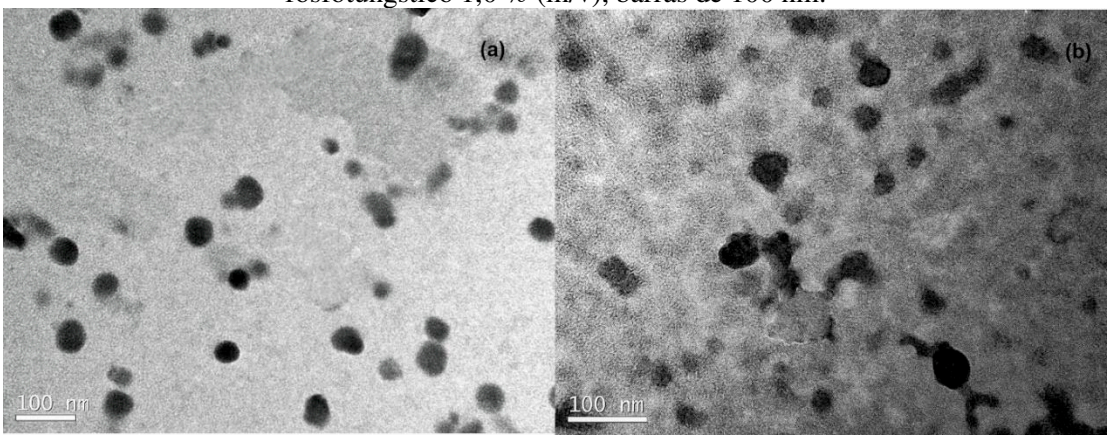

Fonte: elaborada pela autora.

Figura 7 – Derivada de segunda ordem da transmitância (%) obtida a partir de espectroscopia de absorção no infravermelho com transformada de Fourier para a pramlintida (Pram) (a), sulfato de dextrana (DexS) (b), brometo de cetiltrimetilamônio

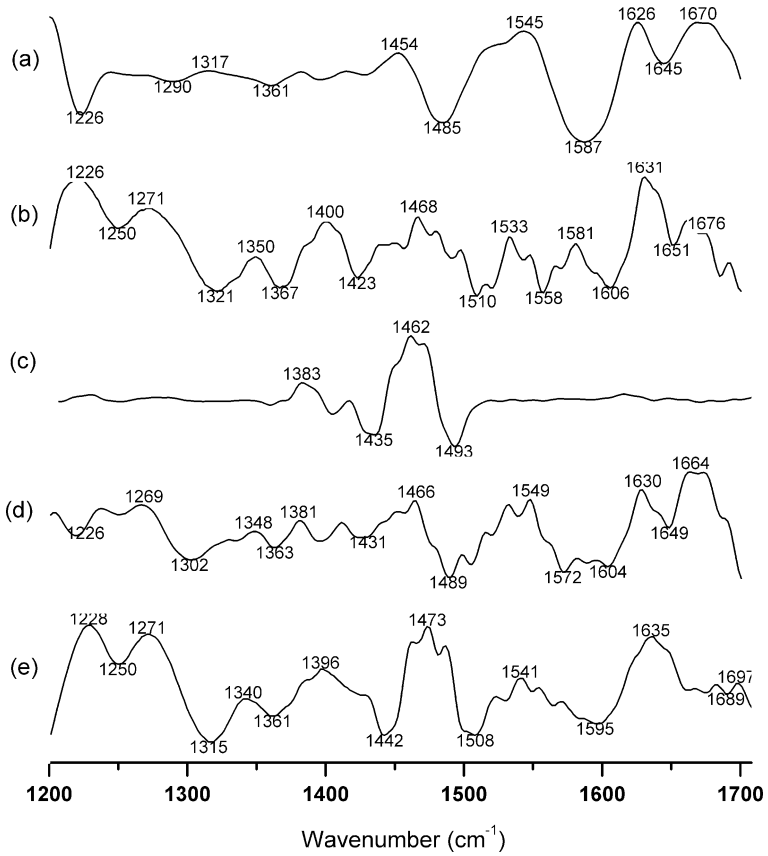

Fonte: elaborada pela autora

Tabela 2 – Composição e caracterização físico-química dos nanocomplexos de polieletrólitos (PECs)

PEC ID	P80 (mg/mL)	S80 (mg/mL)	Tamanho (nm)		PdI		Potencial zeta (mV)		EA (%)
			Água	FNS	Água	FNS	Água	FNS	
PEC_{P80}	3,0	-	283 ± 7,7	>4000	0,31	muito elevado	-43,6 ± 2,05	não avaliado	>99
$PEC_{P80/S80}$	3.0	1.0	168 ± 7,8	275 ± 12,6	0,39	0,34	-32,9 ± 3,1	-12,5 ± 2,2	>99

de sulfato de dextrana/pramlintida estabilizados com tensoativos não iônicos.
PEC ID: identificação dos complexos de polieletrólitos; P80: polissorbato 80; S80: monooleato de sorbitano; PdI: índice de polidispersão; EA: eficiência de associação. Fonte: elaborada pela autora.

Os resultados obtidos com a adição de tensoativos não-iônicos na $PEC_{DexS/Pram}$ são apresentados na *Tabela 2.* A adição de polissorbato 80 (tensoativo não-iônico, hidrofílico) na concentração final de 3,0 mg/mL, resultou na formação de nanopartículas PEC_{P80} com tamanho de 283 ± 7,7 nm (PdI 0,31 ± 0,02) e potencial zeta de -43,6 ± 2,05 mV, no pH original das suspensões. Essas nanopartículas não foram estáveis após tratamento com FNS. A adição de

monooleato de sorbitana (tensoativo não-iônico, lipofílico) na concentração de 1,0 mg/mL através de sua dispersão na suspensão de nanopartículas com sonda de ultrassom resultou na formação de nanopartículas $PEC_{P80/S80}$ com tamanho de 168 ± 7,8 nm (PdI 0,39 ± 0,06). O potencial zeta para essas formulações foi de -32,9 ± 3,1 mV, no pH original das suspensões. Essas nanopartículas demonstraram estabilidade coloidal após o tratamento com FNS, apresentando tamanho de 275 ± 12,6 nm (PdI 0,34 ± 0,04) e potencial zeta de -12,5 ± 2,2 mV. A eficiência de associação para essas nanopartículas foi > 99 %.

4 CONCLUSÕES

A adição de tensoativos, assim como proposto na literatura foi capaz de levar a obtenção de nanopartículas de polieletrólitos estáveis em forças iônicas compatíveis com meios biológicos (ex.: FNS). Porém a necessidade de tratamento com sonda de ultrassom para obtenção das $PEC_{P80/S80}$ consiste em uma desvantagem, já que pode levar a precipitação do peptídeo por si. Já para as PEC_{CTAB}, parte do fármaco desassociado devido a competição pelos sítios de ligação e a potencial toxicidade do tensoativo catiônico, foram consideradas desvantagens. Para as demais nanopartículas (PEC_{P80} e PEC_{QOS}) os resultados obtidos na caracterização físico-química preliminar não foram adequados (tamanho de partícula elevado, baixa estabilidade coloidal após tratamento com FNS ou baixa incorporação do fármaco).

REFERÊNCIAS

JUG, Mario; HAFNER, Anita; LOVRIĆ, Jasmina; KREGAR, Maja Lusina; PEPIĆ, Ivan; VANIĆ, Željka; CETINA-ČIŽMEK, Biserka; FILIPOVIĆ-GRČIĆ, Jelena. ADMET & DMPK. **ADMET and DMPK**, *[S. l.]*, v. 5, n. 3, p. 173–182, 2017. Disponível em: http://pub.iapchem.org/ojs/index.php/admet/article/view/425/pdf. Acesso em: 17 nov. 2018.

SANTALICES, Irene; GONELLA, Andrea; TORRES, Dolores; ALONSO, María José. Advances on the formulation of proteins using nanotechnologies. **Journal of Drug Delivery Science and Technology**, *[S. l.]*, v. 42, p. 155–180, 2017. DOI: 10.1016/j.jddst.2017.06.018.

SCHUBERT, Jonas; CHANANA, Munish. Coating Matters: Review on Colloidal Stability of Nanoparticles with Biocompatible Coatings in Biological Media, Living Cells and Organisms. Current Medicinal Chemistry, *[S. l.]*, v. 25, n. 35, p. 4553–4586, 2018. DOI: 10.2174/0929867325666180601101859. Disponível em: https://www.eurekaselect.com/162672/article. Acesso em: 28 dec. 2020.

APÊNDICE B – VALIDAÇÃO PARCIAL DE MÉTODO UTILIZADO PARA QUANTIFICAÇÃO DE PRANLINTIDA EM AMOSTRAS ORIUNDAS DE EXPERIMENTOS DE MUCODIFUSÃO E PERMEAÇÃO EM MUCOSA NASAL SUÍNA

APRESENTAÇÃO

Este apêndice é constituído por texto que descreve a validação do método de cromatografia líquida de alta eficiência, com detecção no ultravioleta, utilizado para a quantificação da pranlintida em amostras oriundas dos estudos de mucodifusão e permeação em mucosa nasal suína (*Manuscrito 2*).

VALIDAÇÃO PARCIAL DE MÉTODO UTILIZADO PARA QUANTIFICAÇÃO DE PRANLINTIDA EM AMOSTRAS DE EXPERIMENTOS DE MUCODISUSÃO E PERMEAÇÃO EM MUCOSA NASAL SUÍNA

1 INTRODUÇÃO

A validação parcial, segundo a RDC 166/2017 da ANVISA é a demonstração, por meio de, no mínimo precisão, exatidão e seletividade, de que o método analítico previamente validado tem as características necessárias para a obtenção de resultados com a qualidade exigida (BRAZIL, 2017). Segundo o guia para validação do ICH Q2 (R1), a validação parcial avalia modificações realizadas em um método previamente validado e, seus itens são determinados de acordo com a natureza e extensão das alterações realizadas no método. Ainda, segundo a EMEA a exatidão pode ser inferida se a linearidade, a precisão e a especificidade do método forem demonstradas (EMEA, 2006).

2 MATERIAIS E MÉTODOS

2.1 Matérias-primas, solventes e reagentes

Acetato de pranlintida (Genemed Syn, EUA), sulfato de dextrana Mn 40 kDa, grau de sulfonação entre 17 e 19 % (Sigma Aldrich, EUA), triglicerídeos de cadeia média (NEOBEE®, Stepan, EUA) polissorbato 80 (Tween 80®, Sigma Aldrich, EUA), monooleato de sorbitana (Span 80®, Sigma Aldrich, EUA), dimetilsulfóxido grau reagente (DMSO), mucina do estômago suíno (Sigma Aldrich, EUA), ácido trifluoroacético grau CLAE, acetonitrila grau CLAE, água Milli-Q (Millipore, Merk, EUA), ácido acético, cloreto de sódio, cloreto de potássio e cloreto de cálcio grau reagente. Demais solventes e reagentes utilizados com grau reagente e sem purificação prévia.

2.3 Equipamentos

Ultracentrífuga Optima Max XP (Beckman Counter, EUA); microcentrífuga (MiniStar, Bélgica); leitor de microplacas M200 (Tecan, Suíça); leitor de fluorescência (EnSpire, Perkin Elmer); cromatógrafo líquido (Shimadzu Corporation, Japão), equipado com

detector de arranjo de fotodiodos (SPD-30AM, Shimadzu Corporation, Japão); células de difusão de Franz de parede dupla jaquetada, acopladas a banho com aquecimento e agitador magnético.

2.4 Método para a quantificação da pranlintida por cromatografia líquida com detecção ultravioleta em amostras de teor e eficiência de associação das nanopartículas

A quantificação da pranlintida nas amostras de eficiência de associação (ultrafiltrado) e de teor (nanopartículas extraídas com DMSO) foi realizada por cromatografia líquida de alta eficiência com detecção ultravioleta, utilizando cromatógrafo líquido Shimadzu com detector de arranjo de fotodiodos, no comprimento de onda de 205 nm, equipado com coluna C18 (Zorbax Eclipse Plus; 150 x 4,6 mm, 5 µm) e fase móvel composta por ácido trifluoroacético 0,1 % (v/v, solução A) e acetonitrila: ácido trifluoroacético 0,1 % (v/v, solução B) em gradiente linear de eluição (de 10 até 65 % de B), por 25 minutos, em fluxo de 1,0 mL/min. O volume de injeção utilizado foi de 20 µL. Parâmetros já descritos na literatura, para quantificação da pranlintida (KOWALCZYK et al., 2014) foram utilizados, com algumas modificações. O método foi verificado quanto a linearidade, a precisão e a especificidade, e a exatidão foi inferida pela demonstração desses parâmetros. Esse método foi empregado nos Capítulos I e II nos experimentos de determinação do teor, da eficiência de associação e da dissociação da pranlintida.

2.4.1 Linearidade

As soluções-mãe de pranlintida foram preparadas na concentração de 1,0 mg/mL pela solubilização dos fármacos respectivamente em ácido acético 0,001 M; conforme recomendações do fabricante. A linearidade do método foi verificada no intervalo de 11,3 – 60,0 µg/mL. As amostras foram preparadas pela pipetagem dos volumes de solução-mãe e diluente (água ultrapura), homogeneização com pipeta e filtração através de membrana de éster de celulose com diâmetro de poro de 0,22 µM em sistema composto por seringa e filtro para seringa. A análise dos resultados foi realizada por regressão linear.

2.4.2 Precisão

A precisão do método foi verificada pela repetibilidade dos resultados obtidos para amostras em três níveis de concentração (13,3; 33,3 e 60 µg/mL). As amostras foram preparadas em triplicata a partir de três suspensões de nanopartículas, submetidas a extração com DMSO (incubação em ultrassom por 20 minutos) e diluição com água ultrapura. As análises foram realizadas empregando os parâmetros descritos no item 9.6. As amostras de teor geradas pela extração das suspensões com DMSO foram utilizadas para a avaliação da precisão por se tratar de amostras mais complexas comparadas as de eficiência de associação, geradas pela ultrafiltração-centrifugação das suspensões de nanopartículas. Para remover a interferência no início do cromatograma, causada pela absorção do DMSO no UV 205 nm os cromatogramas foram obtidos entre 6,5 e 25 minutos.

2.4.3 Seletividade

A seletividade do método foi verificada pela análise de amostras geradas pela extração de suspensões de nanopartículas brancas (sem os fármacos) com DMSO, preparadas da mesma forma descrita no item 2.5.2 e analisadas empregando as condições descritas no item 2.5. A seletividade foi avaliada em triplicata de amostras.

2.5 Método para a quantificação da pranlintida por cromatografia líquida com detecção ultravioleta em amostras de estudos de mucodifusão e permeação em mucosal nasal suína

As amostras geradas pelos experimentos de mucodifusão e permeação em mucosa nasal suína (Capítulo II) foram analisadas pelo método descrito no item 2.5. A precisão, a exatidão e a seletividade do método em relação as amostras obtidas nesses experimentos foram avaliadas. As amostras oriundas dos experimentos de permeação foram utilizadas para a determinação desses parâmetros por serem mais complexas em relação às amostras oriundas dos estudos de mucodifusão.

2.5.1 Precisão

A precisão do método foi verificada pela repetibilidade dos resultados obtidos para amostras em três níveis de concentração de pranlintida (13,3; 33,3 e 60 µg/mL). As amostras foram preparadas em triplicata empregando como diluentes o meio aceptor utilizado nas células de difusão Franz (FNS pH 5,5) e a solução extrativa da mucosa nasal suína (mucosa nasal suína cortada em cubos com tamanho de cerca de 5 mm e submetida a extração com solventes usados como fase móvel descrita no item 2.5, na proporção de 60: 40, v/v). As soluções-mãe de pranlintida e os diluentes foram adicionados por pipetagem, homogeneizados e submetidos aos tratamentos correspondentes e a filtração através de membrana de éster de celulose com diâmetro de poro de 0,22 µM em sistema composto por seringa e filtro para seringa. O desvio padrão relativo entre os resultados obtidos para as amostras foi considerado indicativo da precisão do método.

2.5.2 Exatidão

A exatidão do método foi verificada pela recuperação da pranlintida adicionada às amostras obtidas nos experimentos de permeação em mucosa nasal suína, assim como descrito para a precisão (item 2.6.1). As soluções-mãe de pranlintida foram adicionadas às amostras com concentrações conhecidas e a recuperação das concentrações adicionadas foi testada pela obtenção de uma resposta representativa da concentração inicial da amostra mais a concentração adicionada. O percentual de recuperação em relação a concentração teórica foi considerado indicativo da exatidão do método.

2.5.3 Seletividade

A seletividade do método foi verificada em triplicata pela análise de amostras sem pranlintida (FNS e solução extrativa da mucosa), preparadas da mesma forma descrita no item 2.6.1 e analisadas nas condições descritas no item 2.5.

3 RESULTADOS E DISCUSSÃO

3.2 Método para quantificação da pranlintida por cromatografia líquida com detecção ultravioleta

A curva de calibração obtida para a quantificação da pranlintida por CLAE/UV está representada na Figura 1. A análise de regressão linear demonstrou que o desvio da linearidade não foi significativo. O coeficiente de correlação obtido foi r = 0,999. A equação da reta obtida foi Y=26794x-36790.

Figura 3 – Curva de calibração obtida para a quantificação da pranlintida por cromatografia líquida com detecção ultravioleta (CLAE/UV).

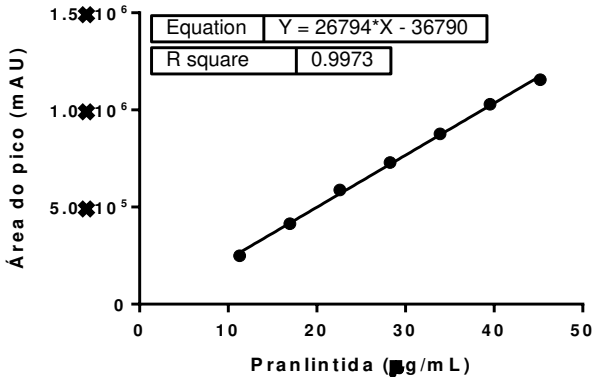

O desvio padrão relativo nas concentrações baixa, média e alta das amostras de teor das nanopartículas foi de 1,43; 2,44 e 2,12 % respectivamente. Amostras sem o fármaco (nanopartículas brancas, NE branca SDex) não apresentaram absorção no comprimento de onda e tempo de retenção dos analitos, demonstrando a especificidade do método (Figura 5).

Para as amostras de permeação da pranlintida em mucosa nasal suína, o desvio padrão relativo nas concentrações baixa, média e alta dos fármacos no meio aceptor da célula de Franz foi de 6,99; 5,62 e 5,80 %. Já o desvio padrão relativo nas concentrações baixa, média e alta dos fármacos na solução extrativa da mucosa foi de 10,6; 3,79 e 1,78 %. A exatidão também foi avaliada para esses experimentos, através da recuperação de quantidades adicionadas das soluções-mãe de pranlintida em amostras com concentrações conhecidas do meio aceptor das células de Franz ou da solução extrativa da mucosa. A recuperação da pranlintida no meio aceptor foi de 83,8 ± 6,99 % para a concentração adicionada de 11,3 µg/mL. Essa recuperação é referente a concentração teórica da amostra que compreende a concentração de pranlintida conhecida mais a concentração adicionada. Na solução extrativa da mucosa a recuperação foi

de 110 ± 11,6 % para a concentração adicionada de 11,3 µg/mL. Ambos o FNS e a solução extrativa da mucosa sem fármacos não apresentaram absorção importante no comprimento de onda e tempo de retenção dos analito, demonstrando a especificidade do método (Figura 2).

Figura 4– Perfil cromatográfico da pranlintida obtido por cromatografia líquida.

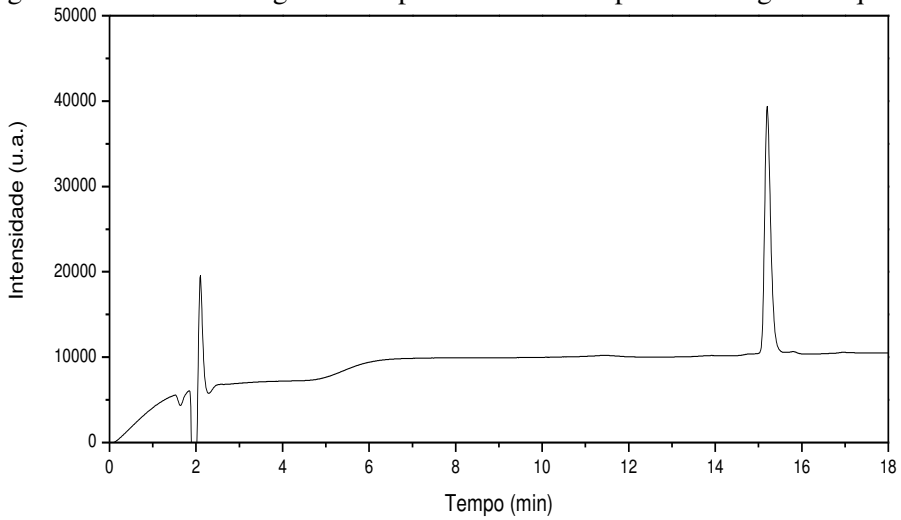

Perfil obtido por cromatografia líquida utilizando comprimento de onda de detecção de 205 nm, coluna de fase reversa C18 Zorbax Eclipse Plus (150 x 4,6 mm, 5 µm; Agilent) e fase móvel composta de (A) ácido trifluoroacético 0,1 % e (B) acetonitrila: ácido trifluoroacético 0,1 % (v/v) em gradiente linear de eluição de 10 – 65 % em 25 minutos. Tempo de retenção (TR) de 15,2 minutos.

Figura 5 – Perfis cromatográficos das nanoemulsões brancas revestidas com sulfato de dextrana extraídas com DMSO, da mucosa nasal suína, extraída com fase móvel (60: 40, v/v, A/B) e do fluido nasal simulado.

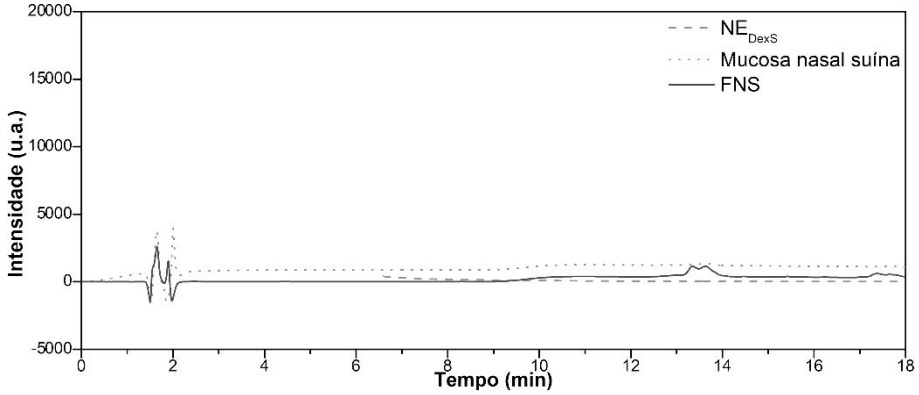

Perfis obtidos por cromatografia líquida, utilizando comprimento de onda de detecção de 205 nm, coluna de fase reversa C18 Zorbax Eclipse Plus (150 x 4,6 mm, 5 µm; Agilent) e fase móvel composta de (A) ácido trifluoroacético 0,1 % e (B) acetonitrila: ácido trifluoroacético 0,1 % (v/v) em gradiente linear de eluição de 10 – 65 % em 25 minutos. Para melhor visualização os perfis foram plotados com um deslocamento no eixo y de 10 % entre eles. Fonte: elaborada pela autora.

4 CONCLUSÕES

O método analítico proposto para quantificação da pranlintida foi verificado e apresentou-se adequado quanto aos critérios de linearidade, precisão, exatidão e seletividade.

REFERÊNCIAS BIBLIOGRÁFICAS

BRAZIL. **RESOLUÇÃO RDC Nº 166, DE 24 DE JULHO DE 2017** - Imprensa Nacional. [S.l: s.n.], 2017

EMEA. **ICH Q2 (R1) Validation of analytical procedures: text and methodology** | European Medicines Agency. [S.l: s.n.], 2006

KOWALCZYK, R. et al. Convergent Chemoenzymatic Synthesis of a Library of Glycosylated An

8 ANEXO

8.1 APRESENTAÇÃO

Certificado de aprovação **CEUA/UFSC n° 6633260819**.

CERTIFICADO

Certificamos que a proposta intitulada "Preparação, caracterização e avaliação in vitro e in vivo de nanoplexos de pranlintida e sulfato de dextrana para administração nasal", protocolada sob o CEUA nº 6633260819 (ID 001426), sob a responsabilidade de **Elenara Maria Teixeira Lemos Senna** *e equipe; Rui Daniel S. Prediger; Carine Zuglianello; Angela Patricia França* - que envolve a produção, manutenção e/ou utilização de animais pertencentes ao filo Chordata, subfilo Vertebrata (exceto o homem), para fins de pesquisa científica ou ensino - está de acordo com os preceitos da Lei 11.794 de 8 de outubro de 2008, com o Decreto 6.899 de 15 de julho de 2009, bem como com as normas editadas pelo Conselho Nacional de Controle da Experimentação Animal (CONCEA), e foi **aprovada** pela Comissão de Ética no Uso de Animais da Universidade Federal de Santa Catarina (CEUA/UFSC) na reunião de 15/10/2019.

We certify that the proposal "Preparation, characterization and in vitro and in vivo evaluation of pramlintide-dextran sulfate nanoplexes for nasal administration", utilizing 132 Heterogenics mice (132 males), protocol number CEUA 6633260819 (ID 001426), under the responsibility of **Elenara Maria Teixeira Lemos Senna** *and team; Rui Daniel S. Prediger; Carine Zuglianello; Angela Patricia França* - which involves the production, maintenance and/or use of animals belonging to the phylum Chordata, subphylum Vertebrata (except human beings), for scientific research purposes or teaching - is in accordance with Law 11.794 of October 8, 2008, Decree 6899 of July 15, 2009, as well as with the rules issued by the National Council for Control of Animal Experimentation (CONCEA), and was **approved** by the Ethic Committee on Animal Use of the Federal University of Santa Catarina (CEUA/UFSC) in the meeting of 10/15/2019.

Finalidade da Proposta: Pesquisa

Vigência da Proposta: de 06/2019 a 12/2019 Área: Ciências da Saúde

Origem:	Biotério Central						
Espécie:	Camundongos heterogênicos	sexo:	Machos	idade:	3 a 3 meses	N:	132
Linhagem:	Camundongos/Swiss			Peso:	40 a 50 g		

Local do experimento: Sala 306, CCB, bloco D

Florianópolis, 25 de fevereiro de 2021

Prof. Dr. Maurício Laterça Martins

Maurício Laterça Martins
Presidente pro tempore da Comissão de Ética no Uso de Animais
Universidade Federal de Santa Catarina

Vice-Presidente da Comissão de Ética no Uso de Animais
Universidade Federal de Santa Catarina